Signatures of the primordial universe in large-scale structure surveys

Nicolas van de Rijt

École Doctorale de l'École Polytechnique
Institut de Physique Théorique du CEA

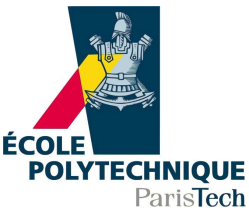

Thèse de Doctorat

présentée par

Nicolas Van de Rijt

Signatures of the primordial universe in large-scale structure surveys

pour obtenir le grade de Docteur de l'École Polytechnique
Spécialité: Physique Théorique

soutenue le 21 juin 2012 devant le jury composé de

Mr Francis Bernardeau	Directeur de thèse
Mr Martin Kilbinger	Examinateur
Mr Julien Lesgourgues	Rapporteur
Mr Simon Prunet	Examinateur
Mr Atsushi Taruya	Rapporteur
Mr Filippo Vernizzi	Directeur de thèse

Abstract

The study of the large-scale structure of the Universe is one of the most important tools used to understand the origin and evolution of the Universe. In this thesis, we focus on two different facets of this study: cosmological perturbation theory and cosmic shear.

Cosmological perturbation theory describes how the large-scale structure of the Universe has been created out of the tiny initial perturbations. This evolution is described using fluid equations, and in this thesis, we introduce new versions of this Boltzmann hierarchy. The advantages and disadvantages of each hierarchy are thoroughly analysed. We also introduce a novel technique, dubbed the eikonal approximation, which enables us to better understand the results of existing perturbation theory approaches. Moreover, its broad range of applicability allows us to generalise many results.

Cosmic shear describes how gravitational lensing deforms the image of the sky. In this thesis, we compute in great detail the bispectrum of cosmic shear to second order in the gravitational potentials. The complete calculation is done on the full sky, making the results much more general than the existing ones. To ease the otherwise impossible numerical calculations, we introduce the (extended) Limber approximation.

L'étude des grandes structures de l'Univers est un des meilleurs moyens pour comprendre l'origine et l'évolution de l'Univers. Dans cette thèse, nous nous spécialisons aussi bien dans la théorie des perturbations aux échelles cosmologiques, que dans le cisaillement cosmique.

La théorie des perturbations aux échelles cosmologiques décrit comment les grandes structures de l'Univers se sont formées à partir des minuscules fluctuations primordiales. Cette évolution est généralement décrite en se servant des équations du mouvement d'un fluide, et dans cette thèse nous introduisons quelques nouvelles versions de cette hiérarchie de Boltzmann. Les avantages et inconvénients de ces nouvelles hiérarchies sont analysés en détail. Nous introduisons aussi une nouvelle technique, appelée l'approximation eikonal, qui nous permet de mieux comprendre les résultats des autres approches utilisées en théorie des perturbations. En outre, grâce à sa généralité, elle nous permet de généraliser une grande quantité de résultats.

Le cisaillement cosmique décrit comment l'effet des lentilles gravitationnelles déforme notre image du ciel. Dans cette thèse, nous étudions de manière détaillée le bispectre du cisaillement cosmique, au deuxième ordre en les potentiels gravitationnels. Le calcul est intégralement fait en "full sky", généralisant ainsi les résultats existants. Pour simplifier les calculs numériques, nous introduisons et généralisons l'approximation dite de Limber.

Acknowledgements

This thesis is the result of three fruitful years of research. And even if there is only one author's name on the cover, I should emphasise that this thesis wouldn't have been possible without...

...my advisors Francis and Filippo. I'd like to thank you for your endless help and support. Your doors were always open, and you were always willing to help and answer my (sometimes stupid) questions. I couldn't have dreamed for better advisors.

...Camille. Without your help, the bispectrum of cosmic shear would still be in its infant stage. Thanks for your joyful collaboration!

...the other cosmologists at the IPhT, i.e. Chiara, Zhiqi, Emiliano and Patrick. Your presence during lunches (thanks Zhiqi for lunchme.php!) and conferences made of these three years an unforgettable experience.

...the secretaries and the IT workers. I can't remember any administrative or computer related issue remaining unresolved for a fraction of a second.

...the other PhD students. Even if we haven't spent a lot of time together, it was always enjoyable to be with you.

...the members of my committee, Messrs Kilbinger, Lesgourgues, Prunet and Taruya. Thank you very much to all of you for accepting to be part of my committee, and especially to Messrs Lesgourgues and Taruya for accepting to be referees.

...my beloved Kathy. I will not start summing up all the reasons I should thank you, because that would take me too long!

Introduction

Gif-sur-Yvette, April 2012

To my successor

Dear successor,

Cosmology is a fantastic bit of science! But there is no point convincing you of this, as you just started a PhD in cosmology. Moreover, there is no doubt you already know a few things about cosmology. Nevertheless, I'm sure that there are much more branches of cosmology than you might think. For sure you know that there exist galaxies and clusters of galaxies in our Universe. And I'd also be utterly surprised if you'd never heard of dark matter or dark energy. Otherwise you wouldn't be reading this, would you? Maybe terms like "cosmic microwave background" and "cosmic inflation" sound familiar to you; you kind of know what they are, but you might not know any equation governing those complicated theories. But... "cosmic shear" and "cosmological perturbation theory", ever heard of? Don't worry, because three years ago, I hadn't.

During your first few years as a researcher, it is unlikely you'll touch on all subjects of cosmology. You'll just focus on a few. If you continue working on the subjects I have been working on – which is not unlikely because there is still a lot to be done – you'll be working on cosmic shear and perturbation theory, with the focus on the latter. Let me explain in a few words what those two subjects consist of, what already has been done by others and by ourselves, and what still could be done by you.

Cosmological perturbation theory is the theory that describes the growth of the initial inhomogeneities into the large-scale structure of the Universe we observe today. Starting with the statistical properties of these initial perturbations, this theory attempts to predict the statistical distribution of large objects like (clusters of) galaxies and dark matter haloes. As the governing fluid equations are highly non-linear and very complicated to solve, many approximation schemes have been proposed in the past. In this thesis, I first present a few new sets of fluid equations, and I later introduce our own eikonal approximation, a generalisation of the so-called renormalised perturbation theory. What still should be done, is the application of our eikonal approximation to these new sets of equations.

As I just did for perturbation theory, let me now also briefly introduce cosmic shear. Gravitational lensing tells us that light – like that coming from stars – is deflected by matter. Because of this, the sky we observe does not exactly correspond to the real Universe; the sky is "sheared". By studying this shear, we can infer properties of the intervening matter. A few years ago, Francis, Filippo and Camille (who is now a post-doc in Cambridge) computed the shear to second order in the gravitational potential. When I joined this team, we started with the computation of the bispectrum (some kind of 3-point function) of this shear. Luckily for you, most of the work has been done now; only the magnetic part of the shear still requires to be analysed.

This thesis is organised exactly as described above. In Part A, I'll derive our new sets of equations, starting from the collisionless Boltzmann equation. I'll also spend some time (in chapter 3) explaining in detail the basic principles of cosmological perturbation theory. In Part B, I'll generalise the standard perturbation theory results by applying our eikonal approximation. Part C tackles the computation of the bispectrum of the cosmic shear, starting with a detailed introduction on cosmic shear and the calculation of the power spectrum.

My dear successor, I've written this thesis for you, based on the sole guideline of usefulness. So don't expect to find a comprehensive review of cosmology (there are plenty of excellent books in the library) or an exhaustive list of references (you can always check the references in our articles). On the other hand, some parts of the information contained in this thesis can also be found in books and reviews, but often using other notations and conventions. Or focussing on details you won't really need to continue our research projects anyway. What I have tried to do, is to write some kind of "read me" to our articles, because if I ask you to read them right away (have a look at pages 57 and 116 if you dare), I reckon you'd be lost rather quickly. So the aim of this thesis is to make our articles understandable to you, a beginning PhD student. Moreover, this thesis should contain all the information you need to continue our projects, like how was the data generated? Or what is the structure of my huge cosmic shear MATHEMATICA notebook? Or even how were the plots constructed? This information is often hidden in the articles, but is obviously crucial for you.

Good luck!

Nicolas

Contents

List of Figures

Part A

Cosmological Perturbation Theory

Chapter 1

Introduction

Contents

1.1 Cosmological perturbation theory

The best description of the Universe we have today assumes that the Universe used to be (almost) homogeneous and isotropic. Nevertheless, little perturbations, likely originating from quantum fluctuations, were present. These little perturbations would eventually become the seeds of the large-scale structure we observe today. An important discipline of cosmology is precisely the study of how these little perturbations evolved into those large-scale structures. This pillar of cosmology is known as cosmological perturbation theory.

Needless to say, cosmological perturbation theory is a very complicated subject. The governing equations (like Einstein's equation) are highly non-linear and the processes generating the primordial perturbations are yet unknown. On the theoretical side, two main difficulties can be distinguished. Firstly, the equations need to be simplified enough so that they can become manageable. Testing the validity of all these approximation is a crucial part of the work. Secondly, a whole new arsenal of techniques needs to be invented in order to "do" something with the equations. Interaction between these two facets is very important, because a better understanding of the techniques used in simple cases can help us in finding better ones. And if these new techniques are more powerful, more complicated (i.e. general) equations can be handled.

The theoretical part of cosmological perturbation theory has evolved in the following way. Basically, progress goes back and forth between the "equations-side" and the "techniques-side". The very first step was the following: using linearised Einstein's general relativity and the linearised Boltzmann equation, a set of linear equations had been obtained. These equations are relatively straightforward to solve, and the predictions of this model (like the cosmic microwave background anisotropies) proved to be extremely

accurate. Next, the non-linear interaction terms were added, and the analysis of their impact was performed using techniques borrowed from field theory. This standard perturbation theory (SPT) approach is doable at low order, but becomes extremely involved as soon as higher-order corrections are taken into account. Nevertheless, groundbreaking results were achieved by introducing the framework of resummed perturbation theory (RPT). In this context, all the non-linear corrections (of a specific type) are taken into account. Unfortunately, this approach suffers from several drawbacks. Firstly, not all the corrections are taken into account, and secondly, a specific assumption is made on the distribution of the initial perturbations.

On the equation-side of the problem, not much progress has been made in the last few years, mostly because the techniques-side could not handle more complicated equations anyway. However, an important comment is in order here. The equations of motion have always been computed making the following approximation: the particles are either relativistic (like photons) or non-relativistic (like dust). Whether this is perfectly true for most of the particles in the Universe, it isn't for neutrinos: as they are light, they used to be relativistic in the early Universe but they turned non-relativistic at some point. This transition is non-trivial and has not yet been incorporated properly in theoretical cosmological perturbation theory.

This thesis handles both sides of cosmological perturbation theory. In chapter 2 the equations of motion are generalised, focussing on neutrinos, and in chapters 4 and 5, the results of RPT are generalised using the so called eikonal approximation. In more details, parts A and B of this thesis are organised as follows. In the remaining of this introductory chapter, we will develop the basic ingredients of cosmology. We will discuss the metric, the matter content of the universe, and how we will describe the various fluids. In the next chapter, chapter 2, we will derive in full details the equations describing the evolution of a fluid, starting from the collisionless Boltzmann equation. Depending on the approximations we will make, we will find different sets of equations. As the standard description of neutrinos neglects relativistic corrections like anisotropic pressure, we will focus on a description where all those corrections are properly taken into account. This is done by introducing generalised momenta. We will precisely show how these new generalised momenta are related to the conventional physical quantities like the energy density, momentum... We will also analyse the Boltzmann equation by expanding the phase space distribution function into spherical harmonics. The calculations are involved, but the results have some great advantages, as will be discussed. In this case as well, we will derive the exact relationship between these newly introduced variables and the conventional ones. Chapter 3 contains an overview of the techniques-side of cosmological perturbation theory. We will show how the equations derived in chapter 2 are used in order to make predictions. Several approaches exist and we will describe both their strengths and shortcomings. In the last section, we will show how perturbation theory can be performed in the framework of spherical harmonics, thereby making yet another bridge between the different hierarchies.

Part B is entirely devoted to the eikonal approximation. After introducing the formalism, we show how the powerful results obtained in RPT can be explained and generalised. In chapter 4 we focus on a universe filled with a single fluid, whereas in chapter 5 we show how the eikonal approximation can be applied in a universe filled with multiple fluids. Future work will involve trying to apply this novel eikonal approximation to the generalised equations; said in order words, trying to incorporate the equations for neutrinos in

the framework of the eikonal approximation.

1.2 FLRW spacetime

On very large scales, our Universe is observed to be statistically homogeneous and isotropic. This cosmological principle [1, 2, 3] is often translated as "we are not in any special place in our Universe". The solution to Einstein's general relativity satisfying these assumptions is given by the Friedmann-Lemaître-Robertson-Walker (FLRW) metric [4]. We will work in a perturbed FLRW spacetime[1] with the metric

$$\mathrm{d}s^2 = a^2(\tau)\left[-(1+2\psi)\mathrm{d}\tau^2 + (1-2\phi)\mathrm{d}\mathbf{x}^2\right], \tag{1.1}$$

where τ is the conformal time, $\mathbf{x}$ are the comoving coordinates, $a(\tau)$ is the scale factor, and ψ and ϕ are the scalar perturbations. We will assume that the scalar perturbations ψ and ϕ are small and consistently drop subleading terms. The metric has been written in conformal Newtonian gauge [5] and we will not consider primordial vector and tensor perturbations. The scale factor a is related to the redshift z as $1 + z = a_0/a$ where a_0 is the scale factor today, and we will take $a_0 = 1$ throughout. Because $a(\tau)$ increases monotonically with time, a can also be used as a time variable.

1.3 Matter content of the Universe

The previous section introduced the FLRW spacetime. But not a word has been said about how the spacetime itself evolves with time. As general relativity intertwines the evolution of the spacetime with the matter content of the Universe, we discuss both at the same time. We will now describe the background evolution of the Universe, i.e. we will neglect the scalar perturbations present in the metric (1.1).

If we assume the Universe to be filled with a "perfect fluid" with pressure p and density ρ, the scale factor $a(\tau)$ satisfies

$$\mathcal{H}^2 = \frac{8\pi G}{3}a^2\rho \qquad \text{and} \qquad \dot{\mathcal{H}} = -\frac{4\pi G}{3}a^2(\rho + 3\mathrm{p}) \tag{1.2}$$

where $\mathcal{H} \equiv (\mathrm{d}a/\mathrm{d}\tau)/a \equiv \dot{a}/a$ is the (conformal) Hubble parameter, and G is Newton's constant. These equations are known as Friedmann's equations and can be derived from Einstein's equations. The Hubble parameter today, denoted by H_0 is measured to be $H_0 = 70.3\,\mathrm{km/s/Mpc}$ and we define the reduced Hubble parameter as $h \equiv H_0/(100\,\mathrm{km/s/Mpc})$ [6].

If our Universe contains more than 1 perfect fluid, eqs. (1.2) are still valid when ρ is taken to be the total matter density, i.e. $\rho = \sum \rho_\alpha$, and p the total pressure, $\mathrm{p} = \sum \mathrm{p}_\alpha$. For each fluid α, it is convenient to introduce the equation-of-state parameter $w_\alpha \equiv \mathrm{p}_\alpha/\rho_\alpha$.

Conservation of energy, found by combining the two Friedmann equations, imposes

$$\frac{\dot{\rho}}{\rho} = -3(1+w)\mathcal{H}. \tag{1.3}$$

[1]The cosmological principle allows for a non-vanishing curvature. However, we will not consider this case.

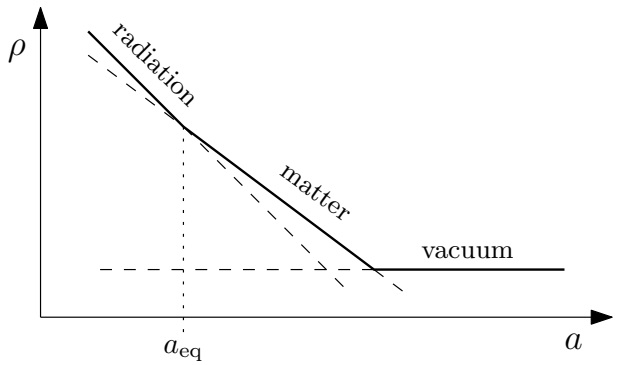

Figure 1.1: The history of the energy density in the Universe. At early times, the Universe was dominated by radiation, until matter took over at "equality". Recently, dark energy has come into play and it will dominate our Universe for eternity, or at least until you have finished reading this thesis.

If w is constant, we can integrate this equation to

$$\rho \propto a^{-3(1+w)}. \tag{1.4}$$

This shows that the equation-of-state parameter w – if constant – fully determines the time evolution of the fluid density. The three types of fluids our Universe (mostly) consists of are matter, radiation and dark energy (vacuum). Their corresponding equation-of-state parameter and exponent ($-3(1+w)$) are given below.

	matter	radiation	vacuum
w	0	1/3	-1
$-3(1+w)$	-3	-4	0

The interpretation of these numbers is very important. One sees that the matter density decays as a^{-3} whereas the radiation energy density decays faster, as a^{-4}. Vacuum energy, by its very nature, does not change in time. The first exponent corresponds to the fact that the energy density of matter gets diluted when the volume increases. And as – until further notice – we live in 3 dimensions, the exponent is 3. Radiation, on top of this dilution, also suffers form the fact that its wavelength gets redshifted, which induces one more factor of $1/a$. A long long time ago, when a was small, the energy content of the Universe was dominated by the radiation. At some point in history, the energy density of radiation and matter became equal. The scale factor at that time is called $a_{\rm eq}$ and it corresponds to a redshift of $z \sim 3000$. After equality, the Universe became matter dominated until the dark energy took over around $z \sim 1$. This is schematically shown on Fig. 1.1.

The Friedmann equations tell us that during radiation domination $a \propto \tau$ and that during matter domination $a \propto \tau^2$. To have a better understanding of these numbers, we can derive how a depends on the cosmic time t, defined[2] through $\mathrm{d}t = a(t)\mathrm{d}\tau$. With this variable, $a \propto t^{1/2}$ during radiation domination, $a \propto t^{2/3}$ during matter domination

[2]It would actually be more correct to say that the conformal time τ is defined out of the cosmic time t using this definition.

and a grows exponentially with (proper) time once the Universe is dominated by vacuum energy. This is why a universe dominated by vacuum energy undergoes an accelerated expansion.

For each fluid α, we define the density parameter Ω_α as

$$\Omega_\alpha(a) \equiv \frac{8\pi G}{3\mathcal{H}^2(a)} a^2 \rho_\alpha(a). \tag{1.5}$$

These quantities are important because the Friedmann equations impose $\sum \Omega_\alpha = 1$. A result different from 1 would impose a non-vanishing curvature term, and we do not consider that case. Even if the definition above makes Ω_α time dependent, we will from now on only consider its value today, i.e.

$$\Omega_\alpha \equiv \frac{8\pi G}{3H_0^2} \rho_\alpha(a_0). \tag{1.6}$$

Combining this with the first Friedmann equation (1.2) and the conservation of energy eq. (1.4), we find

$$\mathcal{H}(a) = aH_0 \left[\sum \Omega_\alpha a^{-3(1+w_\alpha)} \right]^{1/2}. \tag{1.7}$$

The radiation density parameter is denoted by Ω_r, the matter density parameter by Ω_m and the vacuum energy density parameter by Ω_Λ. Recent measurements of these parameters today are $\Omega_\Lambda = 0.729$ and $\Omega_m = 0.271$ [6], confirming the hypothesis that our Universe is flat. Because ρ_r decays away quickly ($\rho_r(a) \propto a^{-4}$), the value of Ω_r today is negligible. Ω_m has two major components, cold dark matter $\Omega_c = 0.226$ and baryons $\Omega_b = 0.0455$.

Not a word has been said yet about neutrinos. The principal reason is that their presence has only little effect on the history of the universe. At all times, their contribution to the energy density is small compared to the dominant fluid. Another reason is that they are neither radiation nor matter: because of their small mass [7, 8], they were still highly relativistic (i.e. like radiation) at equality and turned non-relativistic (i.e. like matter) during matter dominance[3]. Finding an appropriate description of neutrinos, incorporating this transition, will be the subject of chapter 2.

1.4 Particles and fluids

The description of the Universe given in the previous section enables us to understand the basic foundations of cosmology. But even if homogeneity and isotropy are good assumptions on very large scales, they are not good any more on smaller scales as we would like to understand the formation of galaxy clusters and dark matter haloes.

Although we know that the Universe is filled with particles, we will stick to the fluid description. This means that we assume we can define at every point in space-time an energy density, a momentum, etc.. This description of the Universe does not allow for shell-crossings, i.e. points where the momentum is ill-defined, see Fig. 1.2. Shell-crossing occurs in virialized objects like galaxies, so we cannot consider objects of that size using this formalism.

[3]It is yet unknown whether *all* neutrino species are already non-relativistic, but at least 2 are.

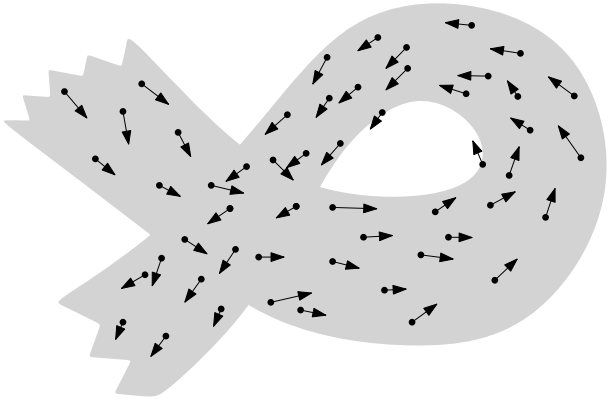

Figure 1.2: Shell-crossing: at some points in spacetime, the direction of the flow is ill-defined because different flows cross each other. At those points, the fluid description breaks down.

For a particle, we define the momentum P^μ through an affine parameter λ as $P^\mu = \mathrm{d}x^\mu/\mathrm{d}\lambda$, and it satisfies the energy-momentum relation

$$P_\mu P^\mu = -m^2, \tag{1.8}$$

where $\mu = 0, 1, 2, 3$ and the Einstein summation convention is used. This definition remains valid in our fluid description, and we define the related quantities q^i and p^i as

$$q^i \equiv a(\tau)p^i \equiv a^2(\tau)(1-\phi)P^i, \tag{1.9}$$

where i runs only over the spatial indices. p^i is the proper momentum measured in a local inertial frame instantaneously at rest with respect to a comoving observer, i.e. with fixed coordinates $\mathbf{x}$, and q^i is the same momentum but corrected for the homogeneous expansion of the Universe [7]. The indices of the comoving momentum P^μ are lowered and raised with the metric. Therefore, we need to use δ^{ij} for p_i and q_i instead. We have

$$P_i P^i = g_{ij}P^i P^j = \delta_{ij}p^i p^j \equiv p^2. \tag{1.10}$$

Finally, we define the comoving energy $\epsilon = \epsilon(\tau, q)$ through

$$P_0 P^0 \equiv -\frac{\epsilon^2}{a^2(\tau)}, \tag{1.11}$$

whence

$$\epsilon^2 = a^2(\tau)\left[m^2 + p^2\right] = a^2(\tau)E^2 \tag{1.12}$$

where E is the proper energy. From the definitions above, it is straightforward to show the following useful identities:

$$\frac{\partial\epsilon}{\partial\tau} = \mathcal{H}\epsilon\left[1 - \frac{q^2}{\epsilon^2}\right] \qquad \text{and} \qquad \frac{\partial\epsilon}{\partial q} = \frac{q}{\epsilon}. \tag{1.13}$$

In this chapter we have introduced our spacetime and the fluid description of the matter content of the Universe. This was enough to derive the time evolution of the spacetime itself. In the next chapter we will derive, using the Boltzmann equation, the time evolution of the fluids.

Chapter 2

The Boltzmann hierarchy

Contents

In this chapter we will derive, in full details, the Botlzmann hierarchy describing the evolution of a fluid, focussing on neutrinos. Using various different sets of variables, we will find various equivalent hierarchies, each one with its advantages and disadvantages. As the derivation is explained step by step, this chapter is rather technical.

2.1 The Boltzmann equation

The fluid we are considering is described by means of its distribution function in phase space, f. The phase space variables we use, are the position $\mathbf{x} = x^i$, the momentum $\mathbf{q} = q^i$ and the conformal time τ. We further decompose the momentum variable into its direction $\hat{n}^i \equiv q^i/q$ and its norm $q^2 \equiv \delta_{ij} q^i q^j$. The spatially averaged distribution function is denoted by $f_0 = f_0(q, \tau)$, and its perturbation by Ψ, i.e.

$$f(\mathbf{x}, \hat{n}^i, q, \tau) = f_0(q, \tau) \left[1 + \Psi(\mathbf{x}, \hat{n}^i, q, \tau)\right]. \tag{2.1}$$

We expand the collisionless Boltzmann equation $\dfrac{\mathrm{d}f}{\mathrm{d}\tau} = 0$ using the chain rule in

$$\frac{\partial f}{\partial x^i}\frac{\mathrm{d}x^i}{\mathrm{d}\tau} + \frac{\partial f}{\partial \hat{n}^i}\frac{\mathrm{d}\hat{n}^i}{\mathrm{d}\tau} + \frac{\partial f}{\partial q}\frac{\mathrm{d}q}{\mathrm{d}\tau} + \frac{\partial f}{\partial \tau} = 0. \tag{2.2}$$

We will now analyze each of these terms one by one.

- $\dfrac{\partial f}{\partial x^i}\dfrac{\mathrm{d}x^i}{\mathrm{d}\tau}$ The first of these two derivatives can be straightforwardly computed by using eq. (2.1), $\frac{\partial f}{\partial x^i} = f_0 \partial_i \Psi$ where the variables on which f_0, f and Ψ depend, have been omitted in order to avoid unnecessary clutter. The second derivative, $\mathrm{d}x^i/\mathrm{d}\tau$, requires slightly more work. By reintroducing an affine parameter λ through $\frac{\mathrm{d}x^i}{\mathrm{d}\tau} = \frac{\mathrm{d}x^i}{\mathrm{d}\lambda}\frac{\mathrm{d}\lambda}{\mathrm{d}\tau}$ we find that

$$\frac{\mathrm{d}x^i}{\mathrm{d}\tau} = \frac{P^i}{P^0} = \frac{q^i}{\epsilon}(1+\phi+\psi). \tag{2.3}$$

The first term of eq. (2.2) can therefore be rewritten as

$$\boxed{\frac{\partial f}{\partial x^i}\frac{\mathrm{d}x^i}{\mathrm{d}\tau} = f_0 \partial_i \Psi \frac{q^i}{\epsilon}(1+\phi+\psi).} \tag{2.4}$$

- $\dfrac{\partial f}{\partial q}\dfrac{\mathrm{d}q}{\mathrm{d}\tau}$ Again, the derivative of f is the easy part, $\frac{\partial f}{\partial q} = \frac{\partial f_0}{\partial q}[1+\Psi] + f_0 \frac{\partial \Psi}{\partial q}$, but the derivative of q will require the use of the temporal part of the geodesic equation,

$$P^0 \frac{\mathrm{d}P^0}{\mathrm{d}\tau} = -\Gamma^0{}_{\alpha\beta} P^\alpha P^\beta. \tag{2.5}$$

To find P^0 in terms of other variables, we combine the metric (1.1), in order to get g_{00}, with eq. (1.11). The result is $P^0 = \frac{\epsilon}{a^2}(1-\psi)$. By plugging this result into the l.h.s. of eq. (2.5), we find

$$P^0 \frac{\mathrm{d}P^0}{\mathrm{d}\tau} = \frac{\epsilon}{a^4}\left[(1-2\psi)\frac{\mathrm{d}\epsilon}{\mathrm{d}\tau} - \epsilon\frac{\mathrm{d}\psi}{\mathrm{d}\tau} - 2\epsilon(1-2\psi)\mathcal{H}\right] \tag{2.6}$$

where $\mathcal{H} \equiv \dot{a}/a$ is the conformal Hubble parameter. Using the identities given in eq. (1.13), we calculate the (total) derivatives of ϵ and ψ, which are found to be

$$\frac{\mathrm{d}\epsilon}{\mathrm{d}\tau} = \frac{1}{\epsilon}\left(a^2 m^2 \mathcal{H} + q\frac{\mathrm{d}q}{\mathrm{d}\tau}\right) \qquad \text{and} \qquad \frac{\mathrm{d}\psi}{\mathrm{d}\tau} = \frac{q}{\epsilon}\hat{n}^i(\partial_i\psi) + \dot{\psi}. \tag{2.7}$$

For the r.h.s. of the temporal part of the geodesic equation eq. (2.5), we need the following Christoffel symbols

$$\Gamma^0{}_{00} = \dot{\psi} + \mathcal{H}, \qquad \Gamma^0{}_{0i} = \partial_i\psi, \qquad \Gamma^0{}_{ij} = \left[-\dot{\phi} + (1-2\phi-2\psi)\mathcal{H}\right]\delta_{ij}. \tag{2.8}$$

By combining these Christoffel symbols with the relation between P^α, q^i and ϵ found in Sec. 1.4, it is straightforward to expand the r.h.s. of the geodesic equation into these last two variables. Equating the result with the l.h.s. given by eq. (2.6), gives, after some simplifications,

$$\frac{\mathrm{d}q}{\mathrm{d}\tau} = -\epsilon\hat{n}^i(\partial_i\psi) + q\dot{\phi}. \tag{2.9}$$

The second term of the Boltzmann equation is therefore given by

$$\boxed{\frac{\partial f}{\partial q}\frac{\mathrm{d}q}{\mathrm{d}\tau} = \left(\frac{\partial f_0}{\partial q}[1+\Psi] + f_0\frac{\partial\Psi}{\partial q}\right)\left(-\epsilon\hat{n}^i(\partial_i\psi) + q\dot{\phi}\right).} \tag{2.10}$$

- $\dfrac{\partial f}{\partial \hat{n}^i}\dfrac{\mathrm{d}\hat{n}^i}{\mathrm{d}\tau}$ Without surprise, the derivative of f w.r.t. $\hat{n}$ does not pose any problem, $\frac{\partial f}{\partial \hat{n}^i} = f_0 \frac{\partial \Psi}{\partial \hat{n}^i}$, but the derivative of $\hat{n}^i$ w.r.t. τ will again require the use of the geodesic equation. To this end, we first rewrite the derivative of $\hat{n}^i$ as the derivative of q^i/q.

$$\frac{\mathrm{d}\hat{n}^i}{\mathrm{d}\tau} = \frac{1}{q}\frac{\mathrm{d}q^i}{\mathrm{d}\tau} + \hat{n}^i \frac{\epsilon}{q}\hat{n}^j(\partial_j\psi) - \hat{n}^i\dot{\phi}, \tag{2.11}$$

where equation (2.9) has been used. The factor $\dfrac{\mathrm{d}q^i}{\mathrm{d}\tau}$ can be found by using the spatial part of the geodesic equation $P^0\frac{\mathrm{d}P^i}{\mathrm{d}\tau} = -\Gamma^i{}_{\alpha\beta}P^\alpha P^\beta$. Using the same machinery as in the previous case, we find for the l.h.s.

$$P^0\frac{\mathrm{d}P^i}{\mathrm{d}\tau} = \frac{\epsilon}{a^4}\left[\frac{\mathrm{d}q^i}{\mathrm{d}\tau}(1+\phi-\psi) + q^i\frac{\mathrm{d}\phi}{\mathrm{d}\tau} - 2q^i(1+\phi-\psi)\mathcal{H}\right]. \tag{2.12}$$

The Christoffel symbols we now need, are those with a spatial contravariant index,

$$\Gamma^i{}_{00} = \partial_i\psi, \quad \Gamma^i{}_{0j} = \left[-\dot{\phi}+\mathcal{H}\right]\delta_{ij}, \quad \Gamma^i{}_{jk} = -(\partial_k\phi)\delta_{ij} - (\partial_j\phi)\delta_{ik} + (\partial_i\phi)\delta_{jk}. \tag{2.13}$$

Plugging these into the r.h.s. of the geodesic equation and performing some simplifications yield

$$\frac{\mathrm{d}q^i}{\mathrm{d}\tau} = -(\partial_i\psi)\epsilon + q^i\dot{\phi} + (\hat{n}^i\hat{n}^j - \delta^{ij})\frac{q^2}{\epsilon}(\partial_j\phi). \tag{2.14}$$

Plugging this back into equation (2.11) gives the desired equation

$$\frac{\mathrm{d}\hat{n}^i}{\mathrm{d}\tau} = (\hat{n}^j\hat{n}^i - \delta^{ij})\left[\frac{\epsilon}{q}\partial_j\psi + \frac{q}{\epsilon}\partial_j\phi\right], \tag{2.15}$$

from which we conclude that

$$\boxed{\frac{\partial f}{\partial \hat{n}^i}\frac{\mathrm{d}\hat{n}^i}{\mathrm{d}\tau} = f_0\frac{\partial\Psi}{\partial\hat{n}^i}(\hat{n}^i\hat{n}^j - \delta^{ij})\left[\frac{\epsilon}{q}\partial_j\psi + \frac{q}{\epsilon}\partial_j\phi\right].} \tag{2.16}$$

- $\dfrac{\partial f}{\partial \tau}$ This is by far the easiest part: $\frac{\partial f}{\partial\tau} = \frac{\partial f_0}{\partial\tau}[1+\Psi] + f_0\frac{\partial\Psi}{\partial\tau}$. An important remark is in order here. As said in the introduction, we focus our derivation on the case of neutrinos. The (equilibrium) phase space distribution function of neutrinos, being fermions, is given by the Fermi-Dirac statistics,

$$f_0 \propto \frac{1}{\exp[\epsilon(q,\tau)/a(\tau)T(a(\tau))] + 1} \tag{2.17}$$

where $T(a)$ is the temperature. When the neutrinos are still relativistic, this reduces to $f_0 \propto (\exp[q/aT(a)] + 1)^{-1}$. But as decoupling takes place long before they become non-relativistic, the unperturbed distribution function maintains this form. Moreover, the temperature of collisionless particles decreases as $T(a) \propto a^{-1}$, so f_0 is τ-independent, i.e. $\partial f_0/\partial\tau = 0$. Therefore,

$$\boxed{\frac{\partial f}{\partial\tau} = f_0\frac{\partial\Psi}{\partial\tau}.} \tag{2.18}$$

We can now combine all the terms given by eqs. (2.4), (2.10), (2.16) and (2.18) to find the full collisionless Boltzmann equation

$$\begin{aligned}\frac{1}{f_0}\frac{\mathrm{d}f}{\mathrm{d}\tau} = 0 \;=\; & \frac{\partial\Psi}{\partial\tau} + \frac{q}{\epsilon}\hat{n}^i\partial_i\Psi \\ & + \left(\frac{\partial \ln f_0}{\partial \ln q}(1+\Psi) + \frac{\partial\Psi}{\partial \ln q}\right)\left(\dot{\phi} - \frac{\epsilon}{q}\hat{n}^i\partial_i\psi\right) \\ & + \frac{\partial\Psi}{\partial\hat{n}^i}\left(\hat{n}^i\hat{n}^j - \delta^{ij}\right)\left(\frac{\epsilon}{q}\partial_j\psi + \frac{q}{\epsilon}\partial_j\phi\right).\end{aligned} \tag{2.19}$$

A different form of this equation can be obtained by using a different set of independent variables. The one that will be the most useful to us later, is the one where q and $\hat{n}^i$ are recombined into the variables q^i. And whereas it is customary to decompose f into a constant part f_0 and a (small) perturbation Ψ like has been done before, we will eventually not do so, as for neutrinos, Ψ is by no means expected to be small. By using eq. (2.14), we find the following (fully equivalent) form of the collisionless Boltzmann equation

$$\boxed{0 = \frac{\mathrm{d}f}{\mathrm{d}\tau} = \frac{\partial f}{\partial\tau} + \frac{q^i}{\epsilon}\partial_i f + \epsilon\frac{\partial f}{\partial q^i}\left[-\partial_i\psi + \frac{q^i}{\epsilon}\dot{\phi} + \left(\hat{n}^i\hat{n}^j - \delta^{ij}\right)\frac{q^2}{\epsilon^2}\partial_j\phi\right].} \tag{2.20}$$

2.2 Moments of the Boltzmann equation

We need to relate the Boltzmann equation (2.20) to observables like the energy density ρ. The energy density is defined as

$$\rho \equiv \int \mathrm{d}^3\mathbf{p}\; E\; f = \int \mathrm{d}^3\mathbf{p}\sqrt{m^2+p^2}\, f. \tag{2.21}$$

But because the independent variable we are working with is q (and not p), we rewrite this as

$$\rho = \int \mathrm{d}^3\mathbf{q}\frac{\epsilon f}{a^4}, \tag{2.22}$$

from which we see that not f but $\epsilon f/a^4$ is the quantity we are the most interested in.

We will construct the Boltzmann hierarchy by integrating the Boltzmann equation (in the new variable $\epsilon f/a^4$) with respect to $\mathrm{d}^3\mathbf{q}$ weighted by products of q^i/ϵ. To that end, we define the quantities A, A^i, A^{ij}, ... as

$$A^{ij\cdots k} \equiv \int \mathrm{d}^3\mathbf{q}\left[\frac{q^i}{\epsilon}\frac{q^j}{\epsilon}\cdots\frac{q^k}{\epsilon}\right]\frac{\epsilon f}{a^4}, \tag{2.23}$$

Obviously, we have that $A = \rho$. The full relationship between the $A^{ij\cdots k}$ and the physical quantities like ρ and p, will be discussed in detail later on (see Sec. 2.3.3).

2.2.1 Zeroth moment

To find the zeroth moment of the Boltzmann equation (2.20), we rewrite this equation into the following equivalent form,

$$\frac{\partial}{\partial\tau}\left(\frac{\epsilon f}{a^4}\right) + \frac{\epsilon f}{a^4}\left(3 + \frac{q^2}{\epsilon^2}\right)\mathcal{H} + \frac{q^i}{\epsilon}\partial_i\left(\frac{\epsilon f}{a^4}\right) + \frac{1}{a^4}\frac{\partial f}{\partial q^i}\left[-\epsilon^2\partial_i\psi + \epsilon q^i\dot{\phi} + q^iq^j\partial_j\phi - q^2\partial_i\phi\right] = 0. \tag{2.24}$$

By directly integrating this equation with respect to $\mathrm{d}^3\mathbf{q}$, we find – using integration by parts – the result

$$\boxed{\frac{\partial A}{\partial \tau} + \left(\mathcal{H} - \dot{\phi}\right)\left(3A + A^{ii}\right) + \partial_i A^i + 2A^i\partial_i(\psi - \phi) = 0.} \tag{2.25}$$

2.2.2 First moment

To find the first moment, we start by multiplying the Boltzmann equation (2.20) by q^i/ϵ. After some manipulations, this becomes

$$\begin{aligned}\frac{\partial}{\partial \tau}\left(\frac{\epsilon f}{a^4}\frac{q^i}{\epsilon}\right) + 4\mathcal{H}\left(\frac{\epsilon f}{a^4}\frac{q^i}{\epsilon}\right) + \partial_j \frac{q^i q^j}{\epsilon^2}\frac{\epsilon f}{a^4} \\ + \frac{1}{a^4}\frac{q^i}{\epsilon}\frac{\partial f}{\partial q^j}\left[-\epsilon^2\partial_j\psi + \epsilon q^j\dot{\phi} + q^j q^k\partial_k\phi - q^2\partial_j\phi\right] = 0.\end{aligned} \tag{2.26}$$

By integrating this expression w.r.t. $\mathrm{d}^3\mathbf{q}$, we find the first moment

$$\boxed{\frac{\partial}{\partial \tau}A^i + 4\left(\mathcal{H} - \dot{\phi}\right)A^i + \partial_j A^{ij} + A\partial_i\psi + A^{ij}\partial_j\psi - 3A^{ij}\partial_j\phi + A^{jj}\partial_i\phi = 0.} \tag{2.27}$$

2.2.3 Second moment

By multiplying the Boltzmann equation by $q^i q^j/\epsilon^2$, we find

$$\begin{aligned}\frac{\partial}{\partial \tau}\left(\frac{\epsilon f}{a^4}\frac{q^i q^j}{\epsilon^2}\right) + 5\mathcal{H}\frac{\epsilon f}{a^4}\frac{q^i q^j}{\epsilon^2} - \mathcal{H}\frac{\epsilon f}{a^4}\frac{q^i q^j q^2}{\epsilon^4} + \partial_k\left(\frac{\epsilon f}{a^4}\frac{q^i q^j q^k}{\epsilon^3}\right) \\ + \frac{1}{a^4}\frac{\partial f}{\partial q^k}\left[-q^i q^j\partial_k\psi + \dot{\phi}\frac{q^i q^j q^k}{\epsilon} + \partial_l\phi\frac{q^i q^j q^k q^l}{\epsilon^2} - \partial_k\phi\frac{q^i q^j q^2}{\epsilon^2}\right] = 0.\end{aligned} \tag{2.28}$$

As before, we integrate this equation with respect to $\mathrm{d}^3\mathbf{q}$ to compute the second moment in the Boltzmann hierarchy,

$$\boxed{\begin{aligned}\frac{\partial}{\partial \tau}A^{ij} + \left(\mathcal{H} - \dot{\phi}\right)\left(5A^{ij} - A^{ijkk}\right) + \partial_k A^{ijk} \\ + A^j\partial_i\psi + A^i\partial_j\psi - 4A^{ijk}\partial_k\phi + A^{jll}\partial_i\phi + A^{ill}\partial_j\phi = 0.\end{aligned}} \tag{2.29}$$

2.2.4 n^{th} moment

It's a straightforward calculation to generalise this result to all moments. By multiplying the Boltzmann equation with $\frac{q^{l_1}}{\epsilon}\cdots\frac{q^{l_n}}{\epsilon}$, and integrating the result, one finds

$$\boxed{\begin{aligned}\frac{\partial}{\partial \tau}A^{l_1\cdots l_n} + \left(\mathcal{H} - \dot{\phi}\right)\left[(n+3)A^{l_1\cdots l_n} - (n-1)A^{l_1\cdots l_n ii}\right] + \sum_{m=1}^{n}\left(\partial_{l_m}\psi\right)A^{l_1\cdots \cancel{l_m}\cdots l_n} \\ + \sum_{m=1}^{n}\left(\partial_{l_m}\phi\right)A^{l_1\cdots \cancel{l_m}\cdots l_n ii} + \partial_i A^{l_1\cdots l_n i} + \left[(2-n)\partial_i\psi - (2+n)\partial_i\phi\right]A^{l_1\cdots l_n i} = 0,\end{aligned}} \tag{2.30}$$

where $l_1\cdots\cancel{l_m}\cdots l_n$ is shorthand notation for $l_1\cdots l_{m-1}l_{m+1}\cdots l_n$, and summation over i is implied.

2.2.5 Hierarchy in Θ_n

Before linearising the Boltzmann equation, we briefly introduce a new notation. To that end we first move from real space to momentum (Fourier) space. Our convention for the Fourier transform of some $\mathbf{x}$-dependent quantity $f(\mathbf{x})$ is

$$\tilde{f}(\mathbf{k}) \equiv \int \frac{\mathrm{d}^3\mathbf{k}}{(2\pi)^3} f(\mathbf{x}) e^{-i\mathbf{k}\cdot\mathbf{x}}, \tag{2.31}$$

and we will always drop the tilde as there is no real risk of ambiguity. The enormous advantage of working in momentum space instead of in real space is that in the linearised equations all the wavemodes $\mathbf{k}$ decouple, i.e. each wavemode $\mathbf{k}$ has its own equation. On the other hand, the product of two $\mathbf{x}$-dependent quantities (like ϕ and A) gets Fourier transformed into the convolution

$$\phi(\mathbf{x})A(\mathbf{x}) \to \int \mathrm{d}^3\mathbf{k}_1\, \mathrm{d}^3\mathbf{k}_2\, \delta_{\mathrm{D}}(\mathbf{k}-\mathbf{k}_1-\mathbf{k}_2)\phi(\mathbf{k}_1)A(\mathbf{k}_2), \tag{2.32}$$

and we will often omit $\int \mathrm{d}^3\mathbf{k}_1 \mathrm{d}^3\mathbf{k}_2 \delta_{\mathrm{D}}(\mathbf{k}-\mathbf{k}_1-\mathbf{k}_2)$ to avoid clutter. For example, in the r.h.s. of eq. (2.36) below, a convolution is implicit. The Fourier transform of a divergence $\partial_{\mathbf{x}}$ is as usual $i\mathbf{k}$.

In this section, we will also restrict ourselves to one pressureless fluid in matter dominance. This implies that[1]

$$\frac{\partial}{\partial\tau}\bar{\rho} = -3\mathcal{H}\bar{\rho} \qquad \text{and} \qquad \frac{\partial}{\partial\tau}\mathcal{H} = -\frac{\mathcal{H}^2}{2}, \tag{2.33}$$

as can be checked using eqs. (1.4) and (1.7).

We now define the new variables Θ_n as

$$\Theta_n(\mathbf{k}) \equiv \frac{ik_{l_1}\cdots ik_{l_n}}{(ik)^n}\frac{(ik)^n}{\bar{\rho}\mathcal{H}^n} A^{l_1\cdots l_n}(\mathbf{k}) \tag{2.34}$$

where summation over the l_i's is implied. These new variables are generalised divergences of $A^{ij\cdots k}$. Rewriting the linear part of the n^{th} moment of the Boltzmann equation (2.30), i.e. keeping the terms with only one $\mathbf{k}$-dependent factor, using these new variables and removing $\dot{\phi}$ together with superhorizon terms, i.e. dropping terms subleading in $k^2/\mathcal{H}^2$, results in the new hierarchy

$$\frac{\partial}{\partial\eta}\Theta_n(\mathbf{k}) + \frac{n}{2}\Theta_n(\mathbf{k}) + \Theta_{n+1}(\mathbf{k}) - \delta_{n,1}\frac{k^2}{\mathcal{H}^2}\psi(\mathbf{k}) = 0, \tag{2.35}$$

where $\eta \equiv \log a$. The last term comes from the fact that $A(\mathbf{k}) = \bar{\rho}(1+\delta(\mathbf{k}))$ (and hence $\Theta_0(\mathbf{k}) = 1+\delta(\mathbf{k})$) contains both a $\mathbf{k}$-independent background term and a $\mathbf{k}$-dependent perturbation term.

It is difficult to find a similar expression for the non-linear interaction. The reason is that the product of k's present in eq. (2.34) necessary to go from $A^{l_1\cdots l_n}(\mathbf{k})$ to $\Theta_n(\mathbf{k})$ does not allow us to go from $A^{l_1\cdots l_n}(\mathbf{k}_1)$ to $\Theta_n(\mathbf{k}_1)$. But if we assume[2] $\mathbf{k}_1 /\!/ \mathbf{k}$, we have that

[1] The first equation can be compared to eq. (2.65) where pressure is not neglected.

[2] It should be emphasised that this assumption is purely technical and not physical as $\mathbf{k}_1$ is an integration variable which should be integrated over the full space.

$k_i/k = (k_1)_i/k_1$ such that the summation in eq. (2.34) can be done with both k and k_1. With this assumption we can write the Boltzmann equation with non-linear interaction as

$$\frac{\partial}{\partial\eta}\Theta_n(\mathbf{k}) + \frac{n}{2}\Theta_n(\mathbf{k}) + \Theta_{n+1}(\mathbf{k}) = n\frac{\mathbf{k}\cdot\mathbf{k}_2}{\mathcal{H}^2}\left(\frac{k}{k_1}\right)^{n-1}\Theta_{n-1}(\mathbf{k}_1)\psi(\mathbf{k}_2). \tag{2.36}$$

We will recover this equation using a totally different approach in Sec. 2.5.

2.3 Linearised equations

2.3.1 Standard formalism

The standard description of the linearised equations builds on the linearised form of the Boltzmann equation given by eq. (2.19), see e.g. [8]. As Ψ, ϕ and ψ are considered small, the equation reduces to

$$\frac{\partial\Psi}{\partial\tau} + \frac{q}{\epsilon}\hat{n}^i\partial_i\Psi + \frac{\partial\ln f_0}{\partial\ln q}\left(\dot{\phi} - \frac{\epsilon}{q}\hat{n}^i\partial_i\psi\right) = 0. \tag{2.37}$$

In momentum space, the only dependence on $\mathbf{k}$ is through its angle with $\hat{n}$, so we define $\mu \equiv \hat{k}\cdot\hat{n}$ and rewrite the linearised Boltzmann equation as

$$\frac{\partial\tilde{\Psi}}{\partial\tilde{\tau}} + \frac{q}{\epsilon}i\mu\tilde{\Psi} + \left(\frac{\partial\phi}{\partial\tilde{\tau}} - \frac{\epsilon}{q}i\mu\psi\right) = 0, \tag{2.38}$$

where $\tilde{\tau} \equiv k\tau$ and $\tilde{\Psi} \equiv \left(\frac{\partial\ln f_0}{\partial\ln q}\right)^{-1}\Psi$. Notice that the fact that the above equation only depends on $\mathbf{k}$ through μ is only true in the linearised equation. The next step is to expand $\tilde{\Psi}$ using Legendre polynomials, introducing the moments $\tilde{\Psi}_l$

$$\tilde{\Psi} = \sum_l (-i)^l(2l+1)\tilde{\Psi}_l P_l(\mu). \tag{2.39}$$

By plugging this expansion into the Boltzmann equation (2.38), one obtains the well-known hierarchy

$$\tilde{\Psi}_0' = -\frac{q}{\epsilon}\,\tilde{\Psi}_1 - \phi', \tag{2.40}$$

$$\tilde{\Psi}_1' = \frac{1}{3}\frac{q}{\epsilon}\,(\tilde{\Psi}_0 - 2\tilde{\Psi}_2) - \frac{1}{3}\frac{\epsilon}{q}\,\psi, \tag{2.41}$$

$$\tilde{\Psi}_l' = \frac{1}{2l+1}\left[l\,\frac{q}{\epsilon}\,\tilde{\Psi}_{l-1} - (l+1)\,\frac{q}{\epsilon}\,\tilde{\Psi}_{l+1}\right] \qquad (l \geq 2), \tag{2.42}$$

where a prime denotes a derivative with respect to $\tilde{\tau}$. To compare this hierarchy with the one given by eqs. (2.25), (2.27) and (2.30), we still need to integrate with respect to dq.

To that end, we define the following physical quantities in the standard way [8]:

$$\bar{\rho}(\tau) = 4\pi \int q^2 \mathrm{d}q \, \frac{\epsilon f_0}{a^4}, \tag{2.43}$$

$$\bar{\mathrm{p}}(\tau) = 4\pi \frac{1}{3} \int q^2 \mathrm{d}q \, \left(\frac{q}{\epsilon}\right)^2 \frac{\epsilon f_0}{a^4}, \tag{2.44}$$

$$\delta\rho(k,\tau) = 4\pi \int q^2 \mathrm{d}q \, \frac{\epsilon f_0}{a^4} \Psi_0, \tag{2.45}$$

$$\delta\mathrm{p}(k,\tau) = 4\pi \frac{1}{3} \int q^2 \mathrm{d}q \, \left(\frac{q}{\epsilon}\right)^2 \frac{\epsilon f_0}{a^4} \Psi_0, \tag{2.46}$$

$$(\bar{\rho} + \bar{\mathrm{p}})\theta(k,\tau) = 4\pi \, k \int q^2 \mathrm{d}q \, \frac{q}{\epsilon} \frac{\epsilon f_0}{a^4} \Psi_1, \tag{2.47}$$

$$(\bar{\rho} + \bar{\mathrm{p}})\sigma(k,\tau) = 4\pi \frac{2}{3} \int q^2 \mathrm{d}q \, \left(\frac{q}{\epsilon}\right)^2 \frac{\epsilon f_0}{a^4} \Psi_2, \tag{2.48}$$

$$(\bar{\rho} + \bar{\mathrm{p}})\Theta(k,\tau) = 4\pi \, k \int q^2 \mathrm{d}q \, \left(\frac{q}{\epsilon}\right)^3 \frac{\epsilon f_0}{a^4} \Psi_1, \tag{2.49}$$

$$(\bar{\rho} + \bar{\mathrm{p}})\Sigma(k,\tau) = 4\pi \frac{2}{3} \int q^2 \mathrm{d}q \, \left(\frac{q}{\epsilon}\right)^4 \frac{\epsilon f_0}{a^4} \Psi_2. \tag{2.50}$$

$\bar{\rho}$ and $\bar{\mathrm{p}}$ are the mean density and pressure respectively, $\delta\rho$ and $\delta\mathrm{p}$ are their first order perturbations; θ is the velocity dispersion, σ the anisotropic stress; Θ and Σ are relativistic corrections to θ and σ respectively. These definitions are only valid in the linear theory as the multipole moments Ψ_l are only well-defined in the linear theory.

The connection between these physical quantities and the $A^{ij\cdots k}$ defined in eq. (2.23) is far from obvious. Whereas its dictionary is relatively transparent for low-order quantities, it gets very involved as soon as one considers high-l Ψ_l's. The bridge is built by introducing yet another Boltzmann hierarchy, using spherical harmonics. We will give here the few essential equations and leave the full treatment of this framework to a later section (see Sec. 2.5, page 22).

2.3.2 Spherical harmonics

In this framework, the phase space distribution function $f(\mathbf{x}, \mathbf{q}, \tau)$ is expanded into spherical harmonics

$$f(\mathbf{x}, \mathbf{q}, \tau) = \sum_{lm} \Psi_{lm}(\mathbf{x}, q, \tau) Y_{lm}(\hat{n}), \tag{2.51}$$

where $\hat{n}$ stands for the direction of $\mathbf{q}$, i.e. $\hat{n} = \hat{q}$. At this point, the direction of $\hat{z}$, which is necessary to define the spherical harmonics, is arbitrary. By combining eqs. (2.1) and (2.39) and equating the result with eq. (2.51), we find, after using the addition theorem for Y_{lm}'s to replace the Legendre polynomial and integrating with respect to $d^2\hat{n}\, Y^*_{l'm'}$,

$$\Psi_{lm} = \sqrt{4\pi}\, f_0\, \delta_{l0}\delta_{m0} + f_0 \frac{\partial \ln f_0}{\partial \ln q} (-i)^l 4\pi Y^*_{lm}(\hat{k}) \tilde{\Psi}. \tag{2.52}$$

As we are free to do so, we will now choose a specific direction for $\hat{z}$. In the linearised case, there is only one $\mathbf{k}$, so we choose $\hat{z} // \mathbf{k}$. With this choice, $Y^*_{lm}(\hat{k})$ reduces

to $\sqrt{(2l+1)/4\pi}\,\delta_{m0}$. Therefore, we find the following relation between the expansion coefficients using spherical harmonics (Ψ_{lm}) and those using Legendre polynomials (Ψ_l),

$$\Psi_{lm} = \sqrt{4\pi}\, f_0\, \delta_{m0} \left[\delta_{l0} + \frac{\partial \ln f_0}{\partial \ln q} (-i)^l \sqrt{2l+1}\, \tilde{\Psi}_l \right]. \tag{2.53}$$

2.3.3 Dictionary

To recover the dictionary relating the physical quantities to the $A^{ij\cdots k}$, we start with the $l=0$, $m=0$ term of eq. (2.53). We find that $\Psi_{00} = \sqrt{4\pi}\, f_0 \left[1 + \Psi_0\right]$, which gives, after inverting eq. (2.51), $\int \mathrm{d}^2\hat{q}\ f\ Y_{00}(\hat{q}) = \sqrt{4\pi}\, f_0 \left[1 + \Psi_0\right]$, which straightforwardly simplifies to $\int \mathrm{d}^2\hat{q}\ f\ = 4\pi\, f_0 \left[1 + \Psi_0\right]$. By adding up eqs. (2.43) and (2.45), it is now easy to see that

$$\boxed{A = \bar{\rho} + \delta\rho,} \tag{2.54}$$

an expected and anticipated result. Doing the very same with eqs. (2.44) and (2.46), one finds

$$\boxed{A^{ii} = 3(\bar{\mathrm{p}} + \delta\mathrm{p}).} \tag{2.55}$$

Specifying the dictionary for the velocity divergence and the dispersion requires more work. We have, using eq. (2.53), that

$$\Psi_1 = \frac{1}{\sqrt{4\pi}} \frac{1}{f_0} \frac{i}{\sqrt{3}} \Psi_{10}. \tag{2.56}$$

We rewrite Ψ_{10} by inverting eq. (2.51) as the angular integral of f times the spherical harmonic Y_{10}^*, resulting in $\Psi_{10} = \int \mathrm{d}^2\hat{q}\, \frac{1}{2}\sqrt{\frac{3}{\pi}} \cos(\theta) f$, but θ is nothing else than $\mu = \hat{q}\cdot\hat{k} = (q^i/q)(k^i/k)$ such that $\Psi_1 = \frac{1}{4\pi}\frac{1}{f_0}\int \mathrm{d}^2\hat{q}\, \frac{ik_i}{k}\frac{q^i}{q} f$. Plugging this into eq. (2.47), we finally find that

$$\boxed{ik_i A^i = (\bar{\rho} + \bar{\mathrm{p}})\theta.} \tag{2.57}$$

Equivalently, we have that

$$\boxed{ik_i A^{ijj} = (\bar{\rho} + \bar{\mathrm{p}})\Theta.} \tag{2.58}$$

Applying the same machinery to $l=2$, $m=0$ gives $(ik_i)(ik_j)A^{ij} = k^2(\bar{\rho}+\bar{\mathrm{p}})\sigma - k^2(\bar{\mathrm{p}} + \delta\mathrm{p})$ and $(ik_i)(ik_j)A^{ijkk} = k^2(\bar{\rho}+\bar{\mathrm{p}})\Sigma - \frac{1}{3}k^2 A^{iijj}$, or equivalently

$$\boxed{\left[\frac{1}{3}k^2\delta_{ij} + (ik_i)(ik_j)\right] A^{ij} = k^2(\bar{\rho} + \bar{\mathrm{p}})\sigma} \tag{2.59}$$

and

$$\boxed{\left[\frac{1}{3}k^2\delta_{ij} + (ik_i)(ik_j)\right] A^{ijkk} = k^2(\bar{\rho} + \bar{\mathrm{p}})\Sigma.} \tag{2.60}$$

The last term we will need to recover the standard linearised hierarchy is A^{ijk}, and we only need it in the form $(ik_i)(ik_j)(ik_k)A^{ijk}$. The contraction of the k's with the q's inside A^{ijk} will obviously give a $\cos^3(\mu)$. As

$$\cos^3(\mu) = \frac{1}{5}\sqrt{\frac{16\pi}{7}}\, Y_{30} + \frac{3}{5}\sqrt{\frac{4\pi}{3}}\, Y_{10}, \tag{2.61}$$

we find that

$$\begin{aligned}(ik_i)(ik_j)(ik_k)A^{ijk} &= (ik)^3\int q^2\mathrm{d}q\frac{\epsilon}{a^4}\left(\frac{q}{\epsilon}\right)^3\int \mathrm{d}^2\hat{q}\left(\frac{1}{5}\sqrt{\frac{16\pi}{7}}Y_{30}+\frac{3}{5}\sqrt{\frac{4\pi}{3}}\Psi_{10}\right)f\\ &= (ik)^3\int q^2\mathrm{d}q\frac{\epsilon}{a^4}\left(\frac{q}{\epsilon}\right)^3\left(\frac{1}{5}\sqrt{\frac{16\pi}{7}}\Psi_{30}+\frac{3}{5}\sqrt{\frac{4\pi}{3}}\Psi_{10}\right).\end{aligned}$$

Assuming Ψ_{30} is of subleading order and recycling eq. (2.56), we finally find that

$$(ik_i)(ik_j)(ik_k)A^{ijk} = -\frac{3}{5}k^2 4\pi\, k\int q^2\mathrm{d}q\,\left(\frac{q}{\epsilon}\right)^3\frac{\epsilon f_0}{a^4}\Psi_1, \tag{2.62}$$

such that $(ik_i)(ik_j)(ik_k)A^{ijk} = -\frac{3}{5}k^2(\bar{\rho}+\bar{\mathrm{p}})\Theta$. Combining this equation with eq. (2.58) leads to

$$\boxed{\left[\frac{1}{3}k^2\delta_{ij}+(ik_i)(ik_j)\right](ik_k)A^{ijk} = -\frac{4}{15}k^2(\bar{\rho}+\bar{\mathrm{p}})\Theta.} \tag{2.63}$$

This completes the dictionary between the $A^{ij\cdots k}$'s and the physical quantities.

2.3.4 Lowest moments

To recover the equations describing the time evolution of ρ, θ and σ, we will perform the substitutions described in the previous section in the linearised version of eqs. (2.25), (2.27) and (2.29). We will further assume our fluid satisfies the equation of state $\bar{\mathrm{p}} = w\bar{\rho}$. Notice that we do not need any Legendre-like expansion of our phase space distribution to recover the equations.

Zeroth moment Performing the substitutions described in Sec. 2.3.3 in the zeroth order moment given by eq. (2.25) gives, after some simplifications,

$$\begin{aligned}\dot{\bar{\rho}}(1+\delta)+\bar{\rho}\dot{\delta}+3\left(\mathcal{H}-\dot{\phi}\right)\left[(1+w)\bar{\rho}+(\delta\rho+\delta\mathrm{p})\right]\\ +\bar{\rho}(1+w)\theta+2\bar{\rho}(1+w)v^i\partial_i(\psi-\phi)=0\end{aligned} \tag{2.64}$$

where we introduced the density contrast $\delta\equiv\delta\rho/\bar{\rho}$. Assuming δ, $\delta\mathrm{p}$, v^i, θ, $\dot{\phi}$ and $\partial_i(\psi-\phi)$ are first-order quantities, the zeroth-order equation is

$$\dot{\bar{\rho}}+3\mathcal{H}\bar{\rho}(1+w)=0. \tag{2.65}$$

Substituting this equation into the first-order equation gives

$$\dot{\delta} = -(1+w)(\theta-3\dot{\phi})-3\mathcal{H}\left(\frac{\delta\mathrm{p}}{\delta\rho}-w\right)\delta. \tag{2.66}$$

First moment Taking the divergence of equation (2.27) yields

$$\begin{aligned}\frac{\partial}{\partial\tau}(\partial_i A^i)+4\partial_i\left[\left(\mathcal{H}-\dot{\phi}\right)A^i\right]+\partial_i\partial_j A^{ij}\\ +\partial_i\left(A\partial_i\psi\right)+\partial_i\left(A^{ij}\partial_j\psi\right)-3\partial_i\left(A^{ij}\partial_j\phi\right)+\partial_i\left(A^{jj}\partial_i\phi\right)=0.\end{aligned} \tag{2.67}$$

Identifying the subleading terms requires some work. By comparing eqs. (2.55) and (2.59) we notice that the leading part of A^{ij} is diagonal and proportional to $\bar{\mathrm{p}}$, i.e. $A^{ij} \sim \bar{\mathrm{p}}\delta^{ij}$ to leading order. Therefore, $\partial_i(A^{ij}\partial_j\psi) \sim \bar{\mathrm{p}}\delta^{ij}\partial_i\partial_j\psi = -\bar{\mathrm{p}}\,k^2\psi$. After removing the subleading terms and performing the necessary substitutions, we find, after some reshuffling,

$$\dot{\theta} = -\mathcal{H}(1-3w)\theta - \frac{\dot{w}}{1+w}\theta + \frac{k^2\delta\mathrm{p}}{\delta\rho}\frac{\delta}{1+w} - k^2\sigma + k^2\psi. \tag{2.68}$$

Second moment To find the equation of motion we are looking for, we first apply the operator

$$\left(\partial_i\partial_j - \frac{1}{3}\nabla^2\delta_{ij}\right), \qquad \text{or equivalently} \qquad \left((ik_i)(ik_j) + \frac{1}{3}k^2\delta_{ij}\right) \tag{2.69}$$

to equation (2.29), which removes the diagonal part of all terms. But as all the non-diagonal parts of all $A^{ij\cdots k}$ are considered as perturbations, we can remove all the terms containing ϕ or ψ. We are therefore left with

$$\left((ik_i)(ik_j) + \frac{1}{3}k^2\delta_{ij}\right)\left[\frac{\partial}{\partial\tau}A^{ij} + \mathcal{H}\left(5A^{ij} - A^{ijkk}\right) + (ik_k)A^{ijk}\right] = 0. \tag{2.70}$$

Using eqs. (2.59), (2.60) and (2.63), we finally get

$$\dot{\sigma} = -\mathcal{H}(2-3w)\sigma - \frac{\dot{w}}{1+w}\sigma + \mathcal{H}\Sigma + \frac{4}{15}\Theta. \tag{2.71}$$

2.4 Non-linear description

2.4.1 Energy-momentum tensor

Introducing the energy-momentum tensor enables us to find a fully non-linear description of the fluid equations of which eqs. (2.66) and (2.68) are the linearised forms [9, 10]. It also allows us to derive the relationship between the $A^{ij\cdots k}$'s and the physical quantities, without having to resort to the *ad hoc* definitions given in eqs. (2.43) to (2.50). Or equivalently, this method actually proves those definitions.

The energy-momentum tensor is defined as

$$T^{\mu\nu} \equiv \int \mathrm{d}P_1\,\mathrm{d}P_2\,\mathrm{d}P_3\;\frac{1}{\sqrt{-g}}\frac{P^\mu P^\nu}{P^0}f. \tag{2.72}$$

By changing the integration variable to q, this becomes

$$T^\mu{}_\nu = \int \mathrm{d}^3\mathbf{q}\;\frac{P^\mu P_\nu}{a^2\epsilon}f. \tag{2.73}$$

A straightforward computation, relying only on the metric (1.1) and eqs. (1.9) and (1.11), relates these quantities to the $A^{ij\cdots k}$'s:

$$T^0{}_0 = -A, \qquad T^0{}_i = (1-\phi-\psi)A_i, \qquad T^i{}_0 = -(1+\phi+\psi)A^i, \qquad T^i{}_j = A^i{}_j. \tag{2.74}$$

We further decompose the energy-momentum tensor in the following way:

$$T^{\mu\nu} = (\mathrm{p}+\rho)U^\mu U^\nu + \mathrm{p}g^{\mu\nu} + \pi^{\mu\nu}, \tag{2.75}$$

where U^μ is the bulk 4-velocity satisfying $U_\mu U^\mu = -1$, and $\pi^{\mu\nu}$ is related to the anisotropic stress. If we assume that the bulk 3-velocity is small, we have that $U^0 = \gamma(1-\psi)/a$. We define the quantity v^i, satisfying $\gamma^2\delta_{ij}v^iv^j = g_{ij}U^iU^j$, as $U^i = \gamma v^i(1+\phi)/a$. Using this decomposition in eq. (2.75) results in

$$\begin{aligned}
T^0{}_0 &= -\gamma^2(\rho + v^2\mathrm{p}) + \pi^0{}_0, &(2.76)\\
T^0{}_i &= \gamma^2(\mathrm{p}+\rho)(1-\psi-\phi)v^i + \pi^0{}_i, &(2.77)\\
T^i{}_0 &= -\gamma^2(\mathrm{p}+\rho)(1+\psi+\phi)v^i + \pi^i{}_0, &(2.78)\\
T^i{}_j &= \gamma^2(\mathrm{p}+\rho)v^iv^j + \mathrm{p}g^i{}_j + \pi^i{}_j. &(2.79)
\end{aligned}$$

A more sensible way to obtain these four expressions (and hence to confirm the decomposition (2.75)) is the following. We define ρ, p and σ^{ij} in the fluid's rest frame as

$$\rho \equiv \int \mathrm{d}^3\mathbf{p}\; Ef, \qquad \mathrm{p} \equiv \frac{1}{3}\int \mathrm{d}^3\mathbf{p}\; \frac{p^2}{E}f, \qquad \sigma^{ij} \equiv \int \mathrm{d}^3\mathbf{p}\; \left(\hat{n}^i\hat{n}^j - \frac{1}{3}\delta^{ij}\right)\frac{p^2}{E}f. \tag{2.80}$$

By boosting $T^\mu{}_\nu$ defined in eq. (2.73) to the rest frame and using that $\mathrm{d}^3\mathbf{p}'/E' = \mathrm{d}^3\mathbf{p}/E$ because it is a Lorentz invariant measure, we find

$$\begin{aligned}
T^0{}_0 &= -\gamma^2(\rho+v^2\mathrm{p}) \underbrace{-\gamma^2 v^iv^j\sigma^{ij}}_{\pi^0{}_0}, &(2.81)\\
T^0{}_i &= (1-\psi-\phi)\big[\gamma^2(\mathrm{p}+\rho)v^i + \underbrace{\gamma v_j\sigma^{ij} + \frac{\gamma(\gamma-1)}{v^2}v_iv_jv_k\sigma^{jk}}_{\pi^0{}_i}\big], &(2.82)\\
T^i{}_j &= \gamma^2(\mathrm{p}+\rho)v^iv^j + \mathrm{p}g^i{}_j + \underbrace{\sigma^{ij} + 2\frac{\gamma-1}{v^2}v^kv^{(i}\sigma^{j)k} + (\gamma-1)^2\frac{v^iv^jv^kv^l}{v^4}\sigma^{kl}}_{\pi^i{}_j}. &(2.83)
\end{aligned}$$

This completes the fully-relativistic correspondence between the energy-momentum tensor and the physical quantities.

2.4.2 Fluid equations

We are now in the position to relate the $A^{ij\cdots k}$'s found previously to the physical quantities ρ, p,... We hereby use the fact that $\pi^0{}_0 = \pi^i{}_0 = \pi^0{}_i = 0$ and $\pi^{ij} = \sigma^{ij}$ to leading order. We also neglect the relativistic corrections given by the γ-factors because we assume the bulk velocities to be small. Based upon these approximations, combining eq. (2.74) with eqs. (2.76–2.79) leads to

$$\begin{aligned}
A &= \rho, &(2.84)\\
A_i &= (\mathrm{p}+\rho)v_i, &(2.85)\\
A^i &= (\mathrm{p}+\rho)v^i, &(2.86)\\
A^i{}_j &= (\mathrm{p}+\rho)v^iv_j + \mathrm{p}g^i{}_j + \pi^i{}_j. &(2.87)
\end{aligned}$$

With this dictionary in mind, we can fully determine the non-linear fluid equations as follows. Making these substitutions in the zeroth and first moments, eqs. (2.25) and (2.27) and removing subleading terms (assuming $\phi, \psi \ll 1$, $\dot{\phi} \ll \mathcal{H}$) results in the following continuity and Euler equations:

$$\begin{cases} \dfrac{\partial \rho}{\partial \tau} + 3\mathcal{H}(\mathrm{p}+\rho) + \partial_i\left[(\mathrm{p}+\rho)v^i\right] &= 0 \\ \dfrac{\partial v^i}{\partial \tau} + \mathcal{H}v^i + v^j\partial_j v^i + \dfrac{1}{\mathrm{p}+\rho}\left(v^i\dfrac{\partial \mathrm{p}}{\partial \tau} + \partial_i \mathrm{p} + \partial_j \pi^{ij}\right) + \partial_i\psi + \dfrac{\pi^{ij}}{\mathrm{p}+\rho}\partial_j(\psi - 3\phi) &= 0. \end{cases} \tag{2.88}$$

To find the scalar equations we are interested in, we first perturb the continuity equation. We define the (homogeneous) background pressure and density, $\bar{\rho}$ and $\bar{\mathrm{p}}$ as

$$\rho = \bar{\rho} + \delta\rho \qquad \text{and} \qquad \mathrm{p} = \bar{\mathrm{p}} + \delta\mathrm{p}. \tag{2.89}$$

We also define the density perturbation δ through $\rho = \bar{\rho}(1+\delta)$. By only keeping the background terms in the first equation, we find the background evolution

$$\dot{\bar{\rho}} + 3\mathcal{H}(\bar{\mathrm{p}} + \bar{\rho}) = 0. \tag{2.90}$$

This result is obviously consistent with the linear result given by eq. (2.65). For a fluid with equation of state $\bar{\mathrm{p}} = w\bar{\rho}$ and sound speed[3] $c_s^2 = \delta\mathrm{p}/\delta\rho$, the continuity equation becomes

$$\dot{\delta} = -(1+w)\theta - 3\mathcal{H}\left(c_s^2 - w\right)\delta - v^i\partial_i\left[\left(c_s^2+1\right)\delta\right] - \left(c_s^2+1\right)\delta\,\theta. \tag{2.91}$$

The same reasoning, applied to the divergence of the Euler equation, yields

$$\begin{aligned} \dot{\theta} = -\frac{\bar{\mathrm{p}}+\bar{\rho}}{\mathrm{p}+\rho}\left[-3\mathcal{H}w\theta + \frac{\dot{w}}{1+w}\theta + \frac{\nabla^2\delta\mathrm{p}}{\delta\rho}\frac{\delta}{1+w} + \frac{\partial_i\partial_j\pi^{ij}}{\bar{\mathrm{p}}+\bar{\rho}}\right] - \mathcal{H}\theta - \nabla^2\psi \\ -\partial_i v^j\,\partial_j v^i - v^i\partial_i\theta - \frac{1}{\mathrm{p}+\rho}\left[\partial_i\pi^{ij}\partial_j(\psi-3\phi) + \pi^{ij}\partial_i\partial_j(\psi-3\phi)\right] \\ -\frac{\bar{\rho}\partial_i w + \partial_i\delta\mathrm{p}\,(1+c_s^2) + \delta\mathrm{p}\partial_i c_s^2}{(\mathrm{p}+\rho)^2}\times \\ \left[\dot{\bar{\rho}}wv^i + \bar{\rho}\dot{w}v^i + \dot{\delta\mathrm{p}}v^i + \partial_i\delta\mathrm{p} + \partial_j\pi^{ij} + \pi^{ij}\partial_j(\psi-3\phi)\right]. \end{aligned} \tag{2.92}$$

When adding to the already made approximations the following two,

$$c_s^2\delta \ll 1 \qquad \text{and} \qquad \frac{\mathcal{H}^2}{k^2} \ll 1, \tag{2.93}$$

these equations simplify to

$$\dot{\delta} = -(1+w)\theta - 3\mathcal{H}\left(c_s^2 - w\right)\delta - v^i\partial_i\delta - \delta\,\theta \tag{2.94}$$

$$\dot{\theta} = (3w-1)\mathcal{H}\theta - \frac{\dot{w}}{1+w}\theta - \frac{\nabla^2\delta\mathrm{p}}{\delta\rho}\frac{\delta}{1+w} - \frac{\partial_i\partial_j\pi^{ij}}{\bar{\mathrm{p}}-\bar{\rho}} - \nabla^2\psi - \partial_i\left(v^j\,\partial_j v^i\right). \tag{2.95}$$

Notice how these equations generalise eqs. (2.66) and (2.68), as the continuity equation now contains the interaction terms $v^i\partial_i\delta$ and $\delta\,\theta$, and the Euler equation $\partial_i(v^j\partial_j v^i)$. These terms were by definition not present in the linearised description.

[3]This definition is only valid in the comoving gauge; the general expression being $v^i\frac{\partial p}{\partial \tau} + \partial_i p = c_s^2\left(v^i\frac{\partial \rho}{\partial \tau} + \partial_i\rho\right)$. However, the difference will not be relevant in our case.

2.4.3 Fully non-linear fluid equations

Yet another hierarchy can be found by limiting the number of approximations. In the following, we will only drop the time derivatives of ϕ, and the subleading terms in ψ, ϕ and v^i. We will not split the density ρ into a homogeneous background part and a perturbation [11]. The equations are found by taking the zeroth and first moment, eqs. (2.25) and (2.27), making the following substitutions:

$$A \to \rho, \qquad A^i \to (\mathrm{p}+\rho)v^i, \qquad A^{ij} \to \mathrm{p}\delta^{ij} + (\mathrm{p}+\rho)v^i v^j. \tag{2.96}$$

This corresponds to what has been found in eqs. (2.84–(2.87)), assuming a vanishing anisotropic stress, i.e. $\pi^{ij} = 0$. We find

$$\begin{cases} \dfrac{\partial \rho}{\partial \tau} + 3\mathcal{H}(\mathrm{p}+\rho) + \partial_i\left[(\mathrm{p}+\rho)v^i\right] &= 0 \\ (\dot{\mathrm{p}}+\dot{\rho})\,v^i + (\mathrm{p}+\rho)\dfrac{\partial v^i}{\partial \tau} + 4\mathcal{H}(\mathrm{p}+\rho)v^i + \partial_i \mathrm{p} + \partial_j\left[(\mathrm{p}+\rho)v^i v^j\right] + (\mathrm{p}+\rho)\partial_i\psi &= 0. \end{cases} \tag{2.97}$$

Using the first equation to get rid of the $\dot{\rho}$ in the second one, we can rewrite the second equation of the system as

$$\mathcal{H}(\mathrm{p}+\rho)v^i - \partial_j\left[(\mathrm{p}+\rho)v^j\right]v^i + (\mathrm{p}+\rho)\frac{\partial v^i}{\partial \tau} = -\frac{\partial \mathrm{p}}{\partial \tau}v^i - \partial_i \mathrm{p} - \partial_j\left[(\mathrm{p}+\rho)v^j v^i\right] - \partial_i\psi, \tag{2.98}$$

which can be simplified to

$$\frac{\partial v^i}{\partial \tau} + \mathcal{H}v^i + v^j\partial_j v^i = -\frac{1}{\mathrm{p}+\rho}\left(v^i\frac{\partial \mathrm{p}}{\partial \tau} + \partial_i \mathrm{p}\right) - \partial_i\psi. \tag{2.99}$$

This shows that most hierarchies found in the literature can be recovered by making the suited approximations and substitutions to the hierarchy in $A^{ij\cdots k}$.

2.5 Spherical harmonics

2.5.1 Boltzmann equation

The approach we will now consider, consists of expanding the distribution function f in spherical harmonics as

$$f(\mathbf{x}, q^i, \tau) = \sum_{lm} \Psi_{lm}(\mathbf{x}, q, \tau)\, Y_{lm}(\hat{n}), \tag{2.100}$$

where $\hat{n}$ stands for the direction of q^i. We need to choose a direction $\hat{z}$ to compute the Y_{lm}'s, but as there is no preferred direction in our set-up, this $\hat{z}$ is arbitrary.

To find the Boltzmann equation in these new variables, we need to integrate equation (2.20) w.r.t. $\mathrm{d}^2\hat{n}$ weighted by $Y^*_{lm}(\hat{n})$. It is obvious that the integrand with $\partial/\partial q^i$ will be difficult. To perform this integration, we will use spherical coordinates to describe q^i. The Cartesian derivative $\partial/\partial q^i$ becomes in this new coordinate system

$$\frac{\partial}{\partial q^i} = \frac{\partial}{\partial q}\hat{e}_q + \frac{1}{q}\frac{\partial}{\partial \theta}\hat{e}_\theta + \frac{1}{q\sin\theta}\frac{\partial}{\partial \varphi}\hat{e}_\varphi, \tag{2.101}$$

which we rewrite using the angular derivatives $\eth$ and $\overline{\eth}$ as[4]

$$\frac{\partial}{\partial q^i} = \frac{\partial}{\partial q}\hat{e}_q - \frac{1}{2q}\left(\eth + \overline{\eth}\right)\hat{e}_\theta - \frac{1}{2qi}\left(\eth - \overline{\eth}\right)\hat{e}_\varphi. \tag{2.102}$$

Let $\mathbf{k}$ be an arbitrary vector. We introduce the following notation:

$${}_0k \equiv \mathbf{k}\cdot\hat{e}_q, \qquad {}_1k \equiv \frac{\mathbf{k}\cdot\hat{e}_\theta + i\mathbf{k}\cdot\hat{e}_\varphi}{\sqrt{2}}, \qquad {}_{-1}k \equiv \frac{-\mathbf{k}\cdot\hat{e}_\theta + i\mathbf{k}\cdot\hat{e}_\varphi}{\sqrt{2}}, \tag{2.103}$$

and

$$k^0 \equiv \mathbf{k}\cdot\hat{z}, \qquad k^1 \equiv \frac{\mathbf{k}\cdot\hat{x} + i\mathbf{k}\cdot\hat{y}}{\sqrt{2}}, \qquad k^{-1} \equiv \frac{-\mathbf{k}\cdot\hat{x} + i\mathbf{k}\cdot\hat{y}}{\sqrt{2}}. \tag{2.104}$$

A property of these variables we will often use later on is

$$\sum_{m=-1}^{1} (-1)^m\ k_1^m\ k_2^{-m} = \mathbf{k}_1\cdot\mathbf{k}_2. \tag{2.105}$$

By explicitly performing the change of basis from $(\hat{x},\hat{y},\hat{z})$ to $(\hat{e}_q,\hat{e}_\theta,\hat{e}_\varphi)$, one can show that the ${}_sk$'s and k^m's are related by

$$k^m = 2\sqrt{\frac{\pi}{3}} \sum_{s=-1,0,1} (-1)^m\ {}_sY_{1m}(\hat{n})\ {}_{-s}k, \tag{2.106}$$

$${}_sk = 2\sqrt{\frac{\pi}{3}} \sum_{m=-1,0,1} (-1)^s\ {}_sY_{1m}(\hat{n})\ k^{-m}, \tag{2.107}$$

where the ${}_sY_{lm}$'s are the spin-weighted spherical harmonics. With this knowledge, it is lengthy but straightforward to compute the angular integral of the Boltzmann equation. We will do so in momentum space, and tackle the terms of eq. (2.20) one by one.

- $\dfrac{\partial f(\mathbf{k})}{\partial\tau}$ This is the easiest part. Multiplying it by $Y^*_{lm}(\hat{n})$ and integrating with respect to $d^2\hat{n}$ gives the first substitution rule,

$$\boxed{\frac{\partial f(\mathbf{k})}{\partial\tau} \to \frac{\partial\Psi_{lm}(\mathbf{k})}{\partial\tau}.} \tag{2.108}$$

  The τ- and q^i-dependence of f and the τ- and q-dependence of Ψ_{lm} have been suppressed to avoid clutter.

- $\dfrac{q^i}{\epsilon}(ik_i)f(\mathbf{k})$ By definition (see eq. (2.103)), we have that $q^ik_i = q\,{}_0k$. We can now use eq. (2.107) to write ${}_0k$ in terms of k^m's. This gives

$$\frac{q^i}{\epsilon}(ik_i)f(\mathbf{k}) = i\frac{q}{\epsilon}\,2\sqrt{\frac{\pi}{3}}\sum_{m'} {}_0Y_{1m'}(\hat{n})\,k^{-m'}\sum_{\tilde{l}\tilde{m}}\Psi_{\tilde{l}\tilde{m}}(\mathbf{k})Y_{\tilde{l}\tilde{m}}(\hat{n}), \tag{2.109}$$

[4]See the Part on cosmic shear, starting on page 77, for a comprehensive discussion on angular derivatives, spin-weighted spherical harmonics and other related objects.

where also eq. (2.100) has been used. Multiplying by $Y^*_{lm}(\hat{n})$ and performing the angular integral results in our second substitution rule,

$$\boxed{\frac{q^i}{\epsilon}(ik_i)f(\mathbf{k}) \to 2i\sqrt{\frac{\pi}{3}}\frac{q}{\epsilon}\sum_{\tilde{l}\tilde{m}m'}\begin{Bmatrix} l & \tilde{l} & 1 \\ -m & \tilde{m} & m' \\ 0 & 0 & 0 \end{Bmatrix}(-1)^m\Psi_{\tilde{l}\tilde{m}}(\mathbf{k})k^{-m'},} \tag{2.110}$$

where $\left\{\vdots\vdots\vdots\right\}$ stands for a Gaunt integral.

- $-\epsilon\dfrac{\partial f(\mathbf{k}_1)}{\partial q^i}(i(k_2)_i)\psi(\mathbf{k}_2)$ By combining eqs. (2.100) and (2.102), we have that

$$\frac{\partial f(\mathbf{k}_1)}{\partial q^i} = \left[\hat{e}_q\frac{\partial}{\partial q} - \hat{e}_\theta\frac{1}{2q}\left(\eth + \overline{\eth}\right) - \hat{e}_\varphi\frac{1}{2qi}\left(\eth - \overline{\eth}\right)\right]\left(\sum_{\tilde{l}\tilde{m}}\Psi_{\tilde{l}\tilde{m}}(\mathbf{k}_1)Y_{\tilde{l}\tilde{m}}(\hat{n})\right). \tag{2.111}$$

Acting with $\eth$ and $\overline{\eth}$ on Y_{lm} raises and lowers the spin of the spherical harmonic in the following way:

$$\eth Y_{lm} = \sqrt{l(l+1)}\ {}_1Y_{lm} \qquad \text{and} \qquad \overline{\eth}Y_{lm} = -\sqrt{l(l+1)}\ {}_{-1}Y_{lm}. \tag{2.112}$$

Therefore, we find that

$$\begin{aligned}\frac{\partial f(\mathbf{k}_1)}{\partial q^i} =& \sum_{\tilde{l}\tilde{m}}\left[\left(\frac{\partial}{\partial q}\Psi_{\tilde{l}\tilde{m}}(\mathbf{k}_1)\right)Y_{\tilde{l}\tilde{m}}(\hat{n})\hat{e}_q - \frac{1}{2q}\Psi_{\tilde{l}\tilde{m}}(\mathbf{k}_1)\left({}_1Y_{\tilde{l}\tilde{m}} - {}_{-1}Y_{\tilde{l}\tilde{m}}\right)\sqrt{l(l+1)}\hat{e}_\theta\right. \\ &\left. -\frac{1}{2qi}\Psi_{\tilde{l}\tilde{m}}(\mathbf{k}_1)\left({}_1Y_{\tilde{l}\tilde{m}} + {}_{-1}Y_{\tilde{l}\tilde{m}}\right)\sqrt{l(l+1)}\hat{e}_\varphi\right].\end{aligned} \tag{2.113}$$

We now need to "dot" this into $(i(k_2)_i)\psi(\mathbf{k}_2)$. We already know that $\hat{e}_q\cdot\mathbf{k}_2 = {}_0k_2$, and that $\hat{e}_\theta\cdot\mathbf{k}_2$ and $\hat{e}_\varphi\cdot\mathbf{k}_2$ are given by linear combinations of ${}_{-1}k_2$ and ${}_1k_2$. Moreover, we use eq. (2.107) to rewrite ${}_0k_2$, ${}_{-1}k_2$ and ${}_1k_2$ in terms of k_2^m's. By multiplying by $Y^*_{lm}(\hat{n})$ and integrating, we finally find

$$\boxed{\begin{aligned}&-\epsilon\frac{\partial f(\mathbf{k}_1)}{\partial q^i}(i(k_2)_i)\psi(\mathbf{k}_2) \to \\ &\quad -2\epsilon\sqrt{\frac{\pi}{3}}\psi(\mathbf{k}_2)\sum_{\tilde{l}\tilde{m}m'}(-1)^m\left[\begin{Bmatrix} l & \tilde{l} & 1 \\ -m & \tilde{m} & m' \\ 0 & 0 & 0 \end{Bmatrix}\frac{\partial}{\partial q}\Psi_{\tilde{l}\tilde{m}}(\mathbf{k}_1)\right. \\ &\qquad \left.-\sqrt{\frac{\tilde{l}(\tilde{l}+1)}{2}}\begin{Bmatrix} l & \tilde{l} & 1 \\ -m & \tilde{m} & m' \\ 0 & 1 & -1 \end{Bmatrix}\left(1+(-1)^{l+\tilde{l}+1}\right)\frac{\Psi_{\tilde{l}\tilde{m}}(\mathbf{k}_1)}{q}\right]ik_2^{-m'}.\end{aligned}} \tag{2.114}$$

- $\epsilon\dfrac{\partial f(\mathbf{k}_1)}{\partial q^i}\dfrac{q^i}{\epsilon}\dot{\phi}(\mathbf{k}_2)$ Dotting eq. (2.113) into q^i selects only the $\hat{e}_q$-part of it. Therefore, it is easy to find that

$$\boxed{\epsilon\frac{\partial f(\mathbf{k}_1)}{\partial q^i}\frac{q^i}{\epsilon}\dot{\phi}(\mathbf{k}_2) \to q\frac{\partial}{\partial q}\Psi_{lm}(\mathbf{k}_1)\ \dot{\phi}(\mathbf{k}_2).} \tag{2.115}$$

- $\epsilon\frac{\partial f(\mathbf{k}_1)}{\partial q^i}(\hat{n}^i\hat{n}^j-\delta^{ij})\frac{q^2}{\epsilon^2}(i(k_2)_j)\phi(\mathbf{k}_2)$ The part containing δ^{ij} is exactly the same as the third term discussed above (see eq. (2.114)), only with ψ and ϕ interchanged, and multiplied by q^2/ϵ^2. Thus

$$\begin{aligned}\epsilon\frac{\partial f(\mathbf{k}_1)}{\partial q^i}(-\delta^{ij})\frac{q^2}{\epsilon^2}(i(k_2)_j)\phi(\mathbf{k}_2)\rightarrow\\ -2\epsilon\frac{q^2}{\epsilon^2}\sqrt{\frac{\pi}{3}}\phi(\mathbf{k}_2)\sum_{\tilde{l}\tilde{m}m'}(-1)^m\left[\begin{Bmatrix} l & \tilde{l} & 1\\ -m & \tilde{m} & m'\\ 0 & 0 & 0\end{Bmatrix}\frac{\partial}{\partial q}\Psi_{\tilde{l}\tilde{m}}(\mathbf{k}_1)\right.\\ \left.-\sqrt{\frac{\tilde{l}(\tilde{l}+1)}{2}}\begin{Bmatrix} l & \tilde{l} & 1\\ -m & \tilde{m} & m'\\ 0 & 1 & -1\end{Bmatrix}\left(1+(-1)^{l+\tilde{l}+1}\right)\frac{\Psi_{\tilde{l}\tilde{m}}(\mathbf{k}_1)}{q}\right]ik_2^{-m'}.\end{aligned} \tag{2.116}$$

The part containing $\hat{n}^i\hat{n}^j$, which we rewrite as q^iq^j/q^2, combines the $(\partial f/\partial q^i)q^i$ discussed in the previous term with the $q^j(k_2)_j = q\,{}_0k_2$ discussed in the second, giving

$$\begin{aligned}\epsilon\frac{\partial f(\mathbf{k}_1)}{\partial q^i}(\hat{n}^i\hat{n}^j)\frac{q^2}{\epsilon^2}(i(k_2)_j)\phi(\mathbf{k}_2)\rightarrow\\ 2\epsilon\frac{q^2}{\epsilon^2}\sqrt{\frac{\pi}{3}}\,\phi(\mathbf{k}_2)\sum_{\tilde{l}\tilde{m}m'}(-1)^m\frac{\partial}{\partial q}\Psi_{\tilde{l}\tilde{m}}(\mathbf{k}_1)\begin{Bmatrix} l & \tilde{l} & 1\\ -m & \tilde{m} & m'\\ 0 & 0 & 0\end{Bmatrix}ik_2^{-m'}.\end{aligned} \tag{2.117}$$

As this cancels with the first row of the previous equation, we can simplify this last substitution rule to

$$\begin{aligned}\epsilon\frac{\partial f(\mathbf{k}_1)}{\partial q^i}(\hat{n}^i\hat{n}^j-\delta^{ij})\frac{q^2}{\epsilon^2}(i(k_2)_j)\phi(\mathbf{k}_2)\rightarrow 2\epsilon\frac{q^2}{\epsilon^2}\sqrt{\frac{\pi}{3}}\phi(\mathbf{k}_2)\sum_{\tilde{l}\tilde{m}m'}(-1)^m\\ \times\sqrt{\frac{\tilde{l}(\tilde{l}+1)}{2}}\begin{Bmatrix} l & \tilde{l} & 1\\ -m & \tilde{m} & m'\\ 0 & 1 & -1\end{Bmatrix}\left(1+(-1)^{l+\tilde{l}+1}\right)\frac{\Psi_{\tilde{l}\tilde{m}}(\mathbf{k}_1)}{q}\Bigg]ik_2^{-m'}.\end{aligned} \tag{2.118}$$

Before combining all the terms, let us discuss what the range of the summations in eqs. (2.110), (2.114) and (2.118) is. As the first row in the Gaunt integrals should satisfy the triangle inequality, we have that $l-1\leq\tilde{l}\leq l+1$. When the last line contains zeros only, the sum of the first row should be even, which imposes $\tilde{l}=l\pm1$. But the $\left(1+(-1)^{l+\tilde{l}+1}\right)$ which is present in the other two cases, enforces the same condition. We conclude that $\boxed{\tilde{l}=l\pm1}$. The third column of the Gaunt integrals enforces $\boxed{|m'|\leq1}$, and as the second line dictates that $-m+\tilde{m}+m'=0$, we have that $\boxed{\tilde{m}=m+m'}$. These conditions suggest us to change to new summation variables, $\Delta l=\pm1$ and $\Delta m=\pm1,0$, such that $\tilde{l}=l+\Delta l$, $m'=\Delta m$ and $\tilde{m}=m-\Delta m$. By combining all this information, we

get to the following form of the Boltzmann equation,

$$\boxed{\begin{aligned}\frac{\partial\Psi_{lm}(\mathbf{k})}{\partial\tau} =& -q\frac{\partial\Psi_{lm}(\mathbf{k}_1)}{\partial q}\dot{\phi}(\mathbf{k}_2)\\ &-\frac{q}{\epsilon}\,\xi_{lm}^{\Delta l\Delta m}\;\Psi_{l+\Delta l\,m+\Delta m}(\mathbf{k})\;ik^{\Delta m}\\ &+\frac{\epsilon}{q}\psi(\mathbf{k}_2)\;\xi_{lm}^{\Delta l\Delta m}\;q\frac{\partial\Psi_{l+\Delta l\,m+\Delta m}(\mathbf{k}_1)}{\partial q}\;ik_2^{\Delta m}\\ &-\left(\frac{\epsilon}{q}\psi(\mathbf{k}_2)+\frac{q}{\epsilon}\phi(\mathbf{k}_2)\right)\zeta_{lm}^{\Delta l\Delta m}\;\Psi_{l+\Delta l\,m+\Delta m}(\mathbf{k}_1)\;ik_2^{\Delta m},\end{aligned}} \tag{2.119}$$

where summation over $\Delta l = \pm 1$ and $\Delta m = -1, 0, 1$ is implied. The coefficients ξ and ζ are given by

$$\xi_{lm}^{\Delta l\Delta m} = 2\sqrt{\frac{\pi}{3}}(-1)^m \begin{Bmatrix} l & l+\Delta l & 1 \\ -m & m+\Delta m & -\Delta m \\ 0 & 0 & 0 \end{Bmatrix}, \tag{2.120}$$

$$\zeta_{lm}^{\Delta l\Delta m} = 4\sqrt{\frac{\pi}{3}}(-1)^m \begin{Bmatrix} l & l+\Delta l & 1 \\ -m & m+\Delta m & -\Delta m \\ 0 & 1 & -1 \end{Bmatrix} \sqrt{\frac{(l+\Delta l)(l+\Delta l+1)}{2}}. \tag{2.121}$$

For $l = m = 0$, these coefficients vanish for $\Delta l = -1$, whereas for $\Delta l = 1$, these are

	$\Delta m = -1$	$\Delta m = 0$	$\Delta m = 1$
$\xi_{00}^{1\Delta m}$	$-1/\sqrt{3}$	$1/\sqrt{3}$	$-1/\sqrt{3}$
$\zeta_{00}^{1\Delta m}$	$2/\sqrt{3}$	$-2/\sqrt{3}$	$2/\sqrt{3}$

(2.122)

When $m = \Delta m = 0$, these coefficients become

	$\Delta l = -1$	$\Delta l = 1$
$\xi_{l0}^{\Delta l\,0}$	$\dfrac{l}{\sqrt{4l^2-1}}$	$\dfrac{l+1}{\sqrt{4l^2+8l+3}}$
$\zeta_{l0}^{\Delta l\,0}$	$\dfrac{l(l-1)}{\sqrt{4l^2-1}}$	$-\dfrac{(l+1)(l+2)}{\sqrt{4l^2+8l+3}}$

(2.123)

Other useful identities are

$$\zeta_{lm}^{1\,\Delta m} = -(l+2)\xi_{lm}^{1\,\Delta m}, \qquad \zeta_{lm}^{-1\,\Delta m} = (l-1)\xi_{lm}^{-1\,\Delta m}, \qquad \xi_{lm}^{-1\,0} = \xi_{l-1\,m}^{1\,0}, \tag{2.124}$$

$$\xi_{0\,0}^{1\,m} = (-1)^m\frac{1}{\sqrt{3}}, \qquad \xi_{1\,m}^{-1\,-m} = \frac{1}{\sqrt{3}}, \tag{2.125}$$

and

$$\xi_{l-1\,m}^{1\,m_1}\;\xi_{l\,m+m_1}^{1\,m_2} = \xi_{l-1\,m}^{1\,m_2}\;\xi_{l\,m+m_2}^{1\,m_1} \qquad (\forall\; m_1, m_2 \in -1, 0, 1). \tag{2.126}$$

This non-trivial commutation relation will be most useful later.

2.5.2 Linearised equations

When linearised, each term in the equations should contain only one k-dependent field. Therefore, we can choose our $\hat{z}$-direction to be in the **k**-direction, such that the only non-vanishing k^m component is k^0, whence $k^0 = k$. Moreover, only Ψ_{00} contains a background term (as we shall see) so that the first, third and fourth terms of eq. (2.119) can be dropped whenever the relevant Ψ_{lm} is not Ψ_{00}. And as the second line contains a spatial gradient, the background term should be removed as well.

To recover eqs. (2.40) to (2.42), we first need to find the relation between the $\tilde{\Psi}_l$'s defined in Sec. 2.3 on page 15 and the Ψ_{lm}'s defined in eq. (2.100). As described in Sec. 2.3.2, the total distribution function f is given by both $f_0(1+\Psi)$ and $\sum \Psi_{lm}\, Y_{lm}$, so by equating them we can find the desired relationship. The $\tilde{\Psi}_l$'s are related to Ψ by

$$\Psi = \frac{\partial \ln f_0}{\partial \ln q} \sum_l (-i)^l (2l+1) \tilde{\Psi}_l \, P_l(\hat{k} \cdot \hat{n}). \tag{2.127}$$

Using the addition theorem for Y_{lm}'s to replace the Legendre polynomials and integrating w.r.t. $d^2\hat{n}\, Y^*_{l'm'}(\hat{n})$, we find

$$\Psi_{lm} = \sqrt{4\pi}\, f_0\, \delta_{l0}\delta_{m0} + f_0 \frac{\partial \ln f_0}{\partial \ln q} (-i)^l 4\pi Y^*_{lm}(\hat{k}) \tilde{\Psi}. \tag{2.128}$$

As discussed earlier, we can now choose $\hat{z} // \mathbf{k}$ such that $Y^*_{lm}(\hat{k}) = \sqrt{(2l+1)/4\pi}\ \delta_{m0}$. The relation between the Ψ_{lm}'s and $\tilde{\Psi}$ is therefore

$$\Psi_{lm} = \sqrt{4\pi}\, f_0\, \delta_{m0} \left[\delta_{l0} + \frac{\partial \ln f_0}{\partial \ln q} (-i)^l \sqrt{2l+1}\, \tilde{\Psi}_l \right]. \tag{2.129}$$

With this knowledge, we are in the position to recover eqs. (2.40) to (2.42) from the Boltzmann equation (2.119). Out of eq. (2.129), we see that we need only consider $m = 0$ moments. For $l = 0$, the Boltzmann equation reduces to

$$\frac{\partial \Psi_{00}}{\partial \tau} = -q \frac{\partial \Psi_{00}}{\partial q} \dot{\phi} - \frac{q}{\epsilon} \xi^{1\,0}_{0\,0}\, \Psi_{10}\, ik^0. \tag{2.130}$$

Because the first term on the r.h.s. contains $\dot{\phi}$, we need only keep the background part in the adjacent Ψ_{00}. Moreover, as discussed above eq. (2.18), $\partial f_0/\partial\tau = 0$ whence we can remove the background term of the l.h.s. Ψ_{00}. Combining all this with the value of $\xi^{1\,0}_{0\,0}$ found in table (2.122), we find

$$\frac{\partial}{\partial \tau} \tilde{\Psi}_0 = -\dot{\phi} - \frac{q}{\epsilon} \tilde{\Psi}_1\, k, \tag{2.131}$$

as desired. For $l = 1$, the computation is slightly more subtle, because the sum over Δl generates more terms, i.e.

$$\frac{\partial \Psi_{10}}{\partial \tau} = \frac{q}{\epsilon} \xi^{\Delta l\,0}_{1\,0}\, \Psi_{1+\Delta l\,0}\, ik + \frac{\epsilon}{q} \psi\, \xi^{-1\,0}_{1\,0}\, q \frac{\partial \Psi_{00}}{\partial q}\, ik - \left(\frac{\epsilon}{q}\psi + \frac{q}{\epsilon}\phi \right) \zeta^{-1\,0}_{1\,0}\, \Psi_{00}\, ik, \tag{2.132}$$

where $\Delta l = \pm 1$. Using table (2.123) we see that the last term vanishes. For the first term on the right hand side, we throw away the background term as it has no spatial gradient

(i.e. is k-independent), but for the second and third terms, we only keep the background term as they are multiplied by ψ or ϕ. Making the transition from Ψ_{lm} to $\tilde{\Psi}_l$ yields

$$\frac{\partial\tilde{\Psi}_1}{\partial\tau} = \frac{1}{3}\frac{q}{\epsilon}\left(\tilde{\Psi}_0 - 2\tilde{\Psi}_2\right)k - \frac{1}{3}\frac{\epsilon}{q}\psi\,k, \tag{2.133}$$

as desired. For $l \leq 2$ no more background terms come into play, so we need only keep the second row of eq. (2.119). Combining this with the values found in table (2.123), gives

$$\begin{aligned}\frac{\partial\Psi_{l0}}{\partial\tau} &= -\frac{q}{\epsilon}\,\xi^{\Delta l\,0}_{l\,0}\,\Psi_{l+\Delta l\,0}\,ik &(2.134)\\ &= -\frac{q}{\epsilon}\,ik\left[\frac{l}{\sqrt{4l^2-1}}\Psi_{l-1\,0} + \frac{l+1}{\sqrt{4l^2+8l+3}}\Psi_{l+1\,0}\right]. &(2.135)\end{aligned}$$

Writing this equation in terms of $\tilde{\Psi}_l$ gives, after some simplifications,

$$\frac{\partial\tilde{\Psi}_l}{\partial\tau} = \frac{q}{\epsilon}\frac{k}{2l+1}\left[l\tilde{\Psi}_{l-1} - (l+1)\tilde{\Psi}_{l+1}\right], \tag{2.136}$$

as desired.

2.5.3 Other hierarchies

In this section, we will derive two other hierarchies, starting from eq. (2.119). In the same way as we went from f via $A^{ij\cdots k}$ to ρ, we will go from Ψ_{lm} to $\rho^{(p)}_{lm}$ by performing the q-integral, and from $\rho^{(p)}_{lm}$ to $\delta^{(p)}_{lm}$ by taking a kind of generalised divergence.

Hierarchy with $\rho^{(p)}_{lm}$

Like announced, to make the connection between the Ψ_{lm}'s and physical quantities, we first perform the q-integral in order to define

$$\rho^{(p)}_{lm}(\mathbf{k},\tau) \equiv \frac{\sqrt{4\pi}}{a^4}\int q^2\mathrm{d}q\left(\frac{q}{\epsilon}\right)^{p+l}\epsilon\,\Psi_{lm}(\mathbf{k},q,\tau). \tag{2.137}$$

By integrating the Boltzmann equation (2.119) like this, we find the new hierarchy

$$\begin{aligned}\frac{\partial}{\partial\tau}\rho^{(p)}_{lm}(\mathbf{k}) = &-\left(\mathcal{H}\delta(\mathbf{k}_2) - \dot{\phi}(\mathbf{k}_2)\right)\left[(3+p+l)\rho^{(p)}_{lm}(\mathbf{k}_1) - (p+l-1)\rho^{(p+2)}_{lm}(\mathbf{k}_1)\right]\\ &- ik^{\Delta m}\,\xi^{\Delta l\Delta m}_{lm}\rho^{(p+1-\Delta l)}_{l+\Delta l\,m+\Delta m}(\mathbf{k})\\ &- ik_2^{\Delta m}\psi(\mathbf{k}_2)\left[(1+p+2l)\,\xi^{-1\,\Delta m}_{lm}\rho^{(p)}_{l-1\,m+\Delta m}(\mathbf{k}_1) + p\,\xi^{1\,\Delta m}_{lm}\rho^{(p-2)}_{l+1\,m+\Delta m}(\mathbf{k}_1)\right]\\ &- ik_2^{\Delta m}\phi(\mathbf{k}_2)\left[(1+p+2l)\,\xi^{-1\,\Delta m}_{lm}\rho^{(p+2)}_{l-1\,m+\Delta m}(\mathbf{k}_1) + p\,\xi^{1\,\Delta m}_{lm}\rho^{(p)}_{l+1\,m+\Delta m}(\mathbf{k}_1)\right]\\ &- ik_2^{\Delta m}\left[\big(2-(p+l)\big)\psi(\mathbf{k}_2) - \big(2+(p+l)\big)\phi(\mathbf{k}_2)\right]\,\xi^{\Delta l\Delta m}_{lm}\rho^{(p+1-\Delta l)}_{l+\Delta l\,m+\Delta m}(\mathbf{k}_1).\end{aligned} \tag{2.138}$$

This expression should be compared with the hierarchy in $A^{l_1\cdots l_n}$ given by equation (2.30).

In the simplest case, when $l = m = p = 0$, this reduces to

$$\begin{aligned}&\frac{\partial}{\partial\tau}\rho^{(0)}_{00}(\mathbf{k}) + \left(\mathcal{H}\delta(\mathbf{k}_2) - \dot{\phi}(\mathbf{k}_2)\right)\left(3\rho^{(0)}_{00}(\mathbf{k}_1) + \rho^{(2)}_{00}(\mathbf{k}_1)\right)\\ &\qquad + ik^{\Delta m}\,\xi^{1\,\Delta m}_{00}\rho^{(0)}_{1\,\Delta m}(\mathbf{k}) + 2ik_2^{\Delta m}\left(\psi(\mathbf{k}_2) - \phi(\mathbf{k}_2)\right)\rho^{(0)}_{1\,\Delta m}(\mathbf{k}_1) = 0,\end{aligned} \tag{2.139}$$

which bears a clear analogy with eq. (2.25).

Hierarchy with $\delta_{lm}^{(p)}$ and θ_n

We now define the new variables $\delta_{lm}^{(p)}$ as

$$\delta_{lm}^{(p)}(\mathbf{k}) \equiv \rho_{lm}^{(p)}(\mathbf{k}) \frac{(ik)^{l+p}}{\bar{\rho}\ \mathcal{H}^{l+p}}. \tag{2.140}$$

This will allow us to remove the superhorizon terms easily. Plugging this definition into equation (2.138) and making the approximation $\mathcal{H}^2/k^2 \ll 1$, gives the equation

$$\begin{aligned} 0 =& \frac{\partial}{\partial\eta}\delta_{lm}^{(p)}(\mathbf{k}) + \frac{p+l}{2}\delta_{lm}^{(p)}(\mathbf{k}) + \frac{k^{\Delta m}}{k}\,\xi_{lm}^{\Delta l\,\Delta m}\,\delta_{l+\Delta l\,m+\Delta m}^{(p+1-\Delta l)}(\mathbf{k}) \\ & - \frac{k_1\,k_2^{\Delta m}}{\mathcal{H}^2}\left(\frac{k}{k_1}\right)^{l+p}\psi(\mathbf{k}_2)\left[(1+p+2l\,)\,\xi_{lm}^{-1\,\Delta m}\,\delta_{l-1\,m+\Delta m}^{(p)}(\mathbf{k}_1) + p\,\xi_{lm}^{1\,\Delta m}\,\delta_{l+1\,m+\Delta m}^{(p-2)}(\mathbf{k}_1)\right], \end{aligned} \tag{2.141}$$

where $\eta \equiv \log a(\tau)$. We make the same approximations as in Sec. 2.2.5, i.e. we are considering a pressureless fluid in matter dominance, with $\dot{\phi} \ll \mathcal{H}$. Note that the second line also contains a linear term: when $l = 1$ and $p = 0$ as $\delta_{00}^{(0)} = 1 + \delta$. We now would like to find a hierarchy resembling the one in Θ_n found in the same section, see eq. (2.36). To that end, we define the new quantities $\epsilon_l^{(p)}$ as follows,

$$\epsilon_l^{(p)}(\mathbf{k}) \equiv \frac{k^{m_1}}{k}\,\xi_{00}^{1\,m_1}\,\frac{k^{m_2}}{k}\,\xi_{1\,m_1}^{1\,m_2}\,\frac{k^{m_3}}{k}\,\xi_{2\,m_1+m_2}^{1\,m_3}\,\cdots\frac{k^{m_l}}{k}\,\xi_{l-1\,m_1+\cdots+m_{l-1}}^{1\,m_l}\,\delta_{l\,m_1+\cdots+m_l}^{(p)}(\mathbf{k}) \tag{2.142}$$

where summation over all $m_i \in \{-1, 0, 1\}$ is implied. As equation (2.141) is valid for all $m \in \{-l, \ldots, l\}$, we can rewrite it as (by dropping the ψ-term)

$$\begin{aligned} 0 =& \frac{\partial}{\partial\eta}\delta_{l\,m_1+\cdots+m_l}^{(p)} + \frac{p+l}{2}\delta_{l\,m_1+\cdots+m_l}^{(p)} + \frac{k^{m_{l+1}}}{k}\,\xi_{l\,m_1+\cdots+m_l}^{1\,m_{l+1}}\,\delta_{l+1\,m_1+\cdots+m_{l+1}}^{(p)} \\ & + \frac{k^{m_{l+1}}}{k}\,\xi_{l\,m_1+\cdots+m_l}^{-1\,m_{l+1}}\,\delta_{l-1\,m_1+\cdots+m_{l+1}}^{(p+2)}, \end{aligned} \tag{2.143}$$

where all m_i's are thus -1, 0 or 1. By multiplying this expression with l factors of $(k^{m_i}/k)\xi_{i\,m_i}^{1\,m_{i+1}}$ like in eq. (2.142) we can translate the equation in $\delta_{lm}^{(p)}$ to an equation in $\epsilon_l^{(p)}$. As we dropped the ψ-term, we only kept linear terms and we can choose $\hat{z}//\mathbf{k}$, such that $k^0 = k$ and all $m_i = 0$. The summation implied in eq. (2.142) therefore reduces to just one term and it is then straightforward to show that

$$\frac{\partial}{\partial\eta}\epsilon_l^{(p)}(\mathbf{k}) + \frac{p+l}{2}\epsilon_l^{(p)}(\mathbf{k}) + \epsilon_{l+1}^{(p)}(\mathbf{k}) + \frac{l^2}{4l^2-1}\epsilon_{l-1}^{(p+2)}(\mathbf{k}) - \delta_{l1}\delta_{p0}\frac{k^2}{\mathcal{H}^2}\psi(\mathbf{k}) = 0, \tag{2.144}$$

where we reintroduced the linear part of the ψ-term. It is much harder to find the same result without assuming $\hat{z}//\mathbf{k}$. The case for which $\mathbf{k}$ lies in the xy-plane, such that $m_i = \pm 1$, is still manageable, but much more technical. The cumbersome calculations rely on the useful property (see eq. (2.126))

$$\xi_{l-1\,m}^{1\,m_1}\,\xi_{l\,m+m_1}^{1\,m_2} = \xi_{l-1\,m}^{1\,m_2}\,\xi_{l\,m+m_2}^{1\,m_1} \qquad (\forall\ m_1, m_2 \in -1, 0, 1). \tag{2.145}$$

We define the "new" quantity Θ_L as

$$\Theta_L(\mathbf{k}) \equiv \sum_{l=0}^{L} C(l, L)\epsilon_l^{(L-l)}(\mathbf{k}) \quad \text{with} \quad C(l, L) \equiv \frac{L!}{l!(L-l)!}\frac{(2l+1)!!(L-l-1)!!}{(L+l+1)!!}, \tag{2.146}$$

where the dummy variable l is even (odd) when L is even (odd). It is long but straightforward to show that this new quantity satisfies

$$\frac{\partial}{\partial\eta}\Theta_L(\mathbf{k}) + \frac{L}{2}\Theta_L(\mathbf{k}) + \Theta_{L+1}(\mathbf{k}) - \delta_{L1}\frac{k^2}{\mathcal{H}^2}\psi(\mathbf{k}) = 0. \tag{2.147}$$

The computation relies on the following property of the $C(l, L)$'s,

$$C(l-1, L) + C(l+1, L)\frac{(l+1)^2}{4(l+1)^2 - 1} = C(l, L+1). \tag{2.148}$$

As the equation for Θ_L computed above is exactly equation (2.35), we can conclude that the two Θ's are actually the same.

Whereas it is perfectly valid to assume $\mathbf{k}//\hat{z}$ in the linear case, when we turn to the non-linear term, we cannot assume that $\mathbf{k}_1//\mathbf{k}_2//\hat{z}$. But to make the connection with eq. (2.36), we will assume $\mathbf{k}_1//\mathbf{k}$, like we did at that point. A similar calculation as the one in the linear case, but now relying on the property

$$C(l+1, L)(L+l+2)\frac{(l+1)^2}{4(l+1)^2 - 1} + C(l-1, L)(L-l+1) = L\,C(l, L-1), \tag{2.149}$$

results in

$$\frac{\partial}{\partial\eta}\Theta_L(\mathbf{k}) + \frac{L}{2}\Theta_L(\mathbf{k}) + \Theta_{L+1}(\mathbf{k}) = L\frac{\mathbf{k}\cdot\mathbf{k}_2}{\mathcal{H}^2}\left(\frac{k}{k_1}\right)^{L-1}\Theta_{L-1}(\mathbf{k}_1)\;\psi(\mathbf{k}_2), \tag{2.150}$$

confirming our conclusion that the Θ_L's defined in this section coincide with the Θ_n's defined in eq. (2.34).

2.6 Conclusion

In this chapter we derived, with all details, the Boltzmann hierarchy. By introducing the standard quantities, we recovered the well known result, as we should. On the other hand, we also introduced new variables like $A^{ij\cdots k}$ and Ψ_{lm} leading to two new hierarchies. Though both are equivalent, it is not clear yet which one is best suited for further calculations. The first one has the advantage of being in close contact with the standard variables whenever the order is small. The second one is attractive as decomposition into the scalar modes, vector modes etc. is well understood. Because of this, truncation of the hierarchy at a certain order is more transparent. We leave a deeper analysis of these hierarchies for the future, though we will show in the next section how both give the same results in the context of perturbation theory.

Chapter 3

Perturbation theory

Contents

Cosmological perturbation theory (CPT) [12] is based on the phenomenon of gravitational instability. Initial overdensities, regardless of how they are created, will attract matter and hence will grow. In the same way, initial voids will become bigger as more and more matter will leave the voids. This runaway process, named gravitational instability, is assumed to be the creator of the large-scale structure we observe today.

From observations of the CMB [6] we can infer the size of the density perturbations at the time of decoupling ($z \sim 1000$) and it is found to have been $\delta \sim 10^{-5}$. Therefore, we can expand the density field at some time τ into new variables $\delta^{(n)}(\tau)$ as $\delta(\tau) = \sum \delta^{(n)}(\tau)$ where $\delta^{(1)}$ is linear in the initial density field δ_{in}, $\delta^{(2)}$ quadratic, etc.

3.1 Equations of motion

In this section, we describe how non-linear perturbation theory can be built out of the non-linear equations found by using the moments of the Boltzmann equation. Throughout this section, we will assume we have just one pressureless ($w = 0$), non-relativistic fluid, like cold dark matter (CDM). The spacetime corresponding to this matter content is Einstein-de Sitter (EdS) spacetime. This means that we can write the Poisson equation on subhorizon scales as

$$\psi(\mathbf{k}) = -\frac{3}{2}\frac{\mathcal{H}^2}{k^2}\delta(\mathbf{k}), \tag{3.1}$$

and that the conformal Hubble rate satisfies $\dot{\mathcal{H}} = -\mathcal{H}^2/2$ [3]. We will only keep the first and second moments of the Boltzmann hierarchy, i.e. the continuity and Euler equations, and neglect all higher-order variables. Our only variables are therefore δ and v^i or its divergence $\theta \equiv ik_j v^j$. Ignoring small-scale shell crossings, we have that our fluid is (and remains) potential, whence $v_j = (-ik_j/k^2)\theta$. This ensures that the truncation of the Boltzmann hierarchy after the first moment is self-consistent.

By making the approximations defined above, the continuity and Euler equations, given by eqs. (2.94) and (2.95) respectively, simplify to

$$\begin{cases} \dot{\delta}(\mathbf{k}) + \theta(\mathbf{k}) &= -\dfrac{k_1^2 + \mathbf{k}_1 \cdot \mathbf{k}_2}{k_1^2}\theta(\mathbf{k}_1)\delta(\mathbf{k}_2), \\ \dot{\theta}(\mathbf{k}) + \mathcal{H}\theta(\mathbf{k}) - k^2\psi(\mathbf{k}) &= -\left(\dfrac{(\mathbf{k}_1 \cdot \mathbf{k}_2)^2}{k_1^2 k_2^2} + \dfrac{\mathbf{k}_1 \cdot \mathbf{k}_2}{k_1^2}\right)\theta(\mathbf{k}_1)\theta(\mathbf{k}_2) \end{cases} \tag{3.2}$$

where on the r.h.s. a convolution $\int \mathrm{d}^3\mathbf{k}_1\, \mathrm{d}^3\mathbf{k}_2\, \delta(\mathbf{k} - \mathbf{k}_1 - \mathbf{k}_2)$ is implied. Note that only the symmetric part of the large parentheses matters, whence we can rewrite it as

$$\begin{cases} \dot{\delta}(\mathbf{k}) + \theta(\mathbf{k}) &= -\dfrac{\mathbf{k}_1 \cdot (\mathbf{k}_1 + \mathbf{k}_2)}{k_1^2}\theta(\mathbf{k}_1)\delta(\mathbf{k}_2), \\ \dot{\theta}(\mathbf{k}) + \mathcal{H}\theta(\mathbf{k}) - k^2\psi(\mathbf{k}) &= -\dfrac{(\mathbf{k}_1 \cdot \mathbf{k}_2)(\mathbf{k}_1 + \mathbf{k}_2)^2}{2k_1^2 k_2^2}\theta(\mathbf{k}_1)\theta(\mathbf{k}_2). \end{cases} \tag{3.3}$$

Minus the coefficients in front of $\theta(\mathbf{k}_1)\delta(\mathbf{k}_2)$ and $\theta(\mathbf{k}_1)\theta(\mathbf{k}_2)$ are commonly known as $\alpha(\mathbf{k}_1, \mathbf{k}_2)$ and $\beta(\mathbf{k}_1, \mathbf{k}_2)$ respectively:

$$\begin{aligned} \alpha(\mathbf{k}_1, \mathbf{k}_2) &\equiv \frac{\mathbf{k}_1 \cdot (\mathbf{k}_1 + \mathbf{k}_2)}{k_1^2}, \\ \beta(\mathbf{k}_1, \mathbf{k}_2) &\equiv \frac{(\mathbf{k}_1 \cdot \mathbf{k}_2)(\mathbf{k}_1 + \mathbf{k}_2)^2}{2k_1^2 k_2^2}. \end{aligned} \tag{3.4}$$

These mode coupling functions play a central role in non-linear perturbation theory.

3.2 Linear perturbation theory

Like said in the introduction, perturbation theory is based on the assumption that δ (and also θ) are small, such that the r.h.s. of eqs. (3.3) can be neglected to leading order. The solutions to the linearised equations are denoted by $\delta^{(1)}$ and $\theta^{(1)}$. Focussing on the linear part of eqs. (3.3), we can combine these two equations into one second-order equation given by

$$\ddot{\delta}^{(1)} + \mathcal{H}\dot{\delta}^{(1)} - \frac{3}{2}\mathcal{H}^2\delta^{(1)} = 0, \tag{3.5}$$

where the Poisson equation (3.1) has been used to replace ψ by $\delta^{(1)}$. The two solutions to this equation are easily found by changing to the time variable $\eta \equiv \ln a$, such that

$$\frac{\partial}{\partial\tau} = \mathcal{H}\frac{\partial}{\partial\eta}, \qquad \frac{\partial\mathcal{H}}{\partial\eta} = -\frac{\mathcal{H}}{2} \qquad \text{and} \qquad \frac{\partial^2}{\partial\tau^2} = -\frac{\mathcal{H}^2}{2}\frac{\partial}{\partial\eta} + \mathcal{H}^2\frac{\partial^2}{\partial\eta^2}, \tag{3.6}$$

whence in this new variable

$$\frac{\partial^2}{\partial\eta^2}\delta^{(1)} + \frac{1}{2}\frac{\partial}{\partial\eta}\delta^{(1)} - \frac{3}{2}\delta^{(1)} = 0. \tag{3.7}$$

The time dependence of the growing mode is $\delta^{(1)} \propto e^{\eta}$, and that of the decaying mode is $\delta^{(1)} \propto e^{(-3/2)\eta}$. By using the assumption that $\delta^{(1)}$ is linear in the initial density field $\delta_{\rm in}$, this corresponds to $\delta^{(1)} = e^{(\eta-\eta_{\rm in})}\,\delta_{\rm in}$ and $\delta^{(1)} = e^{(-3/2)(\eta-\eta_{\rm in})}\,\delta_{\rm in}$ respectively. The initial time is taken at $\eta = \eta_{\rm in}$, and for convenience we will often take $\eta_{\rm in} = 0$.

By using our new time variable and defining $\Theta \equiv -\theta/\mathcal{H}$ (not to be confused with the Θ_n's defined in Sec. 2.2.5), we can rewrite the continuity and Euler equations as

$$\left\{ \begin{array}{rcl} \dfrac{\partial}{\partial\eta}\delta(\mathbf{k}) - \Theta(\mathbf{k}) & = & \alpha(\mathbf{k}_1,\mathbf{k}_2)\;\Theta(\mathbf{k}_1)\;\delta(\mathbf{k}_2), \\ \dfrac{\partial}{\partial\eta}\Theta(\mathbf{k}) + \dfrac{1}{2}\Theta(\mathbf{k}) - \dfrac{3}{2}\delta(\mathbf{k}) & = & \beta(\mathbf{k}_1,\mathbf{k}_2)\;\Theta(\mathbf{k}_1)\;\Theta(\mathbf{k}_2). \end{array} \right. \tag{3.8}$$

The continuity equation shows that linearly, $\Theta^{(1)}$ has the same growing (e^{η}) and decaying ($e^{(-3/2)\eta}$) modes as $\delta^{(1)}$, which justifies the choice of η as time variable and the redefinition of θ to Θ. Moreover, if we only consider the growing mode and neglect the non-linear corrections, we have $\delta^{(1)} = \Theta^{(1)}$. We will recover these results in the next session when introducing a notation more suited to non-linear perturbation theory.

3.3 Non-linear perturbation theory

In non-linear perturbation theory, we keep the interactions given by the r.h.s. of eq. (3.3), or equivalently of eq. (3.8). To second order, there are 4 variables at stake, namely $\delta^{(1)}$, $\Theta^{(1)}$, $\delta^{(2)}$ and $\Theta^{(2)}$. The first two satisfy the linearised equations, the second two

$$\left\{ \begin{array}{rcl} \dfrac{\partial}{\partial\eta}\delta^{(2)}(\mathbf{k}) - \Theta^{(2)}(\mathbf{k}) & = & \alpha(\mathbf{k}_1,\mathbf{k}_2)\;\Theta^{(1)}(\mathbf{k}_1)\;\delta^{(1)}(\mathbf{k}_2), \\ \dfrac{\partial}{\partial\eta}\Theta^{(2)}(\mathbf{k}) + \dfrac{1}{2}\Theta^{(2)}(\mathbf{k}) - \dfrac{3}{2}\delta^{(2)}(\mathbf{k}) & = & \beta(\mathbf{k}_1,\mathbf{k}_2)\;\Theta^{(1)}(\mathbf{k}_1)\;\Theta^{(1)}(\mathbf{k}_2). \end{array} \right. \tag{3.9}$$

To third order, the right hand side of the continuity equation contains combinations of $\Theta^{(2)}\,\delta^{(1)}$ and $\Theta^{(1)}\,\delta^{(2)}$, etc.

To simplify these cumbersome equations, it is convenient to rewrite the system by introducing the doublet $\Psi_a \equiv (\delta, \Theta)^T$, where $a = 1, 2$. The fully non-linear continuity and Euler equations can then be written as

$$\frac{\partial}{\partial\eta}\Psi_a(\mathbf{k}) + \Omega_{ab}\,\Psi_b(\mathbf{k}) = \gamma_{abc}(\mathbf{k},\mathbf{k}_1,\mathbf{k}_2)\Psi_b(\mathbf{k}_1)\Psi_c(\mathbf{k}_2), \tag{3.10}$$

where

$$\Omega_{ab} \equiv \begin{pmatrix} 0 & -1 \\ -\frac{3}{2} & \frac{1}{2} \end{pmatrix}, \tag{3.11}$$

and the non-zero $\gamma_{abc}(\mathbf{k},\mathbf{k}_1,\mathbf{k}_2)$'s are

$$\gamma_{112} = \frac{\alpha(\mathbf{k}_2,\mathbf{k}_1)}{2}, \qquad \gamma_{121} = \frac{\alpha(\mathbf{k}_1,\mathbf{k}_2)}{2} \qquad \text{and} \qquad \gamma_{222} = \beta(\mathbf{k}_1,\mathbf{k}_2). \tag{3.12}$$

Notice that the eigenvalues of $(-\Omega_{ab})$, namely 1 and $-3/2$, correspond to the time dependence of the linear growing and decaying modes. The linear propagator $g_{ab}(\eta,\eta_0)$, which by definition satisfies

$$\frac{\partial}{\partial\eta}g_{ab}(\eta,\eta_0) + \Omega_{ac}(\eta)g_{cb}(\eta,\eta_0) = 0, \tag{3.13}$$

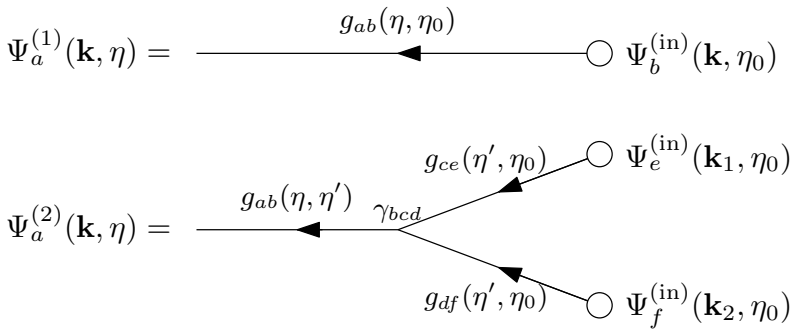

Figure 3.1: Diagrammatic representation of cosmological perturbation theory. The top figure is the diagram of the propagator $g_{ab}(\eta,\eta_{\mathrm{in}})$, the bottom one contains the vertex $\gamma_{bcd}(\mathbf{k}_1,\mathbf{k}_2)$. The circles on the right denote initial conditions.

describes the linear evolution of $\Psi^{(1)} \equiv (\delta^{(1)},\Theta^{(1)})^T$, i.e.

$$\Psi_a^{(1)}(\eta) = g_{ab}(\eta,\eta_0)\Psi_b^{(1)}(\eta_0). \tag{3.14}$$

It can easily be found by exponentiating Ω_{ab}, such that

$$g_{ab}(\eta,\eta_0) = \exp\left[\Omega_{ab}(\eta-\eta_0)\right] = \frac{e^{\eta-\eta_0}}{5}\begin{pmatrix}3 & 2\\ 3 & 2\end{pmatrix} + \frac{e^{(-3/2)(\eta-\eta_0)}}{5}\begin{pmatrix}2 & -2\\ -3 & 3\end{pmatrix}. \tag{3.15}$$

We see that the (adiabatic) growing mode is proportional to $\Psi_a^{(1)} \propto (1,1)^T$, and the (adiabatic) decaying mode to $\Psi_a^{(1)} \propto (1,-3/2)^T$. When $\eta-\eta_0 \gg 1$, the decaying mode becomes negligible, whence $\delta^{(1)} = \Theta^{(1)}$.

An important property of the linear propagator $g_{ab}(\eta,\eta_0)$ is that it enables us to (formally) write down a solution to the equation of motion of $\Psi_a(\eta)$ given in eq. (3.10), namely

$$\begin{aligned}\Psi_a(\mathbf{k},\eta) = {}& g_{ab}(\eta,\eta_0)\Psi_b(\mathbf{k},\eta_0)\\ &+ \int_{\eta_0}^{\eta} \mathrm{d}\tilde{\eta}\; g_{ab}(\eta,\tilde{\eta})\gamma_{bde}(\mathbf{k},\mathbf{k}_1,\mathbf{k}_2)\Psi_d(\mathbf{k}_1,\tilde{\eta})\Psi_e(\mathbf{k}_2,\tilde{\eta}).\end{aligned} \tag{3.16}$$

This equation forms the basis to the diagrammatic representation of cosmological perturbation theory [13]. In this representation, linear propagators, i.e. g_{ab}, are denoted by a line carrying two indices; the vertices, carrying three indices, stand for the interactions, i.e. γ_{abc}. Time flows to the left and integration over intermediate times (respecting causality) is assumed. On the right hand side, we find the initial fields $\Psi_a^{(\mathrm{in})}(\mathbf{k},\eta_0)$. Two examples of diagrams are shown in Fig. 3.1.

We are now in a position to define a series expansion of Ψ_a, in an equivalent way to how we introduced $\delta^{(n)}$ and $\theta^{(n)}$:

$$\Psi_a(\mathbf{k},\eta) \equiv \sum_{n=1}^{\infty} \Psi_a^{(n)}(\mathbf{k},\eta) \tag{3.17}$$

where $\Psi_a^{(n)}$ is of n^{th} order in the initial conditions $\Psi_a^{(\mathrm{in})}$. We further define the kernels $\mathcal{F}_a^{(n)}$ as

$$\Psi_a^{(n)}(\mathbf{k},\eta) \equiv \mathcal{F}_a^{(n)}(\mathbf{k};\mathbf{k}_1,\cdots,\mathbf{k}_n;\eta)\delta_{\mathrm{in}}(\mathbf{k}_1)\cdots\delta_{\mathrm{in}}(\mathbf{k}_n), \tag{3.18}$$

where a convolution $\int \mathrm{d}\mathbf{k}_1 \cdots \mathrm{d}\mathbf{k}_n \delta_{\mathrm{D}}(\mathbf{k} - \sum \mathbf{k}_i)$ is assumed on the right hand side. These quantities, like the linear propagator g_{ab}, correspond to tree-order diagrams. We will later generalise those quantities to diagrams including loops.

If we write the initial conditions as $\Psi_a^{(\mathrm{in})}(\mathbf{k}) = u_a \delta_{\mathrm{in}}(\mathbf{k})$, $\mathcal{F}_a^{(1)}(\eta)$ is related to $g_{ab}(\eta, \eta')$ through $\mathcal{F}_a^{(1)}(\eta) = g_{ab}(\eta, \eta_{\mathrm{in}}) u_b$. We will now assume that the initial conditions are in the (adiabatic) growing mode, i.e. $u_a = (1, 1)^T$, such that $\Psi_1^{(\mathrm{in})} = \Psi_2^{(\mathrm{in})} = \delta_{\mathrm{in}}$. In that case, it is obvious that for $n = 1$ we recover the growing mode of the linear propagator, i.e. $\mathcal{F}_1^{(1)} = \mathcal{F}_2^{(1)} = e^{\eta - \eta_{\mathrm{in}}}$. For $n = 2$, we find

$$\Psi_a^{(2)} = \int_{\eta_0}^{\eta} \mathrm{d}\tilde{\eta}\; g_{ab}(\eta, \tilde{\eta}) \gamma_{bde}(\mathbf{k}, \mathbf{k}_1, \mathbf{k}_2) \left(e^{\tilde{\eta} - \eta_{\mathrm{in}}} \Psi_d^{(\mathrm{in})}(\mathbf{k}_1) \right) \left(e^{\tilde{\eta} - \eta_{\mathrm{in}}} \Psi_e^{(\mathrm{in})}(\mathbf{k}_2) \right). \tag{3.19}$$

Focusing on $a = 1$, i.e. $\delta^{(2)}$, $\mathcal{F}_1^{(2)}$ simplifies to

$$\begin{aligned} \mathcal{F}_1^{(2)} = & \left[\left(e^{\eta - \eta_{\mathrm{in}}} \right)^2 - \left(e^{(\eta - \eta_{\mathrm{in}}) + (\eta_0 - \eta_{\mathrm{in}})} \right) \right] \left(\frac{3}{5} + \frac{1}{2} \mu \left(\frac{k_1}{k_2} + \frac{k_2}{k_1} \right) + \frac{2}{5} \mu^2 \right) \\ & + \frac{4}{35} \left[\left(e^{\eta - \eta_{\mathrm{in}}} \right)^2 - \left(e^{-\frac{3}{2}(\eta - \eta_{\mathrm{in}}) + \frac{7}{2}(\eta_0 - \eta_{\mathrm{in}})} \right) \right] (1 - \mu^2), \end{aligned} \tag{3.20}$$

where $\mu = \dfrac{\mathbf{k}_1 \cdot \mathbf{k}_2}{k_1\, k_2}$. By setting $\eta_{\mathrm{in}} = 0$ for convenience and taking only the fastest growing mode into account, i.e. $e^{2\eta}$, which is equivalent to taking the lower integration bound $\tilde{\eta} \to -\infty$, this simplifies to

$$\mathcal{F}_1^{(2)} \approx e^{2\eta} \left[\frac{5}{7} + \frac{1}{2} \mu \left(\frac{k_1}{k_2} + \frac{k_2}{k_1} \right) + \frac{2}{7} \mu^2 \right]. \tag{3.21}$$

The quantity between the square brackets is commonly known as F_2,

$$\boxed{F_2(\mathbf{k}_1, \mathbf{k}_2) = \frac{5}{7} + \frac{1}{2} \mu \left(\frac{k_1}{k_2} + \frac{k_2}{k_1} \right) + \frac{2}{7} \mu^2,} \tag{3.22}$$

and more generally we have the relationship $\mathcal{F}_1^{(n)} \approx e^{n\eta} F_n$.

It can be shown that the $\mathcal{F}_a^{(n)}$ kernels satisfy the following recursion relation:

$$\begin{aligned} & \mathcal{F}_a^{(n)}(\mathbf{k}_1, \ldots, \mathbf{k}_n; \eta) \delta_{\mathrm{D}} \left(\mathbf{k} - \sum \mathbf{k}_i \right) = \\ & \sum_{m=1}^{n-1} \int_{\eta_0}^{\eta} \mathrm{d}\tilde{\eta}\, g_{ab}(\eta, \tilde{\eta}) \gamma_{bde} \Big(\mathbf{k}, \sum_{i=1}^{m} \mathbf{k}_i, \sum_{i=m+1}^{n} \mathbf{k}_i \Big) \mathcal{F}_d^{(m)}(\mathbf{k}_1, \cdots, \mathbf{k}_m; \tilde{\eta}) \mathcal{F}_e^{(n-m)}(\mathbf{k}_{m+1}, \cdots, \mathbf{k}_n; \tilde{\eta}), \end{aligned} \tag{3.23}$$

where on the r.h.s. symmetrisation over all $\mathbf{k}_i$'s is implied, and $\mathcal{F}_a^{(1)}(\eta) = g_{ab}(\eta, \eta_{\mathrm{in}}) u_b$.

3.4 Multi-point propagators

Before coming to the fully non-linear generalisation of the propagator and the $\mathcal{F}_a^{(n)}$-kernels, we introduce the initial power spectrum of the fields. It is defined by

$$\delta_{\mathrm{D}}(\mathbf{k} + \mathbf{k}') P_{ab}^{(\mathrm{in})}(k) \equiv \left\langle \Psi_a^{(\mathrm{in})}(\mathbf{k}) \Psi_b^{(\mathrm{in})}(\mathbf{k}') \right\rangle, \tag{3.24}$$

which corresponds to the variance of the distribution the initial fields are drawn from. If we assume this distribution to be Gaussian, $P_{ab}^{(\mathrm{in})}(k)$ fully determines it. The fact that $P_{ab}^{(\mathrm{in})}(k)$ does not depend on the direction of $\mathbf{k}$ reflects the assumed isotropy, whereas the Dirac-δ_{D} results from translational invariance (i.e. homogeneity). Writing the initial conditions as $\Psi_a^{(\mathrm{in})} = u_a \delta_{\mathrm{in}}$, we define $P_0(k)$ from $P_{ab}^{(\mathrm{in})}(k) = u_a u_b P_0(k)$. In the diagrammatic representation of cosmological perturbation theory, an initial power spectrum is denoted by $\otimes$. This reflects the fact that for an initial power spectrum, two initial fields, denoted by $\bigcirc$'s on the r.h.s. of Fig. 3.1, are glued together. The initial power spectrum is assumed to be known and what we are often interested in is the equal-time power spectrum

$$\delta_{\mathrm{D}}(\mathbf{k}+\mathbf{k}')P_{ab}(k,\eta) \equiv \langle \Psi_a(\mathbf{k},\eta)\Psi_b(\mathbf{k}',\eta)\rangle \,. \tag{3.25}$$

So the question is how $P_{ab}(k,\eta)$ is related to $P_{ab}^{(\mathrm{in})}(k)$. If we assume growing mode initial conditions, it is clear that linearly

$$P_{ab}(k,\eta) \overset{L}{=} e^{2(\eta-\eta_{\mathrm{in}})} P_{ab}^{(\mathrm{in})}(k) \overset{L}{=} e^{2(\eta-\eta_{\mathrm{in}})} P_0(k). \tag{3.26}$$

The diagram corresponding to this power spectrum is shown on Fig. 3.2.

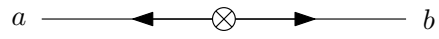

Figure 3.2: Diagrammatic representation of the (linear) power spectrum $P_{ab}(\mathbf{k})$.

The linear propagator $g_{ab}(\eta,\eta_0)$ describes how a field $\Psi_b(\eta_0)$ linearly evolves into the field $\Psi_a(\eta)$. Equivalently, it describes how the field $\Psi_a(\eta)$ depends (linearly) on $\Psi_b(\eta_0)$. The obvious generalisation is thus how $\Psi_a(\eta)$ depends on $\Psi_b(\eta_0)$ taking all the non-linear corrections into account. The non-linear propagator $G_{ab}(\eta,\eta_0)$ is therefore defined as [14, 15, 13]

$$G_{ab}(\mathbf{k},\eta,\eta_0)\delta_{\mathrm{D}}(\mathbf{k}-\mathbf{k}') \equiv \left\langle \frac{\partial \Psi_a(\mathbf{k},\eta)}{\partial \Psi_b(\mathbf{k}',\eta_0)} \right\rangle . \tag{3.27}$$

Focusing on the non-linear propagator starting from initial time η_{in}, we substitute eqs. (3.17) and (3.18) to find

$$\begin{aligned} G_{ab}(\mathbf{k},\eta,\eta_{\mathrm{in}})\delta(\mathbf{k}-\mathbf{k}') = \sum_n \int \mathrm{d}^3\mathbf{k}_1 \cdots \mathrm{d}^3\mathbf{k}_n \delta_{\mathrm{D}}\left(\mathbf{k}-\sum \mathbf{k}_i\right) \mathcal{F}_a^{(n)}(\mathbf{k}_1,\ldots,\mathbf{k}_n) \\ \times \left\langle \frac{\partial}{\partial \delta_{\mathrm{in}}(\mathbf{k}')} \big(\delta_{\mathrm{in}}(\mathbf{k}_1)\cdots\delta_{\mathrm{in}}(\mathbf{k}_n)\big) \right\rangle \end{aligned} \tag{3.28}$$

Whenever n is even, Wick's theorem ensures that the expectation value vanishes for Gaussian initial conditions. The 1-loop correction, of which the diagram is shown on Fig. 3.3, thus corresponds to $n = 3$ and is given by

$$G_{ab}^{(1-\mathrm{loop})}(\mathbf{k},\eta,\eta_{\mathrm{in}}) = 3\int \mathrm{d}^3\mathbf{q}\; \mathcal{F}_a^{(3)}(\mathbf{k},\mathbf{q},-\mathbf{q}) P_{ab}^{(\mathrm{in})}(q). \tag{3.29}$$

The (complicated) expression of $\mathcal{F}_a^{(3)}$ can be found by using the recursion relation given by eq. (3.23).

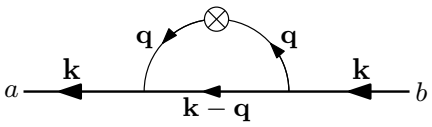

Figure 3.3: Diagrammatic representation of the 1-loop correction to the non-linear propagator $G_{ab}(\mathbf{k}, \eta, \eta')$.

We generalise the $\mathcal{F}_a^{(n)}$-kernels to non-linear multi-point propagators by defining the $(n+1)$-point propagator $\Gamma^{(n)}_{ab_1\ldots b_n}$ through [16, 17]

$$\left\langle \frac{\partial^n \Psi_a(\mathbf{k}, \eta)}{\partial \Psi_{b_1}^{(\mathrm{in})}(\mathbf{k}_1) \cdots \partial \Psi_{b_n}^{(\mathrm{in})}(\mathbf{k}_n)} \right\rangle \equiv \delta_{\mathrm{D}} \left(\mathbf{k} - \sum \mathbf{k}_i \right) \Gamma^{(n)}_{ab_1\ldots b_n}(\mathbf{k}_1, \ldots, \mathbf{k}_n; \eta, \eta_{\mathrm{in}}). \tag{3.30}$$

The δ_{D}-function is due to translational invariance, and for $n = 1$ we recover the 2-point propagator, $\Gamma^{(1)}_{ab}(\mathbf{k}, \eta, \eta_{\mathrm{in}}) = G_{ab}(\mathbf{k}, \eta, \eta_{\mathrm{in}})$. $\Gamma^{(2)}_{abc}$ is the non-linear generalisation of γ_{abc}. The 1-loop corrections to this 3-point propagator (vertex) are shown on Fig. 3.4.

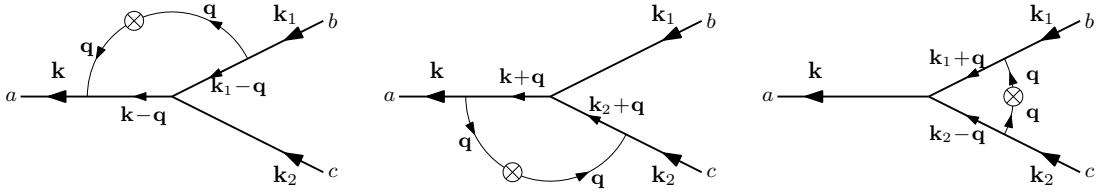

Figure 3.4: Diagrammatic representation of the different 1-loop corrections to the non-linear vertex $\Gamma^{(2)}_{abc}(\mathbf{k}_1, \mathbf{k}_2; \eta, \eta')$.

3.5 Renormalised perturbation theory

In the previous section, we introduced the non-linear propagator G_{ab} and generalised it to the non-linear $(n+1)$-point propagator $\Gamma^{(n)}_{ab_1\cdots b_n}$. Those are the fundamental building blocks of renormalized perturbation theory (RPT). In RPT the same game is played as in Sec. 3.3, but the linear propagator g_{ab} and vertex γ_{abc} are replaced by their non-linear counterparts G_{ab} and $\Gamma^{(2)}_{abc}$. Unfortunately, only the formal definitions, and not the exact expressions, have been disclosed in the previous section. In a certain limit (to be specified below), Crocce and Scoccimarro succeeded in computing the exact expression of the non-linear propagator [15]. This result was later extended by Bernardeau *et al.* to all non-linear $(n+1)$-point propagators in [16].

The bottom line of their calculation resorts on writing the non-linear propagator as

$$G_{ab}(\mathbf{k}, \eta, \eta_0) = g_{ab}(\eta, \eta_0) + \sum_{n=2}^{\infty} \left\langle \frac{\partial \Psi_a^{(n)}(\mathbf{k}, \eta)}{\partial \Psi_b(\mathbf{k}, \eta_0)} \right\rangle. \tag{3.31}$$

In this way, the non-linear corrections can be thought of as memory effects.

The summation of all terms corresponds to the summation of an infinite number of diagrams. In [15], only a specific subset was resummed. To better specify this subset, we need to introduce the concept of *principal line*. The principal line of a diagram is the only

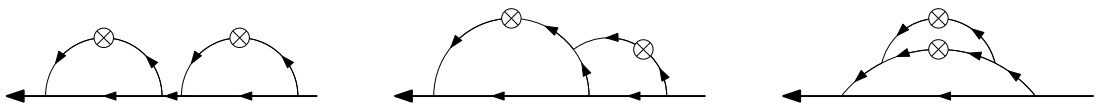

Figure 3.5: Diagrammatic representation of three different 2-loop corrections of the non-linear propagator. The principal line is the thicker line.

line going from right to left without crossing any initial power spectrum. This concept can be generalised to *principal tree* in diagrams with multiple initial fields.
On Fig. 3.5, three different 2-loop diagrams are shown. We see that the leftmost diagram has 4 vertices on the principal line, the middle one 3, and the rightmost 2. In [15], it is argued that the dominant contributions come from the diagrams with the most vertices on the principal line. Therefore, at 2 loops, only the diagrams shown on Fig. 3.6 are taken into account.

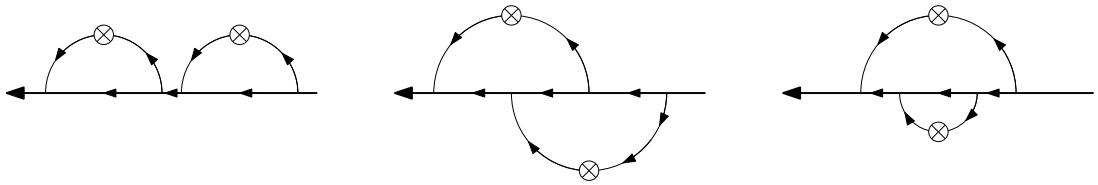

Figure 3.6: Diagrammatic representation of three dominant 2-loop corrections of the non-linear propagator.

Focussing on the high-k limit and assuming that the initial conditions follow a Gaussian distribution and are in the growing mode, it is shown that the fully resummed propagator is given by

$$G_{ab}(\mathbf{k},\eta,\eta_0) = g_{ab}(\eta,\eta_0)\exp\left[-k^2\sigma_{\rm d}^2(e^{\eta}-e^{\eta_0})^2/2\right], \tag{3.32}$$

where $\sigma_{\rm d}^2$ is the variance of the displacement field, defined as

$$\sigma_{\rm d}^2 \equiv \frac{1}{3}\int {\rm d}^3\mathbf{q}\frac{P_0(q)}{q^2}. \tag{3.33}$$

It was later shown in [16] that the same exponential cut-off appears for $(n+1)$-point propagators,

$$\Gamma^{(n)}_{ab_1\ldots b_n}(\mathbf{k}_1,\ldots,\mathbf{k}_n;\eta,\eta_0) = \Gamma^{(n)-{\rm tree}}_{ab_1\ldots b_n}(\mathbf{k}_1,\ldots,\mathbf{k}_n;\eta,\eta_0)\exp\left[-k^2\sigma_{\rm d}^2(e^{\eta}-e^{\eta_0})^2/2\right] \tag{3.34}$$

where $\Gamma^{(n)-{\rm tree}}_{ab_1\ldots b_n}(\mathbf{k}_1,\ldots,\mathbf{k}_n;\eta,\eta_0)$ is the corresponding propagator computed at tree level.

Obtaining these results by brute force resummation was a real tour de force. In the next Part, starting on page 45, we will show how the eikonal approximation can be used to obtain and generalise those results in a more transparent way.

3.6 Other approaches

Renormalised perturbation theory is not the only technique to extend non-linear perturbation theory. In this section, we will briefly describe three other approaches: the time renormalisation group approach by Pietroni and Lesgourgues [18, 19, 20], closure theory by Taruya *et al.* [21, 22] and Langrangian perturbation theory by (amongst others) Matsubara and Valageas [23, 24, 25].

3.6.1 Time renormalisation group

In the time renormalisation group approach (TRG) [18, 19, 20], one uses eq. (3.10) to find a time evolution equation for the power spectrum P_{ab}. In a first place, we define (equal time) higher order correlators of Ψ_a, like the bispectrum B_{abc} and the trispectrum T_{abcd},

$$\langle \Psi_a(\mathbf{k}_1)\Psi_b(\mathbf{k}_2)\Psi_c(\mathbf{k}_3)\rangle = \delta_{\rm D}(\mathbf{k}_1+\mathbf{k}_2+\mathbf{k}_3)B_{abc}(\mathbf{k}_1,\mathbf{k}_2,\mathbf{k}_3), \tag{3.35}$$

$$\langle \Psi_a(\mathbf{k}_1)\Psi_b(\mathbf{k}_2)\Psi_c(\mathbf{k}_3)\Psi_d(\mathbf{k}_4)\rangle = T_{abcd}(\mathbf{k}_1,\mathbf{k}_2,\mathbf{k}_3,\mathbf{k}_4). \tag{3.36}$$

The trispectrum $T_{abcd}(\mathbf{k}_1,\mathbf{k}_2,\mathbf{k}_3,\mathbf{k}_4)$ can be decomposed into its connected and three disconnected parts as

$$T_{abcd}(\mathbf{k}_1,\mathbf{k}_2,\mathbf{k}_3,\mathbf{k}_4) = \delta_{\rm D}(\mathbf{k}_1+\mathbf{k}_2+\mathbf{k}_3+\mathbf{k}_4)T^{\rm c}_{abcd}(\mathbf{k}_1,\mathbf{k}_2,\mathbf{k}_3,\mathbf{k}_4) \tag{3.37}$$

$$+\,\delta_{\rm D}(\mathbf{k}_1+\mathbf{k}_4)\delta_{\rm D}(\mathbf{k}_2+\mathbf{k}_3)P_{ad}(\mathbf{k}_1)P_{bc}(\mathbf{k}_2) \tag{3.38}$$

$$+\,\delta_{\rm D}(\mathbf{k}_1+\mathbf{k}_2)\delta_{\rm D}(\mathbf{k}_3+\mathbf{k}_4)P_{ab}(\mathbf{k}_1)P_{cd}(\mathbf{k}_2) \tag{3.39}$$

$$+\,\delta_{\rm D}(\mathbf{k}_1+\mathbf{k}_3)\delta_{\rm D}(\mathbf{k}_2+\mathbf{k}_4)P_{ac}(\mathbf{k}_1)P_{bd}(\mathbf{k}_2), \tag{3.40}$$

as displayed on Fig. 3.7. In the TRG approach, one assumes a vanishing connected part, $T^{\rm c}_{abcd}(\mathbf{k}_1,\mathbf{k}_2,\mathbf{k}_3,\mathbf{k}_4)=0$. This allows to close the system of equations we derive hereafter.

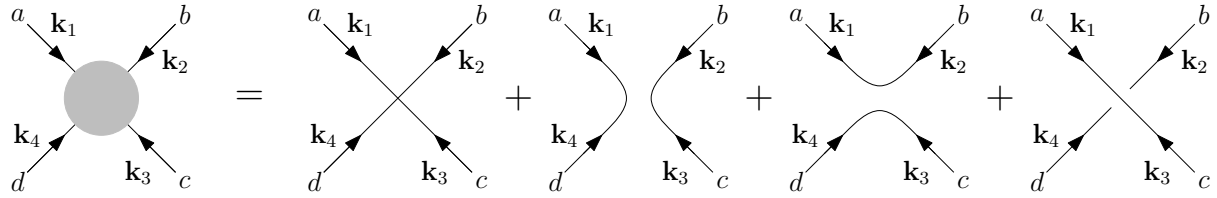

$$T_{abcd}(\mathbf{k}_1,\mathbf{k}_2,\mathbf{k}_3,\mathbf{k}_4) = T^{\rm c}_{abcd}(\mathbf{k}_1,\mathbf{k}_2,\mathbf{k}_3,\mathbf{k}_4) + P_{ad}(\mathbf{k}_1)P_{bc}(\mathbf{k}_2) + P_{ab}(\mathbf{k}_1)P_{cd}(\mathbf{k}_3) + P_{ac}(\mathbf{k}_1)P_{bd}(\mathbf{k}_2)$$

Figure 3.7: Decomposition of the trispectrum $T_{abcd}(\mathbf{k}_1,\mathbf{k}_2,\mathbf{k}_3,\mathbf{k}_4)$ into its connected and three disconnected parts. The $\delta_{\rm D}$-functions have been omitted to avoid clutter.

The time derivative of the power spectrum P_{ab} can be found by plugging eq. (3.10) into $\frac{\partial}{\partial\eta}\langle\Psi_a\Psi_b\rangle$, giving

$$\frac{\partial}{\partial\eta}\langle\Psi_a\Psi_b\rangle = -\Omega_{ad}\langle\Psi_d\Psi_b\rangle + \gamma_{ade}\langle\Psi_d\Psi_e\Psi_b\rangle + \{a\leftrightarrow b\}, \tag{3.41}$$

where the k-dependence has been omitted. Therefore we have that (symbolically)

$$\frac{\partial}{\partial\eta}P = -\Omega P + \gamma B. \tag{3.42}$$

Likewise, we find for the time derivative of the bispectrum B_{abc}, neglecting the connected part of the trispectrum,

$$\frac{\partial}{\partial\eta}B = -\Omega B + \gamma PP. \tag{3.43}$$

Assuming known initial conditions for the power spectrum and the bispectrum (often taken to be zero at early times), these two equations can be solved numerically to find P_{ab} and B_{abc} for any time η. This is the essence of the TRG approach.

3.6.2 Closure theory

Closure theory [21, 22] bears some resemblance with the TRG approach. In both theories, the equations of motion are written in terms of the correlation functions, and not in terms of the fields. In the TRG approach, the infinite hierarchy of equations is truncated by assuming that the connected part of the trispectrum vanishes, $T^{\rm c}_{abcd}(\mathbf{k}_1,\mathbf{k}_2,\mathbf{k}_3,\mathbf{k}_4)=0$, whereas in the closure theory advocated by Taruya *et al.*, the system is closed by borrowing techniques from the theory of turbulence. The approximation is known as the *direct-interaction approximation*. In our terminology, the bispectrum is written in terms of the equal time power spectrum $P_{ab}(\mathbf{k},\eta)$, the different time power spectrum $R_{ab}(\mathbf{k},\eta,\eta')$ defined by $R_{ab}(\mathbf{k},\eta,\eta')\delta_{\rm D}(\mathbf{k}+\mathbf{k}')\equiv\langle\Psi_a(\mathbf{k},\eta)\Psi_b(\mathbf{k}'\eta')\rangle$, and the propagator $G_{ab}(\mathbf{k},\eta,\eta')$. This results in three time evolution equations, one for $P_{ab}(\mathbf{k},\eta)$, one for $R_{ab}(\mathbf{k},\eta,\eta')$ and one for $G_{ab}(\mathbf{k},\eta,\eta')$. Symbolically, this comes down to

$$\frac{\partial}{\partial\eta}P+\Omega P = \gamma\gamma GRR+\gamma\gamma RRG, \tag{3.44}$$

$$\frac{\partial}{\partial\eta}R+\Omega R = \gamma\gamma GRR+\gamma\gamma RRG, \tag{3.45}$$

$$\frac{\partial}{\partial\eta}G+\Omega G = \gamma\gamma GRG. \tag{3.46}$$

The fact that (the r.h.s. of) the first two equations look the same is only because all the subscripts of P, Ω, γ, G and R have been removed, together with several η-integrals. The way the indices of all those terms are contracted is very different, which is also the case for the l.h.s. of these equations.

This set of integro-differential equations can then be integrated numerically. This is most easily done by means of the Born approximation.

3.6.3 Lagrangian perturbation theory

Lagrangian perturbation theory (LPT), pioneered by Buchert and Bouchet in the nineties [26, 27], has been recently reused in order to compare its power with the other approaches [23, 24, 25]. The crucial variable in LPT is not the position $\mathbf{x}$ of the particles at some time τ, but their displacement $\vec{\Psi}$ with respect to their initial position $\mathbf{q}$, i.e.

$$\mathbf{x}(\tau)=\mathbf{q}+\vec{\Psi}(\mathbf{q},\tau). \tag{3.47}$$

Notice that the initial positions $\mathbf{q}$ are comoving so that $\vec{\Psi}$ describes the displacement with respect to the Hubble flow, see Fig. 3.8. In LPT, this displacement is assumed to be small.

Conservation of energy implies that $\bar\rho(1+\delta(\mathbf{x}))\mathrm{d}^3\mathbf{x}=\bar\rho\,\mathrm{d}^3\mathbf{q}$. Physically, this is because in an overdense region the particles are closer together whence the volume element $\mathrm{d}^3\mathbf{x}$ decreases (and vice versa). This suggests that the Jacobian relating the volume elements $\mathrm{d}^3\mathbf{x}$ and $\mathrm{d}^3\mathbf{q}$ will play a crucial role in LPT. As $\partial x_i/\partial q_j=\delta_{ij}+\partial\vec{\Psi}_i/\partial q_j$, we have that

$$J(\mathbf{q},\tau)\equiv\det\left(\delta_{ij}+\frac{\partial\vec{\Psi}_i(\mathbf{q},\tau)}{\partial q_j}\right)=\frac{1}{1+\delta(\mathbf{x},\tau)}. \tag{3.48}$$

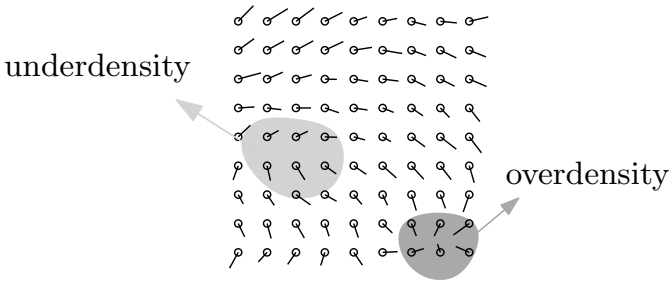

Figure 3.8: Representation of LPT. Each circle ∘ represents an initial condition $\mathbf{q}$, and each line represents the displacement vector $\vec{\Psi}(\mathbf{q})$ associated to it. Diverging displacements vectors create a local underdensity, converging ones an overdensity.

In case of shell crossing, i.e. when particles with different initial positions $\mathbf{q}$ end up in the same position $\mathbf{x}$, the Jacobian vanishes and the description breaks down. Using this Jacobian, we can rewrite the equation of motion of $\mathbf{x}$ into an equivalent equation of motion for $\vec{\Psi}$, which is then solved perturbatively.

LPT has various advantages and disadvantages compared to standard perturbation theory and resummed perturbation theory. The biggest drawback is that physical quantities depend on positions in Eulerian space, and not in Lagrangian space. Therefore, all the results (like the power spectrum) obtained in LPT need to be transformed back to Eulerian space to make predictions or compare with measurements. On the other hand LPT naturally takes into account (i.e. resums) many non-linear corrections present in Eulerian perturbation theory, making its results more precise. Another advantage is that LPT (unlike regular PT) can make predictions in redshift space. And the fact that measurements obtained with galaxy surveys are in redshift space (and not in real space) makes LPT very well suited for comparison with experimental data.

3.7 Perturbation theory with $\delta_{lm}^{(p)}$

We will now describe how perturbation theory can be done in the framework of spherical harmonics. To do so, we start with eq. (2.141). This equation contains the fully non-linear description of a fluid, and therefore it must be possible to recover the standard F_2-kernel of perturbation theory. We assume the order in perturbation theory is given by $l + p$, i.e. we take $l + p \leq 1$ for the linearised equation, and $l + p \leq 2$ for the second order perturbation.

3.7.1 Linear PT

The continuity equation is found by taking $l = p = 0$, and the Euler equation by $l = 1$, $p = 0$. The continuity equation is easily found to be

$$\frac{\partial}{\partial \eta}\epsilon_0^{(0)}(\mathbf{k}) + \epsilon_1^{(0)}(\mathbf{k}) = 0. \tag{3.49}$$

The computation of the Euler equation requires more work. The second row of eq. (2.141) cannot be neglected altogether because $\delta_{00}^{(0)} = 1+\delta$ contains a background part. Moreover,

as we assume we have just one fluid, we can use the Poisson equation to rewrite ψ in terms of $\epsilon_0^{(0)}$,

$$\psi(\mathbf{k}) = -\frac{3}{2}\frac{\mathcal{H}^2}{k^2}\tilde{\epsilon}_0^{(0)}(\mathbf{k}), \tag{3.50}$$

where $\tilde{\epsilon}_0^{(0)}(\mathbf{k}) \equiv \epsilon_0^{(0)}(\mathbf{k}) - 1 = \delta(\mathbf{k})$ is the perturbation part of $\delta_{00}^{(0)}(\mathbf{k})$. Replacing the Newtonian potential in the Euler equation and working through the computation by using the properties of ξ given by eq. (2.125) results in

$$2\frac{\partial}{\partial\eta}\delta_{1m}^{(0)}(\mathbf{k}) + \delta_{10}^{(m)}(\mathbf{k}) + 3\sqrt{3}\ \frac{k^{-m}}{k}\tilde{\epsilon}_0^{(0)}(\mathbf{k}) = 0. \tag{3.51}$$

We now take the "divergence" or this equation by means of eq. (2.142). This leads to

$$2\frac{\partial}{\partial\eta}\epsilon_1^{(0)}(\mathbf{k}) + \epsilon_1^{(0)}(\mathbf{k}) + 3\tilde{\epsilon}_0^{(0)}(\mathbf{k}) = 0. \tag{3.52}$$

Taking the derivative of the continuity equation, after replacing $\epsilon_0^{(0)}$ by $\tilde{\epsilon}_0^{(0)}$ and substituting the Euler equation into the result, gives

$$\frac{\partial^2}{\partial\eta^2}\tilde{\epsilon}_0^{(0)} + \frac{1}{2}\frac{\partial}{\partial\eta}\tilde{\epsilon}_0^{(0)} - \frac{3}{2}\tilde{\epsilon}_0^{(0)} = 0. \tag{3.53}$$

If we assume that the time dependence of $\tilde{\epsilon}_0^{(0)}$ is $\exp(\alpha\eta)$, we find the well known values $\alpha = 1$ and $\alpha = -3/2$. $\epsilon_1^{(0)}$ obviously bears the same time dependence. We will only keep the fastest growing mode, i.e. $\alpha = 1$, such that

$$\tilde{\epsilon}_0^{(0)} \propto \epsilon_1^{(0)} \propto e^{\eta}. \tag{3.54}$$

3.7.2 Second-order PT

In perturbation theory, we assume that the time dependence of second-order variables is the square of that of first-order variables. We will denote the second-order variables with hats, and these are

$$\hat{\delta}_{00}^{(0)}, \qquad \hat{\delta}_{1m}^{(0)}, \qquad \hat{\delta}_{2m}^{(0)}, \qquad \hat{\delta}_{00}^{(2)}, \tag{3.55}$$

or equivalently

$$\hat{\epsilon}_0^{(0)}, \qquad \hat{\epsilon}_1^{(0)} \qquad \hat{\epsilon}_2^{(0)}, \qquad \hat{\epsilon}_0^{(2)}, \tag{3.56}$$

These are all assumed to have $e^{2\eta}$ as time dependence.

The F_2-kernel is defined through

$$\hat{\epsilon}_0^{(0)}(\mathbf{k}) = F_2(\mathbf{k};\mathbf{k}_1,\mathbf{k}_2)\ \tilde{\epsilon}_0^{(0)}(\mathbf{k}_1)\ \tilde{\epsilon}_0^{(0)}(\mathbf{k}_2) \tag{3.57}$$

and describes how the second-order density perturbation depends on the first-order density perturbation.

By only keeping the second-order terms in the Boltzmann equation with $l = p = 0$, we straightforwardly find

$$2\hat{\epsilon}_0^{(0)} + \hat{\epsilon}_1^{(0)} = 0, \tag{3.58}$$

so we see that we need to know $\hat{\epsilon}_1^{(0)}$ in order to find F_2. $\hat{\epsilon}_1^{(0)}$ can be found by keeping the second-order terms in the Boltzmann equation with $l = 1$ and $p = 0$. The result, after taking the divergence, is

$$\frac{5}{2}\hat{\epsilon}_1^{(0)} + \frac{1}{3}\hat{\epsilon}_0^{(2)} + \frac{k^m}{k}\xi_{0\,0}^{1\,m}\frac{k^{\Delta m}}{k}\xi_{1\,m}^{1\,\Delta m}\hat{\delta}_{2,m+\Delta m}^{(0)} + \frac{3}{2}\frac{\mathbf{k}\cdot\mathbf{k}_2}{k_2^2}\tilde{\epsilon}_0^{(0)}(\mathbf{k}_1)\ \tilde{\epsilon}_0^{(0)}(\mathbf{k}_2) + \frac{3}{2}\hat{\epsilon}_0^{(0)} = 0. \quad (3.59)$$

This result introduces two yet unknown quantities, $\hat{\epsilon}_1^{(0)}$ and $\hat{\delta}_{2,m+\Delta m}^{(0)}$. The first one can be found by computing the Boltzmann equation with $l = 0$ and $p = 2$, giving

$$\hat{\delta}_{00}^{(2)} + \frac{k^2}{k_1^2}\frac{k_1 k_2^{\Delta m}}{k_2^2}\xi_{0\,0}^{1\,\Delta m}\ \delta_{1,\Delta m}^{(0)}(\mathbf{k}_1)\ \tilde{\epsilon}_0^{(0)}(\mathbf{k}_2) = 0. \quad (3.60)$$

In this equation, we replace $\delta_{1,\Delta m}^{(0)}(\mathbf{k}_1)$ by using eq. (3.51). Performing the summation on Δm results in

$$\hat{\epsilon}_0^{(2)} = \frac{k^2(\mathbf{k}_1\cdot\mathbf{k}_2)}{k_1^2 k_2^2}\ \tilde{\epsilon}_0^{(0)}(\mathbf{k}_1)\ \tilde{\epsilon}_0^{(0)}(\mathbf{k}_2). \quad (3.61)$$

The term $\hat{\delta}_{2,m+\Delta m}^{(0)}$ requires the same reasoning, together with the not so trivial relation

$$\frac{5}{2}\sqrt{3}\ k^m\ \xi_{0\,0}^{1\,m}\ k^{m_1}\ \xi_{1\,m}^{1\,m_1}\ k_2^{m_2}\ \xi_{2\,m+m_1}^{-1\,m_2}\ k_1^{-(m+m_1+m_2)} = (\mathbf{k}_1\cdot\mathbf{k})(\mathbf{k}_2\cdot\mathbf{k}) - \frac{k^2(\mathbf{k}_1\cdot\mathbf{k}_2)}{3} \quad (3.62)$$

yielding

$$\frac{k^m}{k}\xi_{0\,0}^{1\,m}\frac{k^{\Delta m}}{k}\xi_{1\,m}^{1\,\Delta m}\hat{\delta}_{2,m+\Delta m}^{(0)} = \frac{1}{k_1^2 k_2^2}\left((\mathbf{k}_1\cdot\mathbf{k})(\mathbf{k}_2\cdot\mathbf{k}) - \frac{k^2(\mathbf{k}_1\cdot\mathbf{k}_2)}{3}\right)\tilde{\epsilon}_0^{(0)}(\mathbf{k}_1)\ \tilde{\epsilon}_0^{(0)}(\mathbf{k}_2). \quad (3.63)$$

By combining all the results found above, we have that the Euler equation reduces to

$$\frac{5}{2}\hat{\epsilon}_1^{(0)} + \frac{3}{2}\hat{\epsilon}_0^{(0)} + \left(\frac{(\mathbf{k}_1\cdot\mathbf{k})(\mathbf{k}_2\cdot\mathbf{k})}{k_1^2 k_2^2} + \frac{3}{2}\frac{\mathbf{k}\cdot\mathbf{k}_2}{k_2^2}\right)\tilde{\epsilon}_0^{(0)}(\mathbf{k}_1)\ \tilde{\epsilon}_0^{(0)}(\mathbf{k}_2) = 0. \quad (3.64)$$

F_2 can be solved for by combining this Euler equation with the continuity equation found above, giving

$$F_2(\mathbf{k};\mathbf{k}_1,\mathbf{k}_2) = \frac{2}{7}\left(\frac{(\mathbf{k}_1\cdot\mathbf{k})(\mathbf{k}_2\cdot\mathbf{k})}{k_1^2 k_2^2} + \frac{3}{2}\frac{\mathbf{k}\cdot\mathbf{k}_2}{k_2^2}\right). \quad (3.65)$$

We can rewrite this into the more familiar form by using that $\mathbf{k} = \mathbf{k}_1 + \mathbf{k}_2$, defining $\mu \equiv \dfrac{\mathbf{k}_1\cdot\mathbf{k}_2}{k_1 k_2}$ and symmetrising, giving

$$\boxed{F_2(\mathbf{k}_1,\mathbf{k}_2) = \frac{5}{7} + \frac{1}{2}\left(\frac{k_1}{k_2} + \frac{k_2}{k_1}\right)\mu + \frac{2}{7}\mu^2,} \quad (3.66)$$

which exactly corresponds to eq. (3.22). This shows that the framework of perturbation theory can perfectly be applied in the context of spherical harmonics.

3.8 Conclusion

In this chapter, we introduced the framework of cosmological perturbation theory. In the first place, we analysed the linear equations and showed how a single fluid system has both a growing and a decaying mode. Next, we incorporated the non-linear interaction terms and showed how these are dealt with in standard perturbation theory. We then showed how various techniques (like RPT) manage to do better than SPT, for example by resumming manually an infinite class of corrections. Finally, we proved that, though it might have seemed improbable due to its complexity, perturbation theory can also be performed in the context of spherical harmonics.

Part B

The eikonal approximation

Chapter 4

Single-component fluid

Contents

In this Part, we will show how the results found previously using renormalized perturbation theory (see Sec. 3.5 on page 37) can be recovered using a novel technique dubbed the *eikonal* approximation. In this chapter, we will disclose the derivation in the case of a universe filled with a single fluid.

4.1 Equations of motion

When we introduced the equations of motion (3.8), we assumed the Universe to be filled with just one cold pressureless fluid. We will now extend this to a Universe with only one cold pressureless fluid *and* a cosmological constant, i.e. $\Omega_m + \Omega_\Lambda = 1$. This model is known as ΛCDM and it agrees extremely well with observations. In this case, the Poisson equation on subhorizon scales given by eq. (3.1) gets changed to

$$\psi(\mathbf{k}) = -\frac{3}{2}\Omega_m \frac{\mathcal{H}^2}{k^2}\delta(\mathbf{k}). \tag{4.1}$$

Combining the Euler and continuity equations given by eqs. (3.3) into a second-order equation for δ like we did in eq. (3.5) gives the more general

$$\ddot{\delta}^{(1)} + \mathcal{H}\dot{\delta}^{(1)} - \frac{3}{2}\Omega_m \mathcal{H}^2 \delta^{(1)} = 0. \tag{4.2}$$

Unlike in the CDM case, this cannot be solved in terms of simple powers of a. To proceed, we *define* the two solutions to this second-order equation as D_+ and D_-, and write the general solution to the equation as

$$\delta^{(1)}(\mathbf{k}, \tau) \equiv D_+(\tau)\delta_+^{(1)}(\mathbf{k}) + D_-(\tau)\delta_-^{(1)}(\mathbf{k}) \tag{4.3}$$

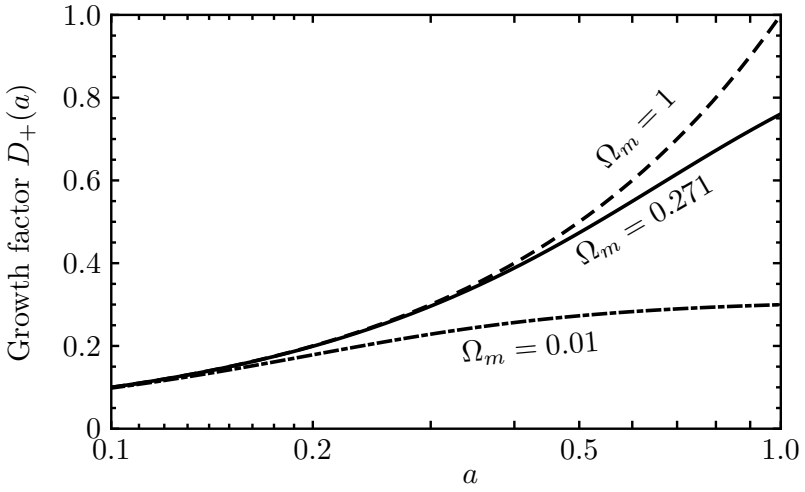

Figure 4.1: The growth factor $D_+(a)$ for three different ΛCDM-cosmologies. In each case, $\Omega_m + \Omega_\Lambda = 1$. The top line, with $\Omega_\Lambda = 0$, corresponds to EdS spacetime, while the middle line, with $\Omega_m = 0.271$, corresponds to our Universe.

where D_+ is the fastest growing mode, and $\delta_+^{(1)}(\mathbf{k})$ and $\delta_-^{(1)}(\mathbf{k})$ are the initial conditions. Using that $\mathrm{d}(\mathcal{H}/a)/\mathrm{d}\tau = -4\pi G a \rho_m = -(3/2)\Omega_m H_0^2/a^{-2}$ in ΛCDM (see eq. (1.2)), it is easy to show that

$$D_- = H_0^{-1}\frac{\mathcal{H}}{a}, \tag{4.4}$$

satisfies eq. (4.2). The growing mode D_+ admits the integral representation

$$D_+ = H_0^2 \frac{\mathcal{H}}{a}\frac{5\Omega_m}{2}\int_0^a \frac{\mathrm{d}\tilde{a}}{\mathcal{H}^3(\tilde{a})} \tag{4.5}$$

where $\mathcal{H}(a) = H_0\sqrt{\Omega_m/a + \Omega_\Lambda a^2}$. The prefactor of D_+ is chosen such that at early times, the EdS results, i.e. $D_+ = a$ and $D_- = a^{-3/2}$ are recovered. On Fig. 4.1 the growth factor D_+ has been shown for three different cosmologies: EdS, our Universe and a universe dominated by a cosmological constant. One can see that a cosmological constant damps the growth of perturbations.

Differentiating eq. (4.3) and defining the growth rates $f_\pm \equiv \mathrm{d}\ln D_\pm/\mathrm{d}\ln a$ we find that the first-order velocity divergence $\theta^{(1)}$ satisfies

$$\frac{\theta^{(1)}(\mathbf{k},\tau)}{\mathcal{H}} = -f_+(\tau)D_+(\tau)\delta_+^{(1)}(\mathbf{k}) - f_-(\tau)D_-(\tau)\delta_-^{(1)}(\mathbf{k}). \tag{4.6}$$

The growth rates can be straightforwardly computed, giving

$$f_- = -\frac{3}{2}\Omega_m\frac{H_0^2}{\mathcal{H}^2 a} \qquad \text{and} \qquad f_+ = -\frac{3}{2}\Omega_m\frac{H_0^2}{\mathcal{H}^2 a}\left(1 - \frac{5}{3}\frac{a}{D_+}\right). \tag{4.7}$$

Notice that in EdS spacetime, $f_+ = 1$. We will now redefine the time variable η and the variable Θ. They used to be $\eta = \ln a$ and $\Theta = -\theta/\mathcal{H}$, and we generalise them now to $\eta \equiv \ln D_+$ and $\Theta \equiv -\theta/(\mathcal{H}f_+)$. By means of these new definitions, we can generalise

eq. (3.8) to

$$\left\{\begin{array}{rcl} \dfrac{\partial}{\partial\eta}\delta(\mathbf{k}) - \Theta(\mathbf{k}) &=& \alpha(\mathbf{k}_1,\mathbf{k}_2)\;\Theta(\mathbf{k}_1)\;\delta(\mathbf{k}_2) \\ \dfrac{\partial}{\partial\eta}\Theta(\mathbf{k}) + \left(\dfrac{3}{2}\dfrac{\Omega_m}{f_+^2} - 1\right)\Theta(\mathbf{k}) - \dfrac{3}{2}\dfrac{\Omega_m}{f_+^2}\delta(\mathbf{k}) &=& \beta(\mathbf{k}_1,\mathbf{k}_2)\;\Theta(\mathbf{k}_1)\;\Theta(\mathbf{k}_2). \end{array}\right. \tag{4.8}$$

We again define $\Psi_a \equiv (\delta, \Theta)^T$ and by combining eqs. (4.3) and (4.6), we see that the linear growing mode still is proportional to $\Psi_a^{(1)} \propto (1,1)^T$, but the decaying mode is now proportional to $\Psi_a^{(1)} \propto (1, f_-/f_+)^T$.

The equations of motion (4.8) can still be written as

$$\frac{\partial}{\partial\eta}\Psi_a(\mathbf{k}) + \Omega_{ab}\,\Psi_b(\mathbf{k}) = \gamma_{abc}(\mathbf{k},\mathbf{k}_1,\mathbf{k}_2)\Psi_b(\mathbf{k}_1)\Psi_c(\mathbf{k}_2), \tag{4.9}$$

but the matrix Ω_{ab} is now time-dependent and is given by

$$\Omega_{ab} = \begin{pmatrix} 0 & -1 \\ -\dfrac{3}{2}\dfrac{\Omega_m}{f_+^2} & \dfrac{3}{2}\dfrac{\Omega_m}{f_+^2} - 1 \end{pmatrix}. \tag{4.10}$$

We can still define a linear propagator $g_{ab}(\eta,\eta_0)$ through

$$\frac{\partial}{\partial\eta}g_{ab}(\eta,\eta_0) + \Omega_{ac}(\eta)g_{cb}(\eta,\eta_0) = 0, \tag{4.11}$$

but the integral representation of the equations of motion, given by eq. (3.16), is not exact any more. However, doing cosmological perturbation theory with the integral representation eq. (3.16) but using as time variable $\eta = \ln D_+$ gives results that are correct to a good approximation [12, 15]. Therefore, we will assume from now on that we can go from the differential representation like eq. (4.9) to the integral representation like eq. (3.16), whether Ω_{ab} is time-independent or not.

4.2 Separation of scales

The eikonal approximation describes how small-scale modes are affected by large-scale modes. This means that we will focus our attention to the large-k limit of the equations of motion described above.

Eq. (4.9) is the starting point for the eikonal approximation. On the r.h.s. the convolution is implicit, i.e.

$$\gamma_{abc}(\mathbf{k},\mathbf{k}_1,\mathbf{k}_2)\Psi_b(\mathbf{k}_1)\Psi_c(\mathbf{k}_2) = \int_{\mathcal{D}} \mathrm{d}^3\mathbf{k}_1\mathrm{d}^3\mathbf{k}_2\delta_{\mathrm{D}}(\mathbf{k}-\mathbf{k}_1-\mathbf{k}_2)\gamma_{abc}(\mathbf{k},\mathbf{k}_1,\mathbf{k}_2)\Psi_b(\mathbf{k}_1)\Psi_c(\mathbf{k}_2) \tag{4.12}$$

The domain of integration $\mathcal{D}$ is twice $\mathbb{R}^3$, and we will split it into two subsets, $\mathcal{D} = \mathcal{S}\cup\mathcal{H}$, where $\mathcal{H}$ is not to be confused with the conformal Hubble rate. The subset $\mathcal{S}$ contains the modes of very different amplitude, i.e. modes for which $k_1 \ll k_2$ or $k_2 \ll k_1$. Notice that as $\mathbf{k} = \mathbf{k}_1 + \mathbf{k}_2$, if $k_1 \ll k_2$, then $k_2 \simeq k$ and vice versa, whence $k_1 \ll k$ or $k_2 \ll k$. We will call these modes the "$\mathcal{S}$oft" modes. On the other hand, the subset $\mathcal{H}$ contains

the remaining modes, i.e. the modes for which $k_1 \simeq k_2$. In this case, $k_1 \simeq k_2 \gtrsim k$, and we will call these modes the "$\mathcal{H}$ard" modes. We therefore write

$$\begin{aligned}\gamma_{abc}(\mathbf{k},\mathbf{k}_1,\mathbf{k}_2)\Psi_b(\mathbf{k}_1)\Psi_c(\mathbf{k}_2) = \\ [\gamma_{abc}(\mathbf{k},\mathbf{k}_1,\mathbf{k}_2)\Psi_b(\mathbf{k}_1)\Psi_c(\mathbf{k}_2)]_{\mathcal{S}} + [\gamma_{abc}(\mathbf{k},\mathbf{k}_1,\mathbf{k}_2)\Psi_b(\mathbf{k}_1)\Psi_c(\mathbf{k}_2)]_{\mathcal{H}}\end{aligned} \tag{4.13}$$

where $[\cdots]_{\mathcal{S}}$ denotes a convolution limited to $\mathcal{S}$, and similarly for $\mathcal{H}$. We will focus our attention to the $\mathcal{S}$-convolution. As $k_1 \ll k$ and $k_2 \simeq k$, or $k_2 \ll k$ and $k_1 \simeq k$, we can approximate it as

$$\begin{aligned}[\gamma_{abc}(\mathbf{k},\mathbf{k}_1,\mathbf{k}_2)\Psi_b(\mathbf{k}_1)\Psi_c(\mathbf{k}_2)]_{\mathcal{S}} \approx \\ \int_{q\ll k} \mathrm{d}^3\mathbf{q}\ \gamma_{abc}(\mathbf{k},\mathbf{q},\mathbf{k})\Psi_b(\mathbf{q})\Psi_c(\mathbf{k}) + \int_{q\ll k} \mathrm{d}^3\mathbf{q}\ \gamma_{abc}(\mathbf{k},\mathbf{k},\mathbf{q})\Psi_b(\mathbf{k})\Psi_c(\mathbf{q}).\end{aligned} \tag{4.14}$$

Because $\gamma_{abc}(\mathbf{k},\mathbf{k}_1,\mathbf{k}_2) = \gamma_{acb}(\mathbf{k},\mathbf{k}_2,\mathbf{k}_1)$, we can simplify this to

$$[\gamma_{abc}(\mathbf{k},\mathbf{k}_1,\mathbf{k}_2)\Psi_b(\mathbf{k}_1)\Psi_c(\mathbf{k}_2)]_{\mathcal{S}} \approx \left(2\int_{q\ll k} \mathrm{d}^3\mathbf{q}\ \gamma_{abc}(\mathbf{k},\mathbf{k},\mathbf{q})\Psi_c(\mathbf{q})\right)\Psi_b(\mathbf{k}). \tag{4.15}$$

Defining the quantity between the parentheses as

$$\Xi_{ab}(\mathbf{k},\eta) \equiv 2\int_{q\ll k} \mathrm{d}^3\mathbf{q}\ \gamma_{abc}(\mathbf{k},\mathbf{k},\mathbf{q})\Psi_c(\mathbf{q},\eta), \tag{4.16}$$

where the η-dependence of $\Psi(\mathbf{q},\eta)$ has been reintroduced to emphasise the time-dependence of Ξ_{ab}, we rewrite the equation of motion eq. (4.9) in the form

$$\frac{\partial}{\partial\eta}\Psi_a(\mathbf{k}) + \Omega_{ab}\,\Psi_b(\mathbf{k}) = \Xi_{ab}(\mathbf{k})\Psi_b(\mathbf{k}) + [\gamma_{abc}(\mathbf{k},\mathbf{k}_1,\mathbf{k}_2)\Psi_b(\mathbf{k}_1)\Psi_c(\mathbf{k}_2)]_{\mathcal{H}}\,. \tag{4.17}$$

In the limit of separation of scales, $\Xi_{ab}(\mathbf{k},\eta)$ does not depend on $\Psi(\mathbf{k},\eta)$ because in this limit we assume that modes of very different sizes (like $\mathbf{q}$ and $\mathbf{k}$) do not talk to each other. Therefore, $\Xi_{ab}(\mathbf{k},\eta)$ only depends on the initial conditions. And as the initial conditions are assumed to be random variables, Ξ_{ab} is also a random variable. In any case, as it is not an interaction term any more, we can rewrite the equation above in the fully equivalent form

$$\boxed{\frac{\partial}{\partial\eta}\Psi_a(\mathbf{k}) + \Omega_{ab}\,\Psi_b(\mathbf{k}) - \Xi_{ab}(\mathbf{k})\Psi_b(\mathbf{k}) = [\gamma_{abc}(\mathbf{k},\mathbf{k}_1,\mathbf{k}_2)\Psi_b(\mathbf{k}_1)\Psi_c(\mathbf{k}_2)]_{\mathcal{H}}\,.} \tag{4.18}$$

4.3 Resummed propagator

The equation above describes a "new" theory, for which we can define a linear propagator ξ_{ab} through

$$\frac{\partial}{\partial\eta}\xi_{ab}(\mathbf{k},\eta,\eta_0) + \big(\Omega_{ac}(\eta) - \Xi_{ac}(\mathbf{k},\eta)\big)\xi_{cb}(\mathbf{k},\eta,\eta_0) = 0. \tag{4.19}$$

We call this new propagator ξ_{ab} the resummed propagator. Notice that as ξ_{ab} depends on Ξ_{ab}, it is also a random variable. Nevertheless, we can translate the equation of motion in its differential representation eq. (4.18) to the integral representation

$$\begin{aligned}\Psi_a(\mathbf{k},\eta) = &\xi_{ab}(\eta,\eta_0)\Psi_b(\mathbf{k},\eta_0) \\ &+ \int_{\eta_0}^{\eta} \mathrm{d}\tilde{\eta}\ \xi_{ab}(\eta,\tilde{\eta})\,[\gamma_{bde}(\mathbf{k},\mathbf{k}_1,\mathbf{k}_2)\Psi_d(\mathbf{k}_1,\tilde{\eta})\Psi_e(\mathbf{k}_2,\tilde{\eta})]_{\mathcal{H}}\,.\end{aligned} \tag{4.20}$$

The question is now how this resummed propagator is related to the non-linear propagator G_{ab} defined in eq. (3.27). In the large-k limit we are considering, the r.h.s. of eq. (4.18) is irrelevant as in this limit $\mathcal{H} \to \varnothing$. Therefore, all the non-linear effects are incorporated in Ξ_{ab} whence ξ_{ab} is closely related to G_{ab}, the only difference being that ξ_{ab} is still dependent on the random variable Ξ. We can therefore recover G_{ab} out of ξ_{ab} by averaging out the random variable Ξ, i.e.

$$G_{ab}(k,\eta,\eta_0) = \left\langle \xi_{ab}(\mathbf{k},\eta,\eta_0) \right\rangle_{\Xi}. \tag{4.21}$$

Even if this equation seems powerful, we have not yet computed what Ξ_{ab} and ξ_{ab} actually are, such that this equation is quite useless so far. Fortunately, in the single-fluid case we are considering in this chapter, Ξ_{ab} and ξ_{ab} explicitly can be written down.

In the definition of Ξ_{ab}, eq. (4.16), we need $\gamma_{abc}(\mathbf{k},\mathbf{k},\mathbf{q})$ with $q \ll k$. But the mode coupling functions $\alpha(\mathbf{k}_1,\mathbf{k}_2)$ and $\beta(\mathbf{k}_1,\mathbf{k}_2)$, defined in eq. (3.4), simplify in this limit to

$$\alpha(\mathbf{q},\mathbf{k}) \approx \frac{\mathbf{q}\cdot\mathbf{k}}{q^2}, \qquad \alpha(\mathbf{k},\mathbf{q}) \approx 0 \qquad \text{and} \qquad \beta(\mathbf{k},\mathbf{q}) = \beta(\mathbf{q},\mathbf{k}) \approx \frac{\mathbf{q}\cdot\mathbf{k}}{2q^2}, \tag{4.22}$$

such that

$$\Xi_{ab}(\mathbf{k},\eta) = \left(\int_{q\ll k} \mathrm{d}^3\mathbf{q} \frac{\mathbf{k}\cdot\mathbf{q}}{q^2} \Theta(\mathbf{q},\eta) \right) \delta_{ab} \equiv \Xi(\mathbf{k},\eta)\delta_{ab}. \tag{4.23}$$

We can therefore rewrite eq. (4.19) as

$$\left(\frac{\partial}{\partial\eta} - \Xi(\mathbf{k},\eta) \right) \xi_{ab}(\mathbf{k},\eta,\eta_0) + \Omega_{ac}(\eta)\xi_{cb}(\mathbf{k},\eta,\eta_0) = 0, \tag{4.24}$$

which is easily solved as we know that g_{ab} is the solution to this equation when $\Xi = 0$. The result is

$$\xi_{ab}(\mathbf{k},\eta,\eta_0) = g_{ab}(\eta,\eta_0) \exp\left[\int_{\eta_0}^{\eta} \mathrm{d}\tilde{\eta}\ \Xi(\mathbf{k},\tilde{\eta}) \right]. \tag{4.25}$$

We need not assume here that the initial conditions are in the growing mode. But if we do so, and add the assumption that the initial conditions follow a Gaussian distribution, it is straightforward to recover eq. (3.32). For the details, I refer to section II.C of our article starting on page 57 of this thesis.

Chapter 5

Multi-component fluids

Contents

Until now, we have assumed that the matter in the Universe is composed of only one fluid. But on page 7, it was said that the matter is composed of baryons (17%) and CDM (83%). And even if treating them as one fluid gives accurate results, we need to drop this assumption to significantly improve accuracy.

The reason why baryons and CDM should not be considered as one fluid is that they have a very different history. CDM moved freely on geodesics for almost its entire history. Baryons on the other hand, being charged particles, were tightly coupled to photons via Thomson scattering until recombination at $z \sim 1000$. This has a clear effect on the power spectrum, and these "baryon acoustic oscillations" (BAOs) have been accurately measured, see e.g. [28] and references therein.

In this chapter, we will redo the derivation of the previous chapter, but in the framework of multi-component fluids.

5.1 Equations of motion

Each fluid α has its own density ρ_α, density perturbation δ_α and velocity divergence Θ_α. The total matter density ρ_m is then given by $\rho_m = \sum \rho_\alpha$ and we define the total density contrast δ_m through

$$\rho_m = (1+\delta_m)\bar{\rho}_m = (1+\delta_m)\sum \bar{\rho}_\alpha \qquad \text{such that} \qquad \delta_m = \sum f_\alpha \delta_\alpha, \tag{5.1}$$

where f_α denotes the fractional contribution of fluid α to the total matter density, i.e. $f_\alpha \equiv \bar{\rho}_\alpha/\bar{\rho}_m$. Note that $\sum f_\alpha = 1$. For each fluid, the equations of motion (3.3) are still valid,

but the Poisson equation (4.1) relates the metric perturbation ψ to the total fluid density perturbation,

$$\psi(\mathbf{k}) = -\frac{3}{2}\Omega_m \frac{\mathcal{H}^2}{k^2}\delta_m(\mathbf{k}). \tag{5.2}$$

This induces the couplings between the different fluids. To write down the equations of motion in a compact form (like e.g. eq. (3.10)), we generalise the vector Ψ_a to

$$\Psi_a = (\delta_1, \Theta_1, \ldots, \delta_n, \Theta_n)^T, \tag{5.3}$$

if the matter is composed of n distinct fluids [29]. The equation of motion in this new variable still reads

$$\frac{\partial}{\partial\eta}\Psi_a(\mathbf{k}) + \Omega_{ab}\Psi_b(\mathbf{k}) = \gamma_{abc}(\mathbf{k}, \mathbf{k}_1, \mathbf{k}_2)\Psi_b(\mathbf{k}_1)\Psi_c(\mathbf{k}_2), \tag{5.4}$$

but Ω_{ab} is not block-diagonal any more. Its elements are given by

$$\Omega_{(2p-1)(2p)} = -1, \qquad \Omega_{(2p)(2p)} = \frac{3}{2}\frac{\Omega_m}{f_+^2} - 1 \qquad \text{and} \qquad \Omega_{(2p)(2q-1)} = -\frac{3}{2}\frac{\Omega_m}{f_+^2}f_q, \tag{5.5}$$

for any integers p and q running from 1 to n. The other elements of Ω_{ab} vanish. The couplings γ_{abc} are given by

$$\begin{aligned}
\gamma_{(2p-1)\,(2p-1)\,(2p)}(\mathbf{k}, \mathbf{k}_1, \mathbf{k}_2) &= \frac{\alpha(\mathbf{k}_2, \mathbf{k}_1)}{2}, \\
\gamma_{(2p-1)\,(2p)\,(2p-1)}(\mathbf{k}, \mathbf{k}_1, \mathbf{k}_2) &= \frac{\alpha(\mathbf{k}_1, \mathbf{k}_2)}{2}, \\
\gamma_{(2p)\,(2p)\,(2p)}(\mathbf{k}, \mathbf{k}_1, \mathbf{k}_2) &= \beta(\mathbf{k}_1, \mathbf{k}_2),
\end{aligned} \tag{5.6}$$

for any integer p. It should be mentioned that these coupling terms only couple different modes of the same fluid, but do not couple different fluids.

The equation of motion (5.4) is a set of $2n$ first-order differential equations; therefore, it has $2n$ solutions. Two of them correspond to the adiabatic growing and decaying mode we found in the single-component fluid. Physically it correspond to the situation where the various fluids start comoving and, as they all follow geodesics, remain comoving; the evolution of the fluids is undistinguishable from that of a single fluid and therefore the single-fluid solutions are also solutions to the multi-component fluid equations of motion.

The eikonal approximation enables us to analyse what the impact is of the other $2n-2$ modes (named the isodensity modes) on the evolution of the fields. As the fastest growing mode is still the adiabatic growing mode, we expect this effect to be rather small at late times because the isodensity modes are supposed to have decayed away.

5.2 Resummed propagator

To apply the eikonal approximation to the multi-component fluid, we perform the same steps as in the single-fluid case. In the first place, we define Ξ_{ab} in the same way as in eq. (4.16), i.e.

$$\Xi_{ab}(\mathbf{k}, \eta) \equiv 2\int_{q\ll k} \mathrm{d}^3\mathbf{q}\; \gamma_{abc}(\mathbf{k}, \mathbf{k}, \mathbf{q})\Psi_c(\mathbf{q}, \eta). \tag{5.7}$$

Unfortunately, Ξ_{ab} does not have a simple form like in eq. (4.23), mostly because Ξ_{ab} is not proportional to δ_{ab} any more. Because of that, we were not able to explicitly solve for the nonlinear propagator ξ_{ab} like in eq. (4.25); therefore, we had to resort to limiting cases or numerical analyses.

I refer to our article starting on page 57 for more details on the data analysis. Nevertheless, how the required data was generated, is described in the next section.

5.3 Data generation

Shortly after recombination, baryons and CDM did not move together: CDM particles had been falling into the potential wells for a long time, baryons on the other hand were just released from the photon gas and had yet to begin their fall. Therefore, both adiabatic and isodensity modes existed at that time. To know how much of each mode was present, we need to compute Ψ_a at $z \sim 1000$, and we use the Boltzmann code CAMB to do so [30].

A difficulty lies in the fact that CAMB is implemented in the synchronous gauge, comoving with CDM, whence $\theta_c^{\mathrm{CAMB}} = 0$ by construction. However, the "gauge" we are working with is the longitudinal gauge for the velocity divergence, and the gauge comoving with the total matter for the density perturbation. Therefore we need to transform the results normally produced by CAMB into our variables in the various gauges. The transformations are given by[1]

$$\theta_c = \sigma k, \qquad \theta_b = \theta_b^{\mathrm{CAMB}} + \sigma k, \qquad \delta_\alpha = \delta_\alpha^{\mathrm{CAMB}} + 3\frac{\mathcal{H}}{k^2} f_b \theta_b^{\mathrm{CAMB}}, \tag{5.8}$$

where σ is the shear[2]. This is implemented by making several changes to CAMB.

To avoid tempering too much with the code, the output is extended but not modified, i.e. the existing columns of the outputted `Transfer` are kept, and new columns are added. As we have four new variables (δ_c, θ_c, δ_b and θ_b), the parameter `Transfer_max` in `modules.f90` needs to be changed from `7` to `11`, and the `write`-line in the subroutine `Transfer_SaveToFiles` present in the same file should be updated to

```
write(fileio_unit,'(11E14.6)')
```

The most important changes are needed in the subroutine `outtransf`, which can be found in the file `equations.f90`. Firstly, the `real` variable `tau` should be added to the `outtransf` parameter list. (Likewise, it has to be added the two times the subroutine is `call`ed in `cmbmain.f90`.) Declarations that need to be added are

```
use ThermoData

real(dl) z,dz,sigma
real(dl) thetaCDMl,thetabl,thetal,deltaCDMcom,deltabcom,deltatot
real(dl) a2,adotoa,etak,vb,tau,cs2,opacity,dopacity
real(dl) grhob_t,grhoc_t,grhor_t,grhog_t,grhov_t,qr,pir,qg,pig
```

These variables are needed to recover the shear `sigma` ($= \sigma$) necessary for the gauge transformations, and it is computed by copying code from the subroutine `derivs`.

[1] See Appendix C of our article for the motivation for this choice of variables, and for the derivation of these transformations.

[2] The shear σ is related to the synchronous gauge variables h_s and η_s through $\sigma = (\dot{h}_s + 6\dot{\eta}_s)/2k$ [5, 31].

```
a2=a*a
etak=y(2)

vb=y(5)

grhob_t=grhob/a
grhoc_t=grhoc/a
grhor_t=grhornomass/a2
grhog_t=grhog/a2
if (w_lam==-1._dl) then
     grhov_t=grhov*a2
else
    grhov_t=grhov*a**(-1-3*w_lam)
end if

if (EV%TightCoupling) then
     call thermo(tau,cs2,opacity,dopacity)
else
     call thermo(tau,cs2,opacity)
end if

gpres=0
grho=grhob_t+grhoc_t+grhor_t+grhog_t+grhov_t

dgrho=grhob_t*clxb+grhoc_t*clxc
dgq=grhob_t*vb

adotoa=sqrt(grho/3)

if (EV%no_nu_multpoles) then
    z=(0.5_dl*dgrho/k + etak)/adotoa
    dz= -adotoa*z - 0.5_dl*dgrho/k
    clxr=-4*dz/k
    qr=-4._dl/3*z
    pir=0
else
    clxr=y(EV%r_ix)
    qr  =y(EV%r_ix+1)
    pir =y(EV%r_ix+2)
endif

if (EV%no_phot_multpoles) then
    if (.not. EV%no_nu_multpoles) then
        z=(0.5_dl*dgrho/k + etak)/adotoa
        dz= -adotoa*z - 0.5_dl*dgrho/k
        clxg=-4*dz/k-4/k*opacity*(vb+z)
        qg=-4._dl/3*z
```

```
        else
            clxg=clxr-4/k*opacity*(vb+z)
            qg=qr
        end if
        pig=0
    else

    clxg=y(EV%g_ix)
    qg=y(EV%g_ix+1)
    if (.not. EV%TightCoupling) pig=y(EV%g_ix+2)
    end if

    dgrho=dgrho + grhog_t*clxg+grhor_t*clxr
    dgq=dgq + grhog_t*qg+grhor_t*qr

    z=(0.5_dl*dgrho/k + etak)/adotoa
    sigma=(z+1.5_dl*dgq/k2)
```

With this `sigma`, we can now apply the gauge transformation rules given by eq. (5.8).

```
    thetaCDMl=k*(sigma)
    thetabl=k*(vb+sigma)

    thetal=CP%omegac/(CP%omegac+CP%omegab)*thetaCDMl
                            +CP%omegab/(CP%omegac+CP%omegab)*thetabl

    deltaCDMcom=clxc+3*adotoa*(thetal-thetaCDMl)/k2
    deltabcom=clxb+3*adotoa*(thetal-thetaCDMl)/k2

    deltatot=CP%omegac/(CP%omegac+CP%omegab)*deltaCDMcom
                            +CP%omegab/(CP%omegac+CP%omegab)*deltabcom
```

These new variables are then exported into the enlarged vector `Arr`.

```
    Arr(8) = deltaCDMcom
    Arr(9) = deltabcom
    Arr(10) = thetaCDMl/adotoa
    Arr(11) = thetabl/adotoa
```

The factor `adotoa` ($= \mathcal{H}$) is added because in our article, θ is defined as $v^i{}_{,i}/\mathcal{H}$ and not simply as $v^i{}_{,i}$, as it is in this thesis. Apart from this factor of $\mathcal{H}$, the 8^{th}, 9^{th}, 10^{th} and 11^{th} column of the outputted data in `Transfer` are exactly Ψ_1, Ψ_3, Ψ_2 and Ψ_4 respectively.

5.4 Article: "Resummed propagators in multicomponent cosmic fluids with the *eikonal* approximation"

PHYSICAL REVIEW D **85,** 063509 (2012)

Resummed propagators in multicomponent cosmic fluids with the *eikonal* approximation

Francis Bernardeau,* Nicolas Van de Rijt,† and Filippo Vernizzi‡
Institut de Physique Théorique, CEA, IPhT, F-91191 Gif-sur-Yvette, France
CNRS, URA 2306, F-91191 Gif-sur-Yvette, France
(Received 23 September 2011; published 13 March 2012)

We introduce the *eikonal* approximation to study the effect of the large-scale motion of cosmic fluids on their small-scale evolution. This approach consists in collecting the impact of the long-wavelength displacement field into a single or finite number of random variables, whose statistical properties can be computed from the initial conditions. For a single dark matter fluid, we show that we can recover the nonlinear propagators of renormalized perturbation theory. These are obtained with no need to assume that the displacement field follows the linear theory. Then we extend the eikonal approximation to many fluids. In particular, we study the case of two nonrelativistic components and we derive their resummed propagators in the presence of isodensity modes. Unlike the adiabatic case, where only the phase of small-scale modes is affected by the large-scale advection field, the isodensity modes change also the amplitude on small scales. We explicitly solve the case of cold dark matter-baryon mixing and find that the isodensity modes induce only very small corrections to the resummed propagators.

DOI: 10.1103/PhysRevD.85.063509 PACS numbers: 98.80.−k

I. INTRODUCTION

The development of wide-field surveys has triggered renewed interest in the implementation of perturbation techniques for the computation of the statistical properties of large-scale structures. Several approaches have been proposed to significantly extend the standard perturbation theory (PT) methods (see [1]). A particularly interesting approach is the so-called renormalized perturbation theory (RPT), pioneered by Crocce and Scoccimarro [2–4]. This method relies on the use of the 2-point propagator as a measure of the memory of the initial conditions. This appears as the fundamental building block from which perturbation theory can be reconstructed and allows to take into account nonlinearities from very small scales, reducing their impact in the neglected terms of the perturbative expansion. This idea was later extended in [5,6] with the introduction of multipoint propagators.

The key result of RPT is that in the high-k limit the propagators can be computed exactly, by summing up an infinite subset of contributions in the standard perturbation theory expansion. However, this result has been proved only for a single pressureless fluid—describing cold dark matter (CDM)—using a technique that seems difficult to extend to more complex scenarios. Thus, there is no systematic way to implement the RPT approach when the content of the cosmic fluid is richer—e.g. when it includes various matter components, nonrelativistic neutrinos, or even modification of gravity—and its application range has been so far limited to simple cosmological models (see however [7]). Note that other approaches, such as the so-called time renormalization group approach [8], do not suffer from such limitations.

On the other hand, the resummation of the propagators can be obtained by a more direct technique than that originally introduced in [2–4]. As mentioned in [9] and explicitly used in [6,10], in the high-k limit it is possible to resum the same class of contributions making use of a single or a finite number of random variables, which describe the effect of the long-wavelength fluctuations on smaller scales. This has been called the α-method [6]. Here we will explicitly present how to compute nonlinear propagators in this framework. Moreover, we will show that this method can be employed to extend the RPT approach to arbitrarily complicated cosmologies. Borrowing the terminology from quantum field theory, where similar techniques are used (see e.g. [11,12]), we propose to dub this method the *eikonal approximation*.

The fluid content of the Universe is richer than a simple single-dark matter component. In practice we know that the properties of the large-scale structure of the Universe can be significantly affected by the presence of a subdominant species. This is the case of baryons, which at high enough redshift behave very differently from CDM. Indeed, the net result of this different behavior is the existence of the baryonic oscillations.

From a theoretical point of view, the CDM-baryon system is very appealing: After decoupling both components are pressureless fluids (at least above the baryonic Jeans scale) and thus follow geodesic motion [13]. However, the matter fluid as a whole cannot be described as a pressureless effective fluid. The reason is that the CDM and baryon fluids are moving at different velocities—see [15] for a study of some of the consequences of this different behavior and their possible observational implications. Such a velocity dispersion induces an effective anisotropic

*francis.bernardeau@cea.fr
†nicolas.van-de-rijt@cea.fr
‡filippo.vernizzi@cea.fr

pressure in the total fluid, modifying its equations of motion. Thus, one is forced to study the system of coupled equations for the CDM and baryons, as previously done in [7]. In particular, this is the system that we will explore with the help of the eikonal approximation.

The plan of the paper is the following. In Sec. II we review the basic concepts of the RPT approach for a single CDM fluid and we discuss the eikonal approximation in this context. In Sec. III we extend this discussion to the multifluid case. In particular, we derive the evolution equations for several gravitationally coupled pressureless fluids, we describe the various modes that appear in this case, and we present how they can be incorporated in the eikonal approximation. Finally, in Sec. IV we illustrate our concepts in the case of the standard CDM-baryon mixing.

II. SINGLE FLUID

In this section we review the basic concepts of the RPT approach with a single perfect fluid, developed in [2,3]. Moreover, we rederive the procedure to resum the nonlinear propagators for cosmic fluids using the eikonal approximation.

A. Equations of motion

We assume the Universe to be filled by one pressureless fluid. We denote its density by ρ, and the density contrast by $\delta \equiv \rho/\bar{\rho} - 1$, where $\bar{\rho}$ is the average energy density. The continuity equation then reads

$$\frac{\partial}{\partial t}\delta + \frac{1}{a}[(1+\delta)u^i]_{,i} = 0, \tag{1}$$

where u^i is the i-component of the peculiar velocity field of the fluid and a comma denotes the partial derivative. The Euler equation is

$$\frac{\partial}{\partial t}u^i + Hu^i + \frac{1}{a}u^j u^i_{,j} = -\frac{1}{a}\phi_{,i}, \tag{2}$$

where H is the Hubble rate, $H \equiv d\ln a/dt$, and ϕ is the gravitational potential. Since we are only interested in the dynamics on subhorizon scales, ϕ is the usual Newtonian potential, satisfying the Poisson equation

$$\Delta\phi = 4\pi G a^2 \bar{\rho}\delta. \tag{3}$$

We also ignore small-scale shell crossings in the fluid. Then, since the gravitational force is potential the fluid velocity remains potential at all orders in the perturbations. Thus, it can be entirely described by the dimensionless velocity divergence, defined by

$$\theta \equiv \frac{u^i_{,i}}{aH}. \tag{4}$$

By using the following convention for the Fourier modes,

$$f(\mathbf{k}) \equiv \int \frac{d^3\mathbf{x}}{(2\pi)^3} f(\mathbf{x}) e^{-i\mathbf{k}\cdot\mathbf{x}}, \tag{5}$$

the equations of motion can then be rewritten in Fourier space as

$$\frac{1}{H}\frac{\partial}{\partial t}\delta(\mathbf{k}) + \theta(\mathbf{k}) = -\alpha(\mathbf{k}_1,\mathbf{k}_2)\theta(\mathbf{k}_1)\delta(\mathbf{k}_2), \tag{6}$$

$$\frac{1}{H}\frac{\partial}{\partial t}\theta(\mathbf{k}) + \frac{1}{H}\frac{d\ln(a^2H)}{dt}\theta(\mathbf{k}) + \frac{3}{2}\Omega_m\delta(\mathbf{k}) = -\beta(\mathbf{k}_1,\mathbf{k}_2)\theta(\mathbf{k}_1)\theta(\mathbf{k}_2), \tag{7}$$

where Ω_m is the reduced matter density and

$$\alpha(\mathbf{k}_1,\mathbf{k}_2) = \frac{(\mathbf{k}_1+\mathbf{k}_2)\cdot\mathbf{k}_1}{k_1^2}, \tag{8}$$

$$\beta(\mathbf{k}_1,\mathbf{k}_2) = \frac{(\mathbf{k}_1+\mathbf{k}_2)^2\mathbf{k}_1\cdot\mathbf{k}_2}{2k_1^2k_2^2}. \tag{9}$$

On the right-hand side of Eqs. (6) and (7), integration over repeated wave modes and a Dirac function $\delta_{\mathrm{D}}(\mathbf{k}-\mathbf{k}_1-\mathbf{k}_2)$ is implied. Note that these equations are valid irrespective of the dark energy equation of state or curvature term.

B. RPT formulation

In order to recast these equations in RPT form let us first discuss their linear solutions. At linear order, the coupling terms in the right-hand side of Eqs. (6) and (7) are absent. We are then left with the usual linear solutions of a pressureless fluid, i.e.

$$\delta(\mathbf{x},t) = D_+(t)\delta_+(\mathbf{x}) + D_-(t)\delta_-(\mathbf{x}), \tag{10}$$

where $D_+(t)$ and $D_-(t)$ correspond to the growing and decaying modes, respectively. The corresponding expression for the dimensionless velocity divergence is

$$\theta(\mathbf{x},t) = -f_+(t)D_+(t)\delta_+(\mathbf{x}) - f_-(t)D_-(t)\delta_-(\mathbf{x}), \tag{11}$$

where f_+ and f_- are the growth rates, defined as $f_\pm \equiv d\ln D_\pm/d\ln a$.

As introduced in [7,16], it is convenient to define the duplet

$$\Psi_a = \begin{pmatrix}\delta \\ \Theta\end{pmatrix}, \tag{12}$$

where Θ is the reduced velocity contrast defined as

$$\Theta(\mathbf{x},t) \equiv -\theta(\mathbf{x},t)/f_+(t) = D_+(t)\delta_+(\mathbf{x}) + \frac{f_-(t)}{f_+(t)}D_-(t)\delta_-(\mathbf{x}), \tag{13}$$

in such a way that the linear growing mode of Θ is the same as that of δ. It is then convenient to rewrite the evolution equation using η as time variable, defined through

$$D_+ d\eta \equiv dD_+. \tag{14}$$

With this definition the equations of motion (6) and (7) can be recast as

$$\frac{\partial}{\partial \eta}\Psi_a(\mathbf{k}) + \Omega_{ab}\Psi_b(\mathbf{k}) = \gamma_{abc}(\mathbf{k}, \mathbf{k}_1, \mathbf{k}_2)\Psi_b(\mathbf{k}_1)\Psi_c(\mathbf{k}_2), \tag{15}$$

where

$$\Omega_{ab} \equiv \begin{pmatrix} 0 & -1 \\ -\frac{3}{2}\frac{\Omega_m}{f_+^2} & \frac{3}{2}\frac{\Omega_m}{f_+^2} - 1 \end{pmatrix}, \tag{16}$$

and the nonzero elements of the coupling matrix γ_{abc} are

$$\begin{aligned} \gamma_{112}(\mathbf{k}, \mathbf{k}_1, \mathbf{k}_2) &\equiv \frac{\alpha(\mathbf{k}_2, \mathbf{k}_1)}{2}, \\ \gamma_{121}(\mathbf{k}, \mathbf{k}_1, \mathbf{k}_2) &\equiv \frac{\alpha(\mathbf{k}_1, \mathbf{k}_2)}{2}, \\ \gamma_{222}(\mathbf{k}, \mathbf{k}_1, \mathbf{k}_2) &\equiv \beta(\mathbf{k}_1, \mathbf{k}_2). \end{aligned} \tag{17}$$

From Eqs. (10) and (13), the growing and decaying solutions are proportional to

$$u_a^{(+)} \propto (1, 1)^T \quad \text{and} \quad u_a^{(-)} \propto (1, f_-/f_+)^T, \tag{18}$$

respectively. It has been widely stressed that f_-/f_+ is very weakly dependent on the background. Indeed, it departs little from the value it takes in an Einstein-de Sitter universe (EdS), i.e. $\Omega_m = 1$, where $f_-/f_+ = -3/2$ [17].

The solutions of the linear equations of motion, obtained from dropping the right-hand side of (15), can be formally written in terms of the *linear* propagator $g_{ab}(\eta, \eta')$. This is such that

$$g_{ab}(\eta, \eta) = \delta_{ab}, \tag{19}$$

and

$$\frac{\partial}{\partial \eta} g_{ab}(\eta, \eta_0) + \Omega_{ac}(\eta) g_{cb}(\eta, \eta_0) = 0. \tag{20}$$

It can be built from a complete set of independent solutions of the evolution equation. For a single fluid we can use $u_a^{(+)}$ and $u_a^{(-)}$ defined in Eq. (18). We then have

$$g_{ab}(\eta, \eta_0) = \sum_\alpha u_a^{(\alpha)}(\eta) c_b^{(\alpha)}(\eta_0), \tag{21}$$

where the coefficients $c_b^{(\alpha)}$ are chosen such that

$$\sum_\alpha u_a^{(\alpha)}(\eta) c_b^{(\alpha)}(\eta) = \delta_{ab}. \tag{22}$$

For an EdS background the explicit form of g_{ab} reads

$$g_{ab}(\eta, \eta_0) = \frac{e^{\eta-\eta_0}}{5}\begin{pmatrix} 3 & 2 \\ 3 & 2 \end{pmatrix} + \frac{e^{-(3/2)(\eta-\eta_0)}}{5}\begin{pmatrix} 2 & -2 \\ -3 & 3 \end{pmatrix}. \tag{23}$$

The linear propagator is useful to formally write the solution for Ψ_a in integral form. Indeed, using Eqs. (12) and (13), the equations of motion (6) and (7) can be written as [16]

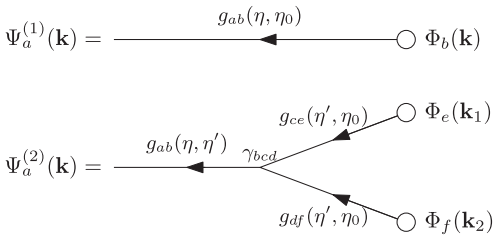

FIG. 1. Diagrammatic representation of the series expansion of $\Psi_a(\mathbf{k})$ up to fourth order in the initial conditions denoted here by $\Phi_a(\mathbf{k})$. Time increases along each segment according to the arrow and each segment bears a factor $g_{cd}(\eta_f - \eta_i)$ if η_i is the initial time and η_f is the final time. At each initial point and each vertex point there is a sum over the component indices; a sum over the incoming wave modes is also implicit and, finally, the time coordinate of the vertex points is integrated from η_0 to the final time η according to the time ordering of each diagram.

$$\begin{aligned} \Psi_a(\mathbf{k}, \eta) = {} & g_{ab}(\eta, \eta_0)\Psi_b(\mathbf{k}, \eta_0) \\ & + \int_{\eta_0}^{\eta} d\eta' g_{ab}(\eta, \eta')\gamma_{bde}(\mathbf{k}, \mathbf{k}_1, \mathbf{k}_2) \\ & \times \Psi_d(\mathbf{k}_1, \eta')\Psi_e(\mathbf{k}_2, \eta'). \end{aligned} \tag{24}$$

As illustrated in Fig. 1, this equation has a diagrammatic representation in the RPT context [2].

Another important quantity introduced in the RPT approach is the nonlinear multipoint propagator. More precisely, the $(n+1)$-point propagator $\Gamma^{(n)}_{ab_1\ldots b_n}$ is defined by

$$\begin{aligned} & \left\langle \frac{\partial^n \Psi_a(\mathbf{k}, \eta)}{\partial \Psi_{b_1}(\mathbf{k}_1, \eta_0) \ldots \partial \Psi_{b_n}(\mathbf{k}_n, \eta_0)} \right\rangle \\ & \quad \equiv \delta_{\mathrm{D}}\Big(\mathbf{k} - \sum_i^n \mathbf{k}_i\Big)\Gamma^{(n)}_{ab_1\ldots b_n}(\mathbf{k}_1, \ldots, \mathbf{k}_n; \eta, \eta_0). \end{aligned} \tag{25}$$

Propagators represent the way the Ψ_a's respond to an infinitesimal change of the modes at an earlier time and they are important in the construction of multipoint spectra [5,6].

In the large-k limit (to be better specified below) these propagators enjoy a remarkable property. Indeed, in [3] it has been shown that in this limit and for Gaussian initial conditions, the nonlinear 2-point propagator $G_{ab} \equiv \Gamma^{(1)}_{ab}$ has a simple expression

$$G_{ab}(k; \eta, \eta_0) = g_{ab}(\eta, \eta_0)\exp[-k^2\sigma_d^2(e^\eta - e^{\eta_0})^2/2], \tag{26}$$

where σ_d^2 is the variance of the initial displacement field. Note that the linear propagator g_{ab} is simply the tree-level analog of G_{ab}. This result has been generalized to $(n+1)$-point propagators with $n \geq 2$ in [5], where it has been shown that

$$\Gamma^{(n)}_{ab_1\ldots b_n} = \Gamma^{(n)\text{-tree}}_{ab_1\ldots b_n}\exp[-k^2\sigma_d^2(e^\eta - e^{\eta_0})^2/2], \tag{27}$$

where $\Gamma^{(n)\text{-tree}}$ is the corresponding propagator computed at tree level.

The exponentiation in Eqs. (26) and (27) has been obtained in [2,3] by summing up an infinite number of diagrams thought to dominate in the large-k limit. In order to identify which diagrams dominate in this limit, the concept of *principal line* and its generalization for the $(n+1)$-point propagators, the *principal* tree, have been introduced. In [3] it has been shown that each diagram contributing to the nonlinear propagator $G_{ab}(k;\eta,\eta_0)$ always contains a unique line that goes from some time η_0 (symbolized by the vertical dotted line) to a final time η. To this line may be attached loops containing power spectra evaluated at an initial time $\eta_{\rm in}$. This is illustrated in Fig. 2, upper panel. The principal line is the unique way to go from η_0 to η without crossing an initial power spectrum $\otimes$, thus moving always in the direction of increasing time. Similarly, for each diagram contributing to $\Gamma^{(n)}_{ab_1\ldots b_n}$ there always exists a unique tree with n branches, the *principal tree*, that joins η_0 to η (see bottom diagram of Fig. 2) [5].

We can now specify under which assumption the relations (26) and (27) have been derived. These are:

(i) The multipoint propagators are dominated by those diagrams in which every loop is directly connected to the principal tree.

(ii) The diagrams are computed and summed up in the limit where the incoming wave modes q_i are soft, i.e. $q_i \ll k$.

As we will show below, the eikonal approximation corresponds exactly to the last assumption. It can incorporate the first one if necessary.

C. Resumming the 2-point propagator with the eikonal approximation

In [6] it has been shown that Eqs. (26) and (27) can be obtained irrespective of the diagrammatic representations and of the nature of the initial conditions. Indeed, the nonlinear fluid equations contain nonlinear terms that couple short and long-wavelength modes. The eikonal approximation corresponds to study the effect of very long-wavelength modes q on the dynamics of a given short-wavelength mode k, in the limit of $q \ll k$. In this limit, space variations of the long-wavelength modes are tiny with respect to the mode k, and the long modes can be treated as an external random background. If we neglect the mode couplings between short scales, the nonlinear fluid equations can be rewritten as linear equations embedded in an external random medium.

Let us be more explicit here. Coupling terms are given by a convolution of fields taken at wave modes $\mathbf{k}_1$ and $\mathbf{k}_2$ such that $\mathbf{k} = \mathbf{k}_1 + \mathbf{k}_2$. These nonlinear terms can be split into two different contributions: the one coming from coupling two modes of very different amplitudes, $k_1 \ll k_2$ or $k_2 \ll k_1$, and the one coming from coupling two modes of comparable amplitudes. In the first case, the small wave

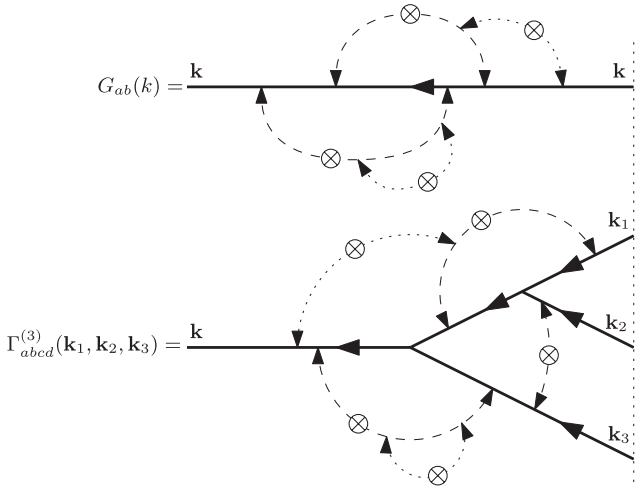

FIG. 2. Example of diagrams contributing to $G_{ab}(k)$ (top) and $\Gamma^{(3)}_{abcd}(\mathbf{k},\mathbf{k}_1,\mathbf{k}_2,\mathbf{k}_3)$ (bottom). The dominant contribution after resuming all possible configurations is expected to come from those diagrams where all loops are directly connected to the principal line (top) or principal tree (bottom). The principal line and tree are drawn with a thick solid line. A symbol $\otimes$ denotes a power spectrum evaluated at initial time $\eta_{\rm in}$. The dominant loops are those drawn by dashed lines, while the subdominant loops are those in dotted lines.

modes ought to be much smaller than $\mathbf{k}$ itself. Let us denote these small modes by $\mathbf{q}$. In the limit of $q \ll k$, the equations of motion (15) can be rewritten as

$$\frac{\partial}{\partial\eta}\Psi_a(\mathbf{k}) + \Omega_{ab}\Psi_b(\mathbf{k}) = \Xi_{ab}(\mathbf{k})\Psi_b(\mathbf{k}) + [\gamma_{abc}(\mathbf{k},\mathbf{k}_1,\mathbf{k}_2)\Psi_b(\mathbf{k}_1)\Psi_c(\mathbf{k}_2)]_{\mathcal{H}}, \tag{28}$$

with

$$\Xi_{ab}(\mathbf{k},\eta) \equiv 2\int_{\mathcal{S}} d^3\mathbf{q}\,\gamma_{abc}(\mathbf{k},\mathbf{k},\mathbf{q})\Psi_c(\mathbf{q},\eta). \tag{29}$$

The key point is that in Eq. (29) the domain of integration is restricted to the soft momenta, for which $q \ll k$. Conversely, on the right-hand side of Eq. (28) the convolution is done excluding the soft domain, i.e. it is over hard modes or modes of comparable size.

In the limit of separation of scales, Ξ_{ab} is a random quantity which depends on the initial conditions. Using Eqs. (8) and (9), for $q \ll k$ the leading expression of the coupling matrix is obtained with the following limit values $\alpha(\mathbf{q},\mathbf{k}) \approx (\mathbf{q}\cdot\mathbf{k})/q^2$, $\alpha(\mathbf{k},\mathbf{q}) \approx 0$, $\beta(\mathbf{q},\mathbf{k}) = \beta(\mathbf{k},\mathbf{q}) \approx (\mathbf{q}\cdot\mathbf{k})/(2q^2)$. Thus, γ_{abc} in Eq. (29) simplifies and Ξ_{ab} becomes proportional to the identity, with

$$\Xi_{ab}(\mathbf{k},\eta) = \Xi(\mathbf{k},\eta)\delta_{ab}, \qquad \Xi(\mathbf{k},\eta) \equiv \int_{\mathcal{S}} d^3\mathbf{q}\,\frac{\mathbf{k}\cdot\mathbf{q}}{q^2}\Theta(\mathbf{q},\eta). \tag{30}$$

Note that only the velocity field Θ (and not the density field δ) contributes to Ξ_{ab}. Furthermore, as $\Theta(\mathbf{x}, \eta)$ is real $\Theta(-\mathbf{q}) = \Theta^*(\mathbf{q})$ and thus Ξ is purely imaginary.

In Eq. (28) we have reabsorbed the effect of the nonlinear coupling with long-wavelength modes in the linear term $\Xi_{ab}\Psi_b$. The solution to this equation can be given in terms of the resummed propagator $\xi_{ab}(\mathbf{k}, \eta, \eta')$ [18] satisfying the equation

$$\left(\frac{\partial}{\partial\eta} - \Xi(\mathbf{k}, \eta)\right)\xi_{ab}(\mathbf{k}, \eta, \eta') + \Omega_{ac}(\eta)\xi_{cb}(\mathbf{k}, \eta, \eta') = 0, \tag{31}$$

and reads

$$\Psi_a(\mathbf{k}, \eta) = \xi_{ab}(\eta, \eta_0)\Psi_b(\mathbf{k}, \eta_0) + \int_{\eta_0}^{\eta} d\eta' \xi_{ab}(\eta, \eta')[\gamma_{bde}(\mathbf{k}, \mathbf{k}_1, \mathbf{k}_2) \times \Psi_d(\mathbf{k}_1, \eta')\Psi_e(\mathbf{k}_2, \eta')]_{\mathcal{H}}, \tag{32}$$

where in the last line the convolution is done on the hard domain $\mathcal{H}$.

In the case of a single fluid, as discussed here, Eq. (31) can be easily solved. Taking into account the boundary condition $\xi_{ab}(\mathbf{k}, \eta, \eta) = \delta_{ab}$, one obtains

$$\xi_{ab}(\mathbf{k}, \eta, \eta_0) = g_{ab}(\eta, \eta_0)\exp\left[\int_{\eta_0}^{\eta} d\eta' \Xi(\mathbf{k}, \eta')\right]. \tag{33}$$

The argument of the exponential is the time integral of the velocity projected along the direction $\mathbf{k}$, i.e. the *displacement* component along $\mathbf{k}$. Note that in their original calculation, Crocce and Scoccimarro assumed that the incoming modes in the soft (i.e. large-scale) lines were in the linear and growing regime. Here we need not make this assumption. Equation (33) is valid irrespective of the fact that the incoming modes in Ξ are in the growing mode or not.

There is another important aspect of Eq. (33). Since $\Xi(\mathbf{k}, \eta)$ is a purely imaginary number, the soft modes change only the phase of the small-scale modes but not their amplitude. Such an effect will then have no impact on the equal-time power spectra. However, it has some impact on the amplitude of the propagators. Indeed, the phase change inevitably damps the correlation between modes at different times. This effect is at the heart of the regularization scheme used by approaches such as RPT.

To illustrate this last point, let us see how one can recover Eq. (26) using the solution (32) and the resummed propagator (33) derived with the eikonal approximation. Deriving Eq. (32) with respect to an initial field $\Psi_b(\mathbf{k}, \eta_0)$ as in Eq. (25), and taking the ensemble average one finds

$$G_{ab}(k, \eta, \eta_0) = \langle\xi_{ab}(\mathbf{k}, \eta, \eta_0)\rangle_{\Xi}. \tag{34}$$

The nonlinear 2-point propagator G_{ab} is given by the ensemble average of $\xi_{ab}(\mathbf{k}, \eta, \eta_0)$ over the realizations of $\Xi(\mathbf{k})$. In general, the expression of the nonlinear propagator introduces the cumulant generating functions of Ξ. Indeed, using (33) Eq. (34) yields

$$G_{ab}(k, \eta, \eta_0) = g_{ab}(\eta, \eta_0)\exp\left(\sum_{p=2}^{\infty}\frac{c_p}{p!}\right), \tag{35}$$

where c_p is the p-order cumulant of the field $\int_{\eta_0}^{\eta} d\eta' \Xi(\mathbf{k}, \eta')$ and for symmetry reasons the sum is restricted to even values of p, thus ensuring that the nonlinear propagators are real.

For Gaussian initial conditions and assuming that at late time the long-wavelength Ξ is in the linear growing mode, cumulants with $p > 2$ in Eq. (35) vanish and we are left with only c_2. This is given by

$$c_2(k) = \int_{\eta_0}^{\eta} d\eta' d\eta'' \langle\Xi(\mathbf{k}, \eta')\Xi(\mathbf{k}, \eta'')\rangle. \tag{36}$$

Then, exploiting the time dependence of the linear growing mode, $\Theta \propto D_+ = e^{\eta - \eta_{\rm in}}$, and using Eq. (30), we have

$$\Xi(\mathbf{k}, \eta) = D_+(\eta)\int_{\mathcal{S}} d^3\mathbf{q}\,\frac{\mathbf{k}\cdot\mathbf{q}}{q^2}\,\Theta(\mathbf{q}, \eta_{\rm in}). \tag{37}$$

Plugging this expression in Eq. (36), we can express c_2 in terms of the initial power spectrum $P_{\rm in}(q)$, defined by

$$\langle\Theta(\mathbf{q}, \eta_{\rm in})\Theta(\mathbf{q}', \eta_{\rm in})\rangle \equiv \delta_{\rm D}(\mathbf{q} + \mathbf{q}')P_{\rm in}(q). \tag{38}$$

Indeed, we have

$$c_2(k) = -k^2\sigma_d^2(e^{\eta - \eta_{\rm in}} - e^{\eta_0 - \eta_{\rm in}})^2, \tag{39}$$

where σ_d^2 gives the variance of the displacement field defined as [2,3]

$$\sigma_d^2 \equiv \frac{1}{3}\int_{\mathcal{S}} d^3\mathbf{q}\,\frac{P_{\rm in}(q)}{q^2}. \tag{40}$$

At this stage σ_d^2 depends on the domain of integration and hence on k. The standard RPT results are obtained by taking the value of σ_d^2 in the large-k limit. We will comment on this assumption in the conclusion. Then, setting here and in the following $\eta_{\rm in} = 0$ for convenience, from Eq. (35) we recover Eq. (26),

$$G_{ab}(k, \eta, \eta_0) = g_{ab}(\eta, \eta_0)\exp(-k^2\sigma_d^2(e^{\eta} - e^{\eta_0})^2/2). \tag{41}$$

D. Higher-order propagators

Although the focus of this paper is on the 2-point propagator, let us comment on the use of the eikonal approximation, in particular, of Eq. (32), in investigating the resummation of higher-order propagators.

The computation of the nonlinear 3-point propagator proceeds by replacing Ψ_d and Ψ_e in the second line of Eq. (32) by the linear solution given by the first line of this equation. Deriving twice with respect to the initial field yields

$$\frac{\partial^2\Psi_a(\mathbf{k},\eta)}{\partial\Psi_b(\mathbf{k}_1,\eta_0)\partial\Psi_c(\mathbf{k}_2,\eta_0)} = \int_{\eta_0}^{\eta} d\eta' \xi_{ad}(\mathbf{k};\eta,\eta')[\gamma_{def}(\mathbf{k},\mathbf{k}_1,\mathbf{k}_2)\xi_{eb}(\mathbf{k}_1;\eta',\eta_0)\xi_{fc}(\mathbf{k}_2;\eta',\eta_0)]_{\mathcal{H}}. \quad (42)$$

This is the same formal expression as for the naked theory except that here the convolution is restricted to the hard-mode domain $\mathcal{H}$. Note that the coupling vertex between modes with hard momenta in the second line is not affected by the use of the eikonal approximation: It is identical to the one of the naked theory. Moreover, it is remarkable to see that, using the form given by Eq. (33), the exponential terms factor out of the time integral and their arguments sum up to give

$$\frac{\partial^2\Psi_a(\mathbf{k},\eta)}{\partial\Psi_b(\mathbf{k}_1,\eta_0)\partial\Psi_c(\mathbf{k}_2,\eta_0)} = \exp\left[\int_{\eta_0}^{\eta} d\eta' \Xi(\mathbf{k},\eta')\right]\int_{\eta_0}^{\eta} d\eta' g_{ad}(\eta,\eta')[\gamma_{def}(\mathbf{k},\mathbf{k}_1,\mathbf{k}_2)g_{eb}(\eta',\eta_0)g_{fc}(\eta',\eta_0)]_{\mathcal{H}}. \quad (43)$$

Finally, taking the ensemble average and using the definition of multipoint propagators, Eq. (25), one obtains in the Gaussian case

$$\Gamma^{(2)}_{abc}(\eta,\eta_0) = \Gamma^{(2)\text{-tree}}_{abc}(\eta,\eta_0)\exp(-k^2\sigma_d^2(e^{\eta}-e^{\eta_0})^2/2). \quad (44)$$

This result can be generalized to propagators of any higher order. The formal expressions of the resummed trees computed in the eikonal approximation are obtained from those computed in the naked theory by simply changing the propagators from g_{ab} to ξ_{ab}. Then, for each pair of merging branches with equal initial time, one can factor out the phase similarly to what is done when going from Eq. (42) to (43). Finally, this leaves an overall factor $\exp(\int_{\eta_0}^{\eta} d\eta' \Xi(\mathbf{k},\eta'))$, which can be factorized out, recovering Eq. (27). The eikonal approximation explicitly shows how the results [5,6] can be recovered and generalized to any time-dependent large-scale wave mode.

III. MULTIFLUIDS

In this section we explore the case where the Universe is filled with several noninteracting pressureless fluids and show how the eikonal approximation can be implemented in this case. Because of the gravitational coupling and the expansion, at late time such a system becomes indistinguishable from a single-fluid component. However, during its evolution it can behave very differently from a single perfect fluid depending on the initial conditions.

A. The equations of motion

Denoting each fluid by a subscript α, the continuity equation reads, for each fluid,

$$\frac{\partial}{\partial t}\delta_\alpha + \frac{1}{a}[(1+\delta_\alpha)u^i_\alpha]_{,i} = 0, \quad (45)$$

while the Euler equation reads

$$\frac{\partial}{\partial t}u^i_\alpha + Hu^i_\alpha + \frac{1}{a}u^j_\alpha u^i_{\alpha,j} = -\frac{1}{a}\phi_{,i}. \quad (46)$$

The Poisson equation (3), where now δ is the density contrast of the total fluid energy density, i.e.

$$\rho_m \equiv \sum_\alpha \rho_\alpha \equiv (1+\delta_m)\bar{\rho}_m, \quad (47)$$

allows to close the system. This introduces couplings between the fluids.

In Fourier space, the equations of motion become now

$$\frac{1}{H}\frac{\partial}{\partial t}\delta_\alpha(\mathbf{k}) + \theta_\alpha(\mathbf{k}) = -\alpha(\mathbf{k}_1,\mathbf{k}_2)\theta_\alpha(\mathbf{k}_1)\delta_\alpha(\mathbf{k}_2), \quad (48)$$

$$\frac{1}{H}\frac{\partial}{\partial t}\theta_\alpha(\mathbf{k}) + \frac{1}{H}\frac{d\ln(a^2H)}{dt}\theta_\alpha(\mathbf{k}) + \frac{3}{2}\Omega_m\delta_m(\mathbf{k}) = -\beta(\mathbf{k}_1,\mathbf{k}_2)\theta_\alpha(\mathbf{k}_1)\theta_\alpha(\mathbf{k}_2), \quad (49)$$

where θ_α is the dimensionless divergence of the velocity field of the fluid α and Ω_m is the reduced total density of the pressureless fluids. The coupling between the fluids is only due to the term δ_m appearing in the Euler equation.

Before studying these equations let us discuss the equations for the total fluid. As we are describing here a collection of pressureless particles, it is tempting to write down the equations of motion for the total fluid. The continuity equation is simply identical to Eq. (1). The total fluid velocity u^i is defined by

$$u^i \equiv \sum_\alpha f_\alpha u^i_\alpha, \quad (50)$$

where $f_\alpha \equiv \rho_\alpha/\rho_m$, and its evolution equation reads

$$\frac{\partial}{\partial t}u^i + Hu^i + \frac{1}{a}u^j u^i_{,j} = -\frac{1}{a}\phi_{,i} - \frac{1}{a\rho_m}(\rho_m\sigma^{ij})_{,j}, \quad (51)$$

where and σ_{ij} is the velocity dispersion of the mean fluid, given by

$$\sigma^{ij} \equiv \sum_\alpha f_\alpha u^i_\alpha u^j_\alpha - u^i u^j. \quad (52)$$

Thus, due to the multifluid nature of the system, the Euler equation contains an anisotropic stress term. One can write down an equation of motion for this term, but this will involve higher moments of the fluid distribution and so on. Thus, the complete description of the total fluid at nonlinear order requires an infinite hierarchy of equations in the moments of the fluid. Another consequence of this expression is that, even though the velocity field of each

fluid remains potential, the total velocity field is no longer potential. Indeed, we expect that it develops a rotational part due to the presence of the dissipative term σ^{ij} [19].

B. Adiabatic and isodensity modes

As we did for the single-fluid case, let us study the linear evolution of the multifluid system by dropping the right-hand side of Eqs. (48) and (49). Since at linear order there is no anisotropic stress σ^{ij}, which is second order in the velocities, the two linear solutions (10) and (13) found in the single-fluid case are expected to be also solutions of the linear multifluid system. This corresponds to the case where all the fluids start comoving and, as they all follow geodesic motion, remain comoving during their entire evolution. Analogously to the jargon adopted in the physics of the early Universe, these solutions correspond to the so-called growing and decaying *adiabatic* modes. Note that if only these two modes are initially excited, the right-hand side of Eq. (52) vanishes and the total fluid is indistinguishable from a pure dark matter fluid.

However, the presence of multiple components gives birth also to *isocurvature* or rather, given our scales of interest, *isodensity* modes. To examine their properties, let us turn to the equations describing the multicomponent system, Eqs. (48) and (49). In this case it is convenient to introduce a multiplet Ψ_a which generalizes the duplet defined in Eq. (12), i.e. [16]

$$\Psi_a = (\delta_1, \Theta_1, \delta_2, \Theta_2, \ldots)^T, \tag{53}$$

where $\Theta_\alpha \equiv -\theta_\alpha/f_+(t)$. Thus, for N components Ψ_a has $2N$ elements. Equations (48) and (49) can then be rewritten as Eq. (15) where in this case the matrix elements of Ω_{ab} are given by

$$\begin{aligned} \Omega_{(2p-1)(2p)} &= -1, \\ \Omega_{(2p)(2p)} &= \frac{3}{2}\frac{\Omega_m}{f_+^2} - 1, \\ \Omega_{(2p)(2q-1)} &= -\frac{3}{2}\frac{\Omega_m}{f_+^2} f_q, \end{aligned} \tag{54}$$

for any integers p and q running from 1 to N and where all the other elements of Ω_{ab} vanish. The nonzero elements of the coupling matrix γ_{abc} are

$$\begin{aligned} \gamma_{(2p-1)(2p-1)(2p)}(\mathbf{k}, \mathbf{k}_1, \mathbf{k}_2) &= \frac{\alpha(\mathbf{k}_2, \mathbf{k}_1)}{2}, \\ \gamma_{(2p-1)(2p)(2p-1)}(\mathbf{k}, \mathbf{k}_1, \mathbf{k}_2) &= \frac{\alpha(\mathbf{k}_1, \mathbf{k}_2)}{2}, \\ \gamma_{(2p)(2p)(2p)}(\mathbf{k}, \mathbf{k}_1, \mathbf{k}_2) &= \beta(\mathbf{k}_1, \mathbf{k}_2), \end{aligned} \tag{55}$$

for any integer p. Note that there are no explicit couplings between different species in the γ_{abc}-matrices.

The isodensity modes are obtained under the constraint that the total density contrast vanishes, i.e. $\delta = 0$. Since the evolution equations decouple under this constraint, the time dependence of these modes can be easily inferred. One solution is given by

$$\begin{aligned} \Theta_\alpha^{(\mathrm{is})}(\eta) &\propto \exp\Big[-\int^\eta d\eta' \Big(\frac{3}{2}\frac{\Omega_m}{f_+^2} - 1\Big)\Big], \\ \delta_\alpha^{(\mathrm{is})}(\eta) &= \int^\eta d\eta' \Theta_\alpha^{(\mathrm{is})}(\eta'), \end{aligned} \tag{56}$$

with

$$\sum_\alpha f_\alpha \Theta_\alpha^{(\mathrm{is})} = 0, \tag{57}$$

which automatically ensures that $\sum_\alpha f_\alpha \delta_\alpha^{(\mathrm{is})} = 0$. Note that as Ω_m/f_+^2 departs little from the value taken in an EdS cosmology, i.e. $\Omega_m/f_+^2 = 1$, the isodensity modes are expected to depart very weakly from

$$\Theta_\alpha^{(\mathrm{is})}(\eta) \propto \exp(-\eta/2), \quad \delta_\alpha^{(\mathrm{is})}(\eta) = -2\Theta_\alpha^{(\mathrm{is})}(\eta). \tag{58}$$

A second set of isodensity modes is given by

$$\Theta_\alpha^{(\mathrm{ci})}(\eta) = 0, \qquad \delta_\alpha^{(\mathrm{ci})}(\eta) = \text{ Constant}, \tag{59}$$

again with

$$\sum_\alpha f_\alpha \delta_\alpha^{(\mathrm{ci})} = 0. \tag{60}$$

To be specific, let us concentrate now on the case of two fluids and assume an EdS background. In this case the growing and decaying solutions are proportional, respectively, to

$$u_a^{(+)} \propto (1, 1, 1, 1)^T, \qquad u_a^{(-)} \propto (1, -3/2, 1, -3/2)^T. \tag{61}$$

Moreover, the isodensity modes are proportional to

$$u_a^{(\mathrm{is})} \propto (-2f_2, f_2, 2f_1, -f_1)^T, \qquad u_a^{(\mathrm{ci})} \propto (f_2, 0, -f_1, 0)^T. \tag{62}$$

We are then in position to write down the linear propagator $g_{ab}(\eta, \eta_0)$ satisfying Eqs. (21) with (22). For two fluids and an EdS background it reads [7]

$$g_{ab}(\eta,\eta_0)=\frac{e^{\eta-\eta_0}}{5}\begin{pmatrix}3f_1 & 2f_1 & 3f_2 & 2f_2\\ 3f_1 & 2f_1 & 3f_2 & 2f_2\\ 3f_1 & 2f_1 & 3f_2 & 2f_2\\ 3f_1 & 2f_1 & 3f_2 & 2f_2\end{pmatrix} + \frac{e^{-(3/2)(\eta-\eta_0)}}{5}\begin{pmatrix}2f_1 & -2f_1 & 2f_2 & -2f_2\\ -3f_1 & 3f_1 & -3f_2 & 3f_2\\ 2f_1 & -2f_1 & 2f_2 & -2f_2\\ -3f_1 & 3f_1 & -3f_2 & 3f_2\end{pmatrix} + e^{-(1/2)(\eta-\eta_0)}\begin{pmatrix}0 & -2f_2 & 0 & 2f_2\\ 0 & f_2 & 0 & -f_2\\ 0 & 2f_1 & 0 & -2f_1\\ 0 & -f_1 & 0 & f_1\end{pmatrix} + \begin{pmatrix}f_2 & 2f_2 & -f_2 & -2f_2\\ 0 & 0 & 0 & 0\\ -f_1 & -2f_1 & f_1 & 2f_1\\ 0 & 0 & 0 & 0\end{pmatrix}. \tag{63}$$

In the following we explore how this propagator is changed by the coupling with the long-wavelength modes in the eikonal approximation.

C. Resummation of the propagator with the eikonal approximation

Let us study the resummed propagator in the presence of more than one fluid. For simplicity, we will restrict the study to the two-fluid case and an EdS background.

The eikonal equation, Eq. (28) with (29), also holds in the multifluid case. However, in this case Ξ_{ab} is given by a sum of adiabatic contributions, for which the fluid displacements are the same, and isodensity contributions, for which their weighted sum vanishes, i.e.,

$$\Xi_{ab}(\mathbf{k},\eta) = \Xi^{(\mathrm{ad})}(\mathbf{k},\eta)\delta_{ab} + \Xi^{(\mathrm{is})}_{ab}(\mathbf{k},\eta), \tag{64}$$

where $\Xi^{(\mathrm{is})}_{ab}$ takes the form

$$\Xi^{(\mathrm{is})}_{ab} = \Xi^{(\mathrm{is})}h_{ab}, \qquad h_{ab}\equiv\begin{pmatrix}f_2 & 0 & 0 & 0\\ 0 & f_2 & 0 & 0\\ 0 & 0 & -f_1 & 0\\ 0 & 0 & 0 & -f_1\end{pmatrix}. \tag{65}$$

If we assume Ξ_{ab} to be in the linear regime, then

$$\Xi^{(\mathrm{ad})}(\mathbf{k},\eta)\equiv\int_{\mathcal{S}} d^3\mathbf{q}\frac{\mathbf{k}\cdot\mathbf{q}}{q^2}(\Theta^{(+)}(\mathbf{q},\eta)+\Theta^{(-)}(\mathbf{q},\eta)), \tag{66}$$

where $\Theta^{(+)}$ and $\Theta^{(-)}$ are, respectively, the growing and decaying adiabatic modes of the long-wavelength displacement field. The isodensity contribution $\Xi^{(\mathrm{is})}_{ab}$ contains the decaying isodensity mode given in Eq. (58), so that it reads

$$\Xi^{(\mathrm{is})}\equiv\frac{1}{f_2}\int_{\mathcal{S}} d^3\mathbf{q}\frac{\mathbf{k}\cdot\mathbf{q}}{q^2}\Theta^{(\mathrm{is})}_1 = -\frac{1}{f_1}\int_{\mathcal{S}} d^3\mathbf{q}\frac{\mathbf{k}\cdot\mathbf{q}}{q^2}\Theta^{(\mathrm{is})}_2. \tag{67}$$

Note that, because of Eq. (59), the constant isodensity mode does not contribute to Ξ_{ab}.

We are now interested in computing the resummed propagator in the eikonal approximation under the modulation of the long-wavelength modes in Eq. (64). As the adiabatic modes in Ξ_{ab} are proportional to the identity, their effect can be incorporated in exactly the same manner as in the single-fluid case. The adiabatic modes will contribute to the resummed propagator by a multiplicative factor of the exponential of the adiabatic displacement field, as in Eq. (33),

$$\xi_{ab}(\mathbf{k};\eta,\eta_0) = \xi_{ab}(\mathbf{k};\eta,\eta_0;\Xi^{(\mathrm{ad})}=0)\exp\left[\int_{\eta_0}^{\eta} d\eta'\Xi^{(\mathrm{ad})}(\mathbf{k},\eta')\right]. \tag{68}$$

Note again that, as in the single-fluid case, the soft adiabatic modes induce a phase change but do not affect the amplitude of the small-scale modes.

Including the isodensity mode in the resummed propagator proved difficult. We have not been able to find a closed analytic form for it. Thus, we have to rely either on numerical studies or on perturbative calculations. As an example, in Fig. 3 we show the effect of the soft isodensity mode on the small-scale modes, by plotting the evolution of the resummed CDM and baryon density modes with $\Xi^{(\mathrm{ad})}=0$, i.e.,

$$\begin{aligned}\delta_c(\eta,\Xi^{(\mathrm{is})}) &\equiv \xi_{1a}(k;\eta,\eta_{\mathrm{in}};\Xi^{(\mathrm{ad})}=0)\Psi_a(\eta_{\mathrm{in}}),\\ \delta_b(\eta,\Xi^{(\mathrm{is})}) &\equiv \xi_{3a}(k;\eta,\eta_{\mathrm{in}};\Xi^{(\mathrm{ad})}=0)\Psi_a(\eta_{\mathrm{in}}),\end{aligned} \tag{69}$$

normalized to the growing mode e^{η}. Initial conditions are chosen such that $\Psi_a(\eta_{\mathrm{in}})=(1,1,0.15,0.15)^T$ and we have taken $|\Xi^{(\mathrm{is})}(k,\eta_{\mathrm{in}})|=25$. At early time the CDM and baryon density mode grow more slowly than e^{η} (upper panel) and since $|\Xi^{(\mathrm{is})}|\gg 1$ the phases of the two modes rapidly evolve (lower panel). At late time the phases are fixed and the density modes evolve according to the standard adiabatic growing mode. Let us study these two limiting behaviors.

1. Early-time behavior

As $\Xi^{(\mathrm{is})}$ is a decaying mode, it can become arbitrarily large at early time. Let us consider a mode k for which initially $|\Xi^{(\mathrm{is})}|\gg 1$. This means that $\mathbf{k}\cdot\mathbf{v}_{\mathcal{S}}$, i.e. the displacement field of the soft modes along $\mathbf{k}$, is much larger than the Hubble flow. In other words, the time scale of the motion of the large-scale modes is much shorter than the time scale of growth of the small-scale ones, set by the Hubble time.

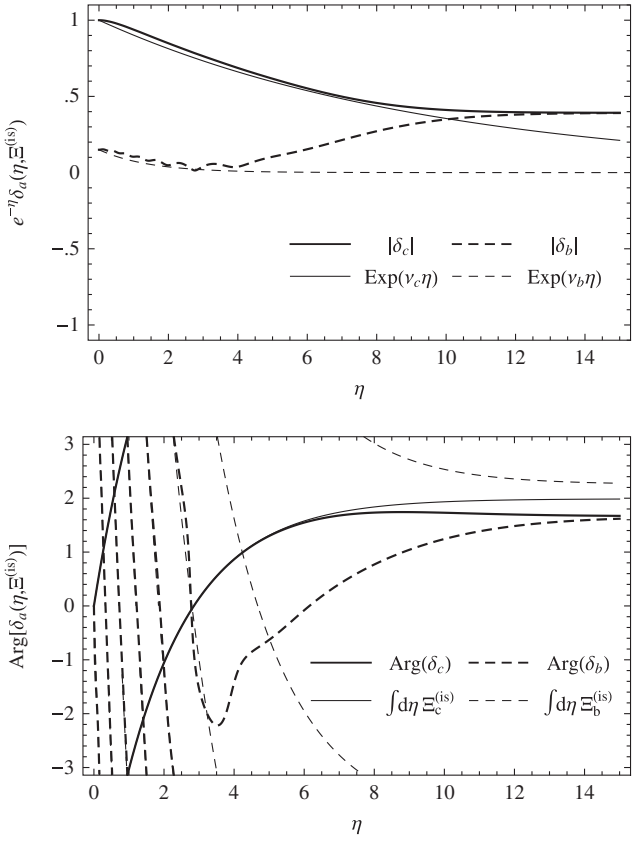

FIG. 3. Evolution of the amplitudes (upper panel) and phases (lower panel) of the resummed density modes with $\Xi^{(ad)} = 0$, i.e. $\delta_c(\eta, \Xi^{(is)})$ and $\delta_b(\eta, \Xi^{(is)})$ as defined in Eq. (69) for CDM (thick solid line) and baryons (thick dashed line). The initial conditions are chosen such that $\Psi_a(\eta_{in}) = (1, 1, 0.15, 0.15)^T$ and $|\Xi^{(is)}(\eta_{in})| = 25$. Thin lines represent the analytic solutions at early times of Eq. (75).

We can grasp the nature of the early-time evolution by making the following change of variable,

$$\tilde{\Psi}_a(\eta) = \Psi_a(\eta)\exp\Big[-\int_{\eta_0}^{\eta} d\eta' \Xi_{aa}(\eta')\Big], \tag{70}$$

where there is no summation over a in Ξ_{aa}. In this case the first line (i.e. the large-k part) of Eq. (28) can be rewritten in terms of $\tilde{\Psi}_a$ as

$$\frac{\partial}{\partial\eta}\tilde{\Psi}_a(\eta) + \tilde{\Omega}_{ab}\tilde{\Psi}_b(\eta) = \tilde{\Xi}_{ab}(\eta)\tilde{\Psi}_b(\eta), \tag{71}$$

where

$$\tilde{\Omega}_{ab} \equiv \begin{pmatrix} 0 & -1 & 0 & 0 \\ -3f_1/2 & 1/2 & 0 & 0 \\ 0 & 0 & 0 & -1 \\ 0 & 0 & -3f_2/2 & 1/2 \end{pmatrix}, \tag{72}$$

and

$$\tilde{\Xi}_{ab} \equiv \begin{pmatrix} 0 & 0 & 0 & 0 \\ 0 & 0 & 3f_2 e^{-i\varphi}/2 & 0 \\ 0 & 0 & 0 & 0 \\ 3f_1 e^{i\varphi}/2 & 0 & 0 & 0 \end{pmatrix}, \tag{73}$$

with

$$\varphi(\eta) \equiv -i\int_{\eta_0}^{\eta} d\eta' \Xi^{(is)}(\eta'). \tag{74}$$

The two fluids are only coupled through $\tilde{\Xi}_{ab}$. However, $\Xi^{(is)}$ in Eq. (74) is purely imaginary: At early time the coupling term contributes to a rapidly changing phase φ. When the time scale of these oscillations is much shorter than that of structure growth, this force term can effectively be neglected and the different species decouple. Indeed, the velocity difference (in the direction along $\mathbf{k}$) between the coherent flows of the two species is large enough that the short modes of one fluid do not gravitationally see those of the other fluid.

The system we are left with is given by Eq. (71) with a vanishing right-hand side. For an EdS background the solution of this equation is given by [20]

$$\tilde{\delta}_\alpha \propto \exp(\nu_\alpha^{(\pm)}\eta), \tag{75}$$

with

$$\nu_\alpha^{(\pm)} = \frac{1}{4}(-1 \pm \sqrt{1 + 24 f_\alpha}). \tag{76}$$

The growing solutions in Eq. (75) explain the early-time evolution shown in Fig. 3. At early time, both CDM and baryons grow more slowly than e^η and their phases are dominated by their respective large-scale isocurvature displacement fields, as accounted for by the change of variable (70).

2. Late-time behavior

As the isodensity mode decays, one expects to recover at late time the single-fluid propagator $g_{ab}(\eta, \eta_0) \times \exp\Big[\int_{\eta_0}^{\eta} d\eta' \Xi^{(ad)}(\eta')\Big]$. More precisely, we can compute how the propagator ξ_{ab} deviates from the adiabatic one with a perturbative analysis. Indeed, since $\Xi_{ab}^{(is)}$ becomes small at late time, one can compute $\xi_{ab}(\mathbf{k}; \eta, \eta_0)$ perturbatively in $\Xi^{(is)}$.

Solving the first line of Eq. (28) at first order in $\Xi^{(is)}$ yields,

$$\xi_{ad}(\mathbf{k}, \eta, \eta_0) \approx \exp\Big(\int_{\eta_0}^{\eta} d\eta' \Xi^{(ad)}(\mathbf{k}, \eta')\Big)\Big[g_{ad}(\eta, \eta_0) + \int_{\eta_0}^{\eta} d\eta' g_{ab}(\eta, \eta')\Xi_{bc}^{(is)}(\mathbf{k}, \eta')g_{cd}(\eta', \eta_0)\Big]. \tag{77}$$

By plugging into this equation the expressions of the linear propagator g_{ab} from Eq. (63) and of $\Xi^{(\mathrm{is})}_{ab}$ from Eq. (65), and integrating in time yields

$$\xi_{ab}(\mathbf{k};\eta,\eta_0) \approx [g_{ab}(\eta,\eta_0) + \Xi^{(\mathrm{is})}(\mathbf{k},0)e^{-\eta_0/2}C_{ab}(\eta,\eta_0)]\exp\left(\int_{\eta_0}^{\eta} d\eta' \Xi^{(\mathrm{ad})}(\mathbf{k},\eta')\right), \tag{78}$$

with

$$\begin{aligned} C_{ab}(\eta,\eta_0) \equiv f_1 f_2 \Bigg[& \frac{2e^{\eta-\eta_0}}{5}\begin{pmatrix} 1 & 1 & -1 & -1 \\ 1 & 1 & -1 & -1 \\ 1 & 1 & -1 & -1 \\ 1 & 1 & -1 & -1 \end{pmatrix} + \frac{e^{(1/2)(\eta-\eta_0)}}{5}\begin{pmatrix} 12 & 8 & 12\frac{f_2}{f_1} & 8\frac{f_2}{f_1} \\ 3 & 2 & 3\frac{f_2}{f_1} & 2\frac{f_2}{f_1} \\ -12\frac{f_1}{f_2} & -8\frac{f_1}{f_2} & -12 & -8 \\ -3\frac{f_1}{f_2} & -2\frac{f_1}{f_2} & -3 & -2 \end{pmatrix} \\ & + 2\begin{pmatrix} \frac{f_2}{f_1}-3 & 2\frac{f_2}{f_1}-3 & 1-3\frac{f_2}{f_1} & 2-3\frac{f_2}{f_1} \\ 0 & 0 & 0 & 0 \\ 3\frac{f_1}{f_2}-1 & 3\frac{f_1}{f_2}-2 & 3-\frac{f_1}{f_2} & 3-2\frac{f_1}{f_2} \\ 0 & 0 & 0 & 0 \end{pmatrix} + e^{-(1/2)(\eta-\eta_0)}\begin{pmatrix} 4-2\frac{f_2}{f_1} & 8-8\frac{f_2}{f_1} & 4\frac{f_2}{f_1}-2 & 8\frac{f_2}{f_1}-8 \\ -2 & 2\frac{f_2}{f_1}-4 & 1-\frac{f_2}{f_1} & 4-2\frac{f_2}{f_1} \\ 2-4\frac{f_1}{f_2} & 8-8\frac{f_1}{f_2} & 2\frac{f_1}{f_2}-4 & 8\frac{f_1}{f_2}-8 \\ \frac{f_1}{f_2}-1 & 2\frac{f_1}{f_2}-4 & 2 & 4-2\frac{f_1}{f_2} \end{pmatrix} \\ & + 2e^{-(\eta-\eta_0)}\begin{pmatrix} 0 & 2\frac{f_2}{f_1}-3 & 0 & 3-2\frac{f_2}{f_1} \\ 0 & 3-\frac{f_2}{f_1} & 0 & \frac{f_2}{f_1}-3 \\ 0 & 2\frac{f_1}{f_2}-3 & 0 & 3-2\frac{f_1}{f_2} \\ 0 & 3-\frac{f_1}{f_2} & 0 & \frac{f_1}{f_2}-3 \end{pmatrix} + \frac{e^{-(3/2)(\eta-\eta_0)}}{5}\begin{pmatrix} -2 & 8 & 2 & -8 \\ 3 & -12 & -3 & 12 \\ -2 & 8 & 2 & -8 \\ 3 & -12 & -3 & 12 \end{pmatrix} \\ & + \frac{2e^{-2(\eta-\eta_0)}}{5}\begin{pmatrix} -1 & 1 & -\frac{f_2}{f_1} & \frac{f_2}{f_1} \\ 1 & -1 & \frac{f_2}{f_1} & -\frac{f_2}{f_1} \\ \frac{f_1}{f_2} & -\frac{f_1}{f_2} & 1 & -1 \\ -\frac{f_1}{f_2} & \frac{f_1}{f_2} & -1 & 1 \end{pmatrix}\Bigg]. \end{aligned} \tag{79}$$

Note that this result is written in terms of $\Xi^{(\mathrm{is})}$ taken at the initial time $\eta_{\mathrm{in}} = 0$, so that the time dependence of $\Xi^{(\mathrm{is})}$ is included in Eq. (78) and in the square bracket of Eq. (79). As expected by Eq. (65), the corrections to the propagator due to the isodensity mode are invariant under exchange of $f_1 \leftrightarrow -f_2$ and $1, 2 \leftrightarrow 3, 4$ in the matrix indices a, b. Furthermore, $C_{ab}(\eta,\eta) = 0$.

The final expression of the nonlinear propagator is obtained after the ensemble average of $\Xi^{(\mathrm{is})}(0) \times \exp\left[\int_{\eta_0}^{\eta} d\eta' \Xi^{(\mathrm{ad})}(\eta')\right]$ has been taken. We recall here that the different modes that enter in Ξ_{ab} are not statistically independent. The ensemble average can be written as (see Appendix A),

$$\langle \Xi^{(\mathrm{is})}(0) e^{\int_{\eta_0}^{\eta} d\eta' \Xi^{(\mathrm{ad})}(\eta')} \rangle = \sum_p \frac{x_{1,p-1}}{(p-1)!} \exp\left(\sum_{q=2}^{\infty} \frac{c_q}{q!}\right), \tag{80}$$

where c_q is the q-order cumulant of the adiabatic modes and $x_{1,p-1}$ is a p-order cross-cumulant defined as

$$x_{1,p-1} \equiv \left\langle \Xi^{(\mathrm{is})}(0) \left(\int_{\eta_0}^{\eta} d\eta' \Xi^{(\mathrm{ad})}(\eta')\right)^{p-1} \right\rangle_c. \tag{81}$$

The explicit values of such coefficients depend on the precise model. For Gaussian initial conditions only c_2 and $x_{1,1}$ are nonzero. Then, Eq. (80) can be rewritten as

$$\left\langle \Xi^{(\mathrm{is})}(0) \exp\left(\int_{\eta_0}^{\eta} d\eta' \Xi^{(\mathrm{ad})}(\eta')\right)\right\rangle = x_{1,1} \exp\left(\frac{c_2}{2}\right), \tag{82}$$

where

$$c_2 = \int_{\eta_0}^{\eta} d\eta' d\eta'' \langle \Xi^{(\mathrm{ad})}(\eta') \Xi^{(\mathrm{ad})}(\eta'')\rangle, \tag{83}$$

$$x_{1,1} = \int_{\eta_0}^{\eta} d\eta' \langle \Xi^{(\mathrm{is})}(0) \Xi^{(\mathrm{ad})}(\eta')\rangle. \tag{84}$$

At late time $\Xi^{(\mathrm{ad})}$ is dominated by the growing mode. Thus, we can express it as on the right-hand side of Eq. (37) and we can use Eq. (39) for c_2. For $x_{1,1}$ we find

$$x_{1,1} = -k^2\sigma_\times^2(e^{\eta} - e^{\eta_0}), \tag{85}$$

where $\sigma_\times^2$ is the cross-correlation between the initial isodensity and the adiabatic modes,

$$\sigma_\times^2 \equiv \frac{1}{3}\int d^3\mathbf{q}\,\frac{C_{\rm in}(q)}{q^2}, \tag{86}$$

with $C_{\rm in}$ defined by

$$\langle \Theta^{(\rm is)}(\mathbf{q},0)\Theta^{(\rm ad)}(\mathbf{q}',0)\rangle = \delta_{\rm D}(\mathbf{q}+\mathbf{q}')C_{\rm in}(q). \tag{87}$$

Finally, the ensemble average in Eq. (82) can be written as

$$\langle \Xi^{(\rm is)} e^{\int_{\eta_0}^{\eta} d\eta' \Xi^{(\rm ad)}(\eta')}\rangle = -k^2\sigma_\times^2(e^\eta - e^{\eta_0})e^{-k^2\sigma_d^2(e^\eta-e^{\eta_0})^2/2}, \tag{88}$$

so that the nonlinear propagator reads, at first order,

$$G_{ab}(\mathbf{k};\eta,\eta_0) \approx [g_{ab}(\eta,\eta_0) - k^2\sigma_\times^2(e^\eta - e^{\eta_0})e^{-\eta_0/2}C_{ab}(\eta,\eta_0)] \times e^{-k^2\sigma_d^2(e^\eta-e^{\eta_0})^2/2}. \tag{89}$$

It is possible to compute the nonlinear propagator at higher orders in $\Xi^{(\rm is)}$. In particular, in Appendix B we derive a recurrence formula for the most growing mode of the resummed propagator, to any order in $\Xi^{(\rm is)}$. We are now in the position to illustrate the effect discussed in this section in a practical case, i.e. the mixture of baryons and cold dark matter after decoupling.

IV. CDM AND BARYONS AFTER DECOUPLING

As an application, in this section we consider the case of baryons and CDM particles just after decoupling. This situation is illustrative of the concepts that we introduced in this paper. Here we focus on the behavior of the propagators on scales which are interesting for PT calculations, i.e. $k \lesssim 1h\ \mathrm{Mpc}^{-1}$. We will see that for such statistical objects and such scales the impact of isodensity modes is very small. We leave the calculations of power spectra for further studies.

The first step of our analysis is to properly identify the isodensity modes after recombination. We will assume that the *primordial* (i.e. before horizon crossing) large-scale perturbations are strictly adiabatic. In this case each fluid component is proportional to the same random field, for instance, the primordial curvature perturbation $\zeta(\mathbf{k})$. We can assume that at the initial time $\eta_{\rm in} = 0$ the different fluid variables are in the linear regime. Then, they can be written in terms of the initial linear transfer functions $T_a(k,0)$ as

$$\Psi_a(\mathbf{k},0) = T_a(k,0)\zeta(\mathbf{k}). \tag{90}$$

We will use CAMB [21] to generate the initial CDM and baryon transfer functions, assuming the following cosmological parameters: $\Omega_c = 0.233$, $\Omega_b = 0.0461$, $\Omega_\Lambda = 0.721$, $h = 0.700$, $n_s = 0.96$, $A_\zeta = 2.46\times10^{-9}$ and massless neutrino species.

A remark is in order here. Cosmological fluctuations, such as those described by the CAMB code, obey linear general relativistic equations. On large scales, i.e. on scales comparable with the Hubble radius, these equations may considerably deviate from the Newtonian equations used in RPT, also at the linear level. Thus, one may worry that the transfer functions generated by CAMB will be affected by these deviations, which are gauge dependent. However, as shown in Appendix C, for a set of *pressureless* fluids there exists a choice of variables for which at linear order the relativistic equations *exactly* reduce to the Newtonian equations. For the density contrasts of cold dark matter and baryons, this choice corresponds to take the energy density perturbations in a gauge comoving to the total fluid. For the velocity divergences this corresponds to take them in the longitudinal gauge. In the limit where we can neglect radiation energy and momentum, the dynamics of these variables is well described by the Newtonian equations even on super-Hubble scales.

Finally, note that even though $\Omega_\Lambda \neq 0$, we will use the linear propagator derived in Sec. III in a EdS universe. Indeed, as explained in [3] most of the cosmological dependence is encoded in the linear growth function D_+ and using the propagators derived for an EdS universe is a very good approximation.

A. The linear modes after decoupling

In Fig. 4 we show the transfer functions for the different fluid variables normalized to the transfer function of the total matter perturbation δ_m. We choose redshift $z = 900$ as initial time $\eta_{\rm in} = 0$. At this redshift the energy density and momentum density of the radiation are still important (of the order of 20%). However, we will neglect their contributions in our treatment. Moreover, since on super-horizon scales the transfer functions are all approximately equal, then $f_+ \simeq 1$ and we will take $\Theta_\alpha = -\theta_\alpha$. Note that, contrary to what has been done in [7], one cannot consistently assume that the density and velocity transfer functions are the same.

The linear evolution of each mode can be constructed by applying the linear propagator g_{ab} given in Eq. (63). In particular, $g_{ab}^{(+)}(\eta,\eta_0)$, $g_{ab}^{(-)}(\eta,\eta_0)$, $g_{ab}^{(\rm is)}(\eta,\eta_0)$, and $g_{ab}^{(\rm ci)}(\eta,\eta_0)$ are the growing and decaying adiabatic, and the decaying and constant isodensity time-dependent projectors, given, respectively, by the first, second, third, and fourth term on the right-hand side of Eq. (63). In terms of these projectors one can define the transfer function for each mode as

$$\begin{aligned} T^{(+)}(k,\eta) &\equiv (f_c,0,f_b,0)g_{ab}^{(+)}(\eta,0)T_b(k,0),\\ T^{(-)}(k,\eta) &\equiv (f_c,0,f_b,0)g_{ab}^{(-)}(\eta,0)T_b(k,0),\\ T^{(\rm is)}(k,\eta) &\equiv (0,1,0,-1)g_{ab}^{(\rm is)}(\eta,0)T_b(k,0),\\ T^{(\rm ci)}(k,\eta) &\equiv (1,0,-1,0)g_{ab}^{(\rm ci)}(\eta,0)T_b(k,0). \end{aligned} \tag{91}$$

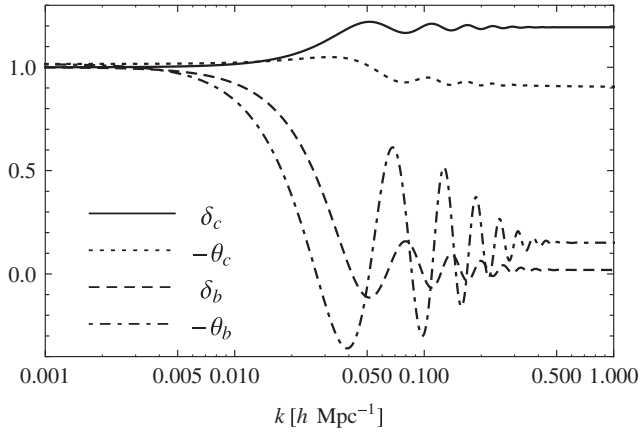

FIG. 4. Shape and amplitude of the transfer functions at $z = 900$. The transfer functions are plotted in units of the total density transfer function. From top to bottom we have the CDM density transfer function (continuous line), the CDM velocity transfer function (dotted line), the baryon density transfer function (dashed line), and the baryon velocity transfer function (dotted-dashed line). On superhorizon scales they are all approximately equal, denoting that $f_+ \simeq 1$. One can observe that at this high redshift the baryon transfer functions are highly suppressed.

These definitions have been chosen in such a way that

$$T_a = T^{(+)}u_a^{(+)} + T^{(-)}u_a^{(-)} + T^{(\mathrm{is})}u_a^{(\mathrm{is})} + T^{(\mathrm{ci})}u_a^{(\mathrm{ci})}. \quad (92)$$

These quantities are shown on Fig. 5 where we plot the amplitude of the transfer functions $T^{(-)}$, $T^{(\mathrm{is})}$, and $T^{(\mathrm{ci})}$ at initial time, normalized to the amplitude of $T^{(+)}$. Note that from these results one can compute the r.m.s. of $\Xi^{(\mathrm{is})}$ that appeared in the previous section. One finds that

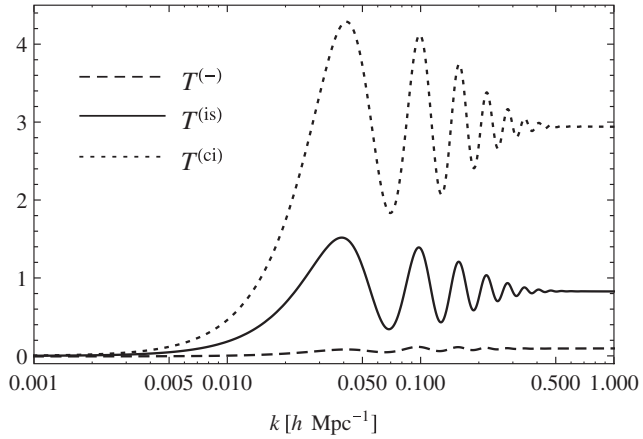

FIG. 5. The transfer functions at $z = 900$, normalized to the adiabatic growing mode. From bottom to top, the adiabatic decaying mode (dashed line), the isodensity decaying mode (continuous line), and the isodensity constant mode (dotted line).

$$\langle \Xi^{(\mathrm{is})^2} \rangle^{1/2} = 8.6 \times 10^{-3} \frac{k}{h\,\mathrm{Mpc}^{-1}}, \quad (93)$$

at redshift $z = 900$, showing that for our scales of interest, $k \lesssim 1h\ \mathrm{Mpc}^{-1}$, the effects of the isocurvature modes can only be small. The explicit dependence of the propagators on the isodensity modes is shown in the following.

B. The nonlinear propagators

In the presence of the decaying isodensity mode, the resummed propagator is no longer proportional to the free field propagator. The effect of the isodensity mode on the resummed propagator is modulated by the matrix $C_{ab}(\eta, \eta_0)$ in Eq. (79). To show this modulation, let us define the quantities

$$\begin{aligned} R_{\delta_c}(k, \eta) &\equiv C_{1a}(\eta, 0)T_a(k, 0)/T_{\delta_c}(k, \eta), \\ R_{\delta_b}(k, \eta) &\equiv C_{3a}(\eta, 0)T_a(k, 0)/T_{\delta_b}(k, \eta), \end{aligned} \quad (94)$$

where

$$\begin{aligned} T_{\delta_c}(k, \eta) &\equiv g_{1a}(\eta, 0)T_a(k, 0), \\ T_{\delta_b}(k, \eta) &\equiv g_{3a}(\eta, 0)T_a(k, 0). \end{aligned} \quad (95)$$

In Fig. 6 we have plotted these quantities as a function of scale and for different redshifts $z = 500$, 200, 40, 10, 3, corresponding to $D_+ = 1.99$, 5.26, 25.71, 95.47, 258.43. In Fig. 7 we have plotted R_{δ_c} and R_{δ_b} as a function of redshift and for different scales $k = 0.001$, 0.01, 0.1, 1 in units of $h\,\mathrm{Mpc}^{-1}$. At small redshift (large η) R_{δ_c} and R_{δ_b} are dominated by the most growing mode of the matrix C_{ab}, i.e. the first term in Eq. (79) which grows as e^η, so that they are independent of redshift. At higher redshift the decaying modes in the matrix C_{ab} become important and for $z = 900$, corresponding to the initial time $\eta_{\mathrm{in}} = 0$, R_{δ_c} and R_{δ_b} go to zero. Note that R_{δ_b} becomes infinite twice around $z \sim 700$. This is because at early times, right after recombination, the linear baryon density contrast is positive and its decaying isodensity mode dominates over the growing adiabatic mode. Later on it reaches a negative minimum where the growing adiabatic mode starts dominating. Thus $T_{\delta_b}(k, \eta)$ crosses zero twice.

The entire effect of the isodensity mode on the propagator is represented by the second term in the square bracket in Eq. (89), which for $\eta_0 = \eta_{\mathrm{in}} = 0$ is

$$-k^2 r_\times \sigma_d^2 (D_+(\eta) - 1) C_{ab}(\eta, 0). \quad (96)$$

Here the parameter $r_\times$ is the ratio of the isodensity-adiabatic displacement cross-correlation $\sigma_\times^2$ to the variance of the adiabatic displacement field σ_d^2,

$$r_\times \equiv \frac{\sigma_\times^2}{\sigma_d^2} = \frac{\int d\ln q T^{(\mathrm{is})}(q, 0) T^{(+)}(q, 0) q^{n_s - 3}}{\int d\ln q [T^{(+)}(q, 0)]^2 q^{n_s - 3}}. \quad (97)$$

(In the second equality we have neglected the adiabatic decaying mode.) At $z = 900$ this is $r_\times \simeq 0.85$. For

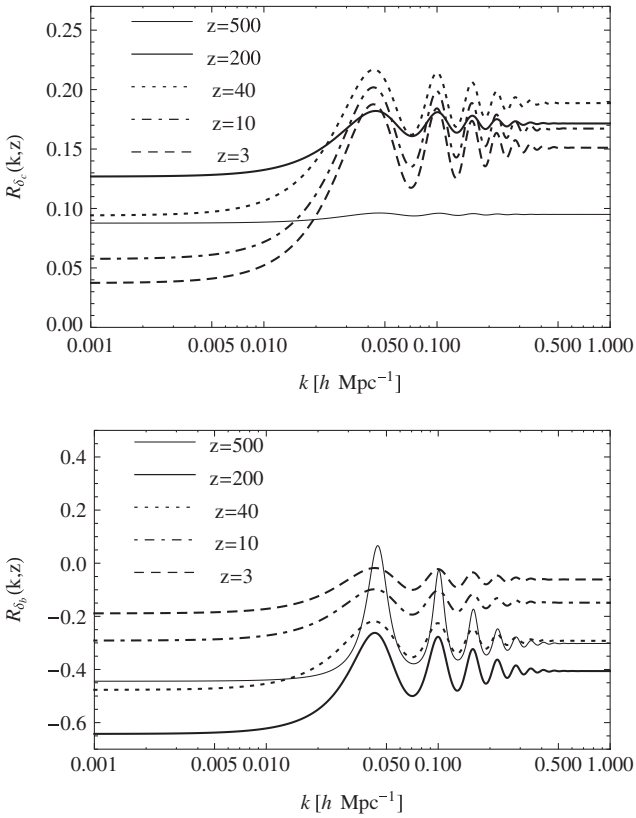

FIG. 6. The quantities $R_{\delta_c} \equiv C_{1a}(z, z_{\rm in} = 900)T_a(k, z_{\rm in} = 900)/T_{\delta_c}(k, z)$ (upper panel) and $R_{\delta_b} \equiv C_{3a}(z, z_{\rm in} = 900)T_a(k, z_{\rm in} = 900)/T_{\delta_b}(k, z)$ (lower panel) as a function of scale at different redshifts.

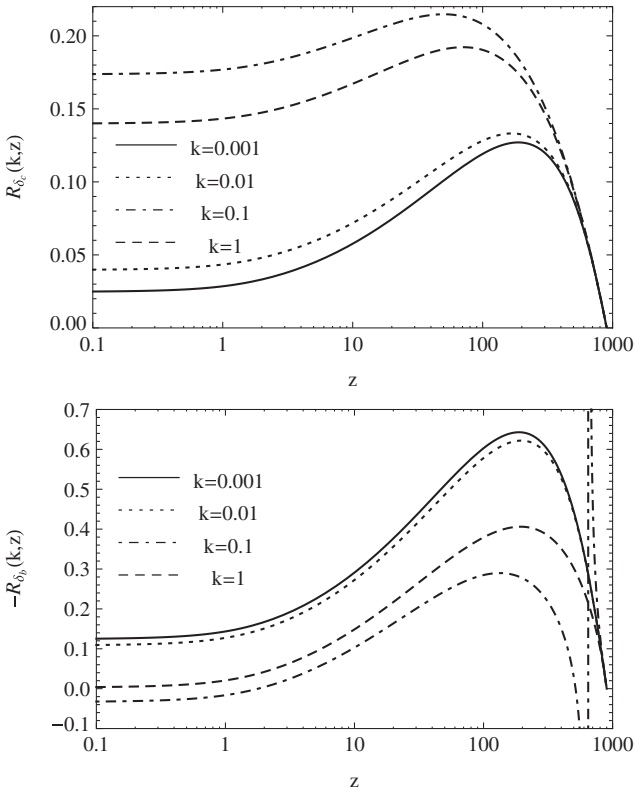

FIG. 7. The quantities R_{δ_c} (upper panel) and R_{δ_b} (lower panel) as a function of redshift at different scales.

$k\sigma_d D_+ \gg 1$ the nonlinear propagator goes quickly to zero, due to the exponential damping in Eq. (89). Thus, the key quantity responsible for suppressing the effect at low redshift is actually the time dependence in Eq. (96) given by $D_+(z) - 1$. For scales $k < k_d \equiv (\sigma_d D_+)^{-1}$, the corrective term (96) is always found to be extremely small.

In order to be more quantitative, in Fig. 8 we show the effect of the isodensity mode on the nonlinear propagator by plotting $G_{\delta_c}/G^{(\rm ad)}_{\delta_c} - 1$ and $G_{\delta_b}/G^{(\rm ad)}_{\delta_b} - 1$ as a function of redshift and at fixed scale k_d, where

$$G_{\delta_c}(k, \eta) \equiv G_{1a}(k; \eta, 0)T_a(k, 0),$$
$$G_{\delta_b}(k, \eta) \equiv G_{3a}(k; \eta, 0)T_a(k, 0), \tag{98}$$

and $G^{(\rm ad)}_{\delta_c}(k, z)$ and $G^{(\rm ad)}_{\delta_b}(k, z)$ are the same quantities in the adiabatic case—i.e. for $\Xi^{(\rm is)} = 0$. We have used that the value of the variance of the displacement field is $\sigma_d \simeq 9.2 \times 10^{-3} h^{-1}\,\mathrm{Mpc}$ at $z = 900$. For $z \leq 50$ we find that the effect is less that $\sim 1\%$ and for $z \leq 9$ less than $\sim 1‰$. Note that the effects are of different signs between CDM and baryons.

Another example where these effects could be significant is when the isodensity modes are set at much lower

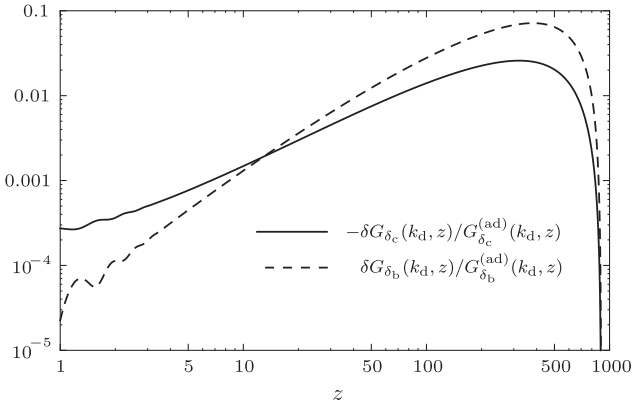

FIG. 8. Effect of the isodensity mode on the nonlinear propagators normalized to the adiabatic nonlinear propagators, $\delta G_{\delta_c}/G^{(\rm ad)}_{\delta_c} \equiv G_{\delta_c}/G^{(\rm ad)}_{\delta_c} - 1$ and $\delta G_{\delta_b}/G^{(\rm ad)}_{\delta_b} \equiv G_{\delta_b}/G^{(\rm ad)}_{\delta_b} - 1$, where $G^{(\rm ad)}_{\delta_c}$ and $G^{(\rm ad)}_{\delta_b}$ are the CDM and baryon nonlinear propagators in absence of isodensity mode, computed at fixed scale k_d, as a function of redshifts. The oscillations appearing for $z \lesssim 3$ are due to the oscillatory behavior of the transfer functions at $k \lesssim 0.4$. Note that the effect on the CDM propagator is plotted with the sign changed.

redshift. This is potentially the case for massive neutrinos. However, massive neutrinos cannot be fully considered as nonrelativistic particles during their cosmological history as their behavior is determined by a whole set of extra modes, such as pressure fluctuations and anisotropic stresses. We leave the study of this special case for the future.

V. CONCLUSIONS

The eikonal approximation provides an efficient formalism within which exact resummation in the high-k limit can be performed explicitly or numerically. We were able to recover the standard results obtained in [2,3,5,6] concerning the nonlinear 2-point and multipoint propagators describing the gravitational instabilities of a single pressureless fluid. In particular, the propagators are corrected by an exponential cutoff whose scale is fixed by the amplitude of the displacement field along the wave-mode $\mathbf{k}$. We have shown this irrespective of the growth rate of the displacement field and of whether it follows the linear regime, thus extending the standard results previously quoted.

Note that this formalism is based on a mode separation between large-scales and small-scales. Indeed, we have assumed that the large-scale modes with momentum $\mathbf{q}$, collected in the random variable Ξ, are much smaller that the small-scale modes $\mathbf{k}$. In Fig. 9 we show the contribution from adiabatic modes to the variance of the displacement field, σ_d, per logarithmic interval. As one can see, most of the contribution comes from modes with $q \lesssim 0.1h\,\mathrm{Mpc}^{-1}$ but that of smaller modes, with $q \approx 0.1$–$1h\,\mathrm{Mpc}^{-1}$ is not negligible. This suggests that, for $k \approx 0.1$–$0.3h\,\mathrm{Mpc}^{-1}$, a better description of the damping could be obtained by setting a UV cutoff for q in Eq. (40).

We have then extended the eikonal approximation to multiple pressureless fluids. In this case one can identify two types of modes: two adiabatic modes and two isodensity modes per added species. Isodensity modes are responsible for new effects. Indeed, their large-scale flow changes the phase but also (unlike the adiabatic modes) the amplitude of small scales. Thus, the growth of structure and consequently the amplitude of propagators and spectra are affected in a more complex way than in the purely adiabatic case. In this paper we focus our results on the propagators, leaving the study of power spectra for future work.

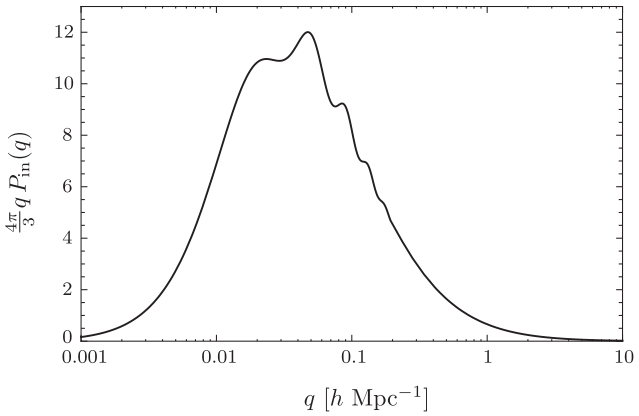

FIG. 9. Mode contribution per log interval to the variance of the displacement field from the adiabatic modes, Eq. (40), at $z = 0$.

In contrast to the single-fluid case, where the effect of large-scale adiabatic modes can be taken into account analytically, for the isodensity modes we have not been able to find an analytic form for the resummed propagator. In this case, one should rely on a numerical or a perturbative approach. The latter is sufficient when one considers the case of CDM-baryon mixing. For this example, we found that the impact of isodensity modes on the propagators is very small at low redshift and for scales of interest for standard PT, i.e. for $k \lesssim 1h\,\mathrm{Mpc}^{-1}$. However, there might be cases where the impact of large-scale modes is more significant, for instance when the scale of interest are close to the nonlinear regime at the time the isodensity modes are set in. This is expected to be the case for massive neutrinos. Although we did not address this case explicitly, we stress that the eikonal method can be used irrespective of the field content of the system. We leave the case of massive neutrinos for further studies.

ACKNOWLEDGMENTS

We thank the participants of the PTchat workshop at IPhT in Saclay for interesting discussions. F. V. wishes to thank Antonio Riotto and Ravi Sheth for fruitful conversations.

APPENDIX A: COMPUTATION OF MOMENTS

We want to compute the value of

$$g_n = \langle \Xi^n \exp(\mathcal{D}) \rangle, \tag{A1}$$

where Ξ and $\mathcal{D}$ are two random variables whose statistical properties are entirely characterized by their joint cumulants,

$$x_{p,q} = \langle \Xi^p \mathcal{D}^q \rangle_c. \tag{A2}$$

It is convenient to introduce the auxiliary function $\exp(\mathcal{D} + \lambda\Xi)$ and to notice that

$$g_n = \frac{d^n}{d\lambda^n} \langle \exp(\mathcal{D} + \lambda\Xi) \rangle|_{\lambda=0}. \tag{A3}$$

The ensemble average that appears in this expression can be written in terms of the cumulants generating function of $\mathcal{D} + \lambda\Xi$ as

$$g_n = \frac{d^n}{d\lambda^n} \exp\left(\sum_{p=0}^{\infty} \sum_{q=0}^{p} \frac{1}{q!} \frac{1}{(p-q)!} x_{q,p-q} \lambda^q\right)\Big|_{\lambda=0}, \tag{A4}$$

which can be rewritten as

$$g_n = \exp\left(\sum_{p=0}^{\infty} \frac{x_{0,p}}{p!}\right) \frac{d^n}{d\lambda^n} \exp\left(\sum_{q=1}^{n} \frac{X_q}{q!} \lambda^q\right)\Big|_{\lambda=0}, \tag{A5}$$

where

$$X_q = \sum_{p=q}^{\infty} \frac{1}{(p-q)!} x_{q,p-q}. \tag{A6}$$

g_n can then be formally expressed in terms of X_q as

$$g_0 = \exp\left(\sum_{p=0}^{\infty} \frac{x_{0,p}}{p!}\right), \tag{A7}$$

$$g_1 = X_1 g_0, \tag{A8}$$

$$g_2 = (X_1^2 + X_2) g_0, \tag{A9}$$

$$g_3 = (X_1^3 + 3X_1 X_2 + X_3) g_0, \tag{A10}$$

$$\ldots.$$

Note that for a unit g_0 the relation between X_q and g_n is exactly the one relating cumulants of order q with moments of order n. Thus, in general this relation is obtained by the Arbogast-Faà di Bruno formulas.

These relations greatly simplify in the case of Gaussian initial conditions, assuming—without loss of generality—that $x_{0,0} = x_{1,0} = x_{0,1} = 0$. Indeed, in this case only X_1 and X_2 are nonzero,

$$X_1 = x_{1,1}, \qquad X_2 = x_{2,0}, \tag{A11}$$

so that

$$g_0 = \exp\left(\frac{x_{0,2}}{2!}\right), \tag{A12}$$

$$g_1 = x_{1,1} g_0, \tag{A13}$$

$$g_2 = (x_{1,1}^2 + x_{2,0}) g_0, \tag{A14}$$

$$g_3 = (x_{1,1}^3 + 3x_{1,1} x_{2,0}) g_0, \tag{A15}$$

$$\ldots.$$

APPENDIX B: HIGHER-ORDER TIME DEPENDENCE

It is possible to compute the nonlinear propagator at higher orders in $\Xi^{(\mathrm{is})}$ using the expansion

$$\xi_{af}(\mathbf{k}, \eta, \eta_0) = g_{af}(\eta, \eta_0) \exp\left(\int_{\eta_0}^{\eta} d\eta' \Xi^{(\mathrm{ad})}(\mathbf{k}, \eta')\right) + \xi_{af}^{(1)}(\mathbf{k}, \eta, \eta_0) + \xi_{af}^{(2)}(\mathbf{k}, \eta, \eta_0) + \cdots, \tag{B1}$$

where

$$\begin{aligned} \xi_{af}^{(1)} &\equiv \exp\left(\int_{\eta_0}^{\eta} d\eta' \Xi^{(\mathrm{ad})}(\mathbf{k}, \eta')\right) \int_{\eta_0}^{\eta} d\eta' g_{ab}(\eta, \eta') \Xi_{bc}^{(\mathrm{is})}(\mathbf{k}, \eta') g_{cf}(\eta', \eta_0), \\ \xi_{af}^{(2)} &\equiv \exp\left(\int_{\eta_0}^{\eta} d\eta' \Xi^{(\mathrm{ad})}(\mathbf{k}, \eta')\right) \int_{\eta_0}^{\eta} d\eta' \int_{\eta_0}^{\eta'} d\eta'' g_{ab}(\eta, \eta') \Xi_{bc}^{(\mathrm{is})}(\mathbf{k}, \eta') g_{cd}(\eta', \eta'') \Xi_{de}^{(\mathrm{is})}(\mathbf{k}, \eta'') g_{ef}(\eta'', \eta_0), \ldots. \end{aligned} \tag{B2}$$

In particular, here we derive an explicit expression for the most growing solution to the integrals above, in terms of a recurrence formula.

The key point is to show that the fastest growing mode of the amplitude of the corrections to the resummed propagator goes as the adiabatic growing mode, i.e. $\propto e^{\eta - \eta_0}$, to all orders in $\Xi^{(\mathrm{is})}$. Let us consider the amplitude of the nth-order correction. From Eq. (B2) and using that $g_{ab}^{(\lambda)}(\eta, \eta_0) \propto e^{\lambda(\eta - \eta_0)}$ and $\Xi_{ab}^{(\mathrm{is})}(\eta) \propto e^{-(1/2)\eta}$ ($\eta_{\mathrm{in}} = 0$), its time dependence is proportional to n nested integrals, given by

$$\mathcal{I}^{(n)} \equiv \int_{\eta_0}^{\eta} d\eta_1 e^{\lambda_0(\eta - \eta_1)} e^{-(1/2)\eta_1} \int_{\eta_0}^{\eta_1} d\eta_2 e^{\lambda_1(\eta_1 - \eta_2)} e^{-(1/2)\eta_2} \cdots \int_{\eta_0}^{\eta_{n-1}} d\eta_n e^{\lambda_{n-1}(\eta_{n-1} - \eta_n)} e^{-(1/2)\eta_n} e^{\lambda_n(\eta_n - \eta_0)}, \tag{B3}$$

where each λ_i can take the values $\{1, 0, -1/2, -3/2\}$. As we are only interested in the fastest growing mode, we take $\lambda_0 = 1$.

We define

$$\alpha_{ij} \equiv \lambda_j - \lambda_i - \frac{j - i}{2}, \tag{B4}$$

satisfying $\alpha_{ij} + \alpha_{jk} = \alpha_{ik}$. It is important to note that $\alpha_{0i} < 0$ for $i \neq 0$. Then, we can rewrite the integrals above as

$$C\int_{\eta_0}^{\eta} d\eta_1 e^{\alpha_{01}\eta_1}\int_{\eta_0}^{\eta_1} d\eta_2 e^{\alpha_{12}\eta_2}\int_{\eta_0}^{\eta_{n-1}} d\eta_n e^{\alpha_{n-1,n}\eta_n} \quad \text{(B5)}$$

with $C \equiv e^{\lambda_0\eta}e^{-\lambda_n\eta_0}$. By performing an integration by parts on η_1, we find the boundary term

$$C\left[\frac{e^{\alpha_{01}\eta_1}}{\alpha_{01}}\int_{\eta_0}^{\eta_1} d\eta_2 e^{\alpha_{12}\eta_2}\cdots\int_{\eta_0}^{\eta_{n-1}} d\eta_n e^{\alpha_{n-1,n}\eta_n}\right]_{\eta_1=\eta_0}^{\eta_1=\eta}, \quad \text{(B6)}$$

and the remaining integrals

$$-C\int_{\eta_0}^{\eta} d\eta_1 \frac{e^{\alpha_{01}\eta_1}}{\alpha_{01}} e^{\alpha_{12}\eta_1}\cdots\int_{\eta_0}^{\eta_{n-1}} d\eta_n e^{\alpha_{n-1,n}\eta_n}. \quad \text{(B7)}$$

The lower bound for the boundary term obviously vanishes. Therefore, the boundary term contains an $e^{\alpha_{01}\eta}$ factor making it subleading with respect to the remaining integrals, which for large η become constant. To see this, we perform $(n-2)$ more integration by parts, every time dropping the boundary term for the very same reason, until we are left with

$$(-1)^{n-1}\frac{C}{\alpha_{01}\alpha_{02}\cdots\alpha_{0,n-1}}\int_{\eta_0}^{\eta} d\eta_n e^{\alpha_{0n}\eta_n}. \quad \text{(B8)}$$

The leading term of this integral is independent of η,

$$(-1)^n\prod_{i=1}^{n}\frac{C}{\alpha_{0i}}e^{\alpha_{0n}\eta_0}, \quad \text{(B9)}$$

and by replacing C by its definition, we have

$$\mathcal{I}^{(n)} = \prod_{i=1}^{n}\frac{1}{\alpha_{i0}}e^{-(n/2)\eta_0}e^{\eta-\eta_0}. \quad \text{(B10)}$$

Now that we have studied the time dependence, we can reintroduce the time-independent matrices $h_{ab}g_{bc}^{(\lambda_i)}$ in (B2) and sum over λ_i in each of the integrals of Eq. (B3). Let us define the time-independent matrices

$$A_{ab}^{(0)} \equiv g_{ab}^{(1)}, \quad A_{ab}^{(i)} \equiv \sum_{\lambda=1,0,-1/2,-3/2}\frac{h_{ac}g_{cb}^{(\lambda)}}{1+i/2-\lambda}, \quad i\geq 1, \quad \text{(B11)}$$

where h_{ab} is defined in Eq. (65), $g_{ab}^{(\lambda)} \equiv g_{ab}^{(\lambda)}(\eta_0,\eta_0)$ are the time-independent projectors on the right-hand side of Eq. (63), and the sum runs over $\lambda = 1, 0, -1/2, -3/2$ corresponding to the 4 linear modes $+$, ci, is and $-$. The denominator $(1 + i/2 - \lambda)$ is exactly the α_{i0} of Eq. (B10). It is easy to verify that the most growing solution for $\xi_{ab}^{(n)}$ in Eq. (B1) is then given by

$$\xi_{ab}^{(n)}(\mathbf{k},\eta,\eta_0) = [\Xi^{(\mathrm{is})}(\mathbf{k},0)e^{-\eta_0/2}]^n\left[\mathbf{A}^{(0)}\prod_{i=1}^{n}\mathbf{A}^{(i)}\right]_{ab} \times e^{\eta-\eta_0}\exp\left(\int_{\eta_0}^{\eta} d\eta'\Xi^{(\mathrm{ad})}(\mathbf{k},\eta')\right). \quad \text{(B12)}$$

This equation formally generalizes the expression for the most growing mode contained in Eqs. (78) and (79) to any order. Note that the time dependence is the same as the *linear* growing mode, i.e. $\propto e^{\eta}$. Ensemble averages of these quantities can be taken using the equations given in appendix A.

APPENDIX C: TREATING SUPERHORIZON SCALES

Let us consider a linearly perturbed FLRW metric in longitudinal gauge with only scalar perturbations. In the absence of anisotropic stress the two metric potentials are identical and the metric simply reads

$$ds^2 = a^2(\tau)[-(1+2\phi_{\mathrm{lon}})d\tau^2 + (1-2\phi_{\mathrm{lon}})d\mathbf{x}^2], \quad \text{(C1)}$$

where τ is the conformal time defined by $d\tau = dt/a(t)$.

Combining the 00 and the $0i$ components of Einstein's equations gives, in Fourier space, [22]

$$k^2\phi_{\mathrm{lon}} = -\frac{3}{2}\mathcal{H}^2(\delta_{\mathrm{lon}} + 3\mathcal{H}^2\theta_{\mathrm{lon}}/k^2), \quad \text{(C2)}$$

where δ_{lon} and θ_{lon} are the total density contrast and dimensionless velocity divergence [23], respectively, in longitudinal gauge and $\mathcal{H} \equiv d\ln a/d\tau$ is the conformal Hubble rate. Moreover, in this gauge, the continuity and Euler equations for a single-fluid read, at linear order, [22]

$$\delta'_{\mathrm{lon}} = -\mathcal{H}\theta_{\mathrm{lon}} + 3\phi'_{\mathrm{lon}}, \quad \text{(C3)}$$

$$\theta'_{\mathrm{lon}} = -(\mathcal{H}'/\mathcal{H} + \mathcal{H})\theta_{\mathrm{lon}} + k^2\phi_{\mathrm{lon}}/\mathcal{H}, \quad \text{(C4)}$$

where a prime denotes the derivative with respect to conformal time.

One can check that, at the linear level, the Newtonian Euler equation (2) is the same as its relativistic version, Eq. (C4), while the continuity equations (1) and (C3) differ by the term $3\phi'_{\mathrm{lon}}$. Indeed, for instance, using that $a \propto \tau^2$ in matter dominance, one can check that the solutions to the above equations are

$$\phi_{\mathrm{lon}}(k,\tau) = \phi_+(k) + (k\tau)^{-5}\phi_-(k), \quad \text{(C5)}$$

and

$$\delta_{\mathrm{lon}} = -\left(2+\frac{1}{6}(k\tau)^2\right)\phi_+ - \left(\frac{1}{6}(k\tau)^{-3} - 3(k\tau)^{-5}\right)\phi_-, \quad \text{(C6)}$$

$$\theta_{\mathrm{lon}} = \frac{1}{6}(k\tau)^2\phi_+ - \frac{1}{4}(k\tau)^{-3}\phi_-. \quad \text{(C7)}$$

Thus, Eq. (C7) correctly describes the growing and decaying solutions of θ in the Newtonian limit, Eq. (11), with $\theta_+ \propto a$ and $\theta_- \propto a^{-3/2}$, even on super-Hubble scales, while for $\delta_{\rm lon}$ we recover the Newtonian case, Eq. (10), only in the limit $k\tau \gg 1$.

One can define a quantity which obeys the Newtonian continuity equation even on super-Hubble scales. The comoving energy density perturbation, defined as

$$\begin{aligned}\delta_{\rm com} &\equiv \delta_{\rm lon} + 3\mathcal{H}^2\theta_{\rm lon}/k^2 \\ &= -\tfrac{1}{6}[(k\tau)^2\phi_+ + (k\tau)^{-3}\phi_-],\end{aligned} \tag{C8}$$

does this job. Indeed, replacing $\phi'_{\rm lon}$ using the $0i$ components of Einstein's equation [22], and using Eq. (C4), Eq. (C3) reads

$$\delta'_{\rm com} = -\mathcal{H}\theta_{\rm lon}, \tag{C9}$$

thus reproducing the linear part of the continuity equations in the Newtonian limit, Eq. (1). Moreover, in terms of this variable Eq. (C2) becomes a Poisson-like equation,

$$k^2\phi_{\rm lon} = -\frac{3}{2}\mathcal{H}^2\delta_{\rm com}, \tag{C10}$$

reproducing Eq. (3).

We conclude that at linear level the Newtonian equations (1)–(3) describe the relativistic dynamics once we interpret the Newtonian potential ϕ as the metric potentials in longitudinal gauge $\phi_{\rm lon}$, the Newtonian density contrast δ as the *comoving* energy density perturbation $\delta_{\rm com}$ and θ as the dimensionless velocity divergence in longitudinal gauge, $\theta_{\rm lon}$.

The case of many fluids is not very different. In this case one can show that for each species α the relativistic perturbation variable which satisfies the Newtonian continuity equation is the energy density perturbation comoving to the *total* fluid,

$$\delta_{\alpha,\rm com} \equiv \delta_{\alpha,\rm lon} + 3\mathcal{H}^2\theta_{\rm lon}/k^2, \tag{C11}$$

where $\theta_{\rm lon}$ is the total dimensionless velocity divergence in longitudinal gauge,

$$\theta_{\rm lon} \equiv \sum_\alpha f_\alpha \theta_{\alpha,\rm lon}. \tag{C12}$$

Using this variable, Eq. (C2) becomes a Poisson equation while the velocity divergence in longitudinal gauge for each species α, $\theta_{\alpha,\rm lon}$, naturally satisfies the Newtonian Euler equation.

Let us connect these variables with those of CAMB in the case of a mixture of cold dark matter and baryons. CAMB uses synchronous gauge comoving with cold dark matter [21]. Using the gauge transformation between synchronous and longitudinal gauge [22] we have that

$$\begin{aligned}\delta_{\alpha,\rm CAMB} &= \delta_{\alpha,\rm lon} + 3\mathcal{H}\sigma, \\ \theta_{\alpha,\rm CAMB} &= \theta_{\alpha,\rm lon} - \sigma k^2/\mathcal{H},\end{aligned} \tag{C13}$$

where σ is the shear. This is related to the usual synchronous metric perturbation variables $h_{\rm syn}$ and $\eta_{\rm syn}$, respectively, the trace and traceless part of the spatial metric, by $\sigma = (h'_{\rm syn} + 6'_{\rm syn})/2k^2$. Using these equations, since in CAMB the dark matter velocity vanishes, $\theta_{c,\rm CAMB} = 0$, we have

$$\begin{aligned}\theta_{c,\rm lon} &= \sigma k^2/\mathcal{H}, \\ \theta_{b,\rm lon} &= \theta_{b,\rm CAMB} + \sigma k^2/\mathcal{H}, \\ \delta_{\alpha,\rm com} &= \delta_{\alpha,\rm CAMB} + 3\mathcal{H}^2 f_b \theta_{b,\rm CAMB}/k^2.\end{aligned} \tag{C14}$$

[1] F. Bernardeau, S. Colombi, E. Gaztañaga, and R. Scoccimarro, Phys. Rep. **367**, 1 (2002).
[2] M. Crocce and R. Scoccimarro, Phys. Rev. D **73**, 063519 (2006).
[3] M. Crocce and R. Scoccimarro, Phys. Rev. D **73**, 063520 (2006).
[4] M. Crocce and R. Scoccimarro, Phys. Rev. D **77**, 023533 (2008).
[5] F. Bernardeau, M. Crocce, and R. Scoccimarro, Phys. Rev. D **78**, 103521 (2008).
[6] F. Bernardeau, M. Crocce, and E. Sefusatti, Phys. Rev. D **82**, 083507 (2010).
[7] G. Somogyi and R. E. Smith, Phys. Rev. D **81**, 023524 (2010).
[8] M. Pietroni, J. Cosmol. Astropart. Phys. 10 (2008) 036.
[9] P. Valageas, Astron. Astrophys. Rev. **484**, 79 (2008).
[10] F. Bernardeau and P. Valageas, Phys. Rev. D **78**, 083503 (2008).
[11] H. D. I. Abarbanel and C. Itzykson, Phys. Rev. Lett. **23**, 53 (1969).
[12] M. Levy and J. Sucher, Phys. Rev. **186**, 1656 (1969).
[13] Another case studied in PT with two components following geodesic motion is a mixture of CDM and clustering quintessence [14]. However, in this case the initial conditions are such that the two fluids remain comoving during their evolution and isodensity modes do not develop.
[14] E. Sefusatti and F. Vernizzi, J. Cosmol. Astropart. Phys. 3 (2011) 047.
[15] D. Tseliakhovich and C. Hirata, Phys. Rev. D **82**, 083520 (2010).
[16] R. Scoccimarro, in *The Onset of Nonlinearity in Cosmology*, edited by J. N. Fry, J. R. Buchler, and H. Kandrup (New York Academy Sciences Annals, New York, 2001), Vol. 927, pp. 13+.

[17] It is straightforward to show that for ΛCDM $f_- = -\frac{3}{2}\Omega_m \frac{H_0^2}{H^2 a^3}$ and $f_+/f_- = 1 - \frac{5}{3}\frac{a}{D_+}$.

[18] In this paper we will indistinguishably use the term of propagator for both ξ_{ab} and G_{ab} although the latter is the ensemble average of the former.

[19] We are here in a situation comparable to that encountered in Lagrangian space where the displacement is found to be nonpotential at order three and beyond in PT.

[20] J. R. Bond, G. Efstathiou, and J. Silk, Phys. Rev. Lett. **45**, 1980 (1980).

[21] A. Lewis, A. Challinor, and A. Lasenby, Astrophys. J. **538**, 473 (2000).

[22] C.-P. Ma and E. Bertschinger, Astrophys. J. **455**, 7 (1995).

[23] Note that contrary to the notation of [22], here θ denotes the *dimensionless* velocity divergence so that $\theta_{\rm our} \equiv \theta_{\rm MB}/\mathcal{H}$.

Part C

Cosmic Shear

Chapter 6

Cosmic Shear

Contents

6.1 Introduction

Cosmic shear is the result of a physical phenomenon known as gravitational lensing. This phenomenon, predicted by Einstein's general relativity, describes how light is deflected by massive objects. Nonetheless this is generically true, we will focus our attention on the following specific situation: the light emitted by a distant galaxy is deflected by the presence of massive objects between the galaxy itself and us, see Fig. 6.1. Quantitatively, these massive objects induce perturbations in the metric, which impact the geodesic equation for photons. Because of this deflection, we see the galaxy at a place different from its real position.

Figure 6.1: An example of gravitational lensing: the light emitted by the galaxy is deflected by the massive dark matter halo.

On the figure above, it is suggested that the apparent (observed) position of the galaxy is "higher" than its actual position. Though this is completely true, there is more going on. If we do not any more assume that the galaxy is a point source, its shape will also

be distorted. The reason is that the light rays passing closer to the halo will be deflected more than those passing further away.

Cosmic shear describes how the observed sky differs from what the sky would look like without gravitational lensing, i.e. how the image of the sky is distorted. And today, the only way to measure this shear is to measure the (change in) ellipticity of galaxies. On Fig. 6.2, we show how gravitational lensing affects the shape (hence the ellipticity) of an observed galaxy. Even if the change looks dramatic on this cartoon, the effect is typically of the order of only 1% [32]. As this is absolutely negligible compared to the variance in the intrinsic ellipticities of galaxies, we need to measure the ellipticity of a huge number of galaxies to capture a significant signal. Future wide-field surveys like Euclid will be able to probe the cosmic shear field.

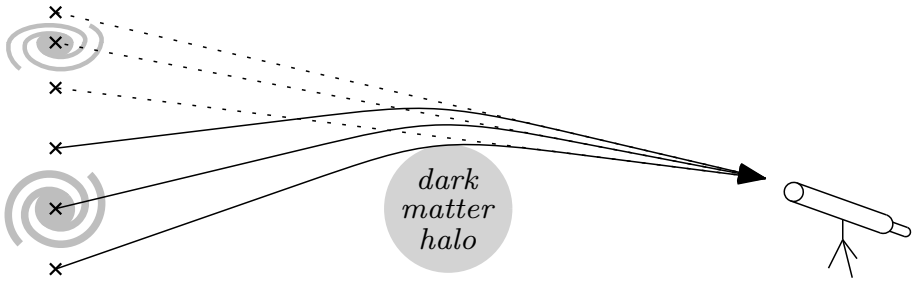

Figure 6.2: The deformation of the image of a galaxy due to gravitational lensing. The deflection of the light coming from three points (say stars) of the galaxy is displayed and their apparent positions are shown. As the light coming from the lower point is deflected more than that of the upper point, the image is not only displaced, but also deformed.

6.2 Objectives

The main goal of this Part is to compute the bispectrum of the cosmic shear, starting from the expression given in [33]. This expression, which will be repeated in the following sections, consists of the shear on the full sky, to second order in the gravitational potentials. The first-order shear will be derived in detail in order to introduce all the quantities and symbols needed for the analysis of the second-order shear. The second-order expression will be stated "as such", the derivation being rather technical and lengthy. The last section of this chapter briefly introduces the concepts of power spectrum and bispectrum in the context of cosmic shear.

In the next two chapters, 7 and 8, we will compute the power spectrum and the bispectrum of cosmic shear respectively. Unfortunately, this will involve long and technical calculations. We will also disclose how the various formulae can be implemented in MATHEMATICA, using the Limber approximation. In chapter 9, we will discuss the results and compare these to the bispectrum generated by a primordial non-Gaussianity.

We will perform the full analysis on the full sky, i.e. without making the so called flat sky approximation. This will allow us to find expressions for the shear (and its power spectrum and bispectrum) that are also valid on large scales, i.e. for small multipoles.

6.3 Shear at first order

At first order in the gravitational potentials, the metric takes the perturbed FLRW form introduced in eq. (1.1), i.e.[1]

$$\mathrm{d}s^2 = a^2(\tau)\left[-(1+2\psi)\mathrm{d}\tau^2 + (1-2\phi)\mathrm{d}\mathbf{x}^2\right]. \tag{6.1}$$

It can be shown that at first order, gravitational lensing only depends on the sum of the two potentials, whence we define the lensing potential[2]

$$\Psi \equiv \frac{\psi+\phi}{2}. \tag{6.2}$$

Before tackling the shear, we first show what the deflection angle of a point source is. Using the lensing potential Ψ, the deflection angle $\vec{\alpha}$, see Fig. 6.3, is given by

$$\vec{\alpha} = 2\int_0^{\chi_S} \mathrm{d}\chi\, \frac{\chi_S - \chi}{\chi_S}\, \nabla_\perp \Psi(\chi), \tag{6.3}$$

where $\nabla_\perp$ denotes the change of Ψ perpendicular to the line of sight and χ parametrises the line of sight [3, 2, 1]. Both $\vec{\alpha}$ and Ψ obviously depend on the direction of observation $\hat{n}$. This result for $\vec{\alpha}$ can easily be found using the geodesic equation for photons.

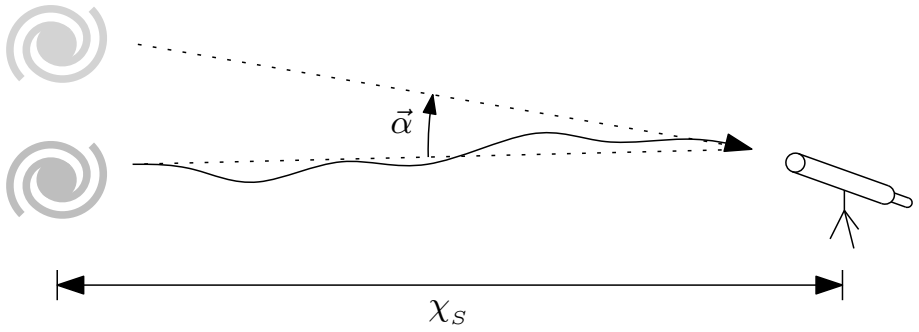

Figure 6.3: The apparent displacement of a distant galaxy due to intervening matter. The distance to the source is denoted by χ_S and $\vec{\alpha}$ denotes the deflection angle.

When each point of the galaxy is displaced in the same way, i.e. has the same deflection angle, the entire galaxy is displaced but not deformed. Cosmic shear is therefore a measure for the *change* in deflection angle between nearby points; because of this, it should not be a surprise that the expression for the shear contains one more gradient than eq. (6.3). The framework that describes the propagation of two nearby light bundles is that of the Sachs equation (see [33] and references therein). For the Sachs equation, we consider two nearby geodesics, say x^μ and $x^\mu + \xi^\mu$, connected by an infinitesimal deviation vector ξ^μ which vanishes at the observer. Let λ be an affine parameter, such that the wave vector k^μ is given by $k^\mu = \mathrm{d}x^\mu/\mathrm{d}\lambda$. The Sachs equation then states that

$$\frac{D^2\xi^\mu}{D\lambda^2} = R^\mu{}_{\nu\alpha\beta}\xi^\beta k^\nu k^\alpha, \tag{6.4}$$

[1]Notice that the graviational potentials ψ and ϕ are interchanged with respect to [33] in order to maintain consistency within this thesis. Fortunately, the impact of this change is very limited because...

[2]...of this.

where $D/D\lambda$ is the covariant derivative and $R^{\mu}{}_{\nu\alpha\beta}$ the Riemann tensor. The next step is to define a 2D-hypersurface orthogonal to both k^μ and the 4-velocity of the observer. We call the 2D-hypersurface the "screen" and denote its basis vectors by $\{n_1^\mu, n_2^\mu\}$. The screen is then parallel transported back along the geodesic, defining the subspace $\{n_1^\mu(\lambda), n_2^\mu(\lambda)\}$. Rewriting the Sachs equation by projecting it on this subspace gives

$$\frac{\mathrm{d}^2\xi^a}{\mathrm{d}\lambda^2} = \mathcal{R}^a{}_b\xi^b, \tag{6.5}$$

where $a = 1, 2$ corresponds to projection on n_1^μ and n_2^μ respectively, and

$$\mathcal{R}_{ab} \equiv R_{\mu\nu\rho\sigma}k^\nu k^\rho n_a^\mu n_b^\sigma. \tag{6.6}$$

This equation is solved by introducing the Jacobi mapping, the 2×2-matrix $\mathcal{D}_{ab}$, which satisfies

$$\frac{\mathrm{d}^2}{\mathrm{d}\lambda^2}\mathcal{D}_{ab} = \mathcal{R}_{ac}\mathcal{D}_{cb}, \tag{6.7}$$

with at the observer $\mathcal{D}_{ab}(0) = 0$ and $\mathrm{d}\mathcal{D}_{ab}/\mathrm{d}\lambda|_{\lambda=0} = \delta_{ab}$. This mapping exactly describes how the vector ξ^a, connecting the geodesics, changes in time, as $\xi^a = \mathcal{D}_{ab}\theta_O^b$ where θ_O^b is the angle between the two geodesics at the observer. The Jacobi mapping $\mathcal{D}_{ab}$ contains all the modes of the shear like the convergence (magnification) and rotation. To proceed, we decompose it into its spin-0 and spin-2 component as

$$\begin{aligned} {}_0\mathcal{D} &\equiv \mathcal{D}_{11} + \mathcal{D}_{22} + i(\mathcal{D}_{12} - \mathcal{D}_{21}), & (6.8)\\ {}_2\mathcal{D} &\equiv \mathcal{D}_{11} - \mathcal{D}_{22} + i(\mathcal{D}_{12} + \mathcal{D}_{21}), & (6.9) \end{aligned}$$

and we define the trace of $\mathcal{D}_{ab}$, which is the real part of the spin-0 component, as $\mathcal{D} \equiv \mathcal{D}_{11}+\mathcal{D}_{22}$. What we observe is the reduced shear, the ratio of the anisotropic and isotropic deformations, and it is given by[3]

$$\boxed{\gamma = -{}_2\mathcal{D}/\mathcal{D}.} \tag{6.10}$$

The reduced shear γ is a spin-2 quantity. Physically, this corresponds to the fact that if one turns γ by $\pi = (2\pi)/2$ on the sky, one obtains the same result[4]. The mathematical objects that are needed to describe a spin-2 field are the spin-weighted spherical harmonics ${}_sY_{lm}$ and the spin raising and lowering operators $\eth$ and $\overline{\eth}$. In spherical coordinates, these operators are defined as

$$\begin{aligned} \eth({}_sX) &\equiv -(\sin\theta)^s\left(\frac{\partial}{\partial\theta} + \frac{i}{\sin\theta}\frac{\partial}{\partial\varphi}\right)(\sin\theta)^{-s}({}_sX), & (6.11)\\ \overline{\eth}({}_sX) &\equiv -(\sin\theta)^{-s}\left(\frac{\partial}{\partial\theta} - \frac{i}{\sin\theta}\frac{\partial}{\partial\varphi}\right)(\sin\theta)^{s}({}_sX), & (6.12) \end{aligned}$$

[3]In [34], the shear is denoted by γ and the reduced shear by g. However, we will denote the reduced shear by γ to be consistent with our article starting on page 116. Moreover, we will often omit the adjective "reduced", so whenever we talk about the shear γ, we effectively mean the reduced shear γ.

[4]In general, rotating a spin-s field ${}_sX$ by α changes it phase by $s\alpha$, i.e. ${}_sX \to e^{is\alpha}{}_sX$. This implies that it is invariant under a rotation by $(2\pi)/s$.

where ${}_sX(\theta,\varphi)$ is a spin-s field. As the name of these operators suggests, $\eth_s X$ is a spin-$(s+1)$ field, and $\overline{\eth}_s X$ is a spin-$(s-1)$ field. Note that in general $\eth$ and $\overline{\eth}$ do not commute: their commutation relation is given by

$$(\overline{\eth}\eth - \eth\overline{\eth})\ {}_sX = 2s\ {}_sX. \tag{6.13}$$

If $s = 0$, we see that $\eth\overline{\eth} = \overline{\eth}\eth$ and it is straightforward to show that it coincides with the standard Laplacian on the sphere.

The (regular) spherical harmonics Y_{lm} are spin-0 quantities on the sphere. It is well known that they are the eigenfunctions of the Laplacian, with eigenvalue $-l(l+1)$,

$$\nabla^2 Y_{lm}(\theta,\varphi) = -l(l+1)Y_{lm}(\theta,\varphi), \tag{6.14}$$

and that they satisfy the orthogonality relation

$$\int \mathrm{d}^2\hat{n}\ Y_{lm}(\theta,\varphi)Y^*_{\tilde{l}\tilde{m}}(\theta,\varphi) = \delta_{l\tilde{l}}\delta_{m\tilde{m}}. \tag{6.15}$$

Out of these spin-0 spherical harmonics, we can construct spin-s objects by applying the operators $\eth$ and $\overline{\eth}$ onto them. We define the spin-weighted spherical harmonics ${}_sY_{lm}$

$$\begin{aligned} \text{ł}(l,s)\ {}_sY_{lm}(\theta,\varphi) &\equiv \eth^s Y_{lm}(\theta,\varphi), \\ \text{ł}(l,s)\ {}_{-s}Y_{lm}(\theta,\varphi) &\equiv (-1)^s\overline{\eth}^s Y_{lm}(\theta,\varphi), \end{aligned} \tag{6.16}$$

where $\text{ł}(l,s) \equiv \sqrt{\dfrac{(l+s)!}{(l-s)!}}$ and $0 \leq s \leq l$. Note that when $l \gg s$, $\text{ł}(l,s) \sim l^s$. Many useful properties of these spin-weighted spherical harmonics, which are straightforward generalisations of the properties of the spin-0 spherical harmonics Y_{lm}'s, can be found in the appendix starting on page 143. A multipole moment l corresponds on the sky to an angular scale $\sim \pi/l$. Current surveys like CFHTLS, covering a limited part of the sky, cannot access multipoles smaller that $l \sim 15$. Future surveys like Euclid, being (almost) full sky, will access multipoles as low as $\sim$ few, which is why a full sky treatment and the extended Limber approximation are necessary, as we shall see. The smallest scales that can be probed correspond to $l \sim$ few thousands.

We are now in a position to express the shear γ using these spin raising and lowering operators. In order to compute γ to first order in Ψ, we need to solve eq. (6.7) to first order in ψ and ϕ [33]. First, we reparametrise the photon geodesic, such that $x^0(\lambda(\tau)) = \tau_0 - \tau$ where τ_0 is the conformal time today. Moreover, it is convenient to define $\chi \equiv \tau_0 - \tau$, such that $k^0 = \mathrm{d}\chi/\mathrm{d}\lambda$. By computing $\mathcal{R}_{ab}$ and k^0 to first order in ϕ and ψ, we can integrate eq. (6.7) twice and find the Jacobi mapping

$$\mathcal{D}_{ab}(\chi_S) = (1-\phi(\chi_S))\chi_S\delta_{ab} + \int_0^{\chi_S} \mathrm{d}\chi \left[4\Psi - 2(\chi_S - \chi)\dot{\Psi}\right]\delta_{ab} - e^i_a e^j_b \int_0^{\chi_S} \mathrm{d}\chi(\chi_S - \chi)\chi 2\Psi_{,ij} \tag{6.17}$$

where the spatial basis at the observer has been written as $n^\mu_a(0) = (0, \mathbf{e}_a)$. It is exactly this contraction between $\mathbf{e}_a$ and the derivatives of Ψ that can be written in terms of spin raising and lowering operators. For example, $e^i_+ e^j_+ \Psi_{,ij} = (1/\chi^2)\eth^2\Psi$, where $\mathbf{e}_+ \equiv \mathbf{e}_1 + i\mathbf{e}_2$. I refer to Sec. 3 of [33] for many more useful relations.

Working through the lengthy computation of ${}_2\mathcal{D}$ and $\mathcal{D}$ using these properties, we eventually find the simple result

$$\boxed{\gamma = \int_0^{\chi_S} \mathrm{d}\chi \, \frac{\chi_S - \chi}{\chi_S \chi} \not{\partial}^2 \Psi.} \tag{6.18}$$

Like before, γ depends on the direction $\hat{n}$.

A remark is in order here. In this section, the shear γ has been computed for a source at a distance χ_S. However, what we observe are redshifts, not distances. So what we are interested in is the shear for a source at redshift z, whence we need to take into account the perturbations to the distance-redshift relation. Luckily, this is a second-order effect and therefore we need not take this correction into account when computing the shear only to first order.

6.4 Shear at second order

In this section, we will merely state the expression for the shear at second order. First, we need to generalise the first-order metric eq. (6.1) to second order. We still assume that the primordial perturbations are scalar ones. However, to second order we cannot neglect the (dynamically created) vector and tensor perturbations. In the so-called generalised Poisson gauge, the metric reads

$$\mathrm{d}s^2 = a^2(\tau) \left[-e^{2\psi} \mathrm{d}\tau^2 + 2\omega_i \mathrm{d}\tau \mathrm{d}x^i + \left(e^{-2\phi} \delta_{ij} + h_{ij} \right) \mathrm{d}x^i \mathrm{d}x^j \right], \tag{6.19}$$

where the vector component ω_i is divergenceless ($\partial_i \omega_i = 0$), and the tensor component h_{ij} is both divergenceless and traceless ($\partial_i h_{ij} = 0 = h_{ii}$). Both ω_i and h_{ij} are thus second-order quantities, while ψ and ϕ are first-order quantities.

The second-order corrections to eq. (6.18) can be put into three categories: geometrical corrections, dynamical corrections and redshift corrections. It should be noted that this decomposition is not physical as it is not gauge invariant. Nevertheless, being very convenient, we will stick to it.

Geometrical corrections are found by solving the Einstein equations to second order in the (primordial) perturbations ψ and ϕ. As in the first-order case, these will only depend on the lensing potential Ψ. An example of a second-order geometrical correction is the coupling between two lenses.

Dynamical corrections are found by computing the second-order evolution of the fields. This includes both the results of non-linear perturbation theory describing the second-order evolution of ψ and ϕ, and the processes responsible for creating vector and tensor perturbations. These will turn out to be the largest and smallest contributions respectively.

Redshift corrections are due to the inhomogeneity of the redshift of the sources. These are the Sachs-Wolfe, the Doppler and the integrated Sachs-Wolfe effects.

The following equation contains all the geometrical and redshift corrections [33]. As the dynamical corrections require a different treatment, they are given in a separate equation.

The numbering of the terms between the square brackets corresponds to the numbering used in the MATHEMATICA notebook. [0] is the first-order term found in eq. (6.18), [1]–[8] are the geometrical corrections and [9]–[11] the redshift corrections. As the third, fourth and fifth term have the very same dependence on χ, they are united into [2].

$$
\begin{aligned}
\gamma \;=\; & \int_0^{\chi_S} \mathrm{d}\chi\, \frac{\chi_S-\chi}{\chi_S\chi}\, \not\partial^2\Psi(\chi) && [0]\\
& - \int_0^{\chi_S} \mathrm{d}\chi\, \frac{\chi_S-\chi}{\chi_S\chi}\, \not\partial^2\Psi^2(\chi) && [1]\\
& - \int_0^{\chi_S} \mathrm{d}\chi\, \frac{\chi_S-\chi}{\chi_S\chi}\, \not\partial \left(\not\partial^2\Psi(\chi) \int_0^{\chi} \mathrm{d}\chi'\, \frac{\chi-\chi'}{\chi\chi'}\, \overline{\not\partial}\Psi(\chi') \right) && [2]\\
& - \int_0^{\chi_S} \mathrm{d}\chi\, \frac{\chi_S-\chi}{\chi_S\chi}\, \not\partial \left(\overline{\not\partial}\not\partial\Psi(\chi) \int_0^{\chi} \mathrm{d}\chi'\, \frac{\chi-\chi'}{\chi\chi'}\, \not\partial\Psi(\chi') \right) && [2]\\
& -2 \int_0^{\chi_S} \mathrm{d}\chi\, \frac{\chi_S-\chi}{\chi_S\chi}\, \not\partial\Psi(\chi) \int_0^{\chi} \mathrm{d}\chi'\, \frac{\chi-\chi'}{\chi\chi'}\, \not\partial\Psi(\chi') && [2]\\
& +2 \int_0^{\chi_S} \mathrm{d}\chi\, \frac{\chi_S-\chi}{\chi_S\chi}\, \Psi(\chi) \frac{1}{\chi} \int_0^{\chi} \mathrm{d}\chi'\, \not\partial^2\Psi(\chi') && [3]\\
& +2 \int_0^{\chi_S} \mathrm{d}\chi\, \frac{1}{\chi_S}\, \Psi(\chi) \int_0^{\chi} \mathrm{d}\chi'\, \frac{1}{\chi'} \not\partial^2\Psi(\chi') && [4]\\
& +2 \int_0^{\chi_S} \mathrm{d}\chi\, \frac{1}{\chi_S\chi}\, \not\partial^2 \left(\Psi(\chi) \int_0^{\chi} \mathrm{d}\chi'\, \Psi(\chi') \right) && [5]\\
& + \int_0^{\chi_S} \mathrm{d}\chi\, \frac{\chi_S-\chi}{\chi_S\chi}\, \overline{\not\partial}\not\partial\Psi(\chi) \int_0^{\chi_S} \mathrm{d}\chi'\, \frac{\chi_S-\chi'}{\chi_S\chi'}\, \not\partial^2\Psi(\chi') && [6]\\
& -2 \int_0^{\chi_S} \mathrm{d}\chi\, \frac{1}{\chi_S}\, \Psi(\chi) \int_0^{\chi_S} \mathrm{d}\chi'\, \frac{\chi_S-\chi'}{\chi_S\chi'}\, \not\partial^2\Psi(\chi') && [7]\\
& -2 \int_0^{\chi_S} \mathrm{d}\chi\, \frac{\chi_S-\chi}{\chi_S\chi}\, \not\partial^2 \left(\dot\Psi(\chi) \int_0^{\chi} \mathrm{d}\chi'\, \Psi(\chi') \right) && [8]\\
& -2 \frac{1+z_S}{{\chi_S}^2 H_S} \left(\int_0^{\chi_S} \mathrm{d}\chi\, \dot\Psi(\chi) \right) \left(\int_0^{\chi_S} \mathrm{d}\chi'\, \not\partial^2\Psi(\chi') \right) && [9]\\
& + \frac{1+z_S}{\chi_S^2 H_S} \psi(\chi_S) \int_0^{\chi_S} \mathrm{d}\chi\, \not\partial^2\Psi(\chi) && [10]\\
& - \frac{1+zS}{\chi_S^2 H_S}\, (\hat n \cdot \mathbf{v}_S) \int_0^{\chi_S} \mathrm{d}\chi\, \not\partial^2\Psi(\chi) && [11]
\end{aligned}
\tag{6.20}
$$

It should be noted that [2] and [6] contain four angular derivatives, whereas all the others only contain two. In eq. (6.16), we see that to every such operator a factor of l is associated. Therefore, we expect that these terms will dominate when we consider large l's. It is for this reason that we will call [2] and [6] the standard geometrical terms, and all the others (i.e. [1], [3], [4], [5], [7] and [8]) the geometrical corrections.

The dynamical corrections have much simpler expressions, comparable to the first-order expression $\gamma^{[0]}$ (by which we denote the [0] part of γ in eq. (6.20)), because we only

need one potential to have a second-order result. These corrections are given by

$$\begin{aligned}\gamma = & \int_0^{\chi_S} \mathrm{d}\chi \, \frac{\chi_S - \chi}{\chi_S \chi} \, \not{\partial}^2 \psi_N^{(2)}(\chi) \\ & + \int_0^{\chi_S} \mathrm{d}\chi \, \frac{\chi_S - \chi}{\chi_S \chi} \, \not{\partial}^2 \left[\frac{1}{2} \left(\psi_R^{(2)}(\chi) + \phi_R^{(2)}(\chi) \right) - \frac{1}{2} \omega_r(\chi) - \frac{1}{4} h_{rr}(\chi) \right] \\ & - \int_0^{\chi_S} \mathrm{d}\chi \, \frac{\chi_S - \chi}{\chi_S \chi} \, \frac{1}{2\chi} \not{\partial} \big({}_1\omega(\chi) + {}_1h_r(\chi) \big) \\ & - \frac{1}{4} {}_2h(\chi_S)\end{aligned} \tag{6.21}$$

where $\omega_r \equiv \hat{n}^i \omega_i$ and $h_{rr} \equiv \hat{n}^i \hat{n}^j h_{ij}$ are spin-0 quantities, ${}_1\omega \equiv \hat{e}_+^i \omega_i$ and ${}_1h_r \equiv \hat{e}_+^i \hat{n}^j h_{ij}$ are spin-1 quantities, and ${}_2h \equiv \hat{e}_+^i \hat{e}_+^j h_{ij}$ is a spin-2 quantity. Here, we have that $\hat{e}_+ \equiv \hat{e}_\theta + i\hat{e}_\varphi$ where $\hat{e}_\theta$ and $\hat{e}_\varphi$ are orthogonal to $\hat{n}$, and to each other. The first term of the equation above, containing the second-order Newtonian potential $\psi_N^{(2)}$, is called the standard dynamical term, whereas the other terms are named the scalar ($\psi_R^{(2)}$ and $\phi_R^{(2)}$), vector (ω_r and ${}_1\omega$) and tensor (h_{rr}, ${}_1h_r$ and ${}_2h$) dynamical corrections.

To finish this section, we will disclose how all these new variables are related to Ψ. In the first place, we show how the first-order lensing potential $\Psi^{(1)}(\chi)$ is related to the primordial perturbations. As at first order $\phi^{(1)} = \psi^{(1)} = \Psi^{(1)}$, we have that

$$\Psi^{(1)}(\chi, \hat{n}) = \int \frac{\mathrm{d}^3\mathbf{k}}{(2\pi)^3} \, g(\chi) T(k) \, \Phi_{\mathbf{k}} \, e^{i\mathbf{k}\cdot\hat{n}\chi}, \tag{6.22}$$

where $g(\chi)$ is the growth-suppression factor, defined as $g(\chi) \equiv D_+(\chi)/a(\chi)$, $T(k)$ the matter transfer function and $\Phi_{\mathbf{k}}$ the primordial perturbation in momentum space [35]. In EdS we have that $g(\chi) = 1$ such that $\dot{\Psi} = 0$. In our ΛCDM Universe however, g is given by

$$g(a) = \frac{5\Omega_m}{2a} \sqrt{\Omega_m a^{-3} + \Omega_\Lambda} \int_0^a \frac{\mathrm{d}\tilde{a}}{\left(\tilde{a} \sqrt{\Omega_m \tilde{a}^{-3} + \Omega_\Lambda} \right)^3}, \tag{6.23}$$

as computed in eq. (4.5), and $a = 1/(1+z)$ is related to χ via

$$\chi(z) = \frac{1}{H_0} \int_0^z \frac{\mathrm{d}\tilde{z}}{\sqrt{\Omega_m (1+\tilde{z})^3 + \Omega_\Lambda}}. \tag{6.24}$$

For the matter transfer function $T(k)$, we conveniently use the BBKS fit [3]:

$$T(k) = \frac{\log(1 + 0.171\hat{k})}{(0.171\hat{k})} \left[1 + 0.284\hat{k} + \left(1.18\hat{k}\right)^2 + \left(0.399\hat{k}\right)^3 + \left(0.490\hat{k}\right)^4 \right]^{(-1/4)}, \tag{6.25}$$

where $\hat{k} \equiv k/k_{eq}$ and $k_{eq} = 0.073 h^2 \Omega_m \, \mathrm{Mpc}^{-1}$. Unless stated otherwise, we will work in a ΛCDM Universe with $\Omega_m = 0.3$, $\Omega_\Lambda = 0.7$ and $h = 0.65$, but it is straightforward to modify the MATHEMATICA code if one wants to consider other cosmological parameters. Our knowledge of $\Psi^{(1)}$ is now reduced to the knowledge of $\Phi_{\mathbf{k}}$, and it is of this quantity that we will assume specific statistical properties in chapter 7.

The second-order Newtonian potential $\psi_N^{(2)}$ has already been computed in the section discussing non-linear perturbation theory, i.e. Sec. 3.3. However, considering we did so in

EdS, we need to generalise the result to ΛCDM. To a good approximation, the F_2-kernel, which acquires a slight time-dependence, is given by

$$F_2(\mathbf{k}_1, \mathbf{k}_2, \chi) = \frac{1}{2}(1+\varepsilon) + \frac{\mu}{2}\left(\frac{k_1}{k_2} + \frac{k_2}{k_1}\right) + \frac{1}{2}(1-\varepsilon)\mu^2, \tag{6.26}$$

where $\varepsilon(\chi) \simeq {}^3\!/_7\,[\rho_m(\chi)/\rho_{\rm tot}(\chi)]^{-1/143}$ and $\mu = (\mathbf{k}_1 \cdot \mathbf{k}_2)/(k_1 k_2)$. By combining this with the Poisson equation (4.1), relating (order by order) ψ to δ, we find

$$\psi_N^{(2)}(\mathbf{k}, \chi) = -\frac{2}{3}\frac{g^2(\chi)a(\chi)}{H_0^2\Omega_m}\frac{k_1^2\,k_2^2}{k^2}\,T(k_1)T(k_2)F_2(\mathbf{k}_1, \mathbf{k}_2, \chi)\Phi_{\mathbf{k}_1}\Phi_{\mathbf{k}_2}, \tag{6.27}$$

where we used that $\Omega_m(\chi) = (H_0/H(\chi))^2\,a^{-3}\,\Omega_m$ and where a convolution is assumed on the r.h.s. The shape of the other potentials like ϕ_R and ω_i is very similar: a time-dependent coefficient and a convolution of the two transfer functions, a kernel and the two primordial potentials $\Phi_{\mathbf{k}_1}$ and $\Phi_{\mathbf{k}_2}$. Their exact expressions are given by (see eqs. (31)–(34) in our article)

$$\psi_R(\mathbf{k}, \chi) = T(k_1)T(k_2)\left[\frac{\mathbf{k}_1 \cdot \mathbf{k}_2}{k^2} - 3\frac{(\mathbf{k} \cdot \mathbf{k}_1)(\mathbf{k} \cdot \mathbf{k}_2)}{k^4}\right]\Phi_{\mathbf{k}_1}\Phi_{\mathbf{k}_2}, \tag{6.28}$$

$$\phi_R(\mathbf{k}, \chi) = -\frac{2}{3}\psi_R(\mathbf{k}, \chi), \tag{6.29}$$

$$\omega_i(\mathbf{k}, \chi) = -\frac{i4a^{1/2}}{3H_0}\frac{T(k_1)T(k_2)}{k^2}\left[k_1^2 k_2^i + k_2^2 k_1^i - \frac{k^i}{k^2}\left(k_1^2(\mathbf{k} \cdot \mathbf{k}_2) + k_2^2(\mathbf{k} \cdot \mathbf{k}_1)\right)\right]\Phi_{\mathbf{k}_1}\Phi_{\mathbf{k}_2}, \tag{6.30}$$

$$\begin{aligned} h_{ij}(\vec{k}, \chi) = \frac{10}{3}\left[1 - 3j_1(k\tau)/(k\tau)\right]\frac{T(k_1)T(k_2)}{k^4}\big[\big((\mathbf{k}_1 \cdot \mathbf{k}_2)^2 - k_1^2\,k_2^2\big)(\delta^{ij} + \mathbf{k}^i\mathbf{k}^j/k^2) \\ + 2\,k_1^2\,k_2^i\,k_2^j + 2\,k_2^2\,k_1^i\,k_1^j - 4\,k_1^i\,k_2^j\,\mathbf{k}_1 \cdot \mathbf{k}_2\big]\,\Phi_{\mathbf{k}_1}\Phi_{\mathbf{k}_2}. \end{aligned} \tag{6.31}$$

6.5 Decomposition in spherical harmonics

In this section, we introduce the variables we will work with in the remaining of this thesis. As the shear is a spin-2 quantity, we expand it in spin-weighted spherical harmonics of spin 2. We denote the expansion coefficients by ${}_2a_{lm}$,

$$\gamma(\theta, \varphi) = \sum_{lm} {}_2a_{lm}\ {}_2Y_{lm}(\theta, \varphi), \tag{6.32}$$

where (θ, φ) represents the direction of the line of sight $\hat{n}$. The conjugate of γ, γ^*, is a spin-(-2) operator, and can therefore be expanded as

$$\gamma^*(\theta, \varphi) = \sum_{lm} {}_{-2}a_{lm}\ {}_{-2}Y_{lm}(\theta, \varphi). \tag{6.33}$$

These expressions can be inverted by using the orthogonality relation of the spin-weighted spherical harmonics, eq. (10.7), giving

$${}_2a_{lm} = \int \mathrm{d}^2\hat{n}\ \gamma(\hat{n})\ {}_2Y^*_{lm}(\hat{n}) \qquad \text{and} \qquad {}_{-2}a_{lm} = \int \mathrm{d}^2\hat{n}\ \gamma^*(\hat{n})\ {}_{-2}Y^*_{lm}(\hat{n}). \tag{6.34}$$

Based upon these expansion coefficients, we can introduce – like in the context of CMB polarisation – two scalar quantities, usually called the "electric" and "magnetic" parts of γ:

$$E(\hat{n}) \equiv \sum_{lm} a_{E,lm}\, Y_{lm}(\hat{n}), \tag{6.35}$$

$$B(\hat{n}) \equiv \sum_{lm} a_{B,lm}\, Y_{lm}(\hat{n}), \tag{6.36}$$

where the coefficients appearing in the summation are given by

$$a_{E,lm} \equiv -\frac{1}{2}\left({}_{-2}a_{lm} + {}_{2}a_{lm}\right) \qquad \text{and} \qquad a_{B,lm} \equiv -\frac{i}{2}\left({}_{-2}a_{lm} - {}_{2}a_{lm}\right). \tag{6.37}$$

Then, the power spectrum of the shear is defined by making use of these last expansion coefficients. For the electric part, which is the only one we will consider, we define

$$C_l\ \delta_{ll'}\delta_{mm'} \equiv \left\langle a_{E,lm}\ a^*_{E,l'm'}\right\rangle, \tag{6.38}$$

where the two Kronecker δ's are due to the assumed isotropy of the Universe. The lensing bispectrum $B^{XYZ}_{l_1l_2l_3}$ is defined by

$$\langle a_{X,l_1m_1}\ a_{Y,l_2m_2}\ a_{Z,l_3m_3}\rangle \equiv \begin{pmatrix} l_1 & l_2 & l_3 \\ m_1 & m_2 & m_3 \end{pmatrix} B^{XYZ}_{l_1l_2l_3}, \tag{6.39}$$

where X, Y and Z can all be either E or B, and where $(:::)$ is a Wigner-3j symbol. This Wigner-3j symbol is the generalisation of the Kronecker δ's appearing in the definition of the power spectrum. It enforces that the three l's satisfy the triangle inequality. As we will focus our attention to the EEE-bispectrum, we define $B_{l_1l_2l_3} \equiv B^{EEE}_{l_1l_2l_3}$. The reduced bispectrum $b_{l_1l_2l_3}$ is related to $B_{l_1l_2l_3}$ through

$$\langle a_{E,l_1m_1}\ a_{E,l_2m_2}\ a_{E,l_3m_3}\rangle \equiv \mathcal{G}^{m_1m_2m_3}_{l_1l_2l_3} b_{l_1l_2l_3}, \tag{6.40}$$

where $\mathcal{G}^{m_1m_2m_3}_{l_1l_2l_3} \equiv \int \mathrm{d}^2\hat{n}\ Y_{l_1m_1}(\hat{n})Y_{l_2m_2}(\hat{n})Y_{l_3m_3}(\hat{n})$ is a Gaunt integral. It can be recast in the following form,

$$\mathcal{G}^{m_1m_2m_3}_{l_1l_2l_3} = \sqrt{\frac{(2l_1+1)(2l_2+1)(2l_3+1)}{4\pi}} \begin{pmatrix} l_1 & l_2 & l_3 \\ m_1 & m_2 & m_3 \end{pmatrix} \begin{pmatrix} l_1 & l_2 & l_3 \\ 0 & 0 & 0 \end{pmatrix}, \tag{6.41}$$

such that we can write the relation between the bispectrum $B_{l_1l_2l_3}$ and the reduced bispectrum $b_{l_1l_2l_3}$ as

$$\sqrt{\frac{(2l_1+1)(2l_2+1)(2l_3+1)}{4\pi}} \begin{pmatrix} l_1 & l_2 & l_3 \\ 0 & 0 & 0 \end{pmatrix} b_{l_1l_2l_3} = B_{l_1l_2l_3}. \tag{6.42}$$

The integral of three spherical harmonics can be generalised to the integral of three spin-weighted spherical harmonics, which we denote by

$$\begin{aligned} \begin{Bmatrix} l_1 & l_2 & l_3 \\ m_1 & m_2 & m_3 \\ s_1 & s_2 & s_3 \end{Bmatrix} &\equiv \int \mathrm{d}^2\hat{n}\ {}_{s_1}Y_{l_1m_1}(\hat{n})\ {}_{s_2}Y_{l_2m_2}(\hat{n})\ {}_{s_3}Y_{l_3m_3}(\hat{n}) \\ &= \sqrt{\frac{(2l_1+1)(2l_2+1)(2l_3+1)}{4\pi}} \begin{pmatrix} l_1 & l_2 & l_3 \\ m_1 & m_2 & m_3 \end{pmatrix} \begin{pmatrix} l_1 & l_2 & l_3 \\ s_1 & s_2 & s_3 \end{pmatrix}. \end{aligned} \tag{6.43}$$

The computation of the reduced bispectrum forms the core of this part and will be covered in chapter 8.

Chapter 7

Power spectrum

Contents

In this chapter, we will compute, to leading order, the power spectrum of the cosmic shear. This will allow us to introduce parts of the formalism we will need, to compute the bispectrum in the next chapter. We will also thoroughly discuss the Limber approximation which is a key element to facilitate the (otherwise very involved) numerical integrations.

7.1 Angular power spectrum

In this section, we will relate the cosmic shear angular power spectrum to the power spectrum of the initial perturbations $\Phi_{\mathbf{k}}$. We will assume that the $\Phi_{\mathbf{k}}$ are drawn from a Gaussian distribution so that they are fully determined by their power spectrum $P(k)$, defined through

$$\langle \Phi_{\mathbf{k}} \Phi_{\mathbf{k}'} \rangle \equiv (2\pi)^3 \delta_{\mathrm{D}}(\mathbf{k} + \mathbf{k}') P(k). \tag{7.1}$$

For convenience, we will only consider a scale invariant spectrum,

$$P(k) = A_\Phi^2 k^{-3}, \tag{7.2}$$

where A_Φ is the amplitude. The treatment can be easily extended to a non-zero tilt. When plotting the bispectrum, we will weight it by the power spectrum squared, so that the amplitude A_Φ becomes irrelevant.

The leading-order power spectrum can be found by taking the first-order lensing potential $\Psi^{(1)}$ in the first-order shear $\gamma^{[0]}$. By combining eqs. (6.16), (6.20),(6.22) and (6.34), together with the useful property

$$e^{i\mathbf{a}\cdot\mathbf{b}} = 4\pi \sum_{lm} i^l \, j_l(ab) Y_{lm}(\hat{a}) Y_{lm}^*(\hat{b}), \tag{7.3}$$

where j_l is a spherical Bessel function, we find that the expansion coefficient ${}_2a_{lm}^{[0]}$ satisfies

$$ {}_2a_{lm}^{[0]} = i^l \text{ł}(l,2) \int_0^{\chi_S} \mathrm{d}\chi\, W(\chi_S,\chi) \int \frac{\mathrm{d}^3\mathbf{k}}{2\pi^2}\, T(k)\, \Phi_{\mathbf{k}}\, j_l(k\chi)\, Y_{lm}^*(\hat{k}), \tag{7.4} $$

where we introduced the window function $W(\chi_S,\chi)$, defined as

$$ W(\chi_S,\chi) \equiv \frac{\chi_S - \chi}{\chi_S \chi} g(\chi). \tag{7.5} $$

Because $\Phi_{\mathbf{k}}$ is real, it is straightforward to show that ${}_2a_{lm}^{[0]} = {}_{-2}a_{lm}^{[0]}$ whence $a_{E,lm}^{[0]} = -{}_2a_{lm}^{[0]}$ and $a_{B,lm}^{[0]} = 0$. This is why we only consider the electric power spectrum.

Combining the definition of the C_l, given by eq. (6.38), with eq. (7.1), we find

$$ \boxed{C_l = \text{ł}^2(l,2) \int_0^{\chi_S} \mathrm{d}\chi\, W(\chi_S,\chi) \int_0^{\chi_S} \mathrm{d}\chi'\, W(\chi_S,\chi') \int \frac{2k^2\mathrm{d}k}{\pi} T^2(k) P(k) j_l(k\chi) j_l(k\chi'),} \tag{7.6} $$

which can be rewritten in the more convenient form

$$ \boxed{C_l = \text{ł}^2(l,2) \int \frac{2k^2\mathrm{d}k}{\pi} T^2(k) P(k) \left[\int_0^{\chi_S} \mathrm{d}\chi\, W(\chi_S,\chi) j_l(k\chi) \right]^2.} \tag{7.7} $$

Though we need not introduce anything else to come to this result, we nevertheless introduce yet another set of expansion coefficients that will be handy later on. To this end, we expand the (scalar) first-order lensing potential $\Psi^{(1)}(\mathbf{k})$ as

$$ \Psi^{(1)}(\mathbf{k},\chi) = \sum_{lm} a_{lm}(k,\chi) Y_{lm}(\hat{k}). \tag{7.8} $$

It is straightforward to show that the expectation value of the product of two a_{lm}'s is given by

$$ \langle a_{lm}(k,\chi) a_{l'm'}(k',\chi') \rangle = (2\pi)^3 (-1)^{l+m} \delta_{ll'} \delta_{m,-m'} \delta(k-k') \frac{T^2(k)}{k^2} P(k) g(\chi) g(\chi'), \tag{7.9} $$

or equivalently by

$$ \langle a_{lm}(k,\chi) a_{l'm'}^*(k',\chi') \rangle = (2\pi)^3 \delta_{ll'} \delta_{mm'} \delta(k-k') \frac{T^2(k)}{k^2} P(k) g(\chi) g(\chi'). \tag{7.10} $$

These new variables are related to the ${}_2a_{lm}^{[0]}$'s defined previously, by

$$ {}_2a_{lm}^{[0]} = \text{ł}(l,2) \frac{1}{4\pi} \int_0^{\chi_S} \mathrm{d}\chi \frac{\chi_S - \chi}{\chi_S \chi} \int \frac{2k^2\mathrm{d}k}{\pi} i^l j_l(k\chi)\, a_{lm}(k), \tag{7.11} $$

from which eq. (7.6) follows trivially.

7.2 Exact integration

In this section, we will analyse how the expressions for the angular power spectrum can be integrated numerically, without making any approximation. This will enable us to test the accuracy of the Limber approximation we will introduce in the next section. As we have two different descriptions, (7.6) and (7.7), we will analyze both.

The first approach to the numerical calculation of the C_l's consists of starting with eq. (7.6) containing three integrals. To get a better understanding of the integrand, we fix a value for l and χ_S and only perform the k-integration. The result is obviously a function of χ and χ', and can therefore be plotted in 3D. On Fig. 7.1, we show the result for $\chi_S = 100/k_{eq}$ and $l = 5, 15, 25$ in EdS spacetime. It can be seen that the function is dominated by the region $\chi \approx \chi'$. This observation is closely related to the validity of the Limber approximation, as we will see later on.

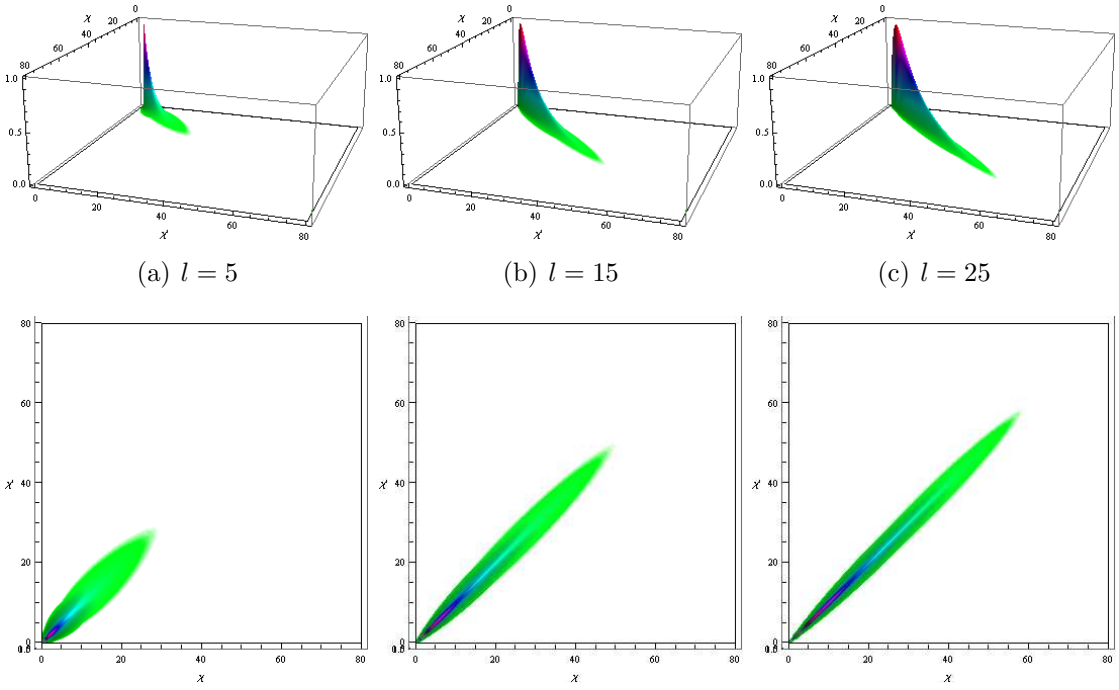

(a) $l = 5$ (b) $l = 15$ (c) $l = 25$

(d) $l = 5$, top view (e) $l = 15$, top view (f) $l = 25$, top view

Figure 7.1: The integrand of equation (7.6) after integrating out k, as a function of χ and χ'. For convenience, we take $\chi_S = 100/k_{eq}$ in an EdS spacetime; χ and χ' are also in units of $1/k_{eq}$. The function is clearly dominated by the region $\chi \approx \chi'$ and this is even more apparent when l gets larger. The functions have been normalised to 1 at their maximum to improve comparability, and the white area corresponds to a normalised value of the integrand ≤ 0.0005.

After this already complicated k-integration, the integrand being a rapidly oscillating function, we still need to perform two more integrations numerically to compute the C_l's. But the other approach, starting with eq. (7.7), only has two integrals to start with, so we will favour that approach.

The fact that eq. (7.7) contains one less integral than eq. (7.6) simplifies the problem significantly. However, as the second integral is squared, it is not possible to implement

it in MATHEMATICA using only one `NIntegrate`. The way around this problem is the following: we construct a suitable chosen sample of values for k, and compute the value of the second integral numerically for all those values. Based upon these outcomes, we construct an interpolating function for the χ-integral. The square of this interpolating function is then numerically integrated, after multiplication with $k^2T^2(k)P(k)$. On Fig. 7.2, we show a `LogLogPlot` of the k-integrand of eq. (7.7), i.e. everything but $\int \mathrm{d}k$, as a function of k for $l = 5, 15, 25$. By means of this plot, we can infer certain properties the chosen sample of k should have. Firstly, it should be distributed logarithmically; the sample should be much more dense for low values of k. Secondly, the peak of the function shifts with l; the sample should take this shift into account. Notice that the function drops quickly for small and large values of k. The sample is constructed such that the integrand is smaller than 10^{-10} at the boundaries. I refer to the `Module` named `ClExact` in my notebook for the details. A high-accuracy computation of a C_l using this approach takes $\mathcal{O}(10\,\mathrm{min})$, and we will use these values as references when checking the validity of the Limber approximation.

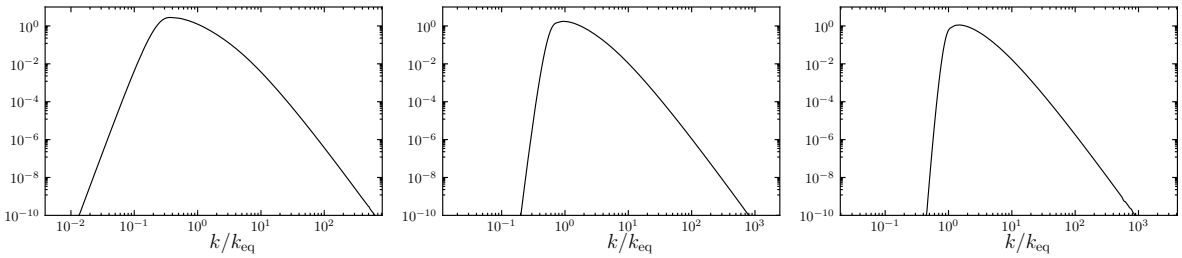

(a) $l = 5$ (b) $l = 15$ (c) $l = 25$

Figure 7.2: The k-integrand of equation (7.7) in units of k_{eq}, as a function of k/k_{eq}. Unlike Fig. 7.1, we plotted this for a ΛCDM Universe and a source at redshift $z_S = 1$ (corresponding to $\chi_S \approx 33/k_{eq}$).

7.3 Limber approximation

The Limber approximation is a useful tool whenever integrals of Bessel functions are involved. We will introduce it using a handwaving argument, and refer to [36] for a very detailed treatment. An ordinary Bessel function $J_\nu(x)$ has the following behaviour: it is approximately zero for $x \ll \nu$, has it first peak at $x \sim \nu$ and oscillates rapidly with decaying amplitude when $x \gg \nu$. Therefore, if $f(x)$ is sufficiently smooth,

$$\int_0^\infty f(x)\, J_\nu(x)\, \mathrm{d}x \propto f(\nu), \tag{7.12}$$

where the constant of proportionality is fixed to unity as we know that $\int J_\nu(x)\mathrm{d}x = 1$. Two equivalent forms, which will be useful to us, are

$$\int_0^\infty f(\chi)\, j_l(k\chi)\, \mathrm{d}\chi \approx \frac{1}{k} f\left(\frac{\nu}{k}\right)\sqrt{\frac{\pi}{2\nu}} \quad \text{and} \quad \int_0^\infty f(k)\, j_l(k\chi)\, \mathrm{d}k \approx \frac{1}{\chi} f\left(\frac{\nu}{\chi}\right)\sqrt{\frac{\pi}{2\nu}}, \tag{7.13}$$

where $\nu = l + 1/2$. The way we generalised $\int J_\nu(x)\mathrm{d}x = 1$ to eq. (7.12) can also be used to generalise the orthogonality property of the spherical Bessel functions, namely $\int \mathrm{d}k\, k^2 j_\nu(kx) j_\nu(kx') = \pi/(2x^2)\delta_\mathrm{D}(x - x')$, to

$$\int_0^\infty \frac{2k^2\, dk}{\pi} P(k) j_l(k\chi) j_l(k\chi') \approx \frac{\delta_\mathrm{D}(\chi - \chi')}{\chi^2} P\left(\frac{\nu}{\chi}\right). \tag{7.14}$$

The appearance of the δ_D equating χ to χ' should be compared to Fig. 7.1. Indeed, the plotted integrand is dominated by the region $\chi \approx \chi'$. The approximation gets better for larger l, i.e. the corrections are $\mathcal{O}(1/\nu^2)$. We can now insert eq. (7.13) into eq. (7.7) or eq. (7.14) into eq. (7.6), the results being obviously equivalent. Nevertheless, care should be taken as the upper boundary of the χ-integral is not infinity. With the first substitution, the result is

$$C_l = \frac{t^2(l,2)}{\nu} \int_{\nu/\chi_S}^\infty \mathrm{d}k\; T^2(k) P(k) W^2\left(\chi_S, \frac{\nu}{k}\right) [1 + \mathcal{O}(1/\nu^2)], \tag{7.15}$$

whereas the second substitution gives, after integrating out the $\delta_\mathrm{D}(\chi - \chi')$, the equivalent

$$C_l = t^2(l,2) \int_0^{\chi_S} \frac{\mathrm{d}\chi}{\chi^2} W(\chi_S, \chi) T^2\left(\frac{\nu}{\chi}\right) P\left(\frac{\nu}{\chi}\right) [1 + \mathcal{O}(1/\nu^2)]. \tag{7.16}$$

The two results are related to each other by the change of variable $k \leftrightarrow \nu/\chi$. Computing the remaining integral numerically is a very easy task. However, as we will see, the approximation is only correct to $\mathcal{O}(1\%)$ when $l \gtrsim 8$. As we want our results to be reliable for much smaller values of l, we need to improve the Limber approximation.

The extended Limber approximation can be found by using subtle properties of the expression [36]

$$\lim_{\epsilon \to 0} \int_0^\infty e^{-\epsilon(x-\nu)} f(x) J_\nu(x)\, \mathrm{d}x, \tag{7.17}$$

resulting in the generalisation of eq. (7.12) to

$$\int_0^\infty f(x)\, J_\nu(x)\, \mathrm{d}x = \left(f(x) - \frac{1}{2} f''(x) - \frac{x}{6} f'''(x)\right)_{x=\nu} + \mathcal{O}(1/\nu^4). \tag{7.18}$$

We can apply this extended Limber approximation to eq. (7.7). To give a first insight into the new result, we here make the approximation that $g(\chi)$ is constant, so that we do not need to bother with its derivatives. Working through the lengthy but straightforward computation gives the better approximation

$$C_l \approx t^2(l,2) \int_0^{\chi_S} \frac{\mathrm{d}\chi}{\chi^2} T^2\left(\frac{\nu}{\chi}\right) P\left(\frac{\nu}{\chi}\right) \left[W^2(\chi_S, \chi) + \frac{1}{8} \frac{W(\chi_S, \chi)}{\nu^2} \left(\frac{5}{\chi} + \frac{1}{\chi_S}\right) g(\chi)\right]. \tag{7.19}$$

We clearly see the $1/\nu^2$ corrections with respect to eq. (7.16). The complete expression, which also takes the derivatives of $g(\chi)$ into account, can be found in the `Module` named `ClLimber2`. In any case, the remaining integral is easily computed numerically and it takes only a fraction of a second, compared to the minutes needed to compute the exact value.

On Fig. 7.3, we compare the different approximations to the exact values. We see that the extended Limber approximation converges much faster, and that its accuracy

is better than 1% even for very small multipoles l. Therefore, we can conclude that the use of the extended Limber approximation is acceptable. This does not only imply an enormous gain of computational time for the angular power spectrum, but also, without this approximation, the computation of the bispectrum would be practically impossible.

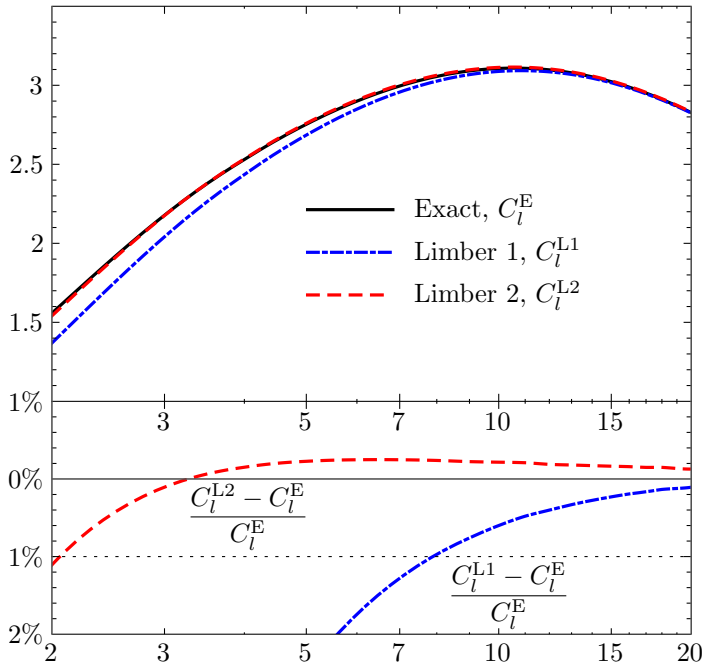

Figure 7.3: The exact values of the angular power spectrum C_l, compared with the Limber approximation (blue) and the extended Limber approximation (red). The source is taken at redshift $z_S = 1$. We see that the accuracy of the extended Limber approximation is better than 1% even for very small l.

Chapter 8

Bispectrum

Contents

In this chapter, we will compute the bispectrum of the cosmic shear, by using the complete expression for γ stated on page 85. As the final expressions are rather long and stated in detail in our article, we will focus our attention on some technical steps that are hidden in our article. We will also describe how the various terms are implemented into MATHEMATICA, after having applied the Limber approximation.

8.1 Introduction

Like said in the previous chapter, we assume that the initial potential $\Phi_{\mathbf{k}}$ follows a Gaussian distribution, implying by Wick's theorem that

$$\langle \Phi_{\mathbf{k}} \Phi_{\mathbf{k}'} \Phi_{\mathbf{k}''} \rangle = 0. \tag{8.1}$$

Therefore, using the first-order $\Psi^{(1)}$ in $\langle \gamma^{[0]} \gamma^{[0]} \gamma^{[0]} \rangle$, gives a vanishing result. To find a non-zero result, we should thus use either the second-order potentials (i.e. the dynamical terms), or the first-order potentials in the second-order terms (i.e. the geometrical and redshift terms). For example, the contribution of term [1] is given by the correlator

$$\langle a^{[0]}_{E,l_1m_1} a^{[0]}_{E,l_2m_2} a^{[1]}_{E,l_3m_3} \rangle + \langle a^{[0]}_{E,l_1m_1} a^{[1]}_{E,l_2m_2} a^{[0]}_{E,l_3m_3} \rangle + \langle a^{[1]}_{E,l_1m_1} a^{[0]}_{E,l_2m_2} a^{[0]}_{E,l_3m_3} \rangle, \tag{8.2}$$

which we will always write as

$$\langle a^{[0]}_{E,l_1m_1} a^{[0]}_{E,l_2m_2} a^{[1]}_{E,l_3m_3} \rangle + 2 \text{ perms.} \tag{8.3}$$

The most simple term to analyze is exactly term [1], so we will start with this one. While analyzing part [2], we will run into the electric and the magnetic part of the bispectrum. As terms [3]–[7] need the very same techniques, we will not discuss them. Term [8] is the first involving $\dot{\Psi}$, so we will discuss it briefly. The redshift terms [9]–[11] all have the same prefactor, so we will consider them together. Moreover, [10] and [11] share the same subtlety, namely a potential evaluated at the source. In the final two sections, we will discuss the standard (Newtonian) dynamical terms and the dynamical corrections given in eq. (6.21) respectively.

8.2 Part [1]

The first part of the second-order shear γ we will analyze is part [1] of eq. (6.20), and we will denoted it by $\mathcal{C}^{[1]}$. It is given by

$$\begin{aligned}\mathcal{C}^{[1]} \equiv -\int_0^{\chi_S}\mathrm{d}\chi_1\,\frac{\chi_S-\chi_1}{\chi_S\chi_1}\int_0^{\chi_S}\mathrm{d}\chi_2\,\frac{\chi_S-\chi_2}{\chi_S\chi_2}\int_0^{\chi_S}\mathrm{d}\chi_3\,\frac{\chi_S-\chi_3}{\chi_S\chi_3}\\ \times\left\langle\partial\!\!\!/^2\Psi(\chi_1,\hat{n}_1)\partial\!\!\!/^2\Psi(\chi_2,\hat{n}_2)\partial\!\!\!/^2\Psi^2(\chi_3,\hat{n}_3)\right\rangle\\ +\ 2\text{ perms},\end{aligned} \tag{8.4}$$

where every $\Psi(\chi,\hat{n})$ is given by eq. (6.22). To improve readability, we will drop the three χ-integrals and window functions for now and define the remaining correlator as $\tilde{\mathcal{C}}^{[1]}$, i.e.,

$$\tilde{\mathcal{C}}^{[1]} \equiv -\left\langle\partial\!\!\!/^2\Psi(\chi_1,\hat{n}_1)\partial\!\!\!/^2\Psi(\chi_2,\hat{n}_2)\partial\!\!\!/^2\Psi^2(\chi_3,\hat{n}_3)\right\rangle, \tag{8.5}$$

so that

$$\mathcal{C}^{[1]} \equiv \int_0^{\chi_S}\mathrm{d}\chi_1\,\frac{\chi_S-\chi_1}{\chi_S\chi_1}\int_0^{\chi_S}\mathrm{d}\chi_2\,\frac{\chi_S-\chi_2}{\chi_S\chi_2}\int_0^{\chi_S}\mathrm{d}\chi_3\,\frac{\chi_S-\chi_3}{\chi_S\chi_3}\,\tilde{\mathcal{C}}^{[1]} +\ 2\text{ perms}. \tag{8.6}$$

There are now two approaches to compute the correlator. The first one, using a convolution in Fourier space, is relatively easy and quickly gives the full result. Unfortunately, this method is not transferable to the other terms. We will therefore introduce a second technique (see Sec. 8.2.2), which is transferable, but more involved.

8.2.1 Convolution

When we write eq. (8.5) in Fourier space, the square becomes a convolution. Substituting the fields Ψ by the primordial fields $\Phi_{\mathbf{k}}$ using eq. (6.22), gives

$$\begin{aligned}\tilde{\mathcal{C}}^{[1]} = -\int\frac{\mathrm{d}^3\mathbf{k}_1\,\mathrm{d}^3\mathbf{k}_2\,\mathrm{d}^3\mathbf{k}_3\,\mathrm{d}^3\mathbf{q}}{(2\pi)^{12}}\,g(\chi_1)g(\chi_2)g^2(\chi_3)T(k_1)T(k_2)T(|\mathbf{k}_3-\mathbf{q}|)T(q)\\ \times\left(\partial\!\!\!/^2 e^{i\mathbf{k}_1\cdot\hat{n}_1\chi_1}\right)\left(\partial\!\!\!/^2 e^{i\mathbf{k}_2\cdot\hat{n}_2\chi_2}\right)\left(\partial\!\!\!/^2 e^{i\mathbf{k}_3\cdot\hat{n}_3\chi_3}\right)\langle\Phi_{\mathbf{k}_1}\Phi_{\mathbf{k}_2}\Phi_{\mathbf{k}_3-\mathbf{q}}\Phi_{\mathbf{q}}\rangle\,.\end{aligned} \tag{8.7}$$

The reason this technique does not work for the other terms is because in those cases, the two Ψ's corresponding to l_3 are not evaluated at the same time χ_3. Applying Wick's theorem to the equation above and using eq. (7.1), gives for the 4-Φ-correlator

$$\langle\Phi_{\mathbf{k}_1}\Phi_{\mathbf{k}_2}\Phi_{\mathbf{k}_3-\mathbf{q}}\Phi_{\mathbf{q}}\rangle = (2\pi)^6\delta_{\mathrm{D}}(\mathbf{k}_1+\mathbf{k}_2+\mathbf{k}_3)P(k_1)P(k_2)\left[\delta_{\mathrm{D}}(\mathbf{k}_1+\mathbf{q})+\delta_{\mathrm{D}}(\mathbf{k}_2+\mathbf{q})\right]. \tag{8.8}$$

The part with $\delta_{\rm D}(\mathbf{k}_3)$ has not been written down because it is singular and does not contribute to $\hat{\mathcal{C}}^{[1]}$. Moreover, as $\mathbf{k}_1$ and $\mathbf{k}_2$ are merely dummy variables and the integrand is symmetric under their exchange, we can trade the $\delta_{\rm D}(\mathbf{k}_2+\mathbf{q})$ with a factor of 2 in front, giving

$$\begin{aligned}\tilde{\mathcal{C}}^{[1]} = &-2\int \frac{\mathrm{d}^3\mathbf{k}_1\,\mathrm{d}^3\mathbf{k}_2\,\mathrm{d}^3\mathbf{k}_3\,\mathrm{d}^3\mathbf{q}}{(2\pi)^{12}}\; g(\chi_1)g(\chi_2)g^2(\chi_3)T(k_1)T(k_2)T(|\mathbf{k}_3-\mathbf{q}|)T(q)\\ &\times\left(\eth^2 e^{i\mathbf{k}_1\cdot\hat{n}_1\chi_1}\right)\left(\eth^2 e^{i\mathbf{k}_2\cdot\hat{n}_2\chi_2}\right)\left(\eth^2 e^{i\mathbf{k}_3\cdot\hat{n}_3\chi_3}\right)\\ &\times(2\pi)^6\delta_{\rm D}(\mathbf{k}_1+\mathbf{k}_2+\mathbf{k}_3)P(k_1)P(k_2)\delta_{\rm D}(\mathbf{k}_1+\mathbf{q}).\end{aligned} \tag{8.9}$$

Using the second $\delta_{\rm D}$ to get rid of the $\mathrm{d}^3\mathbf{q}$-integral gives

$$\begin{aligned}\tilde{\mathcal{C}}^{[1]} = &-2\int \frac{\mathrm{d}^3\mathbf{k}_1\,\mathrm{d}^3\mathbf{k}_2\,\mathrm{d}^3\mathbf{k}_3}{(2\pi)^9}\; g(\chi_1)g(\chi_2)g^2(\chi_3)T^2(k_1)T^2(k_2)P(k_1)P(k_2)\\ &\times\left(\eth^2 e^{i\mathbf{k}_1\cdot\hat{n}_1\chi_1}\right)\left(\eth^2 e^{i\mathbf{k}_2\cdot\hat{n}_2\chi_2}\right)\left(\eth^2 e^{i\mathbf{k}_3\cdot\hat{n}_3\chi_3}\right)(2\pi)^3\delta_{\rm D}(\mathbf{k}_1+\mathbf{k}_2+\mathbf{k}_3).\end{aligned} \tag{8.10}$$

It is now time to tackle the spin raising operators. The trick is to write the $\delta_{\rm D}$-function as the Fourier transform of 1, expand the resulting $3+3=6$ exponentials in spherical Bessel functions and spherical harmonics using, like we did when computing the power spectrum, $e^{i\mathbf{a}\cdot\mathbf{b}} = 4\pi\sum i^l\, j_l(ab)Y_{lm}(\hat{a})Y^*_{lm}(\hat{b})$, and finally let the $\eth$ operators act on the corresponding $Y_{lm}(\hat{n})$. The resulting expression is rather lengthy, but it simplifies easily using orthogonality properties of spherical Bessel functions and spherical harmonics. The resulting expression contains a Gaunt integral which, after writing it in terms of Wigner-3j symbols, allows us to write $\tilde{\mathcal{C}}^{[1]}$ in the form

$$\begin{aligned}\tilde{\mathcal{C}}^{[1]} = &\sum_{l_1m_1}\sum_{l_2m_2}\sum_{l_3m_3}\begin{pmatrix} l_1 & l_2 & l_3\\ m_1 & m_2 & m_3\end{pmatrix}\begin{pmatrix} l_1 & l_2 & l_3\\ 0 & 0 & 0\end{pmatrix}\sqrt{\frac{(2l_1+1)(2l_2+1)(2l_3+1)}{4\pi}}\\ &\times\;(-2)\,\text{ł}(l_1,2)\text{ł}(l_2,2)\text{ł}(l_3,2)g(\chi_1)g(\chi_2)g^2(\chi_3)\\ &\times\int\frac{2k_1^2\mathrm{d}k_1}{\pi}\int\frac{2k_2^2\mathrm{d}k_2}{\pi}T^2(k_1)T^2(k_2)P(k_1)P(k_2)\\ &\times j_{l_1}(k_1\chi_1)j_{l_1}(k_1\chi_3)j_{l_2}(k_2\chi_2)j_{l_2}(k_2\chi_3)\\ &\times\;{}_2Y_{l_1m_1}(\hat{n}_1)\;{}_2Y_{l_2m_2}(\hat{n}_2)\;{}_2Y_{l_3m_3}(\hat{n}_3).\end{aligned} \tag{8.11}$$

The summations together with the last line exactly corresponds to the expansion we are looking for, i.e. we can read off $\langle {}_2a^{[0]}_{l_1m_1}\,{}_2a^{[0]}_{l_2m_2}\,{}_2a^{[1]}_{l_3m_3}\rangle$. Moreover, in the first line, one recognises $\mathcal{G}^{m_1m_2m_3}_{l_1l_2l_3}$ making it straightforward to go from the bispectrum to the reduced bispectrum. Their is just one subtlety: we showed, in the chapter discussing the power spectrum, that $a^{[0]}_{E,lm} = -{}_2a^{[0]}_{lm}$, and for the same reason ($\Phi^2_{\mathbf{k}}$ is also real), $a^{[1]}_{E,lm} = -{}_2a^{[1]}_{lm}$. We should therefore take into account this minus sign when extracting $b_{l_1l_2l_3}$ out of eq. (8.11). The result, after recovering the three χ-integrals, is

$$\boxed{\begin{aligned}b^{[1]}_{l_1l_2l_3} = &\;2\,\text{ł}(l_1,2)\text{ł}(l_2,2)\text{ł}(l_3,2)\\ &\times\int_0^{\chi_S}\mathrm{d}\chi_1\,W(\chi_S,\chi_1)\int_0^{\chi_S}\mathrm{d}\chi_2\,W(\chi_S,\chi_2)\int_0^{\chi_S}\mathrm{d}\chi_3\,W(\chi_S,\chi_3)g(\chi_3)\\ &\times\int\frac{2k_1^2\mathrm{d}k_1}{\pi}\int\frac{2k_2^2\mathrm{d}k_2}{\pi}P(k_1)P(k_2)j_{l_1}(k_1\chi_1)j_{l_1}(k_1\chi_3)j_{l_2}(k_2\chi_2)j_{l_2}(k_2\chi_3)\\ &\quad+\;2\text{ perms.}\end{aligned}} \tag{8.12}$$

Notice that the expression is invariant under the exchange $l_1 \leftrightarrow l_2$ as it should be. Therefore, the factor of 2 can be removed if we change "+ 2 perms" to "+ 5 perms" such that all the permutations, and not only the cyclic ones, are taken into account.

8.2.2 Products of fields

In order to find a technique that can be used for the other terms, we should try to recover eq. (8.12) without assuming that the two Ψ's present in $\gamma^{[1]}$ are evaluated at the same time. To do so, we first use the Leibniz rule to "decouple" the two Ψ's,

$$\eth^2\Psi^2 = 2\left((\eth^2\Psi)\Psi + (\eth\Psi)(\eth\Psi)\right). \tag{8.13}$$

We will thoroughly discuss the first part, i.e. $(\eth^2\Psi(\chi,\hat{n}))\Psi(\chi',\hat{n})$, which we will call [1a]. The other part, say [1b], is completely analogous and we will only state the result at the end of this subsection. Of course, $\chi = \chi'$ in this case, but we will not take this into account, not to lose generality. What we are interested in is the correlator of three ${}_2a_{lm}$'s, but what we know up to now is the correlator of two a_{lm}'s, see eq. (7.9). Therefore, we need to write each ${}_2a_{lm}$ as a function of a_{lm}'s. For part [0], the relation is given by eq. (7.11),

$${}_2a^{[0]}_{lm} = \text{ł}(l,2)\frac{1}{4\pi}\int_0^{\chi_S} \mathrm{d}\chi \frac{\chi_S - \chi}{\chi_S \chi}\int \frac{2k^2\mathrm{d}k}{\pi} i^l j_l(k\chi)\, a_{lm}(k). \tag{8.14}$$

For part [1a], it is more complicated. In appendix 10.2 on page 144, we show the following property. If two spin-0 fields $\Xi_1(\hat{n})$ and $\Xi_2(\hat{n})$ have real space expansion coefficients $\Xi_1(\chi_1,\hat{n}) = \sum a^{\Xi_1}_{lm}(\chi_1)\; Y_{lm}(\hat{n})$ and $\Xi_2(\chi_2,\hat{n}) = \sum a^{\Xi_2}_{lm}(\chi_2)\; Y_{lm}(\hat{n})$ respectively, then the spin-2 field $(\eth^2\Xi_1)\Xi_2$ has the expansion $(\eth^2\Xi_1(\hat{n}))\Xi_2(\hat{n}) = \sum {}_2a_{lm}\;\, {}_2Y_{lm}(\hat{n})$, where the coefficients satisfy

$${}_2a_{lm} = (-1)^m \sum_{l_1,m_1}\sum_{l_2,m_2} \begin{Bmatrix} l & l_1 & l_2 \\ -m & m_1 & m_2 \\ -2 & 2 & 0 \end{Bmatrix} \text{ł}(l_1,2) a^{\Xi_1}_{l_1m_1} a^{\Xi_2}_{l_2m_2}, \tag{8.15}$$

where $\{:::\}$ has been defined in eq. (6.43). If $a^{\Xi_1}_{l_1m_1}$ and $a^{\Xi_2}_{l_2m_2}$ are the Fourier space expansion coefficients, i.e. the expansion coefficients of the Fourier transform of Ξ_1 and Ξ_2 respectively, the above expression gets changed to

$$\begin{aligned} {}_2a_{lm} =& (-1)^m \sum_{l_1,m_1}\sum_{l_2,m_2} \begin{Bmatrix} l & l_1 & l_2 \\ -m & m_1 & m_2 \\ -2 & 2 & 0 \end{Bmatrix} \text{ł}(l_1,2) \\ &\times \frac{1}{4\pi}\int \frac{2k_1^2\mathrm{d}k_1}{\pi} i^{l_1} j_{l_1}(k_1\chi_1) a^{\Xi_1}_{l_1m_1}(k_1) \\ &\times \frac{1}{4\pi}\int \frac{2k_2^2\mathrm{d}k_2}{\pi} i^{l_2} j_{l_2}(k_2\chi_2) a^{\Xi_2}_{l_2m_2}(k_2). \end{aligned} \tag{8.16}$$

This is exactly the expression we are looking for to find ${}_2a_{lm}^{[1a]}$; we just need to add the χ-integral and set $\chi_1 = \chi_2 = \chi$, the result being

$$
\begin{aligned}
{}_2a_{lm}^{[1a]} = \frac{(-1)^m}{(4\pi)^2} \sum_{l_1,m_1} \sum_{l_2,m_2} \begin{Bmatrix} l & l_1 & l_2 \\ -m & m_1 & m_2 \\ -2 & 2 & 0 \end{Bmatrix} \text{ł}(l_1,2) \int_0^{\chi_S} \mathrm{d}\chi \, \frac{\chi_S - \chi}{\chi_S \chi} \\
\times \left(\int \frac{2k_1^2 \mathrm{d}k_1}{\pi} i^{l_1} j_{l_1}(k_1\chi) a_{l_1 m_1}(k_1) \right) \left(\int \frac{2k_2^2 \mathrm{d}k_2}{\pi} i^{l_2} j_{l_2}(k_2\chi) a_{l_2 m_2}(k_2) \right) .
\end{aligned}
\tag{8.17}
$$

Combining twice eq. (8.14) with this equation, gives the three ${}_2a_{lm}$-correlator we are looking for,

$$
\begin{aligned}
\left\langle {}_2a_{l_1 m_1}^{[0]} \; {}_2a_{l_2 m_2}^{[0]} \; {}_2a_{l_3 m_3}^{[1a]} \right\rangle =& (-1)^{m_3} \text{ł}(l_1,2) \text{ł}(l_2,2) \sum_{\substack{l_4,\, m_4 \\ l_5,\, m_5}} i^{l_1+l_2+l_4+l_5} \begin{Bmatrix} l_3 & l_4 & l_5 \\ -m_3 & m_4 & m_5 \\ -2 & 2 & 0 \end{Bmatrix} \text{ł}(l_4,2) \\
& \times \int_0^{\chi_S} \mathrm{d}\chi_1 \, \frac{\chi_S - \chi_1}{\chi_S \chi_1} \int_0^{\chi_S} \mathrm{d}\chi_2 \, \frac{\chi_S - \chi_2}{\chi_S \chi_2} \int_0^{\chi_S} \mathrm{d}\chi_3 \, \frac{\chi_S - \chi_3}{\chi_S \chi_3} \\
& \times \left(\frac{1}{4\pi} \right)^4 \int \frac{2k_1^2 \mathrm{d}k_1}{\pi} \int \frac{2k_2^2 \mathrm{d}k_2}{\pi} \int \frac{2k_4^2 \mathrm{d}k_4}{\pi} \int \frac{2k_5^2 \mathrm{d}k_5}{\pi} \\
& \times j_{l_1}(k_1\chi_1) j_{l_2}(k_2\chi_2) j_{l_4}(k_4\chi_3) j_{l_5}(k_5\chi_3) \\
& \times \langle a_{l_1 m_1}(\chi_1, k_1) a_{l_2 m_2}(\chi_2, k_2) a_{l_4 m_4}(\chi_3, k_4) a_{l_5 m_5}(\chi_3, k_5) \rangle \, .
\end{aligned}
\tag{8.18}
$$

Using Wick's theorem and equation (7.9), we can rewrite the four $a_{lm}(\chi, k)$-correlator in the last line as

$$
\begin{aligned}
& \langle a_{l_1 m_1}(\chi_1, k_1) a_{l_2 m_2}(\chi_2, k_2) a_{l_4 m_4}(\chi_3, k_4) a_{l_5 m_5}(\chi_3, k_5) \rangle \\
& \quad = (2\pi)^6 (-1)^{m_1+l_1} (-1)^{m_2+l_2} \frac{P(k_1)}{k_1^2} \frac{P(k_2)}{k_2^2} T^2(k_1) T^2(k_2) \; g(\chi_1) g(\chi_2) g^2(\chi_3) \\
& \qquad \times \big[\delta_{l_1 l_4} \delta_{m_1,-m_4} \delta_{\mathrm{D}}(k_1 - k_4) \; \delta_{l_2 l_5} \delta_{m_2,-m_5} \delta_{\mathrm{D}}(k_2 - k_5) \\
& \qquad\qquad + \delta_{l_1 l_5} \delta_{m_1,-m_5} \delta_{\mathrm{D}}(k_1 - k_5) \; \delta_{l_2 l_4} \delta_{m_2,-m_4} \delta_{\mathrm{D}}(k_2 - k_4) \big] .
\end{aligned}
\tag{8.19}
$$

The term with the 1-2 and 4-5 δ-functions is singular and has not been written down as it will not contribute to the final result. Formally, it drops out because of an orthogonality relation of the $\{\vdots\}$'s. Using the 4 Kronecker δ's and the 2 δ_{D}'s present in each term, we can remove the four summations and the k_4 and k_5 integrals in eq. (8.18), resulting in the much simpler

$$
\begin{aligned}
\left\langle {}_2a_{l_1 m_1}^{[0]} \; {}_2a_{l_2 m_2}^{[0]} \; {}_2a_{l_3 m_3}^{[1a]} \right\rangle =& \, \text{ł}(l_1,2) \text{ł}(l_2,2) \int \frac{2k_1^2 \mathrm{d}k_1}{\pi} \int \frac{2k_2^2 \mathrm{d}k_2}{\pi} P(k_1) P(k_2) T^2(k_1) T^2(k_2) \\
& \times \int_0^{\chi_S} \mathrm{d}\chi_1 \, W(\chi_S, \chi_1) \int_0^{\chi_S} \mathrm{d}\chi_2 \, W(\chi_S, \chi_2) \int_0^{\chi_S} \mathrm{d}\chi_3 \, W(\chi_S, \chi_3) g(\chi_3) \\
& \times j_{l_1}(k_1\chi_1) j_{l_1}(k_1\chi_3) j_{l_2}(k_2\chi_2) j_{l_2}(k_2\chi_3) \\
& \times \left(\text{ł}(l_1,2) \begin{Bmatrix} l_3 & l_1 & l_2 \\ -m_3 & -m_1 & -m_2 \\ -2 & 2 & 0 \end{Bmatrix} + \text{ł}(l_2,2) \begin{Bmatrix} l_3 & l_2 & l_1 \\ -m_3 & -m_2 & -m_1 \\ -2 & 2 & 0 \end{Bmatrix} \right) .
\end{aligned}
\tag{8.20}
$$

When we apply the same machinery to part [1b], we find the similar result

$$\begin{aligned}\left\langle {}_2a^{[0]}_{l_1m_1}\ {}_2a^{[0]}_{l_2m_2}\ {}_2a^{[1b]}_{l_3m_3}\right\rangle &= \text{ł}(l_1,2)\text{ł}(l_2,2)\int\frac{2k_1^2\mathrm{d}k_1}{\pi}\int\frac{2k_2^2\mathrm{d}k_2}{\pi}P(k_1)P(k_2)T^2(k_1)T^2(k_2)\\ &\times\int_0^{\chi_S}\mathrm{d}\chi_1\,W(\chi_S,\chi_1)\int_0^{\chi_S}\mathrm{d}\chi_2\,W(\chi_S,\chi_2)\int_0^{\chi_S}\mathrm{d}\chi_3\,W(\chi_S,\chi_3)g(\chi_3)\\ &\times j_{l_1}(k_1\chi_1)j_{l_1}(k_1\chi_3)j_{l_2}(k_2\chi_2)j_{l_2}(k_2\chi_3)\\ &\times\left(2\text{ł}(l_1,2)\text{ł}(l_2,2)\begin{Bmatrix} l_3 & l_1 & l_2\\ -m_3 & -m_1 & -m_2\\ -2 & 1 & 1\end{Bmatrix}\right).\end{aligned} \tag{8.21}$$

It can be shown, using several partial integrations inside the spin-weighted Gaunt integrals, that the two big parentheses exactly sum up to $\text{ł}(l_3,2)\mathcal{G}^{000}_{l_1l_2l_3}$ such that

$$\begin{aligned}\left\langle {}_2a^{[0]}_{l_1m_1}\ {}_2a^{[0]}_{l_2m_2}\ {}_2a^{[1a+1b]}_{l_3m_3}\right\rangle &= \text{ł}(l_1,2)\text{ł}(l_2,2)\text{ł}(l_3,2)\mathcal{G}^{000}_{l_1l_2l_3}\\ &\times\int\frac{2k_1^2\mathrm{d}k_1}{\pi}\int\frac{2k_2^2\mathrm{d}k_2}{\pi}P(k_1)P(k_2)T^2(k_1)T^2(k_2)\\ &\times\int_0^{\chi_S}\mathrm{d}\chi_1\,W(\chi_S,\chi_1)\int_0^{\chi_S}\mathrm{d}\chi_2\,W(\chi_S,\chi_2)\int_0^{\chi_S}\mathrm{d}\chi_3\,W(\chi_S,\chi_3)g(\chi_3)\\ &\times j_{l_1}(k_1\chi_1)j_{l_1}(k_1\chi_3)j_{l_2}(k_2\chi_2)j_{l_2}(k_2\chi_3),\end{aligned} \tag{8.22}$$

from which eq. (8.12) immediately follows.

Even if this approach is much more involved than the previous one using the convolution, it is algorithmic. I mean by this that the approach can be applied step by step to all terms of γ, whatever the spin raising and lowering operators are.

8.2.3 Exact integration

Like we did for the power spectrum, we will first try to integrate eq. (8.12) exactly before applying the Limber approximation to it. The trouble is that eq. (8.12) contains five integrals, making it almost impossible to integrate numerically. Fortunately, for fixed k_1 and k_2, the 3 χ-integrals can be calculated quite easily. We therefore need a 2-dimensional sampling of the (k_1,k_2)-space. To facilitate the computation, we focus on an EdS spacetime we source at redshift $z_S=1$. After three full days of computation, we find the following results for four different configurations of (l_1,l_2,l_3). We hereby focus on small values of l to study the precision of the Limber approximation.

(l_1,l_2,l_3)	$b^{[1]}_{l_1l_2l_3}$
$(4,3,3)$	-5.08608
$(4,4,4)$	-4.43533
$(4,5,5)$	-4.31691
$(4,6,6)$	-4.39169

Obviously, three full days is an unreasonably large amount of time for such a small amount of results. We will therefore use, as in the power spectrum case, the Limber approximation.

8.2.4 Limber approximation

The Limber approximation allows us to remove (spherical) Bessel functions. Every time we perform a Limber approximation, we get rid of a Bessel function and an integral. Having four Bessel functions in eq. (8.12), we can remove four integrals, so we are left with only one. The result of the computation is

$$b^{[1],L}_{l_1 l_2 l_3} = \text{ł}(l_1,2)\text{ł}(l_2,2)\text{ł}(l_3,2)\int_0^{\chi_S}\frac{\mathrm{d}\chi}{\chi^4}T^2\left(\frac{\nu_1}{\chi}\right)T^2\left(\frac{\nu_2}{\chi}\right)P\left(\frac{\nu_1}{\chi}\right)P\left(\frac{\nu_2}{\chi}\right)W^3(\chi_S,\chi)g(\chi) + \text{ 5 perms,} \tag{8.23}$$

and this equation can easily be integrated. Using the same parameters as before, we now find the following values:

(l_1,l_2,l_3)	$b^{[1]}_{l_1 l_2 l_3}$	$b^{[1],L}_{l_1 l_2 l_3}$
$(4,3,3)$	-5.08608	-4.73876
$(4,4,4)$	-4.43533	-4.23847
$(4,5,5)$	-4.31691	-4.16807
$(4,6,6)$	-4.39169	-4.26369

The time needed to integrate numerically one of those terms is of the order of $10^{-2}\,\mathrm{s}$, which is much more reasonable than the time needed for the exact integration.

The final step is to apply the second-order Limber approximation to each Bessel function. As can be expected, the result is very involved, and in fact too complicated to write down. I refer to `b1Limber2` in my notebook for the full expression. The results for the same parameters as before are:

(l_1,l_2,l_3)	$b^{[1]}_{l_1 l_2 l_3}$	$b^{[1],L}_{l_1 l_2 l_3}$	$b^{[1],L2}_{l_1,l_2,l_3}$
$(4,3,3)$	-5.08608	-4.73876	-5.04962
$(4,4,4)$	-4.43533	-4.23847	-4.41644
$(4,5,5)$	-4.31691	-4.16807	-4.30234
$(4,6,6)$	-4.39169	-4.26369	-4.37820

One sees that the second-order Limber approximation already gives very accurate results for very small values of l. The computation of the first-order results is approximately twice as fast as the second-order ones.

8.3 Part [2]

The treatment of part [2] (see eq. (6.20)) is very similar to that of part [1]. There are only two differences: a minor one, and a major one. The minor difference is that there is one more χ-integral, meaning that after performing the Limber approximations, there are two integrals left. Fortunately, this requires only few changes in the implementation scheme. Hence, we do not further discuss this difference.

The second, and more important change, is that we cannot say any more that $a^{[2]}_{E,lm} = -{}_2a^{[2]}_{lm}$, like we could for part [1]. The reason is that ${}_2a^{[2]}_{lm} \neq {}_{-2}a^{[2]}_{lm}$ as $\gamma^{[2]}$ cannot be written as the $\eth^2$ of a real function. In appendix 10.2, we show that ${}_2a^{[2]}_{lm}$ and ${}_{-2}a^{[2]}_{lm}$ are related by

simple changes of signs in a Gaunt integral, which itself is equivalent to an overall change of sign depending on the parity of the sum of l's. After taking the three ${}_2a_{lm}$-correlator, we find

$$\left\langle {}_2a^{[0]}_{l_1m_1}\ {}_2a^{[0]}_{l_2m_2}\ {}_2a^{[2]}_{l_3m_3}\right\rangle = (-1)^{l_1+l_2+l_3}\left\langle {}_2a^{[0]}_{l_1m_1}\ {}_2a^{[0]}_{l_2m_2}\ {}_{-2}a^{[2]}_{l_3m_3}\right\rangle, \tag{8.24}$$

which means that

$$\left\langle a^{[0]}_{E,l_1m_1}\ a^{[0]}_{E,l_2m_2}\ a^{[2]}_{E,l_3m_3}\right\rangle = -\frac{1+(-1)^{l_1+l_2+l_3}}{2}\left\langle {}_2a^{[0]}_{l_1m_1}\ {}_2a^{[0]}_{l_2m_2}\ {}_2a^{[2]}_{l_3m_3}\right\rangle. \tag{8.25}$$

Therefore, the (electric) bispectrum $B^{[2],EEE}_{l_1l_2l_3}$ vanishes whenever the sum of l's is odd. For the same reason, the EEB-bispectrum $B^{[2],EEB}_{l_1l_2l_3}$ vanishes whenever the sum of l's is even.

It is not yet obvious that also in this case it is possible to factor $\mathcal{G}^{m_1m_2m_3}_{l_1l_2l_3}$ out of the three $a_{E,lm}$-correlator in order to define the reduced bispectrum. Fortunately, it can be shown that the Gaunt integrals satisfy the following property

$$\begin{Bmatrix} l_1 & l_2 & l_3 \\ m_1 & m_2 & m_3 \\ s_1 & s_2 & s_3 \end{Bmatrix} + \begin{Bmatrix} l_1 & l_2 & l_3 \\ m_1 & m_2 & m_3 \\ -s_1 & -s_2 & -s_3 \end{Bmatrix} = c \begin{Bmatrix} l_1 & l_2 & l_3 \\ m_1 & m_2 & m_3 \\ 0 & 0 & 0 \end{Bmatrix}, \tag{8.26}$$

where c is some coefficient that only depends on the values of l_1, l_2, l_3, s_1, s_2 and s_3. Because of this property, it is sensible to define the reduced bispectrum, even for the parts where the $\mathcal{G}^{m_1m_2m_3}_{l_1l_2l_3}$ does not come out naturally.

For the EEB-bispectrum, it is not possible to define a reduced bispectrum in exactly the same way, as dividing by $\begin{pmatrix} l_1 & l_2 & l_3 \\ 0 & 0 & 0 \end{pmatrix}$ would give singular results for $l_1+l_2+l_3$ odd. Therefore, we define the reduced magnetic bispectrum by dividing the bispectrum by

$$\begin{pmatrix} l_1 & l_2 & l_3 \\ 1 & -1 & 0 \end{pmatrix} - \begin{pmatrix} l_1 & l_2 & l_3 \\ -1 & 1 & 0 \end{pmatrix}. \tag{8.27}$$

Apart from this, the computation of the (reduced) bispectrum is completely similar to the method described in Sec. 8.2.2.

8.4 Part [8]

This term,

$$\gamma^{[8]} = -2\int_0^{\chi_S} d\chi\ \frac{\chi_S-\chi}{\chi_S\chi}\ \eth^2\left(\dot\Psi(\chi)\int_0^{\chi} d\chi'\ \Psi(\chi')\right), \tag{8.28}$$

is slightly different from the others as it contains $\dot\Psi$. During matter dominance, this term vanishes as $g(\chi)=1$ in an EdS spacetime. But in ΛCDM, the growth-suppression factor $g(\chi)$ acquires a time-dependency, see eq. (6.23). This will reflect in a non-vanishing $\dot\Psi$ and hence in a non-vanishing contribution in ΛCDM.

Apart from that, the computation of the reduced bispectrum $b^{[8]}_{l_1l_2l_3}$ is completely analogous to part [5], the only difference being the presence of $g'(\chi_3)$ instead of $g(\chi_3)$. As before, I refer to my notebook or our article for the full expression of $b^{[8]}_{l_1l_2l_3}$.

8.5 Redshift terms

The prefactor of the redshift terms [9]–[11], $(1+z_S)/\chi_S^2 H_S = 1/\chi_S^2 \mathcal{H}_S$ can be computed by means of eqs. (6.24) and (1.7). Apart from this, part [9] has no more subtleties compared to parts [4] and [8]. The next part, part [10], contains one more subtlety: $\psi(\chi_S)$. But as it is multiplied with another potential Ψ, we need ψ only at first order, for which we know that $\psi = \Psi$. Therefore, we can replace $\psi(\chi_S)$ by $\Psi(\chi_S)$ in $\gamma^{[10]}$. For part [11], it is shown in our article (see eqs. (22)–(23)) how $\hat{n}\cdot\mathbf{v}_S$ can be related to the gravitational potentials ϕ and ψ using the $0j$-component of the Einstein equations. Again, as we only need them at first order, we can use Ψ instead. Note that the final expression also contains a derivative of Ψ evaluated at the source, $\dot{\Psi}(\chi_S)$. These potentials evaluated at the source do not complicate in any way the computation of the reduced bispectrum, but they do severely influence the applicability of the Limber approximation.

At first order, the Limber approximation enforces two χ's to be equal, see eq. (7.14). Therefore, applying the Limber approximation to part [10] or [11] would impose one of the integrated χ's to be equal to χ_S. In this case, the window function associated to χ would lead to a vanishing result. Even if taking the second-order Limber approximation resolves the problem of the vanishing result, it is clear that we should not trust the results. In short: the Limber approximation cannot be used on terms containing $j_l(k\chi_S)$.

Luckily, parts [10] and [11] contain only one integral. Therefore even with one less Limber approximation, we are left with only two integrals in the bispectrum. Moreover, the integrals are not coupled, i.e. the bispectrum is a product of two 1D-integrals making its numerical computation fairly easy.

The factor $\hat{n}\cdot\mathbf{v}_S$ in part [11] induces a derivative on the Bessel function evaluated at the source, i.e. $j_l'(k\chi_S)$, the reason being that $(\hat{n}\cdot\mathbf{k}_3)e^{i\mathbf{k}_3\cdot\hat{n}\chi} = -i\partial_\chi e^{i\mathbf{k}_3\cdot\hat{n}\chi}$. To simplify the implementation into MATHEMATICA of this derivative, it is convenient to rewrite it using the following property of spherical Bessel functions,

$$j_l'(x) = \frac{l}{x} j_l(x) - j_{l+1}(x). \tag{8.29}$$

Note that using a different recursion relation for the derivative (many exist) is perfectly valid.

8.6 Newtonian dynamical term

The Newtonian dynamical term (see eqs. (6.21) and (6.27)) is completely analogous to part [1], except for the more complicated window function and the F_2-kernel (6.26). However, the final expression for the (reduced) bispectrum is slightly more complicated because this F_2-kernel makes the $\mathbf{k}_3$-integral non-trivial, whereas it was trivial to go from eq. (8.10) to eq. (8.11). Therefore, the final expression contains two more spherical Bessel

functions and integrals,

$$
\begin{aligned}
b^{\mathrm{N.\,dyn}}_{l_1 l_2 l_3} = {} & \mathit{l}(l_1,2)\mathit{l}(l_2,2)\mathit{l}(l_3,2)\frac{2}{3\Omega_m H_0^2} \\
& \times \int_0^{\chi_S} \mathrm{d}\chi_1 \mathrm{d}\chi_2 \mathrm{d}\chi_3 W(\chi_S,\chi_1) W(\chi_S,\chi_2) W(\chi_S,\chi_3) g(\chi_3) a(\chi_3) \\
& \times \int \frac{2k_1^2 \mathrm{d}k_1}{\pi} \frac{2k_2^2 \mathrm{d}k_2}{\pi} \frac{2k_3^2 \mathrm{d}k_3}{\pi} \frac{k_1^2 k_2^2}{k_3^2} T^2(k_1) T^2(k_2) F_2(k_1,k_2,k_3,\chi_3) P(k_1) P(k_2) \\
& \times \int_0^{\infty} \mathrm{d}\chi\, \chi^2 j_{l_1}(k_1\chi_1) j_{l_1}(k_1\chi) j_{l_2}(k_2\chi_2) j_{l_2}(k_2\chi) j_{l_3}(k_3\chi_3) j_{l_3}(k_3\chi) \\
& + 5 \text{ perms.}
\end{aligned}
\tag{8.30}
$$

Another subtlety lies in the quantity $\mu \equiv (\mathbf{k}_1 \cdot \mathbf{k}_2)/k_1 k_2$ present in the F_2-kernel. Luckily, as $\mathbf{k}_1 + \mathbf{k}_2 + \mathbf{k}_3 = 0$, because of the δ_{D} (see eq. (8.10)), we can rewrite it as $\mu = (k_3^2 - k_1^2 - k_2^2)/2k_1 k_2$.

The first-order Limber approximation of the bispectrum of the Newtonian term is fairly easy to compute; the result resembles the one of part [1],

$$
\begin{aligned}
b^{\mathrm{N.\,dyn}}_{l_1 l_2 l_3} = {} & \mathit{l}(l_1,2)\mathit{l}(l_2,2)\mathit{l}(l_3,2)\frac{\nu_1^2 \nu_2^2}{\nu_3^2}\frac{2}{3\Omega_m H_0^2} \\
& \int_0^{\chi_S} \frac{\mathrm{d}\chi}{\chi^6} W^3(\chi_S,\chi) g(\chi) a(\chi) F_2(\nu_1,\nu_2,\nu_3,\chi) T^2\left(\frac{\nu_1}{\chi}\right) P\left(\frac{\nu_1}{\chi}\right) T^2\left(\frac{\nu_2}{\chi}\right) P\left(\frac{\nu_2}{\chi}\right) \\
& + 5 \text{ perms.}
\end{aligned}
\tag{8.31}
$$

As one can see, the F_2-kernel has ν's as parameters whereas the transfer functions have ν/χ. This is because the F_2-kernel is homogeneous; so we can safely remove the $1/\chi$'s. On the other hand, the second-order Limber approximation is very complicated. The reason is that the higher-order derivatives act on both the window functions and the time-dependent F_2-kernel. To give an idea, the MATHEMATICA code for the second-order Limber approximated Newtonian dynamical term is... 85 cm long.

8.7 Large-scale dynamical terms

The large scale dynamical terms are by far the most difficult parts to be analyzed. So we will handle the scalar, vector and tensor parts separately, by increasing order of difficulty. We will see, especially for the vector and tensor term, that the results get extremely complicated. Fortunately, we saw at first order in the Limber approximation that the resulting bispectra are smaller than all other terms by at least one order of magnitude. Therefore, we make two simplifications. Firstly, we do not compute the second-order Limber approximation, as these corrections would be absolutely negligible compared to the other terms. Secondly, we work in EdS spacetime, i.e. neglecting the dark energy contribution and taking $g(\chi) = 1$.

When removing the dark energy component, the distance-redshift relation is modified. Unfortunately, there are several ways to measure distances in our setup, and it is not clear

yet which one should be kept fixed when removing Ω_Λ. The three options are fixing the redshift, the distance χ_S or the dimensionless distance $\chi_S k_{eq}$ (these two are not the same as k_{eq} is Ω_m-dependent). On Fig. 8.1, we show how these three options change the result. From the plots, we see that it is $\chi_S k_{eq}$ we should keep fixed. The value of z in EdS giving the same $\chi_S k_{eq}$ as $z = 1$ in ΛCDM is $z = 0.278$. Therefore, we will take $z = 0.278$ to compute the large-scale dynamical terms.

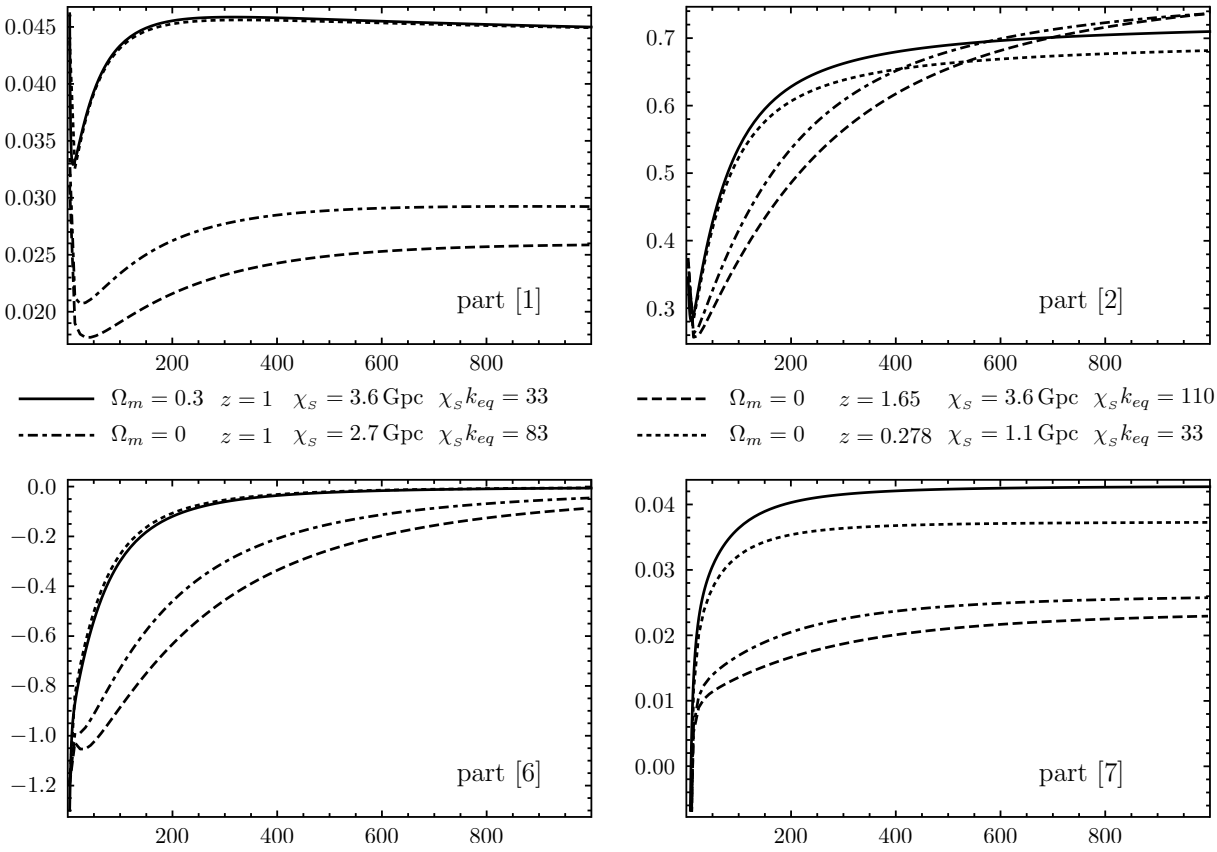

Figure 8.1: Plots of the weighted reduced bispectrum $b^{[i]}_{4,l,l}/(2C_4C_l + C_l^2)$ with $i = 1, 2, 6, 7$, as a function of l. We compare between the results in ΛCDM (continuous line) and EdS at 3 different redshifts (dashdotted: $z = 1$; dashed: $z = 1.65$; dotted: $z = 0.278$). We see that keeping $\chi_S k_{eq}$ fixed is the best approximation.

8.7.1 Scalar parts

The scalar parts, given by $\psi_R^{(2)}$ and $\phi_R^{(2)}$, greatly resembles the Newtonian term discussed previously, the only difference being the kernel. The computation being completely similar, I merely refer to eq. (119) in our article for the result.

8.7.2 Vector parts

The vector part $\omega_r = \hat{n} \cdot \omega_i$ contains factors like $\mathbf{k} \cdot \hat{n}$, and the part with ${}_1\omega$ contains $\hat{e}_+ \cdot \mathbf{k}$. When we handled the velocity term in the redshift corrections, we already encountered $\hat{n} \cdot \mathbf{k}_3$, which introduced a derivative of the spherical Bessel function. Unfortunately, the same trick cannot be applied to $\hat{n} \cdot \mathbf{k}_1$ or $\hat{n} \cdot \mathbf{k}_2$, because it would require us to split the

exponential $e^{\mathbf{k}_3\cdot\hat{n}\chi} = e^{\mathbf{k}_1\cdot\hat{n}\chi}\, e^{\mathbf{k}_2\cdot\hat{n}\chi}$, leading to much more *mess*. The better solution is to use the addition theorem of spherical harmonics,

$$P_l(\hat{a}\cdot\hat{b}) = \frac{4\pi}{2l+1}\sum_{m=-l}^{l} Y^*_{lm}(\hat{a})\; Y_{lm}(\hat{b}), \tag{8.32}$$

where P_l is the l^{th} Legendre polynomial. As $P_1(x) = x$, we have that

$$\hat{a}\cdot\hat{b} = \frac{4\pi}{3}\sum_{m=-1,0,1} Y^*_{1m}(\hat{a})\; Y_{1m}(\hat{b}). \tag{8.33}$$

This introduces yet another, though well controlled, summation. Moreover, the two new spherical harmonics will create Gaunt integrals on places where we used to have $\int \mathrm{d}^2\hat{n} Y_{lm} Y^*_{l'm'}$ which simplified to $\delta_{ll'}\delta_{mm'}$. Fortunately, there is the absolutely flabbergasting property of Gaunt integrals

$$\begin{aligned}
&\sum_{m_1' m_3' M} (-1)^{m_1'+m_3'+M} \mathcal{G}^{-m_1',-m_2,-m_3'}_{l_1',l_2,l'} \mathcal{G}^{-m_3,m_3',M}_{l_3,l_3',1} \mathcal{G}^{-m_1,m_1',-M}_{l_1,l_1',1} \\
&\quad = (-1)^{l_1'+l_3'+1}\sqrt{\frac{(2l_1+1)(2l_2+1)(2l_3+1)}{4\pi}}\frac{3(2l_1'+1)(2l_3'+1)}{4\pi}\begin{pmatrix} l_1 & l_2 & l \\ m_1 & m_2 & m\end{pmatrix} \\
&\qquad \times \begin{pmatrix} l_1 & l_1' & 1 \\ 0 & 0 & 0\end{pmatrix}\begin{pmatrix} l_3' & l_3 & 1 \\ 0 & 0 & 0\end{pmatrix}\begin{pmatrix} l_3' & l_1' & l_2 \\ 0 & 0 & 0\end{pmatrix}\begin{Bmatrix} l_1 & l_2 & l_3 \\ l_3' & 1 & l_1'\end{Bmatrix},
\end{aligned} \tag{8.34}$$

which magically takes care of 3 summations. Nevertheless, the final bispectrum still contains a double summation, but using various properties of the Wigner-3j symbols (like triangle inequalities) reduces these two sums to only 4 terms. These turn out to be relatively simple functions of the l's. Eq. (81) of our article shows the result, before simplifying the five Wigner symbols. Afterwards, when performing the Limber approximation, care should be taken because the changing indices of the spherical Bessel function induce different integration boundaries.

The other subtlety, namely $\hat{e}_+\cdot\mathbf{k}$, can be handled in approximately the same way. The trick is to rewrite it as

$$\hat{e}_+\cdot\mathbf{k} = -\eth(\mathbf{k}\cdot\hat{n}), \tag{8.35}$$

where we used that $\partial_\theta\hat{n} = \hat{e}_\theta$ and $\partial_\varphi\hat{n} = \sin(\theta)\hat{e}_\varphi$. The spin raising operator will then act on the spherical harmonics introduced by eq. (8.33). The remaining calculation is completely similar.

8.7.3 Tensor parts

The tensor parts, those with h_{rr}, ${}_1h_r$ and ${}_2h$, are the *worst*. Not so much because they require yet another bright trick, but because of the incredibly lengthy calculation. As they contain factors like $(\hat{n}\cdot\mathbf{k}_1)(\hat{n}\cdot\mathbf{k}_2)$ or $(\hat{e}_+\cdot\mathbf{k}_1)(\hat{e}_+\cdot\mathbf{k}_2)$, they introduce twice as many new summations and Gaunt integrals as the vectors parts. Each of the three tensor parts contain not less than 16 terms, all with different coefficients. If you really, absolutely, positively want to see the results, have a look at eqs. (121), (123) and (125) of our article. (But I suggest you don't.)

Chapter 9

Results

Contents

In this chapter, we analyse the bispectrum computed in the previous chapter. We will first plot all the parts separately to get a first insight into their respective contributions. We will then explain why some parts depend more than others on the shape of the (l_1, l_2, l_3)-triangle. We will also briefly mention how the bispectra depend on the source redshift and compare the bispectra with the one generated by a primordial non-Gaussianity.

9.1 Plots

On the following page, see Fig. 9.1, we show the weighted reduced bispectrum, i.e.

$$\hat{b}_{l_1 l_2 l_3} \equiv \frac{b_{l_1 l_2 l_3}}{C_{l_1} C_{l_2} + C_{l_2} C_{l_3} + C_{l_3} C_{l_1}} \tag{9.1}$$

for $(l_1, l_2, l_3) = (10, l_s, l_s + \Delta l_s)$ and at source redshift $z_S = 1$, as a function of l_s.[1] Because the sum of the l's has to be even, see eq. (8.25), and the l's have to satisfy the triangle inequality, Δl_s is limited to the values 0, 2, 4, 6, 8, and 10. Except for the dynamical corrections, all calculations have been made using the extended Limber approximation. We summarise here the first observations.

- All plots are approximately flat, i.e. $\hat{b}_{10,l,l+\Delta l}$ is weakly l-dependent when l is large.

[1] See Fig. 9.4 for a figure of the (l_1, l_2, l_3)-triangle.

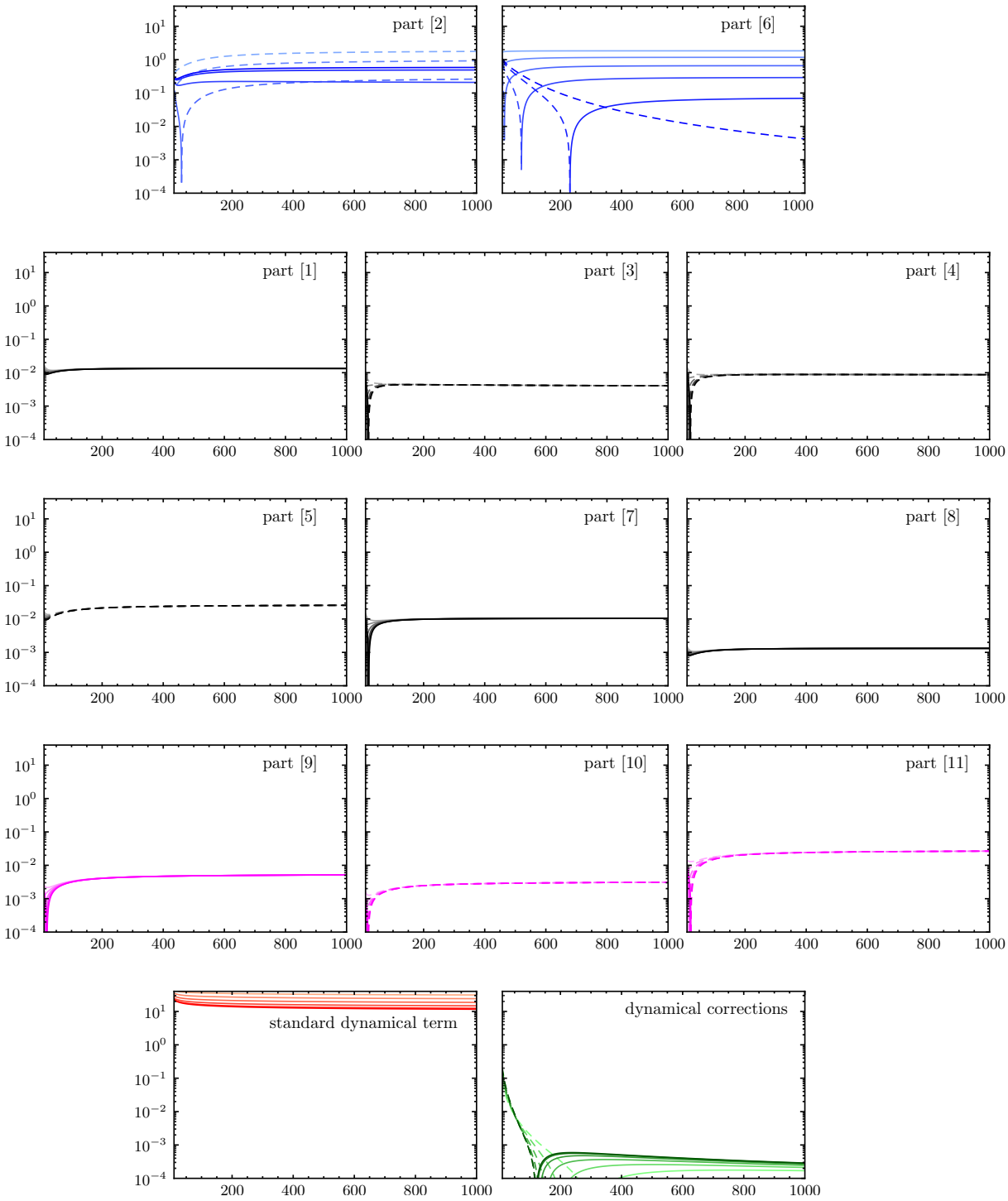

Figure 9.1: Plot of the weighted reduced bispectrum $\hat{b}_{l_1 l_2 l_3}$ for $(l_1, l_2, l_3) = (10, l_s, l_s + \Delta l_s)$ with $4 \leq l_s \leq 1000$ and $0 \leq \Delta l_s \leq 10$. The source is taken at redshift $z_S = 1$. Dashed lines correspond to a negative value for $\hat{b}_{l_1 l_2 l_3}$. The color code corresponds to that used in [34], see Table 1. Dark lines correspond to $\Delta l_s = 0$, light lines to $\Delta l_s = 10$.

- The hierarchy of the corrections is the following: standard dynamical term > standard geometrical terms (i.e. the sum of [2] and [6]) > redshift corrections (i.e. the sum of [9]–[11]) > geometrical corrections (i.e. the sum of [1], [3]–[5], [7]–[8]) > dynamical corrections. This is even more apparent on fig. 3 of our article.

- The standard geometrical and dynamical terms strongly depend on Δl whereas the others don't.

As the dynamical corrections are by far the smallest, we will not discuss them any further. We also see that [3], [8], [9] and [10] are smaller than the others, so to gain computational time, we will not compute them for different source redshifts like we will do for the other parts.

9.2 Analysis of plots

In this section, we explain the three observations made above. As our article contains detailed explanations, term by term, we will merely focus on the basic principles and leave the details to our article (see Sec. 5).

The first step we make to understand the plots, is approximating the transfer function $T(k)$ at the scales of interest. These scales of interest correspond to a multipole $l \sim 1000$ and a distance $\chi_S k_{eq} \sim 30$ whence $k/k_{eq} \sim l/\chi_S k_{eq} \sim 30$. We derive here how we can approximate the transfer function by a power law.

The BBKS transfer function $T(k)$ we use (see eq. (6.25)), is given by

$$T(k) = \frac{\log(1+0.171\hat{k})}{(0.171\hat{k})}\left[1+0.284\hat{k}+\left(1.18\hat{k}\right)^2+\left(0.399\hat{k}\right)^3+\left(0.490\hat{k}\right)^4\right]^{(-1/4)}, \quad (9.2)$$

where $\hat{k} = k/k_{eq}$. In the range we are interested in, we can get rid of the lower powers between the square brackets to find

$$T(k) \approx \frac{\log(1+0.171\hat{k})}{(0.171\hat{k})}\left[0.490\hat{k}\right]^{-1}. \quad (9.3)$$

Writing $\log(1+0.171\hat{k})$ as $\log(0.171\hat{k}) + \log(1+1/0.171\hat{k})$ and dropping the latter as we assume $\hat{k} \gg 1$, gives

$$T(k) \approx \frac{\log(0.171\hat{k})}{0.171 \times 0.490\hat{k}^2}. \quad (9.4)$$

As $\log(x)$ is well approximated by a square root when $x \sim 5$, or more precisely when $\hat{k} \sim 30$, we have that $\log(0.171\hat{k}) \sim \sqrt{0.1\,\hat{k}}$. Therefore, we find the approximation

$$T(k) \approx \frac{12}{\hat{k}^2}\sqrt{0.1\,\hat{k}}. \quad (9.5)$$

Fig. 9.2 shows that this crude approximation is nevertheless a decent one. On the same figure, we also show another approximation $T(k) \sim \sqrt{0.5/\hat{k}}$, which is valid for $\hat{k} \sim 1$.

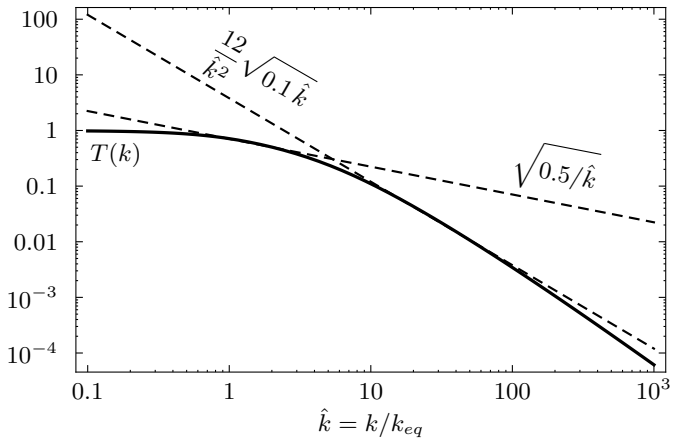

Figure 9.2: Two approximations (dashed lines) to the BBKS transfer function $T(k)$ (thick line). The approximation $T(k) \propto \hat{k}^{-1/2}$ is valid for $\hat{k} \sim 1$ while $T(k) \propto \hat{k}^{-3/2}$ is valid for $\hat{k} \sim 30$.

Of course, there is a much more sensible way to find the effective power when making a power law approximation. Indeed, the power α is given by

$$\alpha \equiv \frac{\mathrm{d}\log T(k)}{\mathrm{d}\log k}, \tag{9.6}$$

which is obviously scale-dependent. On Fig. 9.3, we plot this power and see that the approximations made above ($T(k) \propto \hat{k}^{-1/2}$ and $T(k) \propto \hat{k}^{-3/2}$) are relatively accurate at their respective scales. With this power law approximation, it is easy to approximate the χ- and k-integrals, and to find how they depend on the various l's. The only subtlety is what to do with the window functions and other factors of χ. But as the only length scale in the setup is χ_S, we take $W(\chi_S, \chi) \sim 1/\chi_S$, which is correct up to $\mathcal{O}(1)$ factors.

Using this approximations, it is straightforward to show that $\hat{b}_{10,l_s,l_s+\Delta l_s} \propto l_s^0$ explaining the flatness of the lines in Fig. 9.1.

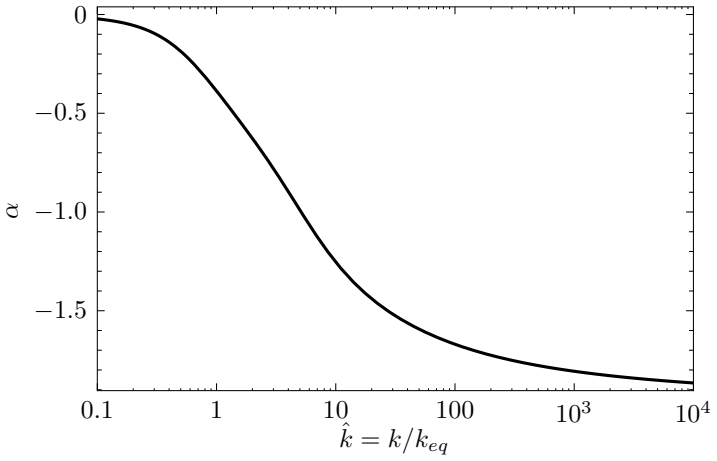

Figure 9.3: The power $\alpha \equiv \frac{\mathrm{d}\log T(k)}{\mathrm{d}\log k}$ as a function of $\hat{k} = k/k_{eq}$. We see that $\alpha(1) \sim -1/2$ and $\alpha(30) \sim -3/2$ which agrees with Fig. 9.2.

Next, we need to get a better understanding of the Wigner-3j symbols, because they

are responsible for the Δl_s-dependence, as we shall see. All the reduced bispectra contain factors of the form

$$\begin{pmatrix} l_1 & l_2 & l_3 \\ s_1 & s_2 & s_3 \end{pmatrix} \begin{pmatrix} l_1 & l_2 & l_3 \\ 0 & 0 & 0 \end{pmatrix}^{-1}, \tag{9.7}$$

where $s_1 + s_2 + s_3 = 0$ and $l_1 + l_2 + l_3 =$ even. The precise values of s_1, s_2 and s_3 depends on the spin raising and lowering operators at hand. Using integration by parts in the Gaunt integrals, they can be reduced to (linear combinations of)

$$\begin{pmatrix} l_1 & l_2 & l_3 \\ 0 & s & -s \end{pmatrix} \begin{pmatrix} l_1 & l_2 & l_3 \\ 0 & 0 & 0 \end{pmatrix}^{-1}, \tag{9.8}$$

where we took $s_1 = 0$ for convenience, but the other two cases, i.e. $s_2 = 0$ or $s_3 = 0$, can also be reached. We will explicitly show what this expression is reduced to for $s = 1$, but we will state its generalisation without proof. By definition, we have that

$$\begin{pmatrix} l_1 & l_2 & l_3 \\ 0 & 1 & -1 \end{pmatrix} = c \int \mathrm{d}^2\hat{n}\; Y_{l_1 m_1}(\hat{n})\; {}_1Y_{l_2 m_2}(\hat{n})\; {}_{-1}Y_{l_3 m_3}(\hat{n}), \tag{9.9}$$

where $c = \left[\begin{pmatrix} l_1 & l_2 & l_3 \\ m_1 & m_2 & m_3 \end{pmatrix} \sqrt{\frac{(2l_1+1)(2l_2+1)(2l_3+1)}{4\pi}} \right]^{-1}$. Writing the spin weighted spherical harmonics as regular spherical harmonics acted upon with spin raising and lowering operators, we find

$$\begin{pmatrix} l_1 & l_2 & l_3 \\ 0 & 1 & -1 \end{pmatrix} = -c \frac{1}{\text{ł}(l_2,1)\text{ł}(l_3,1)} \int \mathrm{d}^2\hat{n}\; Y_{l_1 m_1}(\hat{n})\; \eth Y_{l_2 m_2}(\hat{n})\; \overline{\eth} Y_{l_3 m_3}(\hat{n}). \tag{9.10}$$

By performing integration by parts thrice, we end up with 3 Laplacians (leading to factors of $\text{ł}^2(l,1)$) and the same expression with the operators interchanged. By transforming the "integral representation" back to Wigner-3j symbols, we find

$$\begin{pmatrix} l_1 & l_2 & l_3 \\ 0 & 1 & -1 \end{pmatrix} = -\begin{pmatrix} l_1 & l_2 & l_3 \\ 0 & -1 & 1 \end{pmatrix} - \frac{-\text{ł}^2(l_1,1) + \text{ł}^2(l_2,1) + \text{ł}(l_3,1)}{\text{ł}(l_2,1)\text{ł}(l_3,1)} \begin{pmatrix} l_1 & l_2 & l_3 \\ 0 & 0 & 0 \end{pmatrix}. \tag{9.11}$$

But as the sum of l's is assumed even, the signs of the three lower elements in the Wigner-3j symbol can be changed for free, meaning that the two Wigner-3j symbols on the left are equal. Therefore,

$$\begin{pmatrix} l_1 & l_2 & l_3 \\ 0 & 1 & -1 \end{pmatrix} = -\frac{-\text{ł}^2(l_1,1) + \text{ł}^2(l_2,1) + \text{ł}(l_3,1)}{2\text{ł}(l_2,1)\text{ł}(l_3,1)} \begin{pmatrix} l_1 & l_2 & l_3 \\ 0 & 0 & 0 \end{pmatrix}. \tag{9.12}$$

Assuming the l's are large, we can approximate $\text{ł}(l,1) \sim l$, whence

$$\begin{pmatrix} l_1 & l_2 & l_3 \\ 0 & 1 & -1 \end{pmatrix} \begin{pmatrix} l_1 & l_2 & l_3 \\ 0 & 0 & 0 \end{pmatrix}^{-1} \approx -\frac{-l_1^2 + l_2^2 + l_3^2}{2l_2 l_3} = -\cos(\theta_{23}), \tag{9.13}$$

where θ_{23} is the (interior) angle between l_2 and l_3, see left panel of Fig. 9.4.

More generally, we have that

$$\begin{pmatrix} l_1 & l_2 & l_3 \\ 0 & s & -s \end{pmatrix} \begin{pmatrix} l_1 & l_2 & l_3 \\ 0 & 0 & 0 \end{pmatrix}^{-1} \approx (-1)^s \cos(s\,\theta_{23}), \tag{9.14}$$

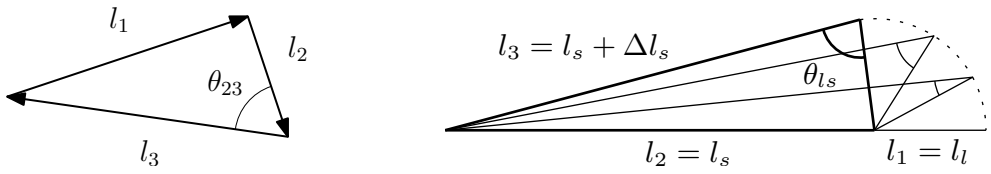

Figure 9.4: The triangle made up of (l_1, l_2, l_3), with, on the left, the angle θ_{23} emphasised. On the right, we show the configuration plotted in Fig. 9.1, i.e. two large l's (corresponding to small scales, whence denoted l_s) and a small l (corresponding to long scales, whence denoted l_l). The angle θ_{ls} dramatically changes with Δl_s, whereas θ_{ss}, the angle between l_s and $l_s + \Delta l_s$, is always small.

as can be checked by applying the same procedure.

With this approximation, we can easily recast the complicated Wigner-3j symbols in a transparent form and understand why [2] and [6] severely depend on Δl_s (see Fig. 9.4, right panel), whereas the other geometrical parts don't. Basically, it is because [2] and [6] depend on the varying $\cos(\theta_{ls})$ whereas [3], [4], [7], [9]–[11] mainly depend on $\cos(\theta_{ss})$ which is close to 1, whatever the value Δl_s is. Because [1], [5] and [8] are of the form $\partial^2(\Psi\Psi)$, their reduced bispectra do not contain any Wigner-3j symbol, whence they are independent of Δl_s.

With these two approximations, we have all the necessary tools to understand the relative sizes of the terms, and their respective Δl-dependence. However, I leave the full treatment of this analysis to Sec. 5 of our article, where it is explained in great detail.

9.3 Signal-to-noise

In this section, we compute the signal-to-noise of the computed bispectrum. For specific configuration (l_1, l_2, l_3), it is given by [37]

$$\frac{S}{N} = \frac{B_{l_1 l_2 l_3}}{\sqrt{\Delta_{l_1 l_2 l_3} C_{l_1} C_{l_2} C_{l_3}}}, \tag{9.15}$$

where $\Delta_{l_1 l_2 l_3} = 1, 2, 6$ if the 3 l's are different, 2 l's are different, or all l's are equal respectively. Note that it is not the reduced bispectrum $b_{l_1 l_2 l_3}$ that has to be used, but the not-reduced $B_{l_1 l_2 l_3}$. When several configurations are taken into account, it is not S/N which has to be summed, but its square,

$$\frac{S}{N} = \left[\sum_{l_1 l_2 l_3} \frac{B^2_{l_1 l_2 l_3}}{\Delta_{l_1 l_2 l_3} C_{l_1} C_{l_2} C_{l_3}} \right]^{1/2}, \tag{9.16}$$

We introduced the weighted bispectrum in such a way that the coefficient A_Φ introduced in equation (7.2) was not relevant. For the signal-to-noise S/N, the factors of A_Φ do not cancel, so we write

$$\frac{S}{N} = A_\Phi \left[\sum_{l_1 l_2 l_3} \left(\frac{B^2_{l_1 l_2 l_3}}{\Delta_{l_1 l_2 l_3} C_{l_1} C_{l_2} C_{l_3}} \right)_{A_\Phi = 1} \right]^{1/2}, \tag{9.17}$$

where the amplitude A_Φ is of the order of 10^{-5}. On Fig. 9.5, we show the signal-to-noise, in units of A_Φ, after summing all configurations with $4 \leq l_l \leq 1000$, $4 \leq l_s \leq 1000$ and $0 \leq \Delta l_s \leq l_l$. We see that for the standard geometrical terms (i.e. parts [2] and [6]) the signal-to-noise is of $\mathcal{O}(1)$ for a source at redshift $z_S \sim 1$, but it gets (slightly) larger for sources further away. Also, as the noise is the same for all contributions, we see that the signal of the redshift corrections decreases rapidly with redshift, but that it dominates the standard geometrical terms for redshifts $z_S \lesssim 0.2$.

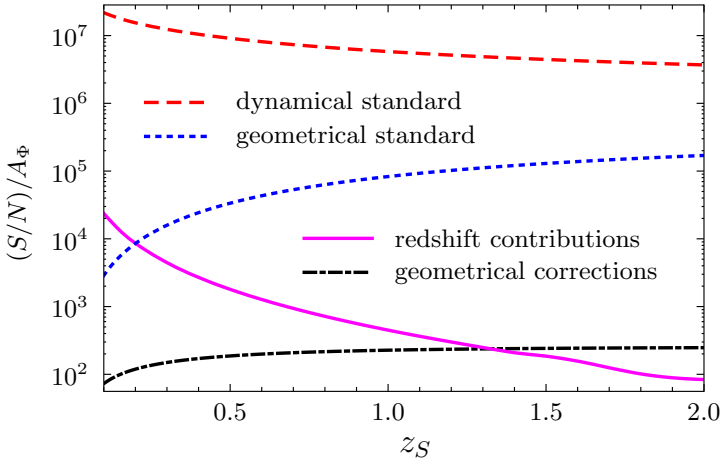

Figure 9.5: S/N as a function of the source redshift z_S for the bispectrum of the standard dynamical term, the standard geometrical terms, the redshift contributions and the geometrical contributions, in units of A_Φ, summing over all configurations with $4 \leq l_l \leq 1000$, $4 \leq l_s \leq 1000$ and $0 \leq \Delta l_s \leq l_l$.

9.4 Primordial non-Gaussianity

In this section, we compare the bispectrum we computed with the bispectrum due to primordial non-Gaussianity. In the introduction of chapter 8, we said that if we assume the primordial perturbations to be Gaussian, we would have that

$$\langle \Phi_{\mathbf{k}} \Phi_{\mathbf{k}'} \Phi_{\mathbf{k}''} \rangle = 0 \qquad \text{whence} \qquad \left\langle \gamma^{[0]} \gamma^{[0]} \gamma^{[0]} \right\rangle = 0. \tag{9.18}$$

So if we now drop this assumption of primordial Gaussianity, we already have a non-zero signal for $\left\langle \gamma^{[0]} \gamma^{[0]} \gamma^{[0]} \right\rangle$. The type of non-Gaussianity we will assume is that of the local type, which satisfies

$$\langle \Phi_{\mathbf{k}_1} \Phi_{\mathbf{k}_2} \Phi_{\mathbf{k}_3} \rangle = (2\pi)^3 \delta_{\mathrm{D}}(\mathbf{k}_1 + \mathbf{k}_2 + \mathbf{k}_3) \times \left[-2 f_{\mathrm{NL}}^{\mathrm{loc}} A_\Phi^2 \left(\frac{1}{k_1^3 k_2^3} + \frac{1}{k_2^3 k_3^3} + \frac{1}{k_3^3 k_1^3} \right) \right], \tag{9.19}$$

where $f_{\mathrm{NL}}^{\mathrm{loc}}$ parametrises the amount of primordial non-Gaussianity. With these initial conditions, it is straightforward to compute the bispectrum associated to local primordial

non-Gaussianity. The result for the reduced bispectrum is

$$\begin{aligned} b^{\rm loc}_{l_1l_2l_3} &= 2f^{\rm loc}_{\rm NL}A^2_\Phi \text{ł}(l_1,2)\text{ł}(l_2,2)\text{ł}(l_3,2) \\ &\times \int_0^{\chi_S} \mathrm{d}\chi_1\,\mathrm{d}\chi_2\,\mathrm{d}\chi_3\, W(\chi_S,\chi_1)\,W(\chi_S,\chi_2)\,W(\chi_S,\chi_3) \int_0^{\chi_S}\mathrm{d}\chi\;\chi^2 \\ &\times \int \frac{2k_1^2\mathrm{d}k_1}{\pi}\frac{2k_2^2\mathrm{d}k_2}{\pi}\frac{2k_3^2\mathrm{d}k_3}{\pi} j_{l_1}(k_1\chi)j_{l_2}(k_2\chi)j_{l_3}(k_3\chi)j_{l_1}(k_1\chi_1)j_{l_2}(k_2\chi_2)j_{l_3}(k_3\chi_3) \\ &\times T(k_1)\,T(k_2)\,T(k_3)\,\left(\frac{1}{k_1^3k_2^3}+\frac{1}{k_2^3k_3^3}+\frac{1}{k_3^3k_1^3}\right). \end{aligned} \tag{9.20}$$

We now compare both the shape and the size of this bispectrum with those of all the other bispectra computed previously. To compare two bispectra, say ${}^1B$ and ${}^2B$, we introduce their scalar product as

$${}^1B\cdot{}^2B \equiv \sum_{l_1,l_2,l_3}\frac{{}^1B_{l_1l_2l_3}\,{}^2B_{l_1l_2l_3}}{\Delta_{l_1l_2l_3}C_{l_1}C_{l_2}C_{l_3}}, \tag{9.21}$$

where, as previously, $\Delta_{l_1l_2l_3}$ equals 1 when all l's are different, 2 when two are equal and 6 when all three l's are equal. Notice that the signal-to-noise of a bispectrum B is given by $(B\cdot B)^{1/2}$. With the above scalar product, one can define a cosine quantifying how two bispectra resemble each other,

$$\cos\left({}^1B,{}^2B\right) \equiv \frac{{}^1B\cdot{}^2B}{\sqrt{({}^1B\cdot{}^1B)({}^2B\cdot{}^2B)}}. \tag{9.22}$$

On Fig. 9.6, we show the cosine between the different parts and the local bispectrum, as a function of the redshift of the source. As before, we summed over all configurations with $4\leq l_l\leq 1000$, $4\leq l_s\leq 1000$ and $0\leq\Delta l_s\leq l_l$. We see that the redshift corrections and the geometrical corrections have a signal which resembles very much that of primordial non-Gaussianity. The fact that the other terms (standard dynamical and geometrical terms) have a very different behavior is totally due to the fact they do depend on Δl_s whereas $b^{\rm loc}$, the reduced bispectrum generated by local primordial non-Gaussianity, does not.

As we now know that the signal created by second-order effects has a similar shape to the one created by a primordial non-Gaussianity of the local type, we need to compute how large the contamination is. In other words, what value of $f^{\rm loc}_{\rm NL}$ would an experiment measure if it did not take into account the second-order corrections. This value of $f^{\rm loc}_{\rm NL}$ is given by

$$f^{\rm loc}_{\rm NL} = \frac{B\cdot B^{\rm loc}}{B^{\rm loc}\cdot B^{\rm loc}}, \tag{9.23}$$

and is shown on Fig. 9.7, where as before the summation is performed over all configurations with $4\leq l_l\leq 1000$, $4\leq l_s\leq 1000$ and $0\leq\Delta l_s\leq l_l$.

The discussion on the source redshift dependence is similar to the one at the end of the signal-to-noise section. The contamination $f^{\rm loc}_{\rm NL}$ is clearly dominated by the standard dynamical terms. Setting aside this well-understood contribution, we see that at low source redshifts, the contamination is mostly due to the redshift contributions.

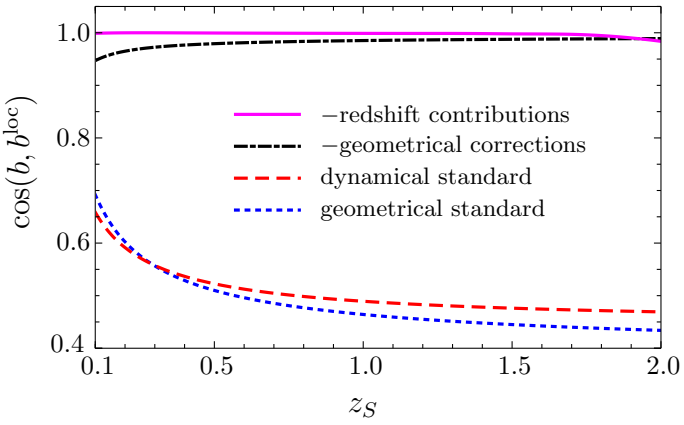

Figure 9.6: The cosine defined in eq. (9.22) between the various terms and the signal created by a primordial non-Gaussianity. The summation is performed over all configurations with $4 \leq l_l \leq 1000$, $4 \leq l_s \leq 1000$ and $0 \leq \Delta l_s \leq l_l$.

9.5 Outlooks

With the computation of the signal-to-noise and $f_{\rm NL}^{\rm loc}$ in the previous sections, we finished the analysis of the electric part of the shear. But we haven't said a word about the magnetic part of it. A crucial property of this magnetic part is that it is absent for the standard dynamical terms, as it is of the form $\eth^2(\Psi\Psi)$. Therefore, we don't have the problem of being completely dominated by this term, like we have for the electric part.

But at the level of the power spectrum, interesting results can also be obtained for the magnetic part. For example, we can define

$$\left\langle a_{E,lm} a^*_{B,l'm'} \right\rangle \equiv \delta_{ll'}\delta_{mm'}\, C_l^{EB} \qquad \text{or} \qquad \left\langle a_{B,lm} a^*_{B,l'm'} \right\rangle \equiv \delta_{ll'}\delta_{mm'}\, C_l^{BB}. \tag{9.24}$$

These quantities vanish at first order (i.e. when only considering $\gamma^{[0]}$), but are non-zero when taking into account all the second-order effects. The trouble is that this loop correction induces two new infinite summations. For example, if we consider the power spectrum of ${}_2a_{lm}^{[1a]}$ (see below eq. (8.13) for the definition[2]), just to get an idea of the formalism, we find

$$\begin{aligned}
\left\langle {}_2a_{lm}^{[1a]} ({}_2a_{l'm'}^{[1a]})^* \right\rangle = & \sum_{l_1 l_2} \begin{pmatrix} l_1 & l_2 & l \\ 2 & 0 & -2 \end{pmatrix} \frac{(2l_1+1)(2l_2+1)}{4\pi} \text{ł}(l_1, 2) \\
& \times \left[\begin{pmatrix} l_1 & l_2 & l \\ 2 & 0 & -2 \end{pmatrix} \text{ł}(l_1, 2) + \begin{pmatrix} l_1 & l_2 & l \\ 0 & 2 & -2 \end{pmatrix} \text{ł}(l_2, 2) \right] \\
& \times \int_0^{\chi_S} \mathrm{d}\chi_1\, W(\chi_S, \chi_1) g(\chi_1) \int_0^{\chi_S} \mathrm{d}\chi_2\, W(\chi_S, \chi_2) g(\chi_2) \\
& \times \int \frac{2k_1^2 \mathrm{d}k_1}{\pi} \int \frac{2k_2^2 \mathrm{d}k_2}{\pi} P(k_1) P(k_2) T^2(k_1) T^2(k_2) \\
& \times j_{l_1}(k_1\chi_1) j_{l_2}(k_2\chi_1) j_{l_1}(k_1\chi_2) j_{l_2}(k_2\chi_2) \\
& \times \delta_{ll'}\, \delta_{mm'}.
\end{aligned} \tag{9.25}$$

[2]Notice that $\langle {}_2a_{lm}^{[0]} ({}_2a_{lm}^{[1a]})^* \rangle$ vanishes if one does not consider primordial non-Gaussianity. If one does, it should be compared to the power spectrum of two terms with second-order ${}_2a_{lm}$'s.

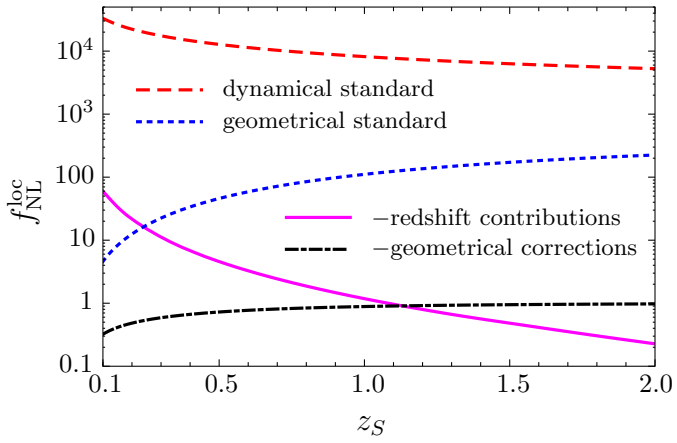

Figure 9.7: The contamination to a primordial local non-Gaussian signal due to the various terms. We see that the redshift corrections contribute to a large contamination when the redshift of the source is small. The summation is performed over all configurations with $4 \leq l_l \leq 1000$, $4 \leq l_s \leq 1000$ and $0 \leq \Delta l_s \leq l_l$.

Apart from the fact that the Limber approximation is tricky because we have "only" two χ-integrals, it is unclear yet how the infinite sums could be handled. A different approach, consisting of making the computation in flat sky, might be worthwhile, as in this set-up the summation becomes a 2D-integral.

9.6 Article: "Cosmic shear bispectrum from second-order perturbations in General Relativity"

PHYSICAL REVIEW D **86,** 023001 (2012)

Cosmic shear bispectrum from second-order perturbations in general relativity

Francis Bernardeau,[1] Camille Bonvin,[2,3] Nicolas Van de Rijt,[1] and Filippo Vernizzi[1]

[1]*CEA, Institut de Physique Théorique, 91191 Gif-sur-Yvette cédex, France and CNRS, URA-2306, 91191 Gif-sur-Yvette cédex, France*

[2]*Kavli Institute for Cosmology Cambridge and Institute of Astronomy, Madingley Road, Cambridge CB3 OHA, UK*

[3]*DAMTP, Centre for Mathematical Sciences, Wilberforce Road, Cambridge CB3 OWA, UK*

(Received 18 January 2012; published 12 July 2012)

Future lensing surveys will be nearly full sky and reach an unprecedented depth, probing scales closer and closer to the Hubble radius. This motivates the study of the cosmic shear beyond the small-angle approximation, including general relativistic corrections that are usually suppressed on sub-Hubble scales. The complete expression of the reduced cosmic shear at second order including all relativistic effects was derived in [F. Bernardeau, C. Bonvin, and F. Vernizzi, Phys. Rev. D **81**, 083002 (2010).]. In the present paper we compute the resulting cosmic shear bispectrum when all these effects are properly taken into account and we compare it to primordial non-Gaussianity of the local type. The new general relativistic effects are generically smaller than the standard nonlinear couplings. However, their relative importance increases at small multipoles and for small redshifts of the sources. The dominant effect among these nonstandard corrections is due to the inhomogeneity of the source redshift. In the squeezed limit, its amplitude can become of the order of the standard couplings when the redshift of the sources is below 0.5. Moreover, while the standard nonlinear couplings depend on the angle between the short and long mode, the relativistic corrections do not and overlap almost totally with local type non-Gaussianity. We find that they can contaminate the search for a primordial local signal by $f_{\rm NL}^{\rm loc} \gtrsim 10$.

DOI: 10.1103/PhysRevD.86.023001 PACS numbers: 95.30.Sf, 98.65.Dx, 98.80.Es, 98.80.Jk

I. INTRODUCTION

With the advent of future wide-field surveys, weak gravitational lensing will become a premier probe of cosmology and an important tool to constrain dark energy, neutrinos and the initial conditions (see for instance [1,2]). In order to fully exploit the potentiality of the convergence and shear fields, it will be important to use their whole statistics. In particular, the lensing bispectrum represents a complementary probe to the power spectrum, as it will provide constraints that are comparable to those obtained from the power spectrum alone [3].

One of the primary interests of wide-field surveys is to look for primordial non-Gaussianities generated in the early universe and the lensing bispectrum represents a natural tool to capture such features [4–8]. Given the current and forecasted constraints on $f_{\rm NL}$, there is a plethora of second-order effects intervening between the initial conditions and the observations that could be potentially relevant. Some of these effects, such as the second-order growth of matter fluctuations in Eulerian perturbation theory, the Born correction, the lens-lens coupling and the nonlinear conversion between the galaxy shape distortion and the (observable) reduced shear, have been thoroughly studied in the past years and are expected to dominate the lensing 3-point statistics on small-angular scales [9–18].

When studying weak lensing one usually restricts the analysis to small angular separations (or large multipole moments), which is justified by the fact that so far cosmic shear surveys have covered only a limited portion of the sky. However, nearly full-sky surveys are currently under preparation and on large angular scales general relativistic second-order couplings will become relevant. These corrections are usually neglected because they are suppressed by the ratio between the scale probed and the Hubble scale, but are important on angular scales of the order of the angular diameter distance to the source. These are analogous to the second-order effects from general relativity affecting the cosmic microwave background (CMB) bispectrum when at least one of the scales probed is larger than the horizon at recombination [19–21]. In the CMB, these effects have been recently found to be negligible for the contamination of Planck searches for a primordial local signal in the squeezed limit [22,23]. In case of cosmic shear observations, these effects however cannot be *a priori* neglected. The aim here is to provide an exhaustive evaluation of the impact of these contributions to observations. Those results extend recent studies on the impact of relativistic corrections to the observations of large-scale galaxy clustering in [24–28].

The complete study of all second-order effects in the cosmic shear, including the general relativistic ones, has been recently undertaken in [29] by solving at second order the Sachs equation [30], which describes the deformation of the cross section of a light bundle, mapping galaxy shapes into their angular images. The main results of this paper are reviewed in Sec. II.

The goal of the current paper is to compute the bispectrum of the electric part of the cosmic shear from all second-order effects and compare the importance of the general relativistic corrections with the standard couplings.

We review the computation of the shear power spectrum in Sec. III where we also present one of the numerical shortcuts we will use throughout the paper, the second-order Limber approximation. The formal expression of the bispectrum, computed in Sec. IV, is determined by two types of nonlinear contributions: the dynamical couplings, which depend on the particular metric solution of Einstein's equations at second order, and the geometrical couplings, so-called because they depend on the geometry of the solution of the Sachs equation at second order. Among the latter we also include the corrections coming from the inhomogeneities of a fixed-redshift source plane. The calculations of Sec. IV involve multiple integrals and complicated manipulations of spherical harmonics and Wigner symbols. (In Appendix C one can find useful relations for these calculations.) We are afraid to say that those calculations are extremely lengthy and technical. Impatient readers can skip this section and go directly to Sec. V. In this section we present our results concentrating on the squeezed limit, where one of the multipole moments l involved in the bispectrum is small and we discuss the functional forms of the resulting terms as well as their relative importance. In Sec. VI we compare our results with the bispectrum generated by primordial non-Gaussianities of the local type and we compute their contamination to a primordial $f_{\rm NL}^{\rm loc}$. Finally, in Sec. VII we conclude and discuss the results of the paper.

II. FULL-SKY LENSING SHEAR AT SECOND ORDER

A. The shear and spin-s spherical harmonics

The shear is characterized by a (2×2)-traceless and symmetric tensor γ_{ab}, whose components are defined with respect to a particular choice of axes about each direction on the sky. This tensor describes the deformation of the image of distant galaxies by the gravitational field of the cosmic structures intervening between emission and observation. The two independent components of γ_{ab}, γ_1 and γ_2, can be conveniently combined into a single complex field representing the shear,

$$\gamma = \gamma_1 + i\gamma_2. \tag{1}$$

Under a right-handed rotation of the axes by an angle α about the line of sight $\hat{n}$, this complex field transforms as $\gamma \to e^{i2\alpha}\gamma$. Thus, it represents a spin-2 field that can be appropriately expanded in terms of spin-weighted spherical harmonics, as

$$\gamma(\hat{n}) = \sum_{lm} {}_2a_{lm}\,{}_2Y_{lm}(\hat{n}). \tag{2}$$

The complex conjugate of γ, $\gamma^* = \gamma_1 - i\gamma_2$, is then a spin-$(-2)$ field, and can therefore be expanded as

$$\gamma^*(\hat{n}) = \sum_{lm} {}_{-2}a_{lm}\,{}_{-2}Y_{lm}(\hat{n}). \tag{3}$$

One can introduce spin raising and lowering operators that can be used to relate quantities of different spin. The spin raising operator is denoted as $\eth$ and the spin lowering operator as $\bar{\eth}$. For a general spin-s field ${}_sX$, these are defined as

$$\eth\,{}_sX \equiv -\sin^s\theta\left(\partial_\theta + i\frac{1}{\sin\theta}\partial_\varphi\right)(\sin^{-s}\theta)\,{}_sX, \tag{4}$$

$$\bar{\eth}\,{}_sX \equiv -\sin^{-s}\theta\left(\partial_\theta - i\frac{1}{\sin\theta}\partial_\varphi\right)(\sin^{s}\theta)\,{}_sX. \tag{5}$$

Note that $\eth$ and $\bar{\eth}$ commute only when applied to a spin-0 quantity. In general one has

$$(\bar{\eth}\eth - \eth\bar{\eth})\,{}_sX = 2s\,{}_sX. \tag{6}$$

These operators can be used to obtain spin-0 quantities. Acting twice with $\bar{\eth}$ and $\eth$, respectively, on γ and γ^* in Eqs. (2) and (3), and using the orthogonality properties of the spherical harmonics one obtains an expression for the expansion coefficients ${}_2a_{lm}$ and ${}_{-2}a_{lm}$ as

$${}_2a_{lm} = \text{ł}(l,-2)\int d\hat{n}\,Y^*_{lm}(\hat{n})\bar{\eth}^2\gamma(\hat{n}), \tag{7}$$

$${}_{-2}a_{lm} = \text{ł}(l,-2)\int d\hat{n}\,Y^*_{lm}(\hat{n})\eth^2\gamma^*(\hat{n}), \tag{8}$$

where for convenience we have defined ł as

$$\text{ł}(l,s) \equiv \sqrt{\frac{(l+s)!}{(l-s)!}}. \tag{9}$$

As for the CMB polarization, we introduce parity eigenstates, spin-0 quantities, called the "electric" and "magnetic" parts of the shear, defined as [31,32]

$$E(\hat{n}) \equiv \sum_{lm} a_{E,lm}Y_{lm}(\hat{n}), \tag{10}$$

$$B(\hat{n}) \equiv \sum_{lm} a_{B,lm}Y_{lm}(\hat{n}), \tag{11}$$

where the coefficients $a_{E,lm}$ and $a_{B,lm}$ are given by

$$a_{E,lm} \equiv -\tfrac{1}{2}({}_{-2}a_{lm} + {}_2a_{lm}), \tag{12}$$

$$a_{B,lm} \equiv -\frac{i}{2}({}_{-2}a_{lm} - {}_2a_{lm}). \tag{13}$$

Under parity transformation, E and B change as $E \to E$ and $B \to -B$. Furthermore, in contrast to the shear components γ_1 and γ_2, these two spin-0 quantities have the advantage of being rotationally invariant.

B. The shear up to second order

We consider a flat Friedmann-Lemaître-Robertson-Walker metric background. In [29] we have computed the shear at second order by using a perturbed metric in

the so-called generalized Poisson gauge. In this gauge the second-order metric reads [33,34]

$$ds^2 = a^2(\eta)[-e^{2\phi}d\eta^2 + 2\omega_i d\eta dx^i + (e^{-2\psi}\delta_{ij} + h_{ij})dx^i dx^j], \quad (14)$$

where the vector component ω_i is divergenceless, $\partial_i\omega_i = 0$, and the tensor component h_{ij} is divergenceless and traceless, $\partial_i h_{ij} = 0 = h_{ii}$. While the scalar perturbations ϕ and ψ contain first- and second-order contributions, since we neglect primordial vector and tensor perturbations, ω_i and h_{ij} are only second-order quantities.

Note that we have chosen to write the gravitational potentials in the metric in the exponential form. This choice is convenient for two reasons. First, up to second order, in this form the metric (14) is conformal to $ds^2 = -e^{2(\phi+\psi)}d\eta^2 + 2\omega_i d\eta dx^i + (\delta_{ij} + h_{ij})dx^i dx^j$ so that the effect of scalar perturbations on null geodesics will be only through the Weyl potential, defined as

$$\Psi \equiv (\phi + \psi)/2. \quad (15)$$

The second reason, which will be explained in more details in Sec. II B 2, is that with this choice the relativistic second-order contributions to ϕ and ψ vanish in the squeezed limit.

In this metric the lensing shear is obtained by solving the Sachs equation [30], which describes linear deformations of the infinitesimal cross section of a light bundle in the optical limit, and maps galaxy intrinsic shapes into their angular images. At *first order* one finds the full-sky expression of the shear field[1]

$$\gamma(\hat{n}) = \int_0^{\chi_S} d\chi \frac{\chi_S - \chi}{\chi_S \chi} \eth^2 \Psi(\chi, \vec{x}), \quad (16)$$

where we have conveniently defined $\chi \equiv \eta_0 - \eta$, where η_0 is the conformal time today, so that $\vec{x} \equiv \hat{n}\chi$ is the background photon geodesic. The subscript S in χ_S refers to the source.

At second order, there are four sources of nonlinearities [29]:

(1) The mapping solution of the Sachs equation is linear in the angular deformation, but it is *nonlinear* in the Weyl potential encountered by the photon from emission to observation. This induces nonlinearities even when using the linear part of the metric.

(2) What we observe is actually the reduced shear [16–18], i.e. the ratio between the anisotropic and isotropic deformations, and there are nonlinear corrections introduced when taking this ratio. These will be proportional to the product of the first-order shear and the first-order convergence.

(3) Observationally, we are mapping galaxies located at a given redshift z_S. Thus, we expect second-order contributions to the observed shear coming from perturbing z_S in the first-order expression (16).

(4) The metric contains second-order terms in the initial conditions. This induces nonlinearities even when using the linear solution of the Sachs equation.

The first three contributions are independent of the *second-order* components of the metric: we will collect them under the name of "geometrical" contributions, because they depend on the geometry of the linear mapping, solution of the Sachs equation at second order. On the other hand, the fourth contribution depends only on the linear mapping at first order, but depends on the particular metric solution of the Einstein equations at second order. Thus, it is natural to call it the "dynamical" contribution. Note that this separation depends on the particular gauge chosen, hence it is not completely physical. However, for reasons that will appear more clearly in the following, it is a convenient distinction that we adopt hereafter.

1. Geometrical couplings

Except for the contribution coming from the perturbation of the redshift, which we discuss below, the geometrical couplings depend exclusively on the Weyl potential Ψ. As explained above, this is a consequence of the choice of the exponential of ϕ and ψ in the form of the metric in Eq. (14). Some of the geometrical couplings dominate in the large-l limit—corresponding to small angular scales—because they contain more operators $\eth$ or $\bar{\eth}$. Indeed, in harmonic space to each of such operators is associated an l factor in the angular power spectrum and bispectrum. These dominant terms, that are standard in the literature, can be written as

$$\begin{aligned}\gamma^{(\mathrm{stan})}_{\mathrm{geom}} = &-\int_0^{\chi_S} d\chi \int_0^{\chi} d\chi' \frac{\chi_S - \chi}{\chi_S \chi}\frac{\chi - \chi'}{\chi \chi'} \\ &\times [\eth(\eth^2\Psi(\chi,\vec{x})\bar{\eth}\Psi(\chi',\vec{x}')) + \bar{\eth}\eth\Psi(\chi,\vec{x})\eth\Psi(\chi',\vec{x}')) \\ &+ 2\eth\Psi(\chi,\vec{x})\eth\Psi(\chi',\vec{x}')] \\ &+ \int_0^{\chi_S} d\chi \int_0^{\chi_S} d\chi' \frac{\chi_S - \chi}{\chi_S \chi}\frac{\chi_S - \chi'}{\chi_S \chi'} \\ &\times \bar{\eth}\eth\Psi(\chi,\vec{x})\eth^2\Psi(\chi',\vec{x}'). \end{aligned} \quad (17)$$

The first two lines contain the usual couplings such as the lens-lens correction and the correction to the Born approximation [9,12–15].[2] The last two lines contain the

[1] Surprisingly, to our knowledge this full-sky expression was explicitly derived only recently in [29] although it is implicit in [35] and in the context of CMB lensing, see for instance [36,37]. The form was painstakingly rederived in [38] in the context of full-sky cosmic shear observations.

[2] For comparison with a recent article in the literature on the subject, by rewriting in the first two lines of Eq. (17) the spin raising and lowering operators in terms of spatial gradients one recovers the second line of Eq. (8) of [16].

correction involved in the relation between the shear and the reduced shear, containing the coupling between the first-order convergence and shear [17,18].

If we relax the small-angle approximation and we consider the full sky, there are other terms which become important [29]. The total geometrical contribution is

$$\gamma_{\rm geom} = \gamma^{\rm (stan)}_{\rm geom} + \gamma^{\rm (corr)}_{\rm geom} + \gamma^{(z)}_{\rm geom}, \tag{18}$$

where the standard terms $\gamma^{\rm (stan)}_{\rm geom}$ are given in Eq. (17), and the new terms, that we can consider as corrections to the small-angle approximation, are given by

$$\gamma^{\rm (corr)}_{\rm geom} = -\int_0^{\chi_S} d\chi \Big[\frac{\chi_S-\chi}{\chi_S\chi}\bar{\not\partial}^2\Psi^2(\chi,\vec{x}) - \frac{2}{\chi_S\chi}\bar{\not\partial}^2\Big((\Psi(\chi,\vec{x}) - (\chi_S-\chi)\dot{\Psi}(\chi,\vec{x})\Big)\int_0^{\chi} d\chi' \Psi(\chi',\vec{x}')\Big)\Big]$$
$$+ 2\int_0^{\chi_S} d\chi \int_0^{\chi} d\chi' \Big(\frac{\chi_S-\chi}{\chi_S\chi^2} + \frac{1}{\chi_S\chi'}\Big)\Psi(\chi,\vec{x})\bar{\not\partial}^2\Psi(\chi',\vec{x}') - 2\int_0^{\chi_S} d\chi \int_0^{\chi_S} d\chi' \frac{\chi_S-\chi'}{\chi_S^2\chi'}\Psi(\chi,\vec{x})\bar{\not\partial}^2\Psi(\chi',\vec{x}'). \tag{19}$$

Note that the third line of Eq. (17) contains only two transverse derivatives and its contribution to the shear is therefore of the same order as the corrections in Eq. (19). Thus, one could be tempted to include this term in the geometrical corrections rather than in the standard contributions. The reason is that classifying terms by counting powers of $\not\partial$ and $\bar{\not\partial}$ operators leads to ambiguities, as in the full sky those operators do not commute. It appears that the third line of (17) can be combined with the second term of the second line of Eq. (17) to form a *single* term containing four spatial gradients,

$$\not\partial\bar{\not\partial}\not\partial\Psi\not\partial\Psi + 2\not\partial\Psi\not\partial\Psi = \bar{\not\partial}\not\partial^2\Psi\not\partial\Psi. \tag{20}$$

For this reason, we have decided to include this term in the standard contribution.

Finally, the other contribution independent of the second-order components of the metric is the one due to the inhomogeneity of the redshift of the sources. This induces a coupling between the photon redshift z_S and the lens,

$$\gamma^{(z)}_{\rm geom} = \frac{1}{\chi_S^2\mathcal{H}_S}\Big(-2\int_0^{\chi_S} d\chi \dot{\Psi}(\chi,\vec{x}) + \phi(\chi_S,\vec{x}_S) - \hat{n}\cdot\vec{v}_S\Big) \times \int_0^{\chi_S} d\chi' \bar{\not\partial}^2\Psi(\chi',\vec{x}'), \tag{21}$$

where $\mathcal{H}$ is the conformal Hubble parameter defined as $\mathcal{H} \equiv d\ln a/d\eta$, $\vec{v}_S$ is the peculiar velocity of the source and a dot denotes a derivative with respect to χ, $\dot{} = \partial_\chi = -\partial_\eta$. Note that the inhomogeneity of the source redshift affects the convergence κ already at first order in perturbation theory [39], but its impact on the shear is only through a coupling with the lens, i.e. of second order.

Since we are interested in ensemble averages over the random field ϕ and ψ, we need to relate the velocity of the source $\vec{v}_S$ to the primordial perturbation at first order. We choose to use the linearized Einstein equations to rewrite $\vec{v}_S$ in terms of the Weyl potential at the source and its time derivative. In doing this we implicitly assume that the source is comoving with the dark matter. At large enough scales this is a legitimate assumption as all matter components are expected to move identically. However, at smaller scales this is clearly an approximation as galaxies typically belong to virialized halos and move independently from the dark matter field. At first order, the $0j$ component of the Einstein equations reads

$$\frac{2}{a^2}\partial_i(\partial_\eta\psi + \mathcal{H}\phi) = -8\pi G\rho_m v^i. \tag{22}$$

Thus, using that $\dot{} = -\partial_\eta$, the dark matter velocity at the source reads, at first order,

$$\vec{v}_S = -\frac{2}{3}\frac{a_S\vec{\nabla}(-\dot{\psi}_S + \mathcal{H}_S\phi_S)}{H_0^2\Omega_m}, \tag{23}$$

where Ω_m is the critical density of matter today, $\Omega_m \equiv 8\pi G\rho_{m,0}/(3H_0^2)$, and we have used that $\rho_m = \rho_{m,0}/a^3$.

Note that the lens-lens correction and the correction to the Born approximation in the first two lines of Eq. (17), can be written as the derivative of a deflection angle. The two shear components associated with these terms are consequently related to the convergence and rotation part of the magnification matrix that contains only 2 degrees of freedom [40]. On the other hand, the geometrical and redshift corrections cannot be written as the derivative of a deflection angle. Hence, due to these relativistic effects the magnification matrix contains in general 4 degrees of freedom: the shear E modes are generically different from the convergence and the shear B modes are different from the rotation.

2. Dynamical couplings

Before moving to the contribution coming from second-order metric perturbations, i.e. the dynamical contribution, let us specify the first-order potentials and the initial conditions. Since we will perform our calculations in a ΛCDM universe, the anisotropic stress vanishes and the traceless part of the ij components of the Einstein equations implies that ϕ and ψ are the same at first order, i.e. $\phi^{(1)} = \psi^{(1)} = \Psi^{(1)}$. Thus the Weyl potential can be decomposed in Fourier space as

$$\Psi^{(1)}(\chi,\hat{n}\chi)=\int\frac{d^3\vec{k}}{(2\pi)^3}g(\chi)T(k)\Phi_{\vec{k}}e^{i\vec{k}\cdot\hat{n}\chi}, \tag{24}$$

where $T(k)$ is the matter transfer function and $g(\chi)$ is the so-called growth-suppression factor, defined as $g(\chi)\equiv D(\chi)/a(\chi)$, where $D(\chi)$ is the linear growth function. Furthermore, Φ is the primordial potential which represents the initial curvature perturbation generated during inflation. During matter dominance, on superhorizon scales it is simply proportional to the curvature perturbation on uniform density hypersurfaces, $\Phi=-(3/5)\zeta$. For the minimal model of inflation ζ is approximately Gaussian [41] and in the following we are going to assume that Φ obeys perfectly Gaussian statistics.

At second order we split both ϕ and ψ into a Newtonian part equal for both potentials, denoted by $\phi_N^{(2)}$, and a relativistic part, denoted, respectively, by $\phi_R^{(2)}$ and $\psi_R^{(2)}$. The Newtonian part dominates on small scales; on these scales the relativistic part is suppressed with respect to the Newtonian part by factors of order $(Ha/k)^2$ and becomes relevant only on large scales. Thus, the Newtonian potential $\phi_N^{(2)}$ dominates in the small angle approximation and its contribution to the shear has been thoroughly studied in the literature [4,9,42]. It is obtained from inserting the second-order Newtonian potential $\phi_N^{(2)}$ into the first-order expression for the shear (16). This yields

$$\gamma_{\rm dyn}^{\rm (stan)}=\int_0^{\chi_S}d\chi\frac{\chi_S-\chi}{\chi_S\chi}\eth^2\phi_N^{(2)}(\chi,\vec{x}). \tag{25}$$

The Newtonian potential $\phi_N^{(2)}$ has been derived in standard Eulerian perturbation theory [43,44] and for ΛCDM it can be written as

$$\phi_N^{(2)}(\chi,\hat{n}\chi)=\int\frac{d^3\vec{k}}{(2\pi)^3}\phi_N^{(2)}(\vec{k},\chi)e^{i\vec{k}\cdot\hat{n}\chi}, \tag{26}$$

with

$$\phi_N^{(2)}(\vec{k},\chi)=-\frac{2g^2a}{3H_0^2\Omega_m}\frac{T(k_1)T(k_2)}{k^2}k_1^2k_2^2F_{2,N}(\vec{k}_1,\vec{k}_2,\chi)\times\Phi_{\vec{k}_1}\Phi_{\vec{k}_2}, \tag{27}$$

where the kernel $F_{2,N}$ is well approximated by

$$F_{2,N}(\vec{k}_1,\vec{k}_2,\chi)=\frac{1}{2}(1+\epsilon)+\frac{\hat{k}_1\cdot\hat{k}_2}{2}\left(\frac{k_1}{k_2}+\frac{k_2}{k_1}\right)+\frac{1}{2}(1-\epsilon)(\hat{k}_1\cdot\hat{k}_2)^2, \tag{28}$$

where $\epsilon(\chi)\simeq\frac{3}{7}[\rho_m(\chi)/\rho_{\rm tot}(\chi)]^{-1/143}$ [44,45].[3] Here and below we implicitly assume integration over repeated momenta, i.e. $\int\frac{d^3\vec{k}_1d^3\vec{k}_2}{(2\pi)^3}\delta_D(\vec{k}-\vec{k}_1-\vec{k}_2)$. Note that the expression for $F_{2,N}$ above is exact in matter dominance, where $\epsilon=3/7$ and $F_{2,N}$ is time independent. For ΛCDM the time dependence of $\phi_N^{(2)}$ cannot be factorized out in the growth-suppression factor $g^2(\chi)$ in front of the integral but $F_{2,N}$ is mildly time dependent. The approximation above to characterize this time dependence reproduces very well the one given in [46].

On large scales the relativistic parts of the scalar potentials $\phi_R^{(2)}$ and $\psi_R^{(2)}$ become important. Also the vector and the tensor modes in the metric, respectively ω_i and h_{ij}, generated at second order are relativistic corrections to the metric of the same order in aH/k as the relativistic potentials $\phi_R^{(2)}$ and $\psi_R^{(2)}$. As they are intrinsically second order, they simply enter linearly in the expression for the shear, yielding

$$\gamma_{\rm dyn}^{\rm (corr)}=\int_0^{\chi_S}d\chi\left[\frac{\chi_S-\chi}{\chi_S\chi}\eth^2\left(\frac{1}{2}(\phi_R^{(2)}(\chi,\vec{x})+\psi_R^{(2)}(\chi,\vec{x}))-\frac{1}{2}\omega_r(\chi,\vec{x})-\frac{1}{4}h_{rr}(\chi,\vec{x})\right)-\frac{1}{2\chi}\eth({}_1\omega(\chi,\vec{x})+{}_1h_r(\chi,\vec{x}))\right]-\frac{1}{4}{}_2h(\chi_S,\vec{x}_S), \tag{29}$$

where we have defined $\omega_r\equiv\hat{n}^i\omega_i$ and $h_{rr}\equiv\hat{n}^i\hat{n}^jh_{ij}$, the spin-1 part of ω_i and h_{ij} respectively as ${}_1\omega\equiv\hat{e}_+^i\omega_i$ and ${}_1h_r\equiv\hat{e}_+^i\hat{n}^jh_{ij}$, and the spin-2 part of h_{ij} as ${}_2h\equiv\hat{e}_+^i\hat{e}_+^jh_{ij}$. Here $\hat{e}_+\equiv\hat{e}_\theta+i\hat{e}_\varphi$ where $\hat{e}_\theta$ and $\hat{e}_\varphi$ are unit vectors orthogonal to the photon propagation $\hat{n}$ and to each other. The term containing ${}_2h$ in the second line of this equation is a boundary term induced by the spin-2 part of the tensor modes, which account for the distortion of the shape at the source. Putting together the dynamical contributions of Eqs. (25) and (29) we obtain [29]

$$\gamma_{\rm dyn}=\gamma_{\rm dyn}^{\rm (stan)}+\gamma_{\rm dyn}^{\rm (corr)}. \tag{30}$$

Let us give here the expressions for the relativistic components of the metric to be put in Eq. (29). For a ΛCDM universe, these have been computed in [47] and their expressions are quite involved. However, as we will see in Sec. V, the effect of the dynamical relativistic terms on the shear bispectrum is extremely small. For this reason we can estimate their contribution by simply using the expressions for the relativistic components in matter dominance, where it is possible to factorize their time and momentum dependence. Indeed, in this case these metric components can be written, in Fourier space, as [20,48]

$$\phi_R^{(2)}(\vec{k},\chi)=\frac{T(k_1)T(k_2)}{k^2}[\vec{k}_1\cdot\vec{k}_2-3(\hat{k}\cdot\vec{k}_1)(\hat{k}\cdot\vec{k}_2)]\Phi_{\vec{k}_1}\Phi_{\vec{k}_2}, \tag{31}$$

$$\psi_R^{(2)}(\vec{k},\chi)=-\frac{2}{3}\phi_R^{(2)}(\vec{k},\chi), \tag{32}$$

[3]Here we have neglected the contributions to $F_{2,N}$ from the radiation era studied in [46]. These can be easily added to the standard dynamical contribution without changing the other corrections.

$$\omega_i(\vec{k},\chi) = -\frac{i4a^{1/2}}{3H_0}\frac{T(k_1)T(k_2)}{k^2}[k_1^2k_2^i + k_2^2k_1^i - \hat{k}^i(k_1^2(\hat{k}\cdot\vec{k}_2) + k_2^2(\hat{k}\cdot\vec{k}_1))]\Phi_{\vec{k}_1}\Phi_{\vec{k}_2}, \quad (33)$$

$$h_{ij}(\vec{k},\chi) = \frac{10}{3}[1-3j_1(k\eta)/(k\eta)]\frac{T(k_1)T(k_2)}{k^4} \times[((\vec{k}_1\cdot\vec{k}_2)^2 - k_1^2k_2^2)(\delta^{ij}+\hat{k}^i\hat{k}^j) + 2k_1^2k_2^ik_2^j + 2k_2^2k_1^ik_1^j - 4k_1^ik_2^j\vec{k}_1\cdot\vec{k}_2]\Phi_{\vec{k}_1}\Phi_{\vec{k}_2}. \quad (34)$$

In the expression for tensor modes, the spherical Bessel function $j_1(x)$ is given by $j_1(x) = \sin(x)/x^2 - \cos(x)/x$.

One can check that this metric solution satisfies Gaussian primordial initial conditions. Indeed, on large scales and at nonlinear order the gauge transformation from the ζ gauge [41] to Poisson gauge (14) is given by $\zeta = -\psi - \frac{2}{3}\phi$ in matter dominance. Thus, Eq. (32) implies Gaussian initial conditions $\zeta^{(2)} = 0$. Furthermore, we note that in the squeezed limit, i.e. when one of the two modes $\vec{k}_1$ and $\vec{k}_2$ is much larger than the other, the second-order relativistic components of the metric given above go to zero. This is another advantage of using the metric (14) with ϕ and ψ in the exponentials.

To summarize, the full sky observed shear up to second order is given by the sum of five contributions, three geometrical and two dynamical [29]:

$$\gamma = \gamma^{(\mathrm{stan})}_{\mathrm{geom}} + \gamma^{(\mathrm{corr})}_{\mathrm{geom}} + \gamma^{(z)}_{\mathrm{geom}} + \gamma^{(\mathrm{stan})}_{\mathrm{dyn}} + \gamma^{(\mathrm{corr})}_{\mathrm{dyn}}. \quad (35)$$

Their expressions are reported, respectively, in Eqs. (17), (19), (21), (25), and (29).

III. ANGULAR POWER SPECTRUM

The aim of this section and of the following one is to give the explicit forms of the spectrum and bispectrum of the shear field. More specifically, we are interested in the spectra of the electric part of the shear field. This section focuses on the power spectrum calculation. To present the formalism it is convenient to introduce the lensing potential Υ through the relation,

$$\gamma(\hat{n}) \equiv \eth^2\Upsilon(\hat{n}), \quad (36)$$

where the shear correlation properties are entirely encoded into the statistical properties of $\Upsilon(\hat{n})$.

A. From metric to shear spectrum

To compute the lensing power spectrum we just need the shear at *linear order* in the Weyl potential. In this case, using the expression for the shear at first order in Eq. (16), Eq. (36) reduces to the usual definition of the lensing potential given in the literature (see e.g. [49]),

$$\Upsilon(\hat{n}) = \int_0^{\chi_S} d\chi \frac{\chi_S - \chi}{\chi_S\chi}\Psi(\chi, \hat{n}\chi). \quad (37)$$

As we will see below when computing the bispectrum, this expression is inappropriate to describe the lensing potential at *second order*, while Eq. (36) remains valid.

The lensing potential Υ is a spin-0 operator. Thus, using the commutation relation (6) one shows that

$$\bar{\eth}^2\gamma = \bar{\eth}^2\eth^2\Upsilon = \eth^2\bar{\eth}^2\Upsilon = \eth^2\bar{\eth}^2\Upsilon^* = \eth^2\gamma^*, \quad (38)$$

where to write the second line we have used that Υ is *real* at first order. From Eqs. (7) and (8), this equation implies that ${}_2a_{lm} = {}_{-2}a_{lm}$ and, using the definition of $a_{E,lm}$, Eq. (12), that

$$a_{E,lm} = -\text{ł}(l,2)\int d\hat{n}Y^*_{lm}(\hat{n})\Upsilon(\hat{n}). \quad (39)$$

Note that $a_{B,lm}$ vanishes at first order (see Eq. (13)). The angular power spectrum C_l^E of the electric part of the shear, $E(\hat{n})$, is defined from the 2-point function,

$$\langle a_{E,lm}a^*_{E,l'm'}\rangle \equiv C_l^E\delta_{ll'}\delta_{mm'}. \quad (40)$$

As at this order the angular power spectrum of the magnetic part of the shear is zero, $C_l^B = 0$, there is no ambiguity in simply setting $C_l \equiv C_l^E$ in what follows.

We then use the Fourier mode decomposition of Eq. (24) for the Weyl potential and expand the plane wave in spherical harmonics, i.e.

$$e^{i\vec{k}\cdot\hat{n}\chi} = 4\pi\sum_{lm} i^l j_l(k\chi)Y_{lm}(\hat{n})Y^*_{lm}(\hat{k}). \quad (41)$$

Combining Eq. (41) with Eqs. (36) and (39), and integrating in $d\hat{n}$ with the orthogonality relation of the spherical harmonics, we obtain an expression for $a_{E,lm}$ as a function of the primordial potential $\Phi_{\vec{k}}$,

$$a_{E,lm} = -i^l\text{ł}(l,2)\int_0^{\chi_S} d\chi W(\chi_S,\chi)\int\frac{d^3\vec{k}}{2\pi^2}j_l(k\chi)Y^*_{lm}(\hat{k})T(k)\Phi_{\vec{k}}, \quad (42)$$

where we have defined the window function W as

$$W(\chi',\chi) \equiv \frac{\chi'-\chi}{\chi'\chi}g(\chi). \quad (43)$$

Finally, using Eq. (42) in the definition of the C_l, Eq. (40), one obtains

$$C_l = \text{ł}^2(l,2)\int_0^{\chi_S} d\chi W(\chi_S,\chi)\int_0^{\chi_S} d\chi' W(\chi_S,\chi') \times\int\frac{2k^2dk}{\pi}T^2(k)P(k)j_l(k\chi)j_l(k\chi'), \quad (44)$$

which can be rewritten in a more compact form as

$$C_l = \text{ł}^2(l,2)\int\frac{2k^2dk}{\pi}P(k)T^2(k) \times\left[\int_0^{\chi_S} d\chi W(\chi_S,\chi)j_l(k\chi)\right]^2. \quad (45)$$

Here $P(k)$ is the power spectrum for the primordial perturbation Φ, defined by

$$\langle \Phi_{\vec{k}} \Phi_{\vec{k}'} \rangle \equiv (2\pi)^3 \delta(\vec{k} + \vec{k}') P(k). \tag{46}$$

For simplicity in our calculations we will only consider a scale invariant spectrum,

$$P(k) = A_\Phi k^{-3}, \tag{47}$$

although all the treatment can be easily extended to a nonzero tilt. In the following we will consider a ΛCDM cosmology with $\Omega_m = 0.3$ today and a Hubble parameter $h = 0.65$. Furthermore, to ease the numerical treatment, for $T(k)$ we will use the Bardeen-Bond-Kaiser-Szalay fitting formula [50].

B. Numerical integrations: The Limber approximation

In practice, integrating Eq. (45) is numerically involved and time consuming. To compute the C_l it is common to employ the so-called Limber approximation [51], which is valid for large l. This is based on the fact that the ordinary Bessel function $J_\nu(x)$, related to the spherical Bessel function $j_l(x)$ by

$$j_l(x) = \sqrt{\frac{\pi}{2x}} J_\nu(x), \qquad \nu \equiv l + 1/2, \tag{48}$$

grows monotonically from zero at $x = 0$ to $x \simeq \nu$ and then rapidly oscillates. For large l an integral of an arbitrary function multiplied by a Bessel function can be approximated by

$$\int dx f(x) J_\nu(x) = f(\nu) + \mathcal{O}(1/\nu^2), \tag{49}$$

which can be written in the following form:

$$\int \frac{2k^2 dk}{\pi} f(k) j_l(k\chi) j_l(k\chi') = \frac{\delta(\chi - \chi')}{\chi^2} f(\nu/\chi)[1 + \mathcal{O}(1/\nu^2)]. \tag{50}$$

Using this approximation one obtains the Limber-approximated C_l as

$$C_l = \mathfrak{l}^2(l, 2) \int_0^{\chi_S} d\chi \frac{W^2(\chi_S, \chi)}{\chi^2} \times T^2(\nu/\chi) P(\nu/\chi)[1 + \mathcal{O}(1/\nu^2)]. \tag{51}$$

This expression approximates the exact C_l, obtained by integrating the full expression in Eq. (45), to better than 1% for $l \gtrsim 8$.

For small l this approximation fails. Since we are interested in studying the shear on the full sky and correlate fields lying at different χ along the line of sight, we need to go beyond the Limber approximation (49). As shown in [52], an integral of an arbitrary function multiplied by a Bessel function admits the series representation

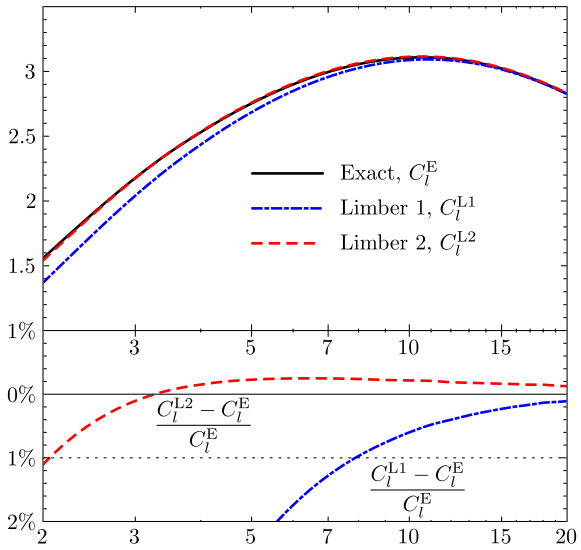

FIG. 1 (color online). Angular power spectrum computed using the exact expression Eq. (45) (*solid black line*), using the Limber approximation at first order as in Eq. (51) [*dotted-dashed blue line*] and at second order as described in Appendix A, Eq. (A1) [*dashed red line*]. The redshift of the source is $z_S = 1$. In the lower panel we have plotted the error made using the first- and second-order Limber approximation. The error made using the second-order approximation is smaller than 1% even at very small l.

$$\int dx f(x) J_\nu(x) = \left[f(x) - \frac{1}{2}\frac{x^2}{\nu^2} f''(x) - \frac{1}{6}\frac{x^3}{\nu^2} f'''(\nu) \right]_{x=\nu} + \mathcal{O}(1/\nu^4). \tag{52}$$

This can be used to go at *second order* in the Limber approximation—i.e. to include corrections of order $1/\nu^2$, such as the second and third terms inside the bracket in the equation above—and to considerably improve the Limber approximation. The expression for the angular power spectrum at second order in the Limber approximation is given in Appendix A, Eq. (A1).

In Fig. 1 we show the angular power spectrum computed using the exact expression Eq. (45) compared with the Limber approximation at first and second order. By going at second order in the Limber approximation, one obtains an agreement with the exact expression to better than 1% for $l \gtrsim 2$.

In practice and for the calculations of the spectra and bispectra, except when otherwise stated, we will employ this improved approximation.

IV. ANGULAR BISPECTRUM

A. The *E*-mode reduced bispectrum

At second order, the lensing potential defined in Eq. (36) is in general a complex quantity. Consequently ${}_2a_{lm}$ and ${}_{-2}a_{lm}$ are not equal anymore. This implies that the second-order shear will generically have both E modes and B modes.

As in the first-order case, we can express $a_{E,lm}$ and $a_{B,lm}$ as a function of the lensing potential. From Eqs. (7) and (8) and using the definition of $a_{E,lm}$ and $a_{B,lm}$, respectively, Eqs. (12) and (13), one finds

$$a_{E,lm} = -\text{ł}(l,-2)\int d\hat{n} Y^*_{lm}(\hat{n})\,\mathrm{Re}[\bar{\eth}^2\gamma(\hat{n})]$$
$$= -\text{ł}(l,2)\int d\hat{n} Y^*_{lm}(\hat{n})\,\mathrm{Re}[\Upsilon(\hat{n})], \quad (53)$$

$$a_{B,lm} = -\text{ł}(l,-2)\int d\hat{n} Y^*_{lm}(\hat{n})\,\mathrm{Im}[\bar{\eth}^2\gamma(\hat{n})]$$
$$= -\text{ł}(l,2)\int d\hat{n} Y^*_{lm}(\hat{n})\,\mathrm{Im}[\Upsilon(\hat{n})]. \quad (54)$$

These expressions relate the electric and magnetic part of the shear, respectively, to *real* and *imaginary* parts of the lensing potentials.

The angular lensing bispectrum $B^{XYZ}_{l_1l_2l_3}$ is defined by

$$\langle a_{X,l_1m_1} a_{Y,l_2m_2} a_{Z,l_3m_3}\rangle \equiv \begin{pmatrix} l_1 & l_2 & l_3 \\ m_1 & m_2 & m_3 \end{pmatrix} B^{XYZ}_{l_1l_2l_3}, \quad (55)$$

where X, Y and Z can be either the electric or magnetic parts of the shear, E and B, and

$$\begin{pmatrix} l_1 & l_2 & l_3 \\ m_1 & m_2 & m_3 \end{pmatrix} \quad (56)$$

is the Wigner $3-j$ symbol. As B vanishes at first order, only expectation values containing three $a_{E,lm}$ or two $a_{E,lm}$ and one $a_{B,lm}$ will be nonzero. For parity reasons, the bispectrum involving three $a_{E,lm}$ will be zero for $l_1+l_2+l_3=$ odd, while the one involving two $a_{E,lm}$ and one $a_{B,lm}$ will be zero for $l_1+l_2+l_3=$ even.

In the following we concentrate on computing the bispectrum of the electric part, which will be simply denoted as $B_{l_1l_2l_3}$, defined as

$$\langle a_{E,l_1m_1} a_{E,l_2m_2} a_{E,l_3m_3}\rangle \equiv \begin{pmatrix} l_1 & l_2 & l_3 \\ m_1 & m_2 & m_3 \end{pmatrix} B_{l_1l_2l_3}. \quad (57)$$

Following the standard CMB notation in the literature [53], we will concentrate on the reduced bispectrum $b_{l_1l_2l_3}$ defined as

$$\langle a_{E,l_1m_1} a_{E,l_2m_2} a_{E,l_3m_3}\rangle \equiv \mathcal{G}^{m_1m_2m_3}_{l_1l_2l_3} b_{l_1l_2l_3}, \quad (58)$$

where

$$\mathcal{G}^{m_1m_2m_3}_{l_1l_2l_3} \equiv \int d\hat{n} Y_{l_1m_1}(\hat{n}) Y_{l_2m_2}(\hat{n}) Y_{l_3m_3}(\hat{n})$$
$$= \sqrt{\frac{(2l_1+1)(2l_2+1)(2l_3+1)}{4\pi}} \times \begin{pmatrix} l_1 & l_2 & l_3 \\ 0 & 0 & 0 \end{pmatrix}\begin{pmatrix} l_1 & l_2 & l_3 \\ m_1 & m_2 & m_3 \end{pmatrix} \quad (59)$$

is the Gaunt integral, which characterizes the angular dependence of the bispectrum. It naturally appears due to translational and rotational invariance on the sky, and enforces m_1, m_2, and m_3 to sum up to zero, and l_1, l_2 and l_3 to satisfy the triangle inequality.

To plot our results, it is convenient to introduce the weighted bispectrum, defined as

$$\hat{b}_{l_1l_2l_3} \equiv \frac{b_{l_1l_2l_3}}{C_{l_1}C_{l_2}+C_{l_1}C_{l_3}+C_{l_2}C_{l_3}}. \quad (60)$$

Note that the weighted bispectrum is independent of the power spectrum normalization A_Φ in Eq. (47).

B. Geometrical contribution

We start by computing the contribution of the geometrical terms to the bispectrum. In order to do this, let us rewrite Eq. (53) by moving the operator $\bar{\eth}^2$ in front of $Y^*_{lm}(\hat{n})$ by integrating by parts twice, and by using Eqs. (C1) and (C2) in Appendix C. After these operations, the coefficient $a_{E,lm}$ becomes

$$a_{E,lm} = (-1)^{m+1}\int d\hat{n}[{}_{-2}Y^*_{lm}(\hat{n})\gamma(\hat{n}) + {}_2Y^*_{lm}(\hat{n})\gamma^*(\hat{n})]. \quad (61)$$

Now, let us initially consider only the standard geometrical contribution, Eq. (17). Plugging this contribution in the above equation, replacing the Weyl potentials by their Fourier components using Eq. (24) and employing the plane wave expansion (41), this can be rewritten as

$$[a^{(\mathrm{stan})}_{\mathrm{geom}}]_{E,lm} = (-1)^{m+1}\sum_{l_1l_2m_1m_2} i^{l_1+l_2}\int d\hat{n}\,{}_{-2}Y^*_{lm}(\hat{n})\{-[\eth(\eth^2 Y^*_{l_1m_1}(\hat{n})\bar{\eth}Y^*_{l_2m_2}(\hat{n}) + \bar{\eth}\eth Y^*_{l_1m_1}(\hat{n})\eth Y^*_{l_2m_2}(\hat{n}))$$
$$+ 2\eth Y^*_{l_1m_1}(\hat{n})\eth Y^*_{l_2m_2}(\hat{n})]\int_0^{\chi_S} d\chi\int_0^{\chi} d\chi' W(\chi_S,\chi)W(\chi,\chi')\mathcal{M}(\chi,\chi')$$
$$+ \bar{\eth}\eth Y^*_{l_1m_1}(\hat{n})Y^*_{l_2m_2}(\hat{n})\int_0^{\chi_S} d\chi\int_0^{\chi_S} d\chi' W(\chi_S,\chi)W(\chi_S,\chi')\mathcal{M}(\chi,\chi')\}$$
$$+ [\eth\leftrightarrow\bar{\eth}], \quad (62)$$

where $\mathcal{M}$ is a function of χ and χ' defined as

$$\mathcal{M}(\chi,\chi') \equiv \int\frac{d^3k_1}{2\pi^2}\frac{d^3k_2}{2\pi^2}T(k_1)T(k_2)j_{l_1}(k_1\chi)j_{l_2}(k_2\chi')Y_{l_1m_1}(\hat{k}_1)Y_{l_2m_2}(\hat{k}_2)\Phi_{\vec{k}_1}\Phi_{\vec{k}_2}. \quad (63)$$

In the fourth line $[\eth \leftrightarrow \bar{\eth}]$ stands for the first three lines (on the right-hand side of the equality) after replacement of the spherical harmonic ${}_{-2}Y^*_{lm}$ by ${}_{2}Y^*_{lm}$ and of all the spatial gradients by their complex conjugates.

We have thus factorized out the projection operators from the time and momentum integrals. We can now make use of the properties of the spin-weighted spherical harmonics, described in Appendix C. It is then straightforward to rewrite the integrals over the angle $\hat{n}$ in terms of the $3-j$ symbols using

$$\int d\hat{n}\, {}_{s_1}Y_{l_1m_1}(\hat{n})\, {}_{s_2}Y_{l_2m_2}(\hat{n})\, {}_{s_3}Y_{l_3m_3}(\hat{n}) = \sqrt{\frac{(2l_1+1)(2l_2+1)(2l_3+1)}{4\pi}} \begin{pmatrix} l_1 & l_2 & l_3 \\ s_1 & s_2 & s_3 \end{pmatrix} \begin{pmatrix} l_1 & l_2 & l_3 \\ m_1 & m_2 & m_3 \end{pmatrix}. \tag{64}$$

Note that the $3-j$ symbol enforces $s_1+s_2+s_3=0$. The fourth line of Eq. (62), $[\eth \leftrightarrow \bar{\eth}]$, gives an identical expression as for the first three lines after sign change of the spin indices s_1, s_2 and s_3. Using the following useful property of the $3-j$ symbols,

$$\begin{pmatrix} l_1 & l_2 & l_3 \\ s_1 & s_2 & s_3 \end{pmatrix} = (-1)^{l_1+l_2+l_3} \begin{pmatrix} l_1 & l_2 & l_3 \\ -s_1 & -s_2 & -s_3 \end{pmatrix}, \tag{65}$$

one finds that for $l_1+l_2+l_3$ even this contribution is identical to the one of the first three lines while for $l_1+l_2+l_3$ odd it is opposite so that all the contributions exactly cancel. Thus, as expected $a_{E,lm}$ vanishes for $l_1+l_2+l_3$ odd.

The bispectrum is then obtained by correlating the second-order $[a^{(\mathrm{stan})}_{\mathrm{geom}}]_{E,lm}$ coefficient in Eq. (62) with the product of two first-order $a_{E,lm}$, whose expression is given in Eq. (42). After taking the expectation value over the primordial perturbations using Wick's theorem and the definition of the primordial power spectrum, Eq. (46), we obtain for the standard geometrical contribution, for $l_1+l_2+l_3$ even,

$$\begin{aligned}
[b^{(\mathrm{stan})}_{\mathrm{geom}}]_{l_1l_2l_3} = {} & -\text{ł}(l_1,2)\text{ł}(l_2,2) \begin{pmatrix} l_1 & l_2 & l_3 \\ 0 & 0 & 0 \end{pmatrix}^{-1} \Bigg[\text{ł}(l_1,3)\text{ł}(l_2,1) \begin{pmatrix} l_1 & l_2 & l_3 \\ 3 & -1 & -2 \end{pmatrix} + \text{ł}^2(l_2,1)\text{ł}(l_1,2) \begin{pmatrix} l_1 & l_2 & l_3 \\ 2 & 0 & -2 \end{pmatrix} \\
& + \text{ł}^2(l_1,1)\text{ł}(l_2,2) \begin{pmatrix} l_1 & l_2 & l_3 \\ 0 & 2 & -2 \end{pmatrix} + \text{ł}(l_1,1)\text{ł}(l_2,1)(l_1+2)(l_1-1) \begin{pmatrix} l_1 & l_2 & l_3 \\ 1 & 1 & -2 \end{pmatrix} \Bigg] \\
& \times \int_0^{\chi_S} d\chi_1 d\chi_2 d\chi_3 \int_0^{\chi_3} d\chi' W(\chi_S,\chi_1) W(\chi_S,\chi_2) W(\chi_S,\chi_3) W(\chi_3,\chi') \mathcal{C}(\chi_1,\chi_3;\chi_2,\chi') \\
& + \text{ł}^2(l_1,1)\text{ł}(l_1,2)\text{ł}^2(l_2,2) \begin{pmatrix} l_1 & l_2 & l_3 \\ 0 & 2 & -2 \end{pmatrix} \begin{pmatrix} l_1 & l_2 & l_3 \\ 0 & 0 & 0 \end{pmatrix}^{-1} \\
& \times \int_0^{\chi_S} d\chi_1 d\chi_2 d\chi_3 \int_0^{\chi_S} d\chi' W(\chi_S,\chi_1) W(\chi_S,\chi_2) W(\chi_S,\chi_3) W(\chi_S,\chi') \mathcal{C}(\chi_1,\chi_3;\chi_2,\chi') + 5\,\text{perms},
\end{aligned} \tag{66}$$

where

$$\mathcal{C}(\chi,\chi';\chi'',\chi''') \equiv \int \frac{2k_1^2 dk_1}{\pi} \frac{2k_2^2 dk_2}{\pi} T^2(k_1) T^2(k_2) j_{l_1}(k_1\chi) j_{l_1}(k_1\chi') j_{l_2}(k_2\chi'') j_{l_2}(k_2\chi''') P(k_1) P(k_2). \tag{67}$$

The bispectrum from the corrections to the geometrical contribution can be straightforwardly computed from Eq. (19), analogously to the calculation for the standard contribution. For $l_1+l_2+l_3$ even we obtain

$$\begin{aligned}
[b^{(\mathrm{corr})}_{\mathrm{geom}}]_{l_1l_2l_3} = {} & \text{ł}(l_1,2)\text{ł}(l_2,2)\text{ł}(l_3,2) \int_0^{\chi_S} d\chi_1 d\chi_2 d\chi_3 W(\chi_S,\chi_1) W(\chi_S,\chi_2) \Bigg[W(\chi_S,\chi_3) g(\chi_3) \mathcal{C}(\chi_1,\chi_3;\chi_2,\chi_3) + \frac{2}{\chi_S\chi_3} (-g(\chi_3) \\
& + (\chi_S-\chi_3) g'(\chi_3)) \int_0^{\chi_3} d\chi' g(\chi') \mathcal{C}(\chi_1,\chi_3;\chi_2,\chi') \Bigg] - 2\text{ł}(l_1,2)\text{ł}^2(l_2,2) \begin{pmatrix} l_1 & l_2 & l_3 \\ 0 & 2 & -2 \end{pmatrix} \begin{pmatrix} l_1 & l_2 & l_3 \\ 0 & 0 & 0 \end{pmatrix}^{-1} \\
& \times \int_0^{\chi_S} d\chi_1 d\chi_2 d\chi_3 W(\chi_S,\chi_1) W(\chi_S,\chi_2) \Bigg[\int_0^{\chi_3} d\chi' \left(\frac{W(\chi_S,\chi_3)}{\chi_3} + \frac{g(\chi_3)}{\chi_S\chi'} \right) g(\chi') \mathcal{C}(\chi_1,\chi_3;\chi_2,\chi') \\
& - \frac{g(\chi_3)}{\chi_S} \int_0^{\chi_S} d\chi' W(\chi_S,\chi') \mathcal{C}(\chi_1,\chi_3;\chi_2,\chi') \Bigg] + 5\,\text{perms}.
\end{aligned} \tag{68}$$

The calculation of the bispectrum from the redshift correction follows from Eq. (21) and proceeds as above. The only complication resides in the spatial gradient in the velocity term, Eq. (23), projected along the line of sight. Using $\hat{n}\cdot\vec{\nabla} e^{i\vec{k}\cdot\hat{n}\chi} = \partial_\chi e^{i\vec{k}\cdot\hat{n}\chi}$, this simply introduces a derivative with respect to χ of the spherical Bessel function in the expansion of plane waves into spherical harmonics. In this case the bispectrum reads

$$[b^{(z)}_{\rm geom}]_{l_1 l_2 l_3} = \mathfrak{H}^2(l_1,2)\mathfrak{H}(l_2,2)\begin{pmatrix} l_1 & l_2 & l_3 \\ 2 & 0 & -2 \end{pmatrix}\begin{pmatrix} l_1 & l_2 & l_3 \\ 0 & 0 & 0 \end{pmatrix}^{-1}\int_0^{\chi_S} d\chi_1 d\chi_2 d\chi_3 W(\chi_S,\chi_1)W(\chi_S,\chi_2)g(\chi_3)$$
$$\times\left\{\frac{1}{\mathcal{H}_S\chi_S^2}\left[2\int_0^{\chi_S} d\chi' g'(\chi')\mathcal{C}(\chi_1,\chi_3;\chi_2,\chi') - g(\chi_S)\mathcal{C}(\chi_1,\chi_3;\chi_2,\chi_S)\right]\right.$$
$$\left.+\frac{2a_S}{3H_0^2\Omega_m\chi_S^3}\left[g(\chi_S)-\frac{g'(\chi_S)}{\mathcal{H}_S}\right]\mathcal{D}(\chi_1,\chi_3;\chi_2,\chi_S)\right\} + 5\,\text{perms}, \tag{69}$$

where

$$\mathcal{D}(\chi,\chi';\chi'',\chi''') \equiv \int \frac{2k_1^2 dk_1}{\pi}\frac{2k_2^2 dk_2}{\pi} T^2(k_1)T^2(k_2) j_{l_1}(k_1\chi) j_{l_1}(k_1\chi') j_{l_2}(k_2\chi'')\frac{\partial j_{l_2}(k_2\chi''')}{\partial \ln\chi'''}P(k_1)P(k_2). \tag{70}$$

C. Dynamical contribution

We compute here the bispectrum from the dynamical terms. Let us start by the Newtonian contribution, Eq. (25). For this contribution the lensing potential is real and reads, using Eq. (36),

$$\Upsilon^{(\rm stan)}_{\rm dyn} = \int_0^{\chi_S} d\chi \frac{\chi_S - \chi}{\chi_S\chi}\phi^{(2)}_N(\chi,\vec{x}). \tag{71}$$

Plugging this expression with (27) into Eq. (53), expanding the plane wave in spherical harmonics and integrating over the angle $\hat{n}$ using the orthogonality of the spherical harmonics we find

$$[a^{(\rm stan)}_{\rm dyn}]_{E,lm} = i^l\mathfrak{H}(l,2)\frac{2}{3H_0^2\Omega_m}\int_0^{\chi_S} d\chi W(\chi_S,\chi)g(\chi)a(\chi)\int\frac{d^3\vec{k}_3}{2\pi^2}Y^*_{lm}(\hat{k}_3)j_l(k_3\chi)$$
$$\times\int\frac{d^3\vec{k}_1 d^3\vec{k}_2}{(2\pi)^3}\delta_D(\vec{k}_3-\vec{k}_1-\vec{k}_2)T(k_1)T(k_2)\frac{k_1^2k_2^2}{k_3^2}F_{2,N}(\vec{k}_1,\vec{k}_2,\chi)\Phi_{\vec{k}_1}\Phi_{\vec{k}_2}, \tag{72}$$

where $F_{2,N}$ is given in Eq. (28).

Using Eq. (42), the expectation value of three $a_{E,lm}$ reads

$$\langle a_{E,l_1m_1}a_{E,l_2m_2}a_{E,l_3m_3}\rangle^{(\rm stan)}_{\rm dyn}$$
$$= -i^{l_1+l_2+l_3}\mathfrak{H}(l_1,2)\mathfrak{H}(l_2,2)\mathfrak{H}(l_3,2)\frac{4}{3H_0^2\Omega_m}\int_0^{\chi_S} d\chi_1 d\chi_2 d\chi_3 W(\chi_S,\chi_1)W(\chi_S,\chi_2)W(\chi_S,\chi_3)g(\chi_3)a(\chi_3)$$
$$\times\int\frac{d^3\vec{k}_1}{2\pi^2}\frac{d^3\vec{k}_2}{2\pi^2}\frac{d^3\vec{k}_3}{2\pi^2}j_{l_1}(k_1\chi_1)j_{l_2}(k_2\chi_2)j_{l_3}(k_3\chi_3)Y^*_{l_1m_1}(\hat{k}_1)Y^*_{l_2m_2}(\hat{k}_2)Y^*_{l_3m_3}(\hat{k}_3)T^2(k_1)T^2(k_2)$$
$$\times\frac{k_1^2k_2^2}{k_3^2}F_{2,N}(\vec{k}_1,\vec{k}_2,\chi_3)P(k_1)P(k_2)(2\pi)^3\delta_D(\vec{k}_1+\vec{k}_2+\vec{k}_3) + 5\,\text{perms}. \tag{73}$$

Now we can write the Dirac delta function in the last line of this expression as

$$\delta_D(\vec{k}_1+\vec{k}_2+\vec{k}_3) = \frac{1}{(2\pi)^3}\int d^3\vec{y}\, e^{i(\vec{k}_1+\vec{k}_2+\vec{k}_3)\cdot\vec{y}}$$
$$= 8\sum_{l_i'm_i'} i^{l_1'+l_2'+l_3'}(-1)^{l_1'+l_2'+l_3'}\mathcal{G}^{m_1'm_2'm_3'}_{l_1'l_2'l_3'}Y_{l_1'm_1'}(\hat{k}_1)Y_{l_2'm_2'}(\hat{k}_2)Y_{l_3'm_3'}(\hat{k}_3)\int_0^\infty d\chi\chi^2 j_{l_1'}(k_1\chi)j_{l_2'}(k_2\chi)j_{l_3'}(k_3\chi), \tag{74}$$

where we have used $\vec{y}\equiv\hat{n}\chi$. Integrating Eq. (73) over the angular directions $d^2\hat{k}_i$ using the above equation and the orthogonality relations of the spherical harmonics, we find for the bispectrum

$$[b_{\rm dyn}^{\rm (stan)}]_{l_1 l_2 l_3} = \text{ł}(l_1,2)\text{ł}(l_2,2)\text{ł}(l_3,2)\frac{2}{3\Omega_m H_0^2}\int_0^{\chi_S} d\chi_1 d\chi_2 d\chi_3 W(\chi_S,\chi_1)W(\chi_S,\chi_2)W(\chi_S,\chi_3)g(\chi_3)a(\chi_3)$$
$$\times\int\frac{2k_1^2dk_1}{\pi}\frac{2k_2^2dk_2}{\pi}\frac{2k_3^2dk_3}{\pi}\frac{k_1^2k_2^2}{k_3^2}T^2(k_1)T^2(k_2)F_{2,N}(k_1,k_2,k_3;\chi_3)P(k_1)P(k_2)$$
$$\times\int_0^\infty d\chi\chi^2 j_{l_1}(k_1\chi_1)j_{l_1}(k_1\chi)j_{l_2}(k_2\chi_2)j_{l_2}(k_2\chi)j_{l_3}(k_3\chi_3)j_{l_3}(k_3\chi) + 5\ \text{perms}, \tag{75}$$

where the kernel $F_{2,N}$ is a function of the amplitudes of the three momenta k_1, k_2, k_3, as easily shown using $\vec{k}_1\cdot\vec{k}_2 = (k_3^2 - k_1^2 - k_2^2)/2$ in Eq. (28).

We now move to the dynamical corrections, Eq. (29). For the rest of this section we will assume matter dominance, so that the growth suppression factor is $g = 1$ and the window function reduces to $W(\chi,\chi') = (\chi - \chi')/(\chi\chi')$. The first two lines of Eq. (29) yield a real lensing potential. For the scalar relativistic contribution coming from the first two terms in Eq. (29), i.e. $(\phi_R^{(2)} + \psi_R^{(2)})/2$, the computation is analogous to the standard scalar part above, the only difference being the kernel. The details of the calculation and the result can be found in Appendix B.

The computation of the vector and tensor contributions is more involved since their kernels depend not only on the amplitude of $\vec{k}_1$ and $\vec{k}_2$ but also on their directions. We present here the computation of the vector modes. The computation of the tensor modes, which is similar, can be found in Appendix B. The vector modes contain two types of terms. The first one comes from the second line of Eq. (29). Using Eq. (33) and after some manipulations it can be written, in Fourier space, as

$$-\frac{1}{2}\omega_r(k_3) = -\frac{i2a^{1/2}}{3H_0}\frac{T(k_1)T(k_2)}{k_3^2}\Phi_{\vec{k}_1}\Phi_{\vec{k}_2}\left[\frac{k_3^2(k_1^2+k_2^2)-(k_1^2-k_2^2)^2}{2k_3^2}(\vec{k}_3\cdot\hat{n}) - k_2^2(\vec{k}_1\cdot\hat{n}) - k_1^2(\vec{k}_2\cdot\hat{n})\right]. \tag{76}$$

The computation of the term proportional to $\vec{k}_3\cdot\hat{n}$ is analogous to the computation of the Doppler term in the redshift correction. Using that

$$i\vec{k}_3\cdot\hat{n}e^{i\vec{k}_3\cdot\hat{n}\chi} = \partial_\chi e^{i\vec{k}_3\cdot\hat{n}\chi}, \tag{77}$$

the time derivative of Fourier modes translates into a time derivative of spherical Bessel functions in the expansion of Eq. (74). The rest of the calculation follows the one for the scalar modes.

The same trick cannot be used for the second and third terms proportional to $\vec{k}_i\cdot\hat{n}$, $i = 1, 2$, since it would require to split the exponential as $e^{i\vec{k}_3\cdot\vec{x}} = e^{i\vec{k}_1\cdot\vec{x}}e^{i\vec{k}_2\cdot\vec{x}}$. This would introduce additional infinite summations over l' and m' in the expansion of the exponential into spherical harmonics. The alternative solution is to expand directly the product $\vec{k}_i\cdot\hat{n}$ into spherical harmonics using

$$\hat{k}_i\cdot\hat{n} = \frac{4\pi}{3}\sum_M Y_{1M}^*(\hat{k}_i)Y_{1M}(\hat{n}). \tag{78}$$

With this expansion we find that the $a_{E,lm}$ coefficient from the second term in the brackets of Eq. (76) reads

$$[a_{\rm dyn}^{\rm (corr)}]_{E,l_3m_3} = -\frac{32i}{9H_0}\text{ł}(l,2)\int_0^{\chi_S} d\chi_3 W(\chi_S,\chi_3)a^{1/2}(\chi_3)\int\frac{k_3^2dk_3}{2\pi^2}\frac{d^3\vec{k}_1 d^3\vec{k}_2}{2\pi^2}T(k_1)T(k_2)\Phi_{\vec{k}_1}\Phi_{\vec{k}_2}\frac{k_1k_2^2}{k_3^2}$$
$$\times\sum_{l_i'm_i'}\sum_{M=-1,0,1}(-1)^{m_3+m_1'+m_2'+m_3'+l_3'}i^{l_1'+l_2'}\mathcal{G}^{l_1',l_2',l_3'}_{-m_1',-m_2',-m_3'}\mathcal{G}^{l,l',1}_{-m_3,m_3',M}Y_{1M}^*(\hat{k}_1)Y_{l_1'm_1'}(-\hat{k}_1)Y_{l_2'm_2'}(-\hat{k}_2)$$
$$\times\int_0^\infty d\chi\chi^2 j_{l_1'}(k_1\chi)j_{l_2'}(k_2\chi)j_{l_3'}(k_3\chi)j_{l_3'}(k_3\chi_3). \tag{79}$$

When computing the 3-point function, one ends up with three spherical harmonics to integrate over $\hat{k}_1$, which give rise to another Gaunt integral. The summation over three Gaunt integrals can then be simplified by using that

$$\sum_{m_1'm_3'M}(-1)^{m_1'+m_3'+M}\mathcal{G}^{l_1',l_2,l'}_{-m_1',-m_2,-m_3'}\mathcal{G}^{l_3,l_3',1}_{-m_3,m_3',M}\mathcal{G}^{l_1,l_1',1}_{-m_1,m_1',-M}$$
$$= (-1)^{l_1'+l_3'+1}\sqrt{\frac{(2l_1+1)(2l_2+1)(2l_3+1)}{4\pi}\frac{3(2l_1'+1)(2l_3'+1)}{4\pi}}$$
$$\times\begin{pmatrix} l_1 & l_2 & l\\ m_1 & m_2 & m\end{pmatrix}\begin{pmatrix} l_1 & l_1' & 1\\ 0 & 0 & 0\end{pmatrix}\begin{pmatrix} l_3' & l_3 & 1\\ 0 & 0 & 0\end{pmatrix}\begin{pmatrix} l_3' & l_1' & l_2\\ 0 & 0 & 0\end{pmatrix}\begin{Bmatrix} l_1 & l_2 & l_3\\ l_3' & 1 & l_1'\end{Bmatrix}, \tag{80}$$

where

$$\begin{Bmatrix} l_1 & l_2 & l_3 \\ l_1' & l_2' & l_3' \end{Bmatrix}$$

denotes the $6-j$ Wigner matrix. The properties of this matrix impose that the only terms in the summation over l_1' and l_3' that give nonzero contributions are those with $l_1' = l_1 \pm 1$ and $l_3' = l_3 \pm 1$. Using the same procedure for the third term in Eq. (76), we find that the bispectrum of the vector contribution $-\frac{1}{2}\omega_r$ reads

$$\begin{aligned}
[b_{\rm dyn}^{\rm (corr)}]_{l_1 l_2 l_3} = & \frac{2}{3H_0}\mathfrak{h}(l_1,2)\mathfrak{h}(l_2,2)\mathfrak{h}(l_3,2)\int_0^{\chi_S} d\chi_1 d\chi_2 d\chi_3 W(\chi_S,\chi_1)W(\chi_S,\chi_2)W(\chi_S,\chi_3)a^{1/2}(\chi_3) \\
& \times \int \frac{2k_1^2 dk_1}{\pi}\frac{2k_2^2 dk_2}{\pi}\frac{2k_3^2 dk_3}{\pi} T^2(k_1)T^2(k_2)P(k_1)P(k_2)\Big\{\frac{(k_1^2+k_2^2)k_3^2-(k_1^2-k_2^2)^2}{2k_3^4} \\
& \times \int_0^\infty d\chi \chi^2 j_{l_1}(k_1\chi_1) j_{l_1}(k_1\chi) j_{l_2}(k_2\chi_2) j_{l_2}(k_2\chi)\partial_{\chi_3} j_{l_3}(k_3\chi_3) j_{l_3}(k_3\chi) \\
& + 2\frac{k_1 k_2^2}{k_3^2}\sum_{\substack{l_1'=l_1\pm 1 \\ l_3'=l_3\pm 1}} (-1)^{l_2} i^{l_1'-l_1+1}(2l_1'+1)(2l_3'+1)\begin{Bmatrix} l_1 & l_2 & l_3 \\ l_3' & 1 & l_1' \end{Bmatrix}\begin{pmatrix} l_1 & l_1' & 1 \\ 0 & 0 & 0 \end{pmatrix}\begin{pmatrix} l_3 & l_3' & 1 \\ 0 & 0 & 0 \end{pmatrix}\begin{pmatrix} l_1' & l_2 & l_3' \\ 0 & 0 & 0 \end{pmatrix}\begin{pmatrix} l_1 & l_2 & l_3 \\ 0 & 0 & 0 \end{pmatrix}^{-1} \\
& \times \int_0^\infty d\chi \chi^2 j_{l_1}(k_1\chi_1) j_{l_1'}(k_1\chi) j_{l_2}(k_2\chi_2) j_{l_2}(k_2\chi) j_{l_3'}(k_3\chi_3) j_{l_3'}(k_3\chi)\Big\} + 5\,\text{perms.}
\end{aligned} \tag{81}$$

The second vector term comes from the third line of Eq. (29) and reads

$$\begin{aligned}
-\frac{1}{2}\eth_1\omega(\hat{n}\chi) = & -\frac{i2a^{1/2}}{3H_0}\int \frac{d^3\vec{k}_3}{(2\pi)^3}\frac{d^3\vec{k}_1 d^3\vec{k}_2}{(2\pi)^3}\delta_D(\vec{k}_3-\vec{k}_1-\vec{k}_2)\frac{T(k_1)T(k_2)}{k_3^2}\Phi_{\vec{k}_1}\Phi_{\vec{k}_2} \\
& \times \eth\Big\{e^{i\vec{k}_3\cdot\hat{n}\chi}\Big[\frac{k_3^2(k_1^2+k_2^2)-(k_1^2-k_2^2)^2}{2k_3^2}(\vec{k}_3\cdot\hat{e}_+)-k_1^2(\vec{k}_2\cdot\hat{e}_+)-k_2^2(\vec{k}_1\cdot\hat{e}_+)\Big]\Big\}.
\end{aligned} \tag{82}$$

Here the new terms are those proportional to $\hat{k}_3\cdot\hat{e}_+$. To compute these terms we rewrite them as $\hat{k}_3\cdot\hat{e}_+ = \eth(\hat{k}_3\cdot\hat{n})$ and then we use the expansion in Eq. (77). The operator $\eth$ acts on the spherical harmonics giving a spin-1 spherical harmonic ${}_1Y_{lm}(\vec{n})$, that results in a Gaunt integral with spin 1. We also have terms proportional to $\hat{k}_i\cdot\hat{e}_+$, $i=1,2$. Again, we rewrite these terms as $\hat{k}_i\cdot\hat{e}_+ = \eth(\hat{k}_i\cdot\hat{n})$ and then we use the expansion in Eq. (78). With this, we find for the bispectrum of the vector term $-\frac{1}{2}\eth_1\omega$,

$$\begin{aligned}
[b_{\rm dyn}^{\rm (corr)}]_{l_1 l_2 l_3} = & \frac{-2}{3H_0}\mathfrak{h}(l_1,2)\mathfrak{h}(l_2,2)\mathfrak{h}(l_3,2)\int_0^{\chi_S} d\chi_1 d\chi_2 d\chi_3 W(\chi_1,\chi_S)W(\chi_2,\chi_S)\frac{\sqrt{a(\chi_3)}}{\chi_3} \\
& \times \int \frac{2k_1^2 dk_1}{\pi}\frac{2k_2^2 dk_2}{\pi}\frac{2k_3^2 dk_3}{\pi} T^2(k_1)T^2(k_2)P(k_1)P(k_2)\Big\{\frac{(k_1^2+k_2^2)k_3^2-(k_1^2-k_2^2)^2}{2k_3^4} \\
& \times \int_0^\infty d\chi \chi^2 j_{l_1}(k_1\chi_1) j_{l_1}(k_1\chi) j_{l_2}(k_2\chi_2) j_{l_2}(k_2\chi) j_{l_3}(k_3\chi_3) j_{l_3}(k_3\chi) \\
& + 2\frac{k_1 k_2^2}{k_3^2}\sum_{\substack{l_1'=l_1\pm 1 \\ l_3'=l_3\pm 1}} (-1)^{l_2} i^{l_1'-l_1+1}\frac{(2l_1'+1)(2l_3'+1)}{\mathfrak{h}(l_3,2)^2}\begin{Bmatrix} l_1 & l_3 & l_2 \\ l_3' & l_1' & 1 \end{Bmatrix}\begin{pmatrix} l_1 & l_2 & l_3 \\ 0 & 0 & 0 \end{pmatrix}^{-1} \\
& \times \Bigg[4l_3'(l_3'+1)\begin{pmatrix} l_1 & l_1' & 1 \\ 0 & 0 & 0 \end{pmatrix}\begin{pmatrix} l_3 & l_3' & 1 \\ 0 & 0 & 0 \end{pmatrix}\begin{pmatrix} l_1' & l_2 & l_3' \\ 0 & 0 & 0 \end{pmatrix} \\
& \times \sqrt{2l_3'(l_3'+1)}(l_3'^2+l_3'+2)\begin{pmatrix} l_1 & l_1' & 1 \\ 0 & 0 & 0 \end{pmatrix}\begin{pmatrix} l_3 & l_3' & 1 \\ 0 & 1 & -1 \end{pmatrix}\begin{pmatrix} l_1' & l_2 & l_3' \\ 0 & 0 & 0 \end{pmatrix}\Bigg] \\
& \times \int_0^\infty d\chi \chi^2 j_{l_1}(k_1\chi_1) j_{l_1'}(k_1\chi) j_{l_2}(k_2\chi_2) j_{l_2}(k_2\chi) j_{l_3'}(k_3\chi_3) j_{l_3'}(k_3\chi)\Big\} + 5\,\text{perms.}
\end{aligned} \tag{83}$$

The computation of the bispectrum from the tensor contribution is analogous to the one above and is reported in Appendix B.

V. RESULTS

We now evaluate the weighted bispectrum from the geometrical and the dynamical terms in a ΛCDM universe. Since we are mainly interested in the impact of the full-sky corrections, which become relevant when one of the modes becomes very long (of the order of the Hubble radius), we compute the bispectrum in the squeezed limit, $l_1 \ll l_2 \simeq l_3$. We label the low multipole corresponding to the long wavelength by l_l, and the two large multipoles, corresponding to the short wavelengths, by l_s and $l_s + \Delta l_s$ respectively (see Fig. 2).

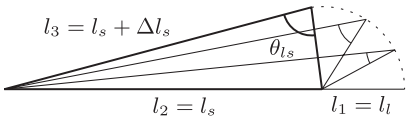

FIG. 2. Possible choice of l_1, l_2 and l_3 in the squeezed limit. Because of the triangle inequality enforced by the Gaunt integral, we let Δl_s vary from 0 to l_l.

In Fig. 3 we plot the various contributions to the weighted bispectrum for two different values of the small multipole l_l and two different values of the redshift of the sources z_S. The amplitudes of the different contributions depend on the redshift of the sources and on the value of the small multipole l_l and, as shown by this figure, there is a clear hierarchy between them.

In the following we are going to discuss their amplitude and their shape, including their redshift dependence. Even though the bispectra shown in Fig. 3 were computed using the second-order Limber approximation, for the following analysis we will make use of the first-order Limber approximation. Moreover, we will assume that the matter transfer function $T(k)$ can be approximated by a power law,

$$T(k = \nu/\chi) \propto \left(\frac{l}{\chi k_{\rm eq}}\right)^{\alpha}, \tag{84}$$

where $k_{\rm eq}$ is the equality scale. Clearly, as shown in Fig. 4 the power α depends on the scales that we consider. At very small l's, $\alpha \to 0$ for a scale invariant spectrum. Using this ansatz, we can employ Eq. (51) to derive how the angular power spectrum C_l scales with l and with the distance of the observer to the source, χ_S. We find

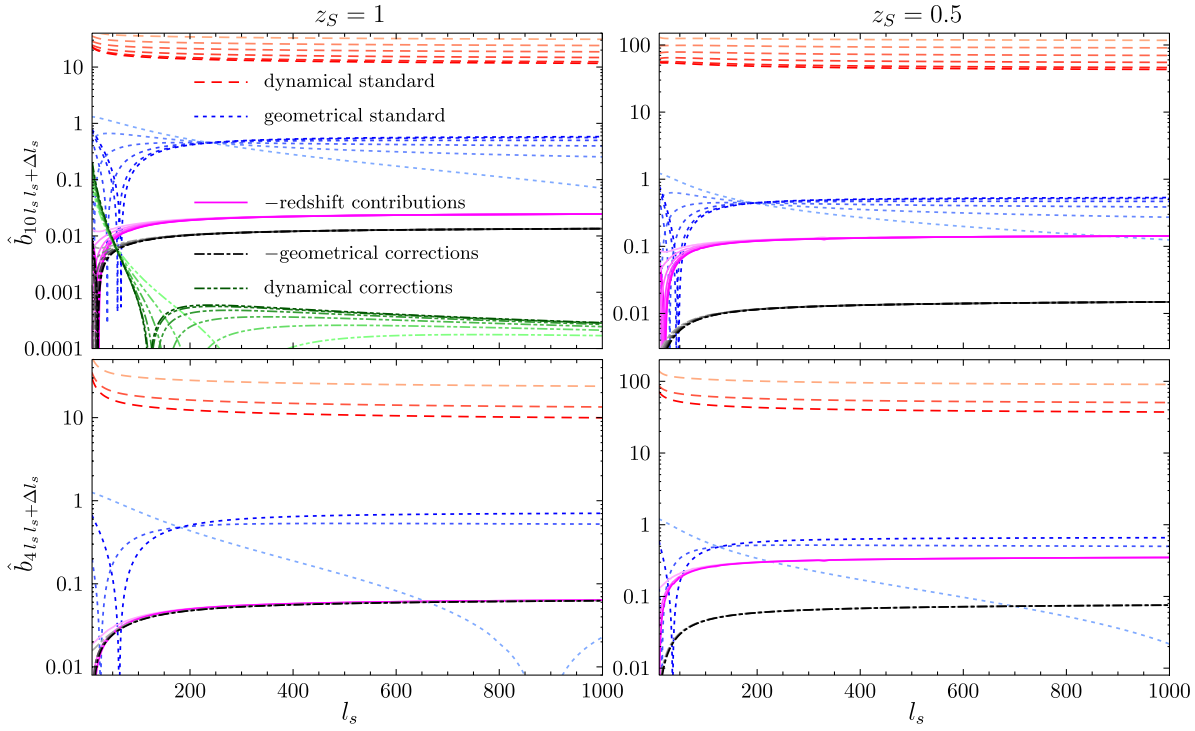

FIG. 3 (color online). The weighted bispectrum in the squeezed limit as a function of l_s, for two different values of the small multipole l_l and two different source redshifts, i.e. $z_S = 1$ (left-hand panels) and $z_S = 0.5$ (right-hand panels). In the top panels we have plotted the weighted bispectrum for $l_l = 10$ and $0 \le \Delta l_s \le 10$ while in the bottom panels we have plotted the case for $l_l = 4$ and $0 \le \Delta l_s \le 4$. The dynamical standard terms are in red, the geometrical standard terms in blue, the redshift contribution in magenta, the geometrical corrections in black and the dynamical corrections in green. For each term Δl_s varies from 0 (darker line) to its maximum (lighter line) by steps of 2. The sign in the legend corresponds to the sign in the large-l_s limit.

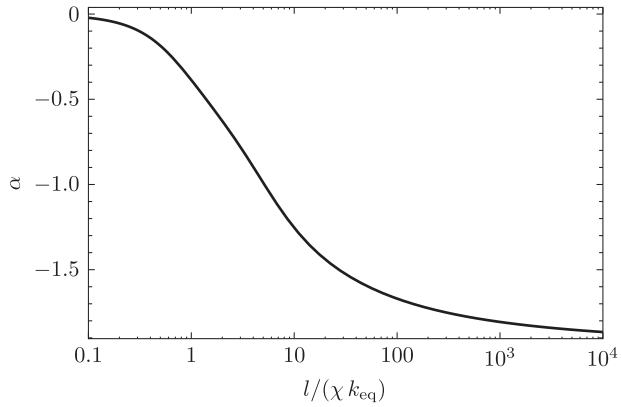

FIG. 4. The power $\alpha \equiv d\ln T/d\ln k$ as a function of $k/k_{\rm eq} = l/(\chi k_{\rm eq})$. For the cosmology chosen in this paper ($h = 0.65$ and $\Omega_m = 0.3$) $k_{\rm eq} = 42.7H_0$ and $\chi(z = 1) = 0.77H_0^{-1}$ so that for $l \sim 1000$, $\alpha \sim -1.5$.

$$C_l \sim l\left(\frac{l}{\chi_S k_{\rm eq}}\right)^{2\alpha}(1 + \mathcal{O}(l^{-2})), \tag{85}$$

The Limber approximated formulae for the bispectrum can be found in Appendix A. For a summary of the color coding in the figures and of the equations giving the expression of the various contributions see Table I.

A. Geometrical correction

We will start by describing the geometrical relativistic correction, Eq. (68), black line in Fig. 3. This contains two terms that we study separately but will give identical behavior. The first term contains a total derivative $\not{\partial}^2(\Psi(\chi,\vec{x})\Psi(\chi',\vec{x}'))$ and its Limber approximation is given by the first two lines of Eq. (A3). Using this equation we can find the scaling behavior of this term,

$$b_{l_1 l_2 l_3} \sim \left(\frac{l_1}{\chi_S k_{\rm eq}}\right)^{2\alpha_1} l_1^{-1}\left(\frac{l_2}{\chi_S k_{\rm eq}}\right)^{2\alpha_2} l_2^{-1} l_3^2 + 5\,\text{perms}. \tag{86}$$

Because the term above is a total gradient there is no modulation dependence on the angle between the short and long mode. We can compute the weighted bispectrum in the squeezed limit by using the expression for the C_l in Eq. (85). Choosing $l_1 = l_l$ gives

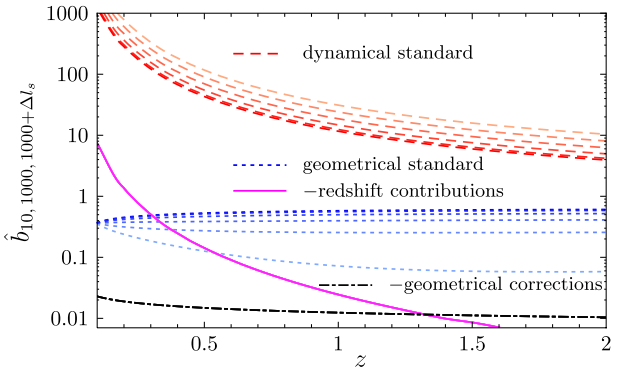

FIG. 5 (color online). The weighted bispectrum in the configuration $l_l = 10$, $l_s = 1000$ and $0 \le \Delta l_s \le 10$, plotted as a function of the redshift of the source z_S. The color coding is the same as in Fig. 3.

$$\hat{b}_{\,l_l l_s l_s+\Delta l_s} \simeq \frac{b_{l_l l_s l_s+\Delta l_s}}{2C_{l_l}C_{l_s}} \sim l_l^{-2}(1 + \mathcal{O}(l_s^{-2})). \tag{87}$$

Thus, the weighted bispectrum for this term does not depend on the short mode l_s and gives rise to a plateau at large l_s, as shown in Fig. 3. Furthermore, as it does not depend on the angle between the short and long mode, it does not depend on Δl_s. However, its dependence on l_l can be clearly seen by comparing the upper and lower panel in Fig. 3. As expected from Eq. (87), this contribution is large from smaller l_l.

Note that the dependence on χ_S drops out in the weighted bispectrum so that the latter depends very mildly on the redshift of the sources z_S, as can be seen by comparing the left- and right-hand panels in Fig. 3. In order to better visualize the redshift dependence, in Fig. 5 we have plotted the weighted bispectrum for a particular configuration ($l_l = 10$, $l_s = 1000$ and $0 \le \Delta l_s \le 10$) as a function of z_S.

Let us discuss now the second term, containing $\Psi(\chi,\vec{x})\not{\partial}^2\Psi(\chi',\vec{x}')$, i.e. a coupling of a spin-0 with a spin-2 field. Its Limber approximation is given by the last three lines of Eq. (A3). By applying the same scaling argument as above we obtain

$$b_{l_1 l_2 l_3} \sim \left(\frac{l_1}{\chi_S k_{\rm eq}}\right)^{2\alpha_1} l_1^{-1}\left(\frac{l_2}{\chi_S k_{\rm eq}}\right)^{2\alpha_2} l_2\cos(2\theta_{23}) + 5\,\text{perms}, \tag{88}$$

TABLE I. Color code for the different contributions to the bispectrum showed in Fig. 3.

Standard dynamical: Newtonian kernel	$\hat{b}^{\rm (stan)}_{\rm dyn}$, Eq. (75)	Red
Standard geometrical: lens-lens, Born corr., reduced shear	$\hat{b}^{\rm (stan)}_{\rm geom}$, Eq. (66)	Blue
Redshift corrections: Doppler, Sachs-Wolfe, ISW	$\hat{b}^{(z)}_{\rm geom}$, Eq. (69)	Magenta
Geometrical corrections	$\hat{b}^{\rm (corr)}_{\rm geom}$, Eq. (68)	Black
Dynamical corrections: scalar, vector and tensor	$\hat{b}^{\rm (corr)}_{\rm dyn}$ Eqs. (81), (83), (B3), (B5), (B7), and (B9),	Green

where θ_{23} is the angle between l_2 and l_3 *inside* the triangle, and we have used the general expression

$$\begin{pmatrix} l_1 & l_2 & l_3 \\ 0 & -s & s \end{pmatrix}\begin{pmatrix} l_1 & l_2 & l_3 \\ 0 & 0 & 0 \end{pmatrix}^{-1} \approx (-1)^s \cos(s\cdot\theta_{23}), \tag{89}$$

valid for large l's. If in the squeezed limit we take $l_1 = l_l$ and $l_2 \simeq l_3 = l_s$, the dominant term in the permutation is the first on the right-hand side of Eq. (88) or the equivalent term with 2 and 3 exchanged. These are proportional to $\cos(2\theta_{23})$—where θ_{23} is the angle between the two short wave modes—which in the squeezed limit goes to 1. Thus, also for this term we expect no modulation on the angle between the short and long mode and for the weighted bispectrum we find the same scaling as for the first term, Eq. (87). Again, the dependence on χ_S drops out in the weighted bispectrum, whence it does not depend on the redshift.

B. Redshift correction

Let us discuss now the redshift correction, Eq. (69), in magenta in Fig. 3. This contribution is of the form $\Psi(\chi,\vec{x})\not{\partial}^2\Psi(\chi',\vec{x}')$ (the Doppler term contains an additional gradient of Ψ, but this has no impact on the Wigner symbols and consequently on the Δl_s dependence of this contribution) and the same arguments as for the second term above can be applied [the first-order Limber approximation for the redshift correction is given in Eq. (A4)]. Hence, the redshift correction is also constant in l_s and is independent of Δl_s, as shown in Fig. 3 (magenta lines). However, the redshift dependence of this contribution is more complex than the one of the geometrical correction and we need to study it in more details.

Indeed, as shown in Eq. (21), the redshift correction is made of three contributions: a Sachs-Wolfe, an integrated Sachs-Wolfe and a Doppler term. Using Eq. (69) we can infer the scaling with the source distance from the observer. In the squeezed limit the first two contributions scale as

$$\hat{b}_{l_l l_s l_s+\Delta l_s} \sim l_l^{-2}\frac{\eta_S}{\chi_S}(1+\mathcal{O}(l_s^{-2})), \tag{90}$$

where η_S is the conformal time at the source. The extra factor η_S/χ_S with respect to the geometrical correction comes from the term in front of the first square bracket of Eq. (69). For the Doppler term one finds

$$\hat{b}_{l_l l_s l_s+\Delta l_s} \sim l_l^{-2}\left(\frac{\eta_S}{\chi_S}\right)^2(1+\mathcal{O}(l_s^{-2})). \tag{91}$$

Thus, for sources at very high redshifts, i.e. such that $\eta_S \lesssim \chi_S$, the redshift correction is typically dominated by the Sachs-Wolfe and integrated Sachs-Wolfe term, and is subdominant with respect to the geometrical correction. For sources at low redshifts $\eta_S \gtrsim \chi_S$ and the Doppler term dominates over the Sachs-Wolfe and integrated Sachs-Wolfe terms, and the redshift correction is larger than the geometrical correction. The redshift of transition is around $z_S \sim 1.2$ but its exact value depends on the particular configuration. This is shown by comparing the left- and right-hand panels in Fig. 3 and more directly in Fig. 5, where for each contribution we plot a particular configuration as a function of the redshift z_S.

A remark is in order here. Naively one would think that the contribution coming from the Doppler term vanishes. Indeed, in the small angle approximation the correlation between the Doppler term and the first-order shear is taken at the same time $\chi = \chi_S$ and vanishes for two reasons: the first-order shear vanishes at the source because of the window function; the Doppler term is longitudinal to the line of sight while the shear is transverse, so that being orthogonal their correlation at the same time vanishes. However, the correlation of the lens with the source does not vanish immediately for $\chi < \chi_S$, but for a given mode l it remains large as long as $\chi_S - \chi \lesssim \chi/l$, after which it decays exponentially (see the Appendix of [20]). In other words, the correlation between the source and the lens decays when the distance from the source is of the order of the typical wavelength. This also implies that the redshift correction is dominated by the configuration in which the Doppler term and one of the first-order shear terms in Eq. (69) is in the long mode.

C. Standard geometrical contribution

We now study the standard geometrical contribution, given in Eq. (66) and shown in blue in Fig. 3. This contribution is given by the collection of the lens-lens coupling, the Born correction, and the nonlinear correction induced by going from the shear to the reduced shear. All these terms contain four transverse derivatives of the Weyl potential and we expect that they dominate over the two contributions discussed above.

Let us start discussing the correction induced by the reduced shear. This term is proportional to $\not{\partial}^2\Psi(\chi,\vec{x})\bar{\not{\partial}}\not{\partial}\Psi(\chi',\vec{x}')$ (see e.g. last line of Eq. (17)) and hence describes the coupling between a spin-2 and a spin-0 field. Using the first-order Limber approximation given in the last two lines of Eq. (A2), the bispectrum scales as

$$b_{l_1 l_2 l_3} \sim \left(\frac{l_1}{\chi_S k_{\rm eq}}\right)^{2\alpha_1} l_1 \left(\frac{l_2}{\chi_S k_{\rm eq}}\right)^{2\alpha_2} l_2 \cos(2\theta_{23}) + 5\,\text{perms}, \tag{92}$$

where we have employed Eq. (89) to rewrite the Wigner symbols in terms of the cosine. If we chose $l_1 = l_l$, the four dominant configurations in the squeezed limit are those containing l_1, i.e., summing up all of them,

$$b_{l_1 l_2 l_3} \sim \left(\frac{l_1}{\chi_S k_{\rm eq}}\right)^{2\alpha_1} l_1 \left(\frac{l_2}{\chi_S k_{\rm eq}}\right)^{2\alpha_2} l_2[\cos(2\theta_{13}) + \cos(2\theta_{12}) + 2\cos(2\theta_{23})], \tag{93}$$

where we have used $l_2 \simeq l_3$. In the squeezed limit $\theta_{23} \to 0$ and $\theta_{12} \to \pi - \theta_{13}$, so that we can write the scaling of the weighted bispectrum as

$$\hat{b}_{l_l l_s l_s+\Delta l_s} \sim (1 + \cos(2\theta_{ls}))(1 + \mathcal{O}(l_s^{-2})). \tag{94}$$

Thus, this contribution is l_s independent for large l_s's but its shape depends on the angle between the long and the short mode. For $\Delta l_s \ll l_s$, $\cos\theta_{ls} \simeq \Delta l_s/l_l$ and $1 + \cos(2\theta_{ls}) \simeq 2(\Delta l_s/l_l)^2$. This can be seen in detail in Fig. 6 (left panel) where we have plotted this contribution separately from the other geometrical standard contributions. One can check that in the large-l_s limit the weighted bispectrum vanishes for $\Delta l_s = 0$, and becomes positive when Δl_s goes to l_l.

We can now concentrate on the lens-lens coupling and the correction to the Born approximation, which are described by the first two lines of Eq. (17). They contain three types of couplings: couplings between a spin-3 and a spin-(-1) field, $\eth^3\Psi(\chi,\vec{x})\bar{\eth}\Psi(\chi',\vec{x}')$, couplings between two spin-1 fields, $\bar{\eth}\eth^2\Psi(\chi,\vec{x})\eth\Psi(\chi',\vec{x}')$, and couplings between a spin-2 and a spin-0 field, $\eth^2\Psi(\chi,\vec{x})\eth\bar{\eth}\Psi(\chi',\vec{x}')$. These types of couplings generate three different Wigner symbols, written in Eq. (66). In order to study the scaling of this contribution we can use the recurrence identities for the Wigner symbols to write

$$\begin{aligned}
\begin{pmatrix} l_1 & l_2 & l_3 \\ 3 & -1 & -2 \end{pmatrix} &= -\sqrt{\frac{(l_3-2)(l_3+3)}{l_2(l_2+1)}}\begin{pmatrix} l_1 & l_2 & l_3 \\ 3 & 0 & -3 \end{pmatrix} \\
&\quad -\sqrt{\frac{(l_1+3)(l_1-2)}{l_2(l_2+1)}}\begin{pmatrix} l_1 & l_2 & l_3 \\ 2 & 0 & -2 \end{pmatrix}, \\
\begin{pmatrix} l_1 & l_2 & l_3 \\ 1 & 1 & -2 \end{pmatrix} &= -\sqrt{\frac{(l_3+2)(l_3-1)}{l_2(l_2+1)}}\begin{pmatrix} l_1 & l_2 & l_3 \\ 1 & 0 & -1 \end{pmatrix} \\
&\quad -\sqrt{\frac{(l_1-1)(l_1+2)}{l_2(l_2+1)}}\begin{pmatrix} l_1 & l_2 & l_3 \\ 2 & 0 & -2 \end{pmatrix},
\end{aligned} \tag{95}$$

so that in the large l's limit we can rewrite all the Wigner symbols in terms of cosines using Eq. (89). Thus, inserting these decompositions into the first-order Limber approximation of the bispectrum given by the first four lines of Eq. (A2), the lens-lens coupling and the correction to the Born approximation scale as

$$\begin{aligned}
b_{l_1 l_2 l_3} \sim &\left(\frac{l_1}{\chi_S k_{\rm eq}}\right)^{2\alpha_1} l_1 \left(\frac{l_2}{\chi_S k_{\rm eq}}\right)^{2\alpha_2} l_2 \\
&\times \Big[\frac{l_1 l_3}{l_2^2}(\cos(3\theta_{13}) + \cos(\theta_{13})) - 2\frac{l_1^2}{l_2^2}\cos(2\theta_{13}) \\
&+ \cos(2\theta_{13}) + \cos(2\theta_{23})\Big] + 5\,\text{perms}.
\end{aligned} \tag{96}$$

Taking the squeezed limit of this expression is subtle: at lowest order in $1/l_s$ (i.e. at zeroth order in the expansion of the cosines in terms of the small angle between the two short wave modes) the expression above vanishes. Thus, we need to compute this expression at least at an order $\mathcal{O}(l_s^{-2})$ higher. Taking into account all the permutations one finds

$$\hat{b}_{l_l l_s l_s+\Delta l_s} \sim (1 - 6\cos^2\theta_{ls})(1 + \mathcal{O}(l_s^{-2})). \tag{97}$$

This contribution is shown in details in Fig. 6 (right panel). Using that $1 - 6\cos^2\theta_{ls} \simeq 1 - 6\Delta l_s^2/l_l^2$ one can check that it is positive for $\Delta l_s \leq 4$.

Summing the reduced shear contribution to the lens-lens coupling and the Born correction, we find that the standard geometrical contribution gives rise to a plateau as a function of l_s. The redshift dependence of the standard geometrical contribution is similar to the one of the geometrical correction. However, its amplitude is much larger due to the absence of the l_l^{-2} suppression present in the geometrical correction. Moreover, it depends on Δl_s, as shown in Fig. 3 (blue lines). As shown in the lower-right panel of Fig. 3, for very small l_l and low z_S, the redshift correction becomes of the same order as the standard geometric contribution.

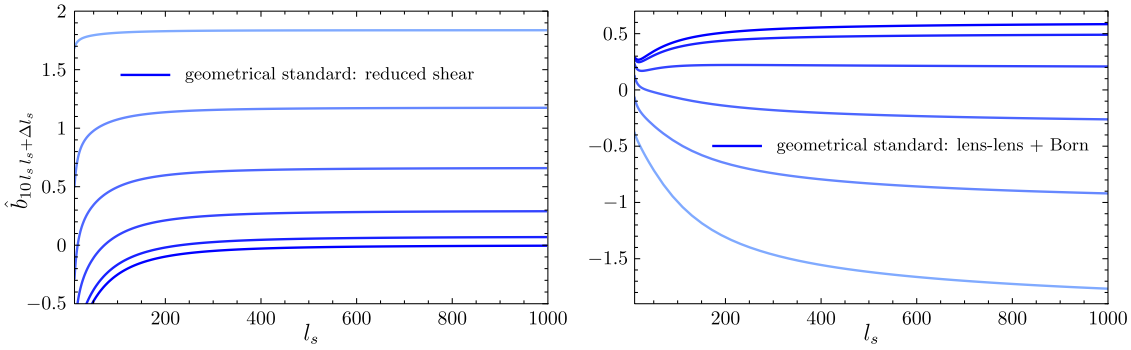

FIG. 6 (color online). The weighted bispectrum from the reduced shear contribution (left panel) and from the lens-lens coupling and the correction to the Born approximation (right panel) at $z_S = 1$, in the squeezed limit: $l_l = 10$ and $0 \leq \Delta l_s \leq 10$. Δl_s varies from 0 (dark blue) to 10 (light blue) by steps of 2. Note that the reduced shear contribution (left panel) increases with Δl_s, whereas the lens-lens coupling and the correction to the Born approximation (right panel) decreases with Δl_s.

D. Dynamical contributions

The largest contribution to the cosmic shear comes from what we have called the standard dynamical contribution. This is given in Eq. (75) and shown in red in Fig. 3. This contribution is proportional to the total transverse Laplacian of a scalar, $\not{\partial}^2\phi_N^{(2)}(\chi,\vec{x})$ [see Eq. (25)], but the scalar $\phi_N^{(2)}$ is not a Gaussian variable: it is related to the Gaussian primordial perturbation Φ by Eqs. (27) and (28). We can compute the scaling of this contribution as we did above for the others. We obtain

$$b_{l_1l_2l_3} \sim \left(\frac{l_1}{\chi_S k_{\rm eq}}\right)^{2\alpha_1} l_1 \left(\frac{l_2}{\chi_S k_{\rm eq}}\right)^{2\alpha_2} l_2 \left(\frac{\eta_0}{\chi_S}\right)^2 F_{2,N}(\vec{l}_1,\vec{l}_2) + 5\,\text{perms}, \tag{98}$$

where, from Eq. (28),

$$F_{2,N}(\vec{l}_1,\vec{l}_2) \equiv \frac{1}{2}(1+\epsilon) + \frac{1}{2}\left(\frac{l_1}{l_2}+\frac{l_2}{l_1}\right)\cos\theta_{12} + \frac{1}{2}(1-\epsilon)\cos^2\theta_{12}. \tag{99}$$

If we take the squeezed limit by choosing $l_l = l_1$, there are four contributions that dominate,

$$b_{l_1l_2l_3} \sim \left(\frac{l_1}{\chi_S k_{\rm eq}}\right)^{2\alpha_1} l_1 \left(\frac{l_2}{\chi_S k_{\rm eq}}\right)^{2\alpha_2} l_2 (2F_{2,N}(\vec{l}_1,\vec{l}_2) + 2F_{2,N}(\vec{l}_1,\vec{l}_3))\left(\frac{\eta_0}{\chi_S}\right)^2, \tag{100}$$

where we have used $l_2 \simeq l_3$. As in the squeezed limit $\cos\theta_{13} = -\cos\theta_{12}$, the terms proportional to $\cos\theta_{12}$ and $\cos\theta_{13}$ cancel and we finally obtain

$$\hat{b}_{l_l l_s l_s+\Delta l_s} \sim 2[(1+\epsilon)+(1-\epsilon)\cos^2\theta_{ls}]\left(\frac{\eta_0}{\chi_S}\right)^2 (1+\mathcal{O}(l_s^{-2})). \tag{101}$$

Thus, as can be checked in Fig. 3, the weighted bispectrum of the standard dynamical contribution does not depend on l_s but depends on the angle between the short and the long mode. This contribution dominates over the standard geometrical contribution because it is enhanced by the term $(\eta_0/\chi_S)^2$. This term decreases at higher redshift, as shown by comparing the left and right panels of Fig. 3 and more clearly in Fig. 5.

The dynamical correction from scalar, vector and tensor modes, see Eqs. (81), (83), (B3), (B5), (B7), and (B9), is shown in green in Fig. 3, left-top panel. For large l_s it is at least 1 order of magnitude smaller than the geometrical correction. Only for $l_s \lesssim 100$ it becomes larger than the geometrical correction and the redshift contribution. We will neglect it in the analysis of the following section.

VI. COMPARISON WITH PRIMORDIAL NON-GAUSSIANITY

A. Local bispectrum

Let us start by studying the effect that a primordial signal would induce on the lensing shear bispectrum. The most common type of non-Gaussianity considered in the literature is the local type, which is typically generated by multifield models [54–57]. For local non-Gaussianity, the first-order primordial potential Φ (which in matter dominance is related to the primordial curvature perturbation ζ by $\Phi = -(3/5)\zeta$) contains a primordial quadratic correction in position space [58],

$$\Phi(\vec{x}) = \Phi_G(\vec{x}) - f_{\rm NL}^{\rm loc}\Phi_G^2(\vec{x}), \tag{102}$$

where Φ_G is a primordial Gaussian potential whose power spectrum is given by Eqs. (46) and (47).[4] Using the above equation together with Eqs. (46) and (47), we can rewrite the 3-point correlation function of Φ in Fourier space as

$$\langle \Phi_{\vec{k}_1}\Phi_{\vec{k}_2}\Phi_{\vec{k}_3}\rangle = (2\pi)^3\delta(\vec{k}_1+\vec{k}_2+\vec{k}_3)B^{\rm loc}(k_1,k_2,k_3), \tag{103}$$

where the local bispectrum is given by

$$B^{\rm loc}(k_1,k_2,k_3) = -2f_{\rm NL}^{\rm loc}A_\Phi^2\left(\frac{1}{k_1^3k_2^3}+\frac{1}{k_1^3k_3^3}+\frac{1}{k_2^3k_3^3}\right). \tag{104}$$

We can use Eq. (42) to compute the angular lensing bispectrum generated by local non-Gaussianity. It is straightforward to show that this is given by

$$\begin{aligned} b^{\rm loc}_{l_1l_2l_3} = {} & -\text{ł}(l_1,2)\text{ł}(l_2,2)\text{ł}(l_3,2)\int_0^{\chi_S} d\chi_1 d\chi_2 d\chi_3 W(\chi_S,\chi_1) \\ & \times W(\chi_S,\chi_2)W(\chi_S,\chi_3)\int_0^{\chi_S} d\chi\chi^2 \int \frac{2k_1^2dk_1}{\pi} \\ & \times \frac{2k_2^2dk_2}{\pi}\frac{2k_3^2dk_3}{\pi} j_{l_1}(k_1\chi)j_{l_2}(k_2\chi)j_{l_3}(k_3\chi)j_{l_1}(k_1\chi_1) \\ & \times j_{l_2}(k_2\chi_2)j_{l_3}(k_3\chi_3)T(k_1)T(k_2)T(k_3)B^{\rm loc}(k_1,k_2,k_3). \end{aligned} \tag{105}$$

Let us use the Limber approximation and the scaling arguments of the previous section to find the behavior of the local bispectrum as a function of the long and short modes. Employing again the relation $T(k) \propto l^\alpha$, one finds

$$b^{\rm loc}_{l_1l_2l_3} \sim \left(\frac{l_1}{\chi_S k_{\rm eq}}\right)^{\alpha_1} l_1^{-1}\left(\frac{l_2}{\chi_S k_{\rm eq}}\right)^{\alpha_2} l_2^{-1}\left(\frac{l_3}{\chi_S k_{\rm eq}}\right)^{\alpha_3} l_3^2 + 5\,\text{perms}. \tag{106}$$

In the squeezed limit we obtain, for the weighted bispectrum,

[4] Note that we use the notation of [59] with a minus sign for $f_{\rm NL}$. This is related to $f_{\rm NL}$ used in CMB computation (which is defined in radiation domination) by $f_{\rm NL} = 10/9 f_{\rm NL}^{\rm CMB}$.

$$\hat{b}^{\rm loc}_{l_l l_s l_s+\Delta l_s} \sim l_l^{-2}\left(\frac{l_l}{\chi_S k_{\rm eq}}\right)^{-\alpha_l}(1+\mathcal{O}(l_s^{-2})). \qquad (107)$$

Thus, on very large scales, where $\alpha_l \to 0$, the local bispectrum behaves as the geometrical correction.

B. Contamination

The estimator of local primordial non-Gaussianity is given by [60]

$$\mathcal{E} = \frac{1}{N_{\rm loc}}\sum_{l_i m_i}\begin{pmatrix} l_1 & l_2 & l_3 \\ m_1 & m_2 & m_3\end{pmatrix}\frac{B^{\rm loc}_{l_1 l_2 l_3}}{\Delta_{l_1 l_2 l_3} C_{l_1} C_{l_2} C_{l_3}} \times \langle a_{E,l_1 m_1} a_{E,l_2 m_2} a_{E,l_3 m_3}\rangle, \qquad (108)$$

where $\Delta_{l_1 l_2 l_3}$ is a combinatorial factor equal to 1 if the three l's are different, to 2 if two of them are equal and to 6 if all of them are equal. If the local bispectrum $B^{\rm loc}_{l_1 l_2 l_3}$ is computed for $f^{\rm loc}_{\rm NL} = 1$, the normalization factor $N_{\rm loc}$ that makes the estimator unbiased ($\langle\mathcal{E}\rangle = f^{\rm loc}_{\rm NL}$) is

$$N_{\rm loc} = \sum_{l_1 l_2 l_3}\frac{(B^{\rm loc}_{l_1 l_2 l_3})^2}{\Delta_{l_1 l_2 l_3} C_{l_1} C_{l_2} C_{l_3}}. \qquad (109)$$

Thus, if this estimator is applied to an arbitrary signal $B^X_{l_1 l_2 l_3}$, this will contaminate the measurement by a value of $f^{\rm loc}_{\rm NL}$ given by

$$f^{\rm loc}_{\rm NL} = \frac{1}{N_{\rm loc}}\sum_{l_1 l_2 l_3}\frac{B^{\rm loc}_{l_1 l_2 l_3} B^X_{l_1 l_2 l_3}}{\Delta_{l_1 l_2 l_3} C_{l_1} C_{l_2} C_{l_3}}. \qquad (110)$$

Before estimating the contamination to the local signal from each of the contributions studied in the previous sections, let us use Eq. (108) to define a natural quantity that characterizes the "superposition" between two different contributions. We define the cosine between two bispectra as [61]

$$\cos(Y,X) \equiv \frac{1}{N_X^{1/2} N_Y^{1/2}}\sum_{l_1 l_2 l_3}\frac{B^X_{l_1 l_2 l_3} B^Y_{l_1 l_2 l_3}}{\Delta_{l_1 l_2 l_3} C_{l_1} C_{l_2} C_{l_3}}, \qquad (111)$$

where the factors $N_{X,Y}$ are defined analogously to $N_{\rm loc}$ in Eq. (109). This quantity ranges from -1 to 1 and its absolute value tells us how much two signals are orthogonal, $\cos(Y,X) \simeq 0$, or superposed, $\cos(Y,X) \simeq \pm 1$. The cosine between the local non-Gaussianity and the contributions to the lensing shear from second-order perturbations is plotted in Fig. 7 as a function of the redshift. For the calculation, we have summed over all l's (with even sum) from 2 to $l_{\rm max} = 1000$. As expected, the geometrical relativistic corrections and the correction due to the redshift perturbation overlap very much with a local non-Gaussianity, contributing with a negative $f^{\rm loc}_{\rm NL}$. Indeed, in the squeezed limit both these corrections have the same l behavior and no dependence on the angle between the short and long mode. The overlap with the standard contributions is much milder. This is due to the fact that in the equilateral limit its amplitude decays less rapidly than the one of the local shape and because part of the standard contributions depend on the angle between the short and long mode, and this part averages to zero when convolved with the local signal.

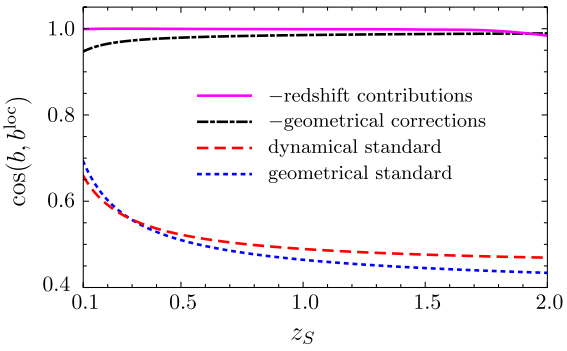

FIG. 7 (color online). Overlap between the local non-Gaussianity and the standard dynamical and geometrical contributions and the geometrical and redshift corrections.

We can now use Eq. (110) to compute the non-Gaussian contamination to the local signal from each of these four contributions. The $f^{\rm loc}_{\rm NL}$ that an experiment looking for a local signal would measure from these contributions is shown in Fig. 8 as a function of the redshift of the source z_S. As expected, the geometrical correction leads to an $f^{\rm loc}_{\rm NL} \sim 1$ and roughly constant with z_S. Even though the redshift correction has the same l dependence as the local signal, at low redshift it is enhanced by a factor $(\eta_S/\chi_S)^2$ and the contamination to $f^{\rm loc}_{\rm NL}$ becomes surprisingly large, $f^{\rm loc}_{\rm NL} \gtrsim 10$ for $z_S \lesssim 0.3$. The overlap between the standard geometrical correction and the local signal strongly depends on the redshift of the sources, and the $f^{\rm loc}_{\rm NL}$ of contamination inherits the same behavior. In this case $f^{\rm loc}_{\rm NL} \gtrsim 100$ for $z_S \gtrsim 0.8$. Finally, as the standard dynamical contribution gets larger and larger at low redshift, its contamination to the local signal does the same. For $z_S \lesssim 1.7$ we have $f^{\rm loc}_{\rm NL} \gtrsim 10^4$.

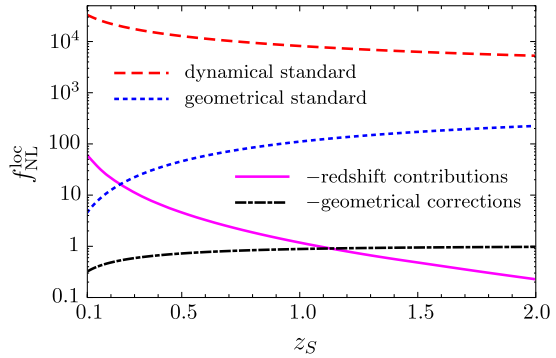

FIG. 8 (color online). The contamination to a primordial local non-Gaussian signal due to the standard dynamical and geometrical contributions and the geometrical and redshift corrections.

VII. CONCLUSION

In this paper we present an exhaustive calculation of the full-sky bispectrum of the shear field as it would be built by an observer measuring shapes of galaxies at a given redshift. The calculation is performed at tree order (i.e. neglecting loop corrections), assuming that the initial curvature perturbation ζ obeys Gaussian statistics, such as after single-field inflation. Furthermore, we study the relative importance of the different couplings and we compare them with primordial non-Gaussianities of the local type.

Our derivation fully exploits and completes the recent study of Ref. [29], where the full-sky second-order expression of the shear field has been computed. This article derives all second-order terms in the metric fluctuations that contribute to the shear field and it is thus the natural starting point of the computation of the tree order bispectrum presented here. In this paper we focus our calculations on the bispectrum of the scalar, i.e. electric, part of the shear field alone. This is somewhat restrictive since the second-order shear field contains a pseudoscalar, i.e. magnetic, mode. We leave the study of the B mode and of the correlators where it is relevant for the future.

The computation of the bispectrum from the formal second-order shear expression is an involved exercise, which includes two steps. The first consists in the formal derivation of the bispectrum in harmonic space. The electric part of the shear field itself is defined from its harmonic space expression, in a way similar to the mode decompositions of the CMB polarization. Its bispectrum is then computed with the help of the decomposition properties of the spherical harmonics and their spin weighted extensions. These results are presented in Sec. IV of the paper where the contribution of each term is fully computed. Then, the second part consists in numerically evaluating the terms that we have found, in the context of the ΛCDM model.

Two approximations are commonly employed for weak lensing calculations, namely, the Limber approximation [62], which consists in neglecting longitudinal modes, as they tend to average out along the line of sight, and the flat sky approximation, which consists in replacing a small portion of the spherical sky with a two-dimensional plane.[5] In order to be consistent with our full-sky treatment, it is *a priori* not possible to employ neither of these two approximations. Abandoning the Limber approximation makes the computations numerically challenging due to the large number of integrations involved and, as a consequence, only a limited number of configurations could be exactly computed. In order to circumvent this problem we have used the higher-order Limber approximation discussed in [51]. Except for a specific type of contributions, we have found that sufficiently high accuracy can be reached with the help of the second-order approximation. The procedure that we have used to implement this approximation to the angular power spectrum and the bispectrum is presented in Appendix A.

Our results are described in Sec. V. In this section we give a precise account of the relative importance of the various contributing terms, as well as of their dependence with the multipole configuration. We distinguish the different contributing terms as geometrical and dynamical, depending on whether they originate from pure general relativistic effects on the line-of-sights or due to the dynamical evolution of the metric field. Note however that this distinction is somewhat arbitrary, since it depends on the gauge choice. Furthermore, in each case we distinguish the standard terms as those which survive at small angular scale, from the nonstandard ones that are mainly relevant at large angular scales.

We discuss the contribution to the bispectrum of the different nonlinear couplings focussing on the squeezed limit configuration, where the nonstandard general relativistic corrections are more likely to play a significant role. In Sec. V we give a precise account of the relative importance of the various contributing terms as well as of their dependence with the multipole configuration. We find that the general relativistic effects, i.e. the nonstandard coupling terms, are typically smaller than the standard nonlinear couplings. However their relative importance increases at smaller source redshifts. Among the new couplings, the dynamical couplings are always much smaller than the others, while those due to the inhomogeneity in the redshift of the source dominate. The latter can even become of the same order of the standard couplings when the redshift of the sources is below 0.5. These results are summarized in Figs. 3 and 5. Note that the bispectrum computed here assumes correlation between sources at the same redshift. Those results could naturally be extended to cases of multiple redshift sources. It increases the number of terms one needs to compute and, lacking motivations to explore specific source plane configurations, we did not try to do it in this paper.

In Sec. VI we finally compute the corresponding level of contamination induced by the standard and nonstandard terms on the amplitude of primordial non-Gaussianities of the local type. Note that, as in the squeezed limit the standard nonlinear couplings depend on the angle between the short and long mode, they differ significantly from a local signal. For $z_S \gtrsim 0.8$, the contamination to $f_{\rm NL}^{\rm loc}$ of the standard geometrical couplings amounts to $f_{\rm NL}^{\rm loc} \gtrsim 100$. On the other hand, the relativistic corrections induce a non-Gaussianity which is mainly of the local type and can contaminate the search for a primordial signal by $f_{\rm NL}^{\rm loc} \sim 1$ to $f_{\rm NL}^{\rm loc} \gtrsim 10$ when the source redshifts vary from 1 to 0.3.

Our investigations did not go as far as computing the signal-to-noise ratio for the bispectrum induced by the general relativistic corrections. However, given the much larger amplitude of the standard contributions, we expect it

[5] Note that these two approximations are not equivalent and one does not necessarily imply the other.

to be rather small. This might not be the case when, besides the only E-mode three-point correlators we have investigated here, quantities involving B modes are also included. Relativistic corrections indeed generically induce B modes with an amplitude *a priori* comparable to the E modes [29]. This is at variance with the standard dynamical couplings that induce second-order E modes only. It ensures that the correlations between E and B modes are only nonvanishing in the presence of general relativistic corrections making such quantities more likely to be observable. We leave such calculations for a future study.

ACKNOWLEDGMENTS

It is a pleasure to thank C. Caprini, R. Durrer, A. Rassat and U. Seljak for useful discussions. F. B. is partly supported by the French Programme National de Cosmologie et Galaxies; C. B. is supported by the Herchel Smith Fund and by Kings College Cambridge.

APPENDIX A: LIMBER APPROXIMATION

1. Power spectrum in the second-order Limber approximation

The expression for the power spectrum with the second-order Limber approximation can be straightforwardly computed by applying the series expansion given by Eq. (52) to the expression for the angular power spectrum, Eq. (45). The result is

$$C_l = \mathfrak{l}^2(l,2)\int_0^{\chi_S}\frac{d\chi}{\chi}T^2(\nu/\chi)P(\nu/\chi)\tilde{W}(\chi) \times\left[\tilde{W}(\chi)-\frac{1}{\nu^2}\left(\chi^2\tilde{W}''(\chi)+\frac{1}{3}\chi^3\tilde{W}'''(\chi)\right)\right] \tag{A1}$$

where $\tilde{W}(\chi)\equiv W(\chi_S,\chi)/\sqrt{\chi}$. By dropping the $1/\nu^2$ term, one easily recovers the first-order Limber-approximated result given by Eq. (51).

2. Geometrical terms in the first-order Limber approximation

We present here the solutions for the bispectrum at first order in the Limber approximation. In our numerical code we go beyond this approximation and we use the second-order Limber approximation. However, the first-order approximation is sufficient to understand qualitatively the scaling of the bispectrum in the squeezed limit.

The bispectrum from the standard geometrical terms reads at first order in the Limber approximation

$$\begin{aligned}[b^{(\mathrm{stan})}_{\mathrm{geom}}]_{l_1l_2l_3} =& \mathfrak{l}(l_1,2)\mathfrak{l}(l_2,2)\begin{pmatrix}l_1&l_2&l_3\\0&0&0\end{pmatrix}^{-1}\Bigg\{\mathfrak{l}(l_1,3)\mathfrak{l}(l_2,1)\left[\begin{pmatrix}l_1&l_2&l_3\\3&-1&-2\end{pmatrix}+\mathrm{c.c.}\right]+\mathfrak{l}^2(l_2,1)\mathfrak{l}(l_1,2)\left[\begin{pmatrix}l_1&l_2&l_3\\2&0&-2\end{pmatrix}+\mathrm{c.c.}\right]\\
&+\mathfrak{l}^2(l_1,1)\mathfrak{l}(l_2,2)\left[\begin{pmatrix}l_1&l_2&l_3\\0&2&-2\end{pmatrix}+\mathrm{c.c.}\right]+\mathfrak{l}(l_1,1)\mathfrak{l}(l_2,1)(l_1+2)(l_1-1)\left[\begin{pmatrix}l_1&l_2&l_3\\1&1&-2\end{pmatrix}+\mathrm{c.c.}\right]\Bigg\}\\
&\times\Bigg[\int_0^{\chi_S}\frac{d\chi}{\chi^3}T^2\left(\frac{\nu_1}{\chi}\right)P\left(\frac{\nu_1}{\chi}\right)W^2(\chi_S,\chi)\int_0^{\chi}\frac{d\chi'}{\chi'^2}T^2\left(\frac{\nu_2}{\chi'}\right)P\left(\frac{\nu_2}{\chi'}\right)W(\chi_S,\chi')g(\chi')-\int_0^{\chi_S}\frac{d\chi}{\chi^2}T^2\left(\frac{\nu_1}{\chi}\right)P\left(\frac{\nu_1}{\chi}\right)W^2(\chi_S,\chi)\\
&\times\int_0^{\chi}\frac{d\chi'}{\chi'^3}T^2\left(\frac{\nu_2}{\chi'}\right)P\left(\frac{\nu_2}{\chi'}\right)W^2(\chi_S,\chi')g(\chi')\Bigg]+\mathfrak{l}^2(l_1,1)\mathfrak{l}(l_1,2)\mathfrak{l}^2(l_2,2)\left[\begin{pmatrix}l_1&l_2&l_3\\0&2&-2\end{pmatrix}+\mathrm{c.c.}\right]\begin{pmatrix}l_1&l_2&l_3\\0&0&0\end{pmatrix}^{-1}\\
&\times\int_0^{\chi_S}\frac{d\chi}{\chi^2}T^2\left(\frac{\nu_1}{\chi}\right)P\left(\frac{\nu_1}{\chi}\right)W^2(\chi_S,\chi)\int_0^{\chi_S}\frac{d\chi'}{\chi'^2}T^2\left(\frac{\nu_2}{\chi'}\right)P\left(\frac{\nu_2}{\chi'}\right)W^2(\chi_S,\chi')+5\,\mathrm{perms},\end{aligned} \tag{A2}$$

where $\nu_i\equiv l_i+1/2$.

The bispectrum from the geometrical corrections is at first order in the Limber approximation

$$\begin{aligned}[b^{(\mathrm{corr})}_{\mathrm{geom}}]_{l_1l_2l_3} =& \mathfrak{l}(l_1,2)\mathfrak{l}(l_2,2)\mathfrak{l}(l_3,2)\Bigg\{\int_0^{\chi_S}\frac{d\chi}{\chi^4}T^2\left(\frac{\nu_1}{\chi}\right)P\left(\frac{\nu_1}{\chi}\right)T^2\left(\frac{\nu_2}{\chi}\right)P\left(\frac{\nu_2}{\chi}\right)W^3(\chi_S,\chi)g(\chi)+2\int_0^{\chi_S}\frac{d\chi}{\chi^3}T^2\left(\frac{\nu_1}{\chi}\right)P\left(\frac{\nu_1}{\chi}\right)W(\chi_S,\chi)\\
&\times\left[-\frac{g(\chi)}{\chi_S}\int_0^{\chi}\frac{d\chi'}{\chi'^2}T^2\left(\frac{\nu_2}{\chi'}\right)P\left(\frac{\nu_2}{\chi'}\right)W(\chi_S,\chi')g(\chi')+g'(\chi)\int_0^{\chi}\frac{d\chi'}{\chi'^2}T^2\left(\frac{\nu_2}{\chi'}\right)P\left(\frac{\nu_2}{\chi'}\right)W(\chi_S,\chi')g(\chi')\right]\Bigg\}\\
&-2\mathfrak{l}(l_1,2)\mathfrak{l}^2(l_2,2)\left[\begin{pmatrix}l_1&l_2&l_3\\0&2&-2\end{pmatrix}+\mathrm{c.c.}\right]\begin{pmatrix}l_1&l_2&l_3\\0&0&0\end{pmatrix}^{-1}\int_0^{\chi_S}\frac{d\chi}{\chi^3}T^2\left(\frac{\nu_1}{\chi}\right)P\left(\frac{\nu_1}{\chi}\right)W(\chi_S,\chi)\\
&\times\left[W(\chi_S,\chi)\int_0^{\chi}\frac{d\chi'}{\chi'^2}T^2\left(\frac{\nu_2}{\chi'}\right)P\left(\frac{\nu_2}{\chi'}\right)W(\chi_S,\chi')g(\chi')+\frac{\chi}{\chi_S}g(\chi)\int_0^{\chi}\frac{d\chi'}{\chi'^3}T^2\left(\frac{\nu_2}{\chi'}\right)P\left(\frac{\nu_2}{\chi'}\right)W(\chi_S,\chi')g(\chi')\right.\\
&\left.-\frac{g(\chi)\chi}{\chi_S}\int_0^{\chi_S}\frac{d\chi'}{\chi'^2}T^2\left(\frac{\nu_2}{\chi'}\right)P\left(\frac{\nu_2}{\chi'}\right)W^2(\chi_S,\chi')\right]+5\,\mathrm{perms}.\end{aligned} \tag{A3}$$

The bispectrum from the redshift corrections is at first order in the Limber approximation

$$[b^{(z)}_{\rm geom}]_{l_1l_2l_3} = \frac{1}{2}\text{ł}^2(l_1,2)\text{ł}(l_2,2)\left[\begin{pmatrix} l_1 & l_2 & l_3 \\ 2 & 0 & -2 \end{pmatrix} + \text{c.c.}\right]\begin{pmatrix} l_1 & l_2 & l_3 \\ 0 & 0 & 0 \end{pmatrix}^{-1}\int_0^{\chi_S}\frac{d\chi}{\chi^2}\frac{d\chi'}{\chi'^2}P\left(\frac{\nu_1}{\chi}\right)T^2\left(\frac{\nu_1}{\chi}\right)P\left(\frac{\nu_2}{\chi'}\right)T^2\left(\frac{\nu_2}{\chi'}\right)W(\chi_S,\chi)W(\chi_S,\chi')$$
$$\times\left\{\frac{1}{\chi_S^2\mathcal{H}_S}\left[2g'(\chi') - \nu_2^{3/2}\sqrt{\frac{2}{\pi}}g(\chi_S)\frac{1}{\chi'}j_{l_2}\left(\frac{\nu_2}{\chi'}\chi_S\right)\right] + \frac{2a_S}{3H_0^2\Omega_m\chi_S^2}\left[g(\chi_S) - \frac{g'(\chi_S)}{\mathcal{H}_S}\right]\nu_2^{5/2}\sqrt{\frac{2}{\pi}}\frac{1}{\chi'^2}j'_{l_2}\left(\frac{\nu_2}{\chi'}\chi_S\right)\right\}$$
$$+ 5\,\text{perms.} \tag{A4}$$

Note that for the redshift corrections we cannot use the Limber approximation on the spherical Bessel functions $j_{l_2}(\frac{\nu_2}{\chi'}\chi_S)$ and $j'_{l_2}(\frac{\nu_2}{\chi'}\chi_S)$. Indeed in this approximation $\chi' \simeq \chi_S$ and the bispectrum vanishes. Hence for these terms we perform the exact integral on χ'.

3. Standard dynamical term in the first-order Limber approximation

By applying the first-order Limber approximation given by Eq. (50) to Eq. (75), it is straightforward to compute the Limber-approximated expression of the standard dynamical term.

$$[b^{(\rm stan)}_{\rm dyn}]_{l_1l_2l_3} = \text{ł}(l_1,2)\text{ł}(l_2,2)\text{ł}(l_3,2)\frac{\nu_1^2\nu_2^2}{\nu_3^2}\frac{2}{3\Omega_m H_0^2}\int_0^{\chi_S}\frac{d\chi}{\chi^6}W^3(\chi_S,\chi)g(\chi)a(\chi)F_{2,N}\left(\frac{\nu_1}{\chi},\frac{\nu_2}{\chi},\frac{\nu_3}{\chi};\chi\right)T^2\left(\frac{\nu_1}{\chi}\right)P\left(\frac{\nu_1}{\chi}\right)T^2\left(\frac{\nu_2}{\chi}\right)P\left(\frac{\nu_2}{\chi}\right)$$
$$+ 5\,\text{perms.} \tag{A5}$$

APPENDIX B: DYNAMICAL CONTRIBUTIONS

We present here the computation of the dynamical scalar and tensor terms. The vector terms are shown in Sec. IV C. Let us start by the scalar terms. The sum of the two relativistic potentials gives, using Eqs. (31) and (32),

$$\frac{1}{2}(\phi_R^{(2)}(\vec{k}_3) + \psi_R^{(2)}(\vec{k}_3)) = T(k_1)T(k_2)F_{2,S}(\vec{k}_1,\vec{k}_2,\vec{k}_3)\Phi_{\vec{k}_1}\Phi_{\vec{k}_2}, \tag{B1}$$

where we define

$$F_{2,S}(k_1,k_2,k_3) \equiv \frac{\vec{k}_1\cdot\vec{k}_2 - 3(\hat{k}_3\cdot\vec{k}_1)(\hat{k}_3\cdot\vec{k}_2)}{6k_3^2}. \tag{B2}$$

For the bispectrum one finds

$$[b^{(\rm corr)}_{\rm dyn,S}]_{l_1l_2l_3} = -\text{ł}(l_1,2)\text{ł}(l_2,2)\text{ł}(l_3,2)\int_0^{\chi_S}d\chi_1 d\chi_2 d\chi_3 W(\chi_S,\chi_1)W(\chi_S,\chi_2)W(\chi_S,\chi_3)\int\frac{2k_1^2dk_1}{\pi}\frac{2k_2^2dk_2}{\pi}\frac{2k_3^2dk_3}{\pi}$$
$$\times T^2(k_1)T^2(k_2)F_{2,S}(k_1,k_2,k_3)P(k_1)P(k_2)\int_0^\infty d\chi\chi^2 j_{l_1}(k_1\chi_1)j_{l_1}(k_1\chi)j_{l_2}(k_2\chi_2)j_{l_2}(k_2\chi)j_{l_3}(k_3\chi_3)j_{l_3}(k_3\chi)$$
$$+ 5\,\text{perms.} \tag{B3}$$

We now compute the tensor terms. We start with the contribution coming from the second line of Eq. (29). Using Eq. (34), after few manipulations one finds

$$-\frac{1}{4}h_{rr}(k_3) = -\frac{5}{3}\left[1 - 3\frac{j_1(k_3\eta)}{k_3\eta}\right]\frac{T(k_1)T(k_2)}{k_3^4}\Phi_{\vec{k}_1}\Phi_{\vec{k}_2}\left[\frac{1}{8}(k_3^4 + (k_1^2-k_2^2)^2 - 2k_3^2(k_1^2+k_2^2))(1+(\hat{k}_3\cdot\hat{n})^2)\right.$$
$$\left. + (\vec{k}_3\cdot\hat{n})(k_2^2(\vec{k}_1\cdot\hat{n}) + k_1^2(\vec{k}_2\cdot\hat{n})) - k_3^2(\vec{k}_1\cdot\hat{n})(\vec{k}_2\cdot\hat{n})\right]. \tag{B4}$$

The computation of this contribution is similar to the one of the vector contribution, Eq. (76). The only new term is the one proportional to the product $(\vec{k}_1\cdot\hat{n})(\vec{k}_2\cdot\hat{n})$. We use the expansion of Eq. (78) twice. As a result, in the computation of the $a_{E,lm}$ we obtain an integral over $d^3\vec{k}_3$ with four spherical harmonics. This integral gives rise to a product of two Gaunt integrals. We then compute the bispectrum regrouping the appropriate Gaunt integrals such that the summation in Eq. (80) can be applied twice. This generates two Wigner $6-j$ symbols, with terms of the form $l_i\pm 2$. With this the bispectrum from the tensor contribution $-\frac{1}{4}h_{rr}$ is

$$
\begin{aligned}
[b_{\rm dyn}^{\rm (corr)}]_{l_1l_2l_3} =& \frac{5}{3}\text{Ɨ}(l_1,2)\text{Ɨ}(l_2,2)\text{Ɨ}(l_3,2)\int_0^{\chi_S} d\chi_1 d\chi_2 d\chi_3 W(\chi_1,\chi_S)W(\chi_2,\chi_S)W(\chi_3,\chi_S)\\
&\times\int\frac{2k_1^2dk_1}{\pi}\frac{2k_2^2dk_2}{\pi}\frac{2k_3^2dk_3}{\pi}T^2(k_1)T^2(k_2)P(k_1)P(k_2)\\
&\times\left[1-\frac{3j_1(k_3(\eta_0-\chi_3))}{k_3(\eta_0-\chi_3)}\right]\left\{\frac{k_3^4+(k_1^2-k_2^2)^2-2k_3^2(k_1^2+k_2^2)}{8k_3^4}\right.\\
&\times\int_0^\infty d\chi\chi^2 j_{l_1}(k_1\chi_1)j_{l_1}(k_1\chi)j_{l_2}(k_2\chi_2)j_{l_2}(k_2\chi)\left(1-\frac{\partial^2_{\chi_3}}{k_3^2}\right)j_{l_3}(k_3\chi_3)j_{l_3}(k_3\chi)\\
&+2\frac{k_1k_2^2}{k_3^4}\sum_{\substack{l_1'=l_1\pm1\\ l_3'=l_3\pm1}}(-1)^{l_2}i^{l_1'-l_1+1}(2l_1'+1)(2l_3'+1)\begin{Bmatrix}l_1 & l_2 & l_3\\ l_3' & 1 & l_1'\end{Bmatrix}\\
&\times\begin{pmatrix}l_1 & l_1' & 1\\ 0 & 0 & 0\end{pmatrix}\begin{pmatrix}l_3 & l_3' & 1\\ 0 & 0 & 0\end{pmatrix}\begin{pmatrix}l_1' & l_2 & l_3'\\ 0 & 0 & 0\end{pmatrix}\begin{pmatrix}l_1 & l_2 & l_3\\ 0 & 0 & 0\end{pmatrix}^{-1}\\
&\times\int_0^\infty d\chi\chi^2 j_{l_1}(k_1\chi_1)j_{l_1'}(k_1\chi)j_{l_2}(k_2\chi_2)j_{l_2}(k_2\chi)\partial_{\chi_3}j_{l_3'}(k_3\chi_3)j_{l_3'}(k_3\chi)\\
&+\frac{k_1k_2}{k_3^2}\sum_{\substack{l_1'=l_1\pm1\\ l_2'=l_2\pm1}}\sum_{\substack{l_3'=l_3\pm1\\ l_3''=l_3'\pm1}}(-1)^{l_3}i^{l_1'-l_1+l_2'-l_2}(2l_1'+1)(2l_2'+1)(2l_3'+1)(2l_3''+1)\\
&\times\begin{Bmatrix}l_1 & l_3 & l_2\\ 1 & l_2' & l_3'\end{Bmatrix}\begin{Bmatrix}l_1 & l_2' & l_3'\\ l_3'' & 1 & l_1'\end{Bmatrix}\begin{pmatrix}l_1 & l_1' & 1\\ 0 & 0 & 0\end{pmatrix}\begin{pmatrix}l_2 & l_2' & 1\\ 0 & 0 & 0\end{pmatrix}\begin{pmatrix}l_3 & l_3' & 1\\ 0 & 0 & 0\end{pmatrix}\begin{pmatrix}l_1' & l_2' & l_3''\\ 0 & 0 & 0\end{pmatrix}\begin{pmatrix}l_1 & l_2 & l_3\\ 0 & 0 & 0\end{pmatrix}^{-1}\\
&\times\left.\int_0^\infty d\chi\chi^2 j_{l_1}(k_1\chi_1)j_{l_1'}(k_1\chi)j_{l_2}(k_2\chi_2)j_{l_2'}(k_2\chi)j_{l_3''}(k_3\chi_3)j_{l_3''}(k_3\chi)\right\}+5\,\text{perms.}
\end{aligned}
\tag{B5}
$$

We then compute the tensor term in the third line of Eq. (29) that reads

$$
\begin{aligned}
-\frac{1}{2}\not{\partial}_1 h_r(\hat{n}\chi) =& -\frac{10}{3}\int\frac{d^3\vec{k}_3}{(2\pi)^3}\frac{d^3\vec{k}_1d^3\vec{k}_2}{(2\pi)^3}\delta_D(\vec{k}_3-\vec{k}_1-\vec{k}_2)[1-3j_1(k_3\eta)/(k_3\eta)]\frac{T(k_1)T(k_2)}{k_3^4}\Phi_{\vec{k}_1}\Phi_{\vec{k}_2}\\
&\times\not{\partial}\left\{e^{i\vec{k}_3\cdot\hat{n}\chi}\left[\frac{1}{8}(k_3^4+(k_1^2-k_2^2)^2-2k_3^2(k_1^2+k_2^2))(\hat{k}_3\cdot\hat{n})(\hat{k}_3\cdot\hat{e}_+)+k_1k_2k_3(\hat{k}_3\cdot\hat{e}_+)(k_2(\hat{k}_1\cdot\hat{n})+k_1(\hat{k}_2\cdot\hat{n}))\right.\right.\\
&\left.\left.+\frac{1}{2}k_1k_2(k_2^2-k_1^2-k_3^2)((\hat{k}_1\cdot\hat{e}_+)(\hat{k}_2\cdot\hat{n})-(\hat{k}_2\cdot\hat{e}_+)(\hat{k}_1\cdot\hat{n}))\right]\right\}.
\end{aligned}
\tag{B6}
$$

The computation of this term is similar to the one of the vector term in Eq. (82) and we find for the bispectrum

$$
\begin{aligned}
[b_{\rm dyn}^{(\rm corr)}]_{l_1 l_2 l_3} &= \frac{10}{3}\text{ł}(l_1,2)\text{ł}(l_2,2)\text{ł}(l_3,2)\int_0^{\chi_S} d\chi_1 d\chi_2 d\chi_3 W(\chi_1,\chi_S)W(\chi_2,\chi_S) \\
&\times \frac{1}{\chi_3^2}\int \frac{2k_1^2dk_1}{\pi}\frac{2k_2^2dk_2}{\pi}\frac{2k_3^2dk_3}{\pi} T^2(k_1)T^2(k_2)P(k_1)P(k_2) \\
&\times \left[1-\frac{3j_1(k_3(\eta_0-\chi_3))}{k_3(\eta_0-\chi_3)}\right]\left\{\frac{k_3^4+(k_1^2-k_2^2)^2-2k_3^2(k_1^2+k_2^2)}{8k_3^5}\right. \\
&\times \sum_{l_3'=l_3\pm1} i^{l_3'-l_3+1}\frac{2l_3'+1}{2l_3+1}\begin{pmatrix} l_3 & l_3' & 1\\ 0 & 0 & 0\end{pmatrix}\begin{pmatrix} l_1 & l_2 & l_3\\ 0 & 0 & 0\end{pmatrix}^{-1} \\
&\times \left[(l_3'^2+l_3'+2)(l_3'+1)l_3'\begin{pmatrix} l_3 & l_3' & 1\\ 0 & 0 & 0\end{pmatrix}+\sqrt{2l_3'(l_3'+1)}(3l_3'^2+3l_3'-2)\begin{pmatrix} l_3 & l_3' & 1\\ 0 & 1 & -1\end{pmatrix}\right] \\
&\times \int_0^\infty d\chi\chi^2 j_{l_1}(k_1\chi_1)j_{l_1}(k_1\chi)j_{l_2}(k_2\chi_2)j_{l_2}(k_2\chi)j_{l_3}(k_3\chi_3)j_{l_3'}(k_3\chi) \\
&- \left.\frac{k_1k_2^2}{k_3^4}\sum_{\substack{l_1'=l_1\pm1\\ l_3'=l_3\pm1}}(-1)^{l_2}i^{l_1'-l_1+1}\frac{(2l_1'+1)(2l_3'+1)}{\text{ł}(l_3,2)^2}\begin{Bmatrix} l_1 & l_3 & l_2\\ l_3' & l_1' & 1\end{Bmatrix}\begin{pmatrix} l_1 & l_1' & 1\\ 0 & 0 & 0\end{pmatrix}\begin{pmatrix} l_1' & l_2 & l_3'\\ 0 & 0 & 0\end{pmatrix}\begin{pmatrix} l_1 & l_2 & l_3\\ 0 & 0 & 0\end{pmatrix}^{-1}\right. \\
&\times \left[(l_3'^2+l_3'+2)(l_3'+1)l_3'\begin{pmatrix} l_3 & l_3' & 1\\ 0 & 0 & 0\end{pmatrix}+\sqrt{2l_3'(l_3'+1)}(3l_3'^2+3l_3'-2)\begin{pmatrix} l_3 & l_3' & 1\\ 0 & 1 & -1\end{pmatrix}\right] \\
&\times \int_0^\infty d\chi\chi^2 j_{l_1}(k_1\chi_1)j_{l_1'}(k_1\chi)j_{l_2}(k_2\chi_2)j_{l_2}(k_2\chi)j_{l_3'}(k_3\chi_3)j_{l_3'}(k_3\chi) \\
&- \chi_3\frac{(k_3^2+k_1^2-k_2^2)k_1k_2}{k_3^4}\sum_{\substack{l_1'=l_1\pm1\\ l_2'=l_2\pm1}}\sum_{\substack{l_3'=l_3\pm1\\ l_3''=l_3'\pm1}}(-1)^{l_3}\frac{i^{l_1'-l_1+l_2'-l_2}}{\text{ł}(l_3,2)^2}(2l_1'+1)(2l_2'+1)(2l_3'+1)(2l_3''+1) \\
&\times \begin{Bmatrix} l_1 & l_3 & l_2\\ 1 & l_2' & l_3'\end{Bmatrix}\begin{Bmatrix} l_1 & l_2' & l_3'\\ l_3'' & 1 & l_1'\end{Bmatrix}\begin{pmatrix} l_1 & l_1' & 1\\ 0 & 0 & 0\end{pmatrix}\begin{pmatrix} l_2 & l_2' & 1\\ 0 & 0 & 0\end{pmatrix}\begin{pmatrix} l_1' & l_2' & l_3''\\ 0 & 0 & 0\end{pmatrix}\begin{pmatrix} l_1 & l_2 & l_3\\ 0 & 0 & 0\end{pmatrix}^{-1} \\
&\times \left[4(l_3''^2+l_3''+2)\begin{pmatrix} l_3 & l_3' & 1\\ 0 & 0 & 0\end{pmatrix}\begin{pmatrix} l_3' & l_3'' & 1\\ 0 & 0 & 0\end{pmatrix}+4(l_3''^2+l_3''+2)\begin{pmatrix} l_3 & l_3' & 1\\ 0 & 1 & -1\end{pmatrix}\begin{pmatrix} l_3' & l_3'' & 1\\ -1 & 0 & 1\end{pmatrix}\right. \\
&+ \sqrt{2l_3''(l_3''+1)}(l_3''^2+l_3''+6)\begin{pmatrix} l_3 & l_3' & 1\\ 0 & 0 & 0\end{pmatrix}\begin{pmatrix} l_3' & l_3'' & 1\\ 0 & -1 & 1\end{pmatrix}+8\sqrt{2l_3''(l_3''+1)}\begin{pmatrix} l_3 & l_3' & 1\\ 0 & 1 & -1\end{pmatrix}\begin{pmatrix} l_3' & l_3'' & 1\\ -1 & 1 & 0\end{pmatrix} \\
&\left.\left.+ 2\text{ł}(l_3'',2)\begin{pmatrix} l_3 & l_3' & 1\\ 0 & -1 & 1\end{pmatrix}\begin{pmatrix} l_3' & l_3'' & 1\\ 1 & -2 & 1\end{pmatrix}\right]\int_0^\infty d\chi\chi^2 j_{l_1}(k_1\chi_1)j_{l_1'}(k_1\chi)j_{l_2}(k_2\chi_2)j_{l_2'}(k_2\chi)j_{l_3''}(k_3\chi_3)j_{l_3''}(k_3\chi)\right\} \\
&+ 5\,\text{perms.}
\end{aligned}
\tag{B7}
$$

Finally we compute the bispectrum of the boundary tensor term, i.e. the last term in Eq. (29)

$$
\begin{aligned}
-\frac{1}{4}h(\hat{n}\chi_S) &= -\frac{5}{6}\int\frac{d^3\vec{k}_3}{(2\pi)^3}\frac{d^3\vec{k}_1 d^3\vec{k}_2}{(2\pi)^3}\delta_D(\vec{k}_3-\vec{k}_1-\vec{k}_2)[1-3j_1(k_3\eta)/(k_3\eta)]\frac{T(k_1)T(k_2)}{k_3^4}\Phi_{\vec{k}_1}\Phi_{\vec{k}_2}2e^{i\vec{k}_3\cdot\hat{n}\chi_S} \\
&\times\left[\frac{1}{4}(k_3^4+(k_1^2-k_2^2)^2-2k_3^2(k_1^2+k_2^2))(\hat{k}_3\cdot\hat{e}_+)^2+2(\vec{k}_3\cdot\hat{e}_+)(k_2^2(\vec{k}_1\cdot\hat{e}_+)+k_1^2(\vec{k}_2\cdot\hat{e}_+))\right. \\
&\left.-2k_3^2(\vec{k}_1\cdot\hat{e}_+)(\vec{k}_2\cdot\hat{e}_+)\right].
\end{aligned}
\tag{B8}
$$

The computation of this term is similar to the previous ones and its bispectrum reads

$$
\begin{aligned}
[b_{\rm dyn}^{\rm (corr)}]_{l_1 l_2 l_3} &= \frac{5}{3}\mathfrak{l}(l_1,2)\mathfrak{l}(l_2,2)\mathfrak{l}(l_3,2)\int_0^{\chi_S} d\chi_1 d\chi_2 W(\chi_1,\chi_S)W(\chi_2,\chi_S) \\
&\times \int \frac{2k_1^2 dk_1}{\pi}\frac{2k_2^2 dk_2}{\pi}\frac{2k_3^2 dk_3}{\pi} T^2(k_1)T^2(k_2)P(k_1)P(k_2)\left[1-\frac{3j_1(k_3(\eta_0-\chi_S))}{k_3(\eta_0-\chi_S)}\right] \\
&\times \left\{-\frac{k_3^4+(k_1^2-k_2^2)^2-2k_3^2(k_1^2+k_2^2)}{16k_3^4}\frac{1}{k_3^2\chi_S^2}\int_0^\infty d\chi\chi^2 j_{l_1}(k_1\chi_1)j_{l_1}(k_1\chi)j_{l_2}(k_2\chi_2)j_{l_2}(k_2\chi)j_{l_3}(k_3\chi_S)j_{l_3}(k_3\chi)\right. \\
&+ \frac{2k_1k_2^2}{k_3^3}\sum_{\substack{l_1'=l_1\pm1\\ l_3'=l_3\pm1}}(-1)^{l_2}i^{l_1'-l_1+1}\frac{(2l_1'+1)(2l_3'+1)}{\mathfrak{l}(l_3,2)^2}\begin{Bmatrix} l_1 & l_3 & l_2\\ l_3' & l_1' & 1\end{Bmatrix}\begin{pmatrix} l_1 & l_1' & 1\\ 0 & 0 & 0\end{pmatrix}\begin{pmatrix} l_1' & l_2 & l_3'\\ 0 & 0 & 0\end{pmatrix}\begin{pmatrix} l_1 & l_2 & l_3\\ 0 & 0 & 0\end{pmatrix}^{-1} \\
&\times\left[4(l_3'+1)l_3'\begin{pmatrix} l_3 & l_3' & 1\\ 0 & 0 & 0\end{pmatrix}+\sqrt{2l_3'(l_3'+1)}(l_3'^2+l_3'+2)\begin{pmatrix} l_3 & l_3' & 1\\ 0 & 1 & -1\end{pmatrix}\right] \\
&\times\frac{1}{k_3\chi_S}\int_0^\infty d\chi\chi^2 j_{l_1}(k_1\chi_1)j_{l_1'}(k_1\chi)j_{l_2}(k_2\chi_2)j_{l_2}(k_2\chi)j_{l_3'}(k_3\chi_3)j_{l_3'}(k_3\chi) \\
&+ \frac{2k_1k_2}{k_3^2}\sum_{\substack{l_1'=l_1\pm1\\ l_2'=l_2\pm1}}\sum_{\substack{l_3'=l_3\pm1\\ l_3''=l_3'\pm1}}(-1)^{l_3}\frac{i^{l_1'-l_1+l_2'-l_2}}{\mathfrak{l}(l_3,2)^2}(2l_1'+1)(2l_2'+1)(2l_3'+1)(2l_3''+1)\begin{Bmatrix} l_1 & l_3 & l_2\\ 1 & l_2' & l_3'\end{Bmatrix}\begin{Bmatrix} l_1 & l_2' & l_3'\\ l_3'' & 1 & l_1'\end{Bmatrix} \\
&\times\begin{pmatrix} l_1 & l_1' & 1\\ 0 & 0 & 0\end{pmatrix}\begin{pmatrix} l_2 & l_2' & 1\\ 0 & 0 & 0\end{pmatrix}\begin{pmatrix} l_1' & l_2' & l_3''\\ 0 & 0 & 0\end{pmatrix}\begin{pmatrix} l_1 & l_2 & l_3\\ 0 & 0 & 0\end{pmatrix}^{-1}\left[4\begin{pmatrix} l_3 & l_3' & 1\\ 0 & 1 & -1\end{pmatrix}\begin{pmatrix} l_3' & l_3'' & 1\\ -1 & 0 & 1\end{pmatrix}\right. \\
&+2\sqrt{2l_3''(l_3''+1)}\begin{pmatrix} l_3 & l_3' & 1\\ 0 & 0 & 0\end{pmatrix}\begin{pmatrix} l_3' & l_3'' & 1\\ 0 & -1 & 1\end{pmatrix}+2\sqrt{2l_3''(l_3''+1)}\begin{pmatrix} l_3 & l_3' & 1\\ 0 & 1 & -1\end{pmatrix}\begin{pmatrix} l_3' & l_3'' & 1\\ -1 & 1 & 0\end{pmatrix} \\
&\left.\left.+\mathfrak{l}(l_3'',2)\begin{pmatrix} l_3 & l_3' & 1\\ 0 & -1 & 1\end{pmatrix}\begin{pmatrix} l_3' & l_3'' & 1\\ 1 & -2 & 1\end{pmatrix}\right]\int_0^\infty d\chi\chi^2 j_{l_1}(k_1\chi_1)j_{l_1'}(k_1\chi)j_{l_2}(k_2\chi_2)j_{l_2'}(k_2\chi)j_{l_3''}(k_3\chi_S)j_{l_3''}(k_3\chi)\right\} \\
&+ 5\,\text{perms.}
\end{aligned}
\tag{B9}
$$

APPENDIX C: SPIN-WEIGHTED SPHERICAL HARMONICS

The spin-weighted spherical harmonics ${}_sY_{lm}(\hat{n})$ are related to the standard spherical harmonics $Y_{lm}(\hat{n})$ by

$$\mathfrak{l}(l,s)\,{}_sY_{lm}(\hat{n}) = \eth^s Y_{lm}(\hat{n}), \tag{C1}$$

$$\mathfrak{l}(l,s)\,{}_{-s}Y_{lm}(\hat{n}) = (-1)^s\bar{\eth}^s Y_{lm}(\hat{n}), \tag{C2}$$

for $s \geq 0$ and $|s| \leq l$. The coefficient $\mathfrak{l}(l,s)$ is defined as

$$\mathfrak{l}(l,s) \equiv \sqrt{\frac{(l+s)!}{(l-s)!}}. \tag{C3}$$

Let us recall here a few useful relations obeyed by the spin-weighted spherical harmonics,

$${}_sY^*_{lm}(\hat{n}) = (-1)^{m+s}\,{}_{-s}Y_{l,-m}(\hat{n}), \tag{C4}$$

$$\bar{\eth}\eth Y_{lm}(\hat{n}) = -\mathfrak{l}^2(l,1)Y_{lm} = -l(l+1)Y_{lm}(\hat{n}), \tag{C5}$$

$$\int d^2\hat{n}\,{}_sY_{lm}(\hat{n})\,{}_sY^*_{l'm'}(\hat{n}) = \delta_{ll'}\delta_{mm'}, \tag{C6}$$

$$\sum_{lm}{}_sY_{lm}(\hat{n})\,{}_sY^*_{lm}(\hat{n}') = \delta(\hat{n}-\hat{n}'). \tag{C7}$$

The operators $\eth$ and $\bar{\eth}$ satisfy the commutation relation

$$(\bar{\eth}\eth - \eth\bar{\eth})\,{}_sY_{lm} = 2s\,{}_sY_{lm}, \tag{C8}$$

such that

$$\bar{\eth}\eth^2 Y_{lm} = -\frac{\mathfrak{l}^2(l,2)}{\mathfrak{l}^2(l,1)}\eth Y_{lm}. \tag{C9}$$

The same relation holds when $\eth$ and $\bar{\eth}$ are interchanged. From this relation we deduce that

$$\bar{\eth}^2\eth^2 Y_{lm} = \mathfrak{l}^2(l,2)Y_{lm}. \tag{C10}$$

Dropping the boundary term when using integration by parts is valid as long as the integrand has spin zero, i.e. $\int d^2\hat{n}\,\eth([\text{spin} = -1]) = \int d^2\hat{n}\,\bar{\eth}([\text{spin} = 1]) = 0$.

[1] I. Debono, A. Rassat, A. Réfrégier, A. Amara, and T. D. Kitching, Ann. Phys. (Leipzig) **19**, 324 (2010).
[2] T. Giannantonio, C. Porciani, J. Carron, A. Amara, and A. Pillepich, Mon. Not. R. Astron. Soc. **422**, 2854 (2012)
[3] J. Berge, A. Amara, and A. Refregier, Astrophys. J. **712**, 992 (2010).
[4] F. Bernardeau, Y. Mellier, and L. van Waerbeke, Astron. Astrophys. **389**, L28 (2002).
[5] M. Takada and B. Jain, Mon. Not. R. Astron. Soc. **344**, 857 (2003).
[6] F. Pace, L. Moscardini, M. Bartelmann, E. Branchini, K. Dolag, M. Grossi, and S. Matarrese, Mon. Not. R. Astron. Soc. **411**, 595 (2011).
[7] D. Jeong, F. Schmidt, and E. Sefusatti, Phys. Rev. D **83**, 123005 (2011).
[8] B. M. Schaefer, A. Grassi, M. Gerstenlauer, and C. T. Byrnes, arXiv:1107.1656v1
[9] F. Bernardeau, L. van Waerbeke, and Y. Mellier, Astron. Astrophys. **322**, 1 (1997).
[10] A. Cooray and W. Hu, Astrophys. J. **548**, 7 (2001).
[11] F. Bernardeau, Y. Mellier, and L. van Waerbeke, Astron. Astrophys. **389**, L28 (2002).
[12] A. Cooray and W. Hu, Astrophys. J. **574**, 19 (2002).
[13] M. Takada and B. Jain, Mon. Not. R. Astron. Soc. **344**, 857 (2003).
[14] S. Dodelson, E W. Kolb, S. Matarrese, A. Riotto, and P. Zhang, Phys. Rev. D **72**, 103004 (2005).
[15] C. Shapiro and A. Cooray, J. Cosmol. Astropart. Phys. 3 (2006) 007.
[16] E. Krause and C. M. Hirata, Astron. Astrophys. **523**, A28 (2010).
[17] S. Dodelson and P. Zhang, Phys. Rev. D **72**, 083001 (2005).
[18] P. Schneider, L. van Waerbeke, B. Jain, and G. Kruse, Mon. Not. R. Astron. Soc. **296**, 873 (1998).
[19] N. Bartolo, S. Matarrese, and A. Riotto, Phys. Rev. Lett. **93**, 231301 (2004).
[20] L. Boubekeur, P. Creminelli, J. Norena, and F. Vernizzi, J. Cosmol. Astropart. Phys. 08 (2008) 028.
[21] C. Pitrou, J.-P. Uzan, and F. Bernardeau, J. Cosmol. Astropart. Phys. 07 (2010) 003.
[22] P. Creminelli, C. Pitrou, and F. Vernizzi, J. Cosmol. Astropart. Phys. 11 (2011) 025.
[23] N. Bartolo, S. Matarrese, and A. Riotto, J. Cosmol. Astropart. Phys. 02 (2012) 017.
[24] J. Yoo, A. L. Fitzpatrick, and M. Zaldarriaga, Phys. Rev. D **80**, 083514 (2009).
[25] C. Bonvin and R. Durrer, Phys. Rev. D **84**, 063505 (2011).
[26] A. Challinor and A. Lewis, Phys. Rev. D **84**, 043516 (2011).
[27] T. Baldauf, U. Seljak, L. Senatore, and M. Zaldarriaga, J. Cosmol. Astropart. Phys. 10 (2011) 031.
[28] J. Yoo, N. Hamaus, U. Seljak, and M. Zaldarriaga, arXiv:1109.0998v1
[29] F. Bernardeau, C. Bonvin, and F. Vernizzi, Phys. Rev. D **81**, 083002 (2010).
[30] R. Sachs, Proc. R. Soc. A **264**, 309 (1961).
[31] M. Kamionkowski, A. Kosowsky, and A. Stebbins, Phys. Rev. D **55**, 7368 (1997).
[32] M. Zaldarriaga and U. Seljak, Phys. Rev. D **55**, 1830 (1997).
[33] E. Bertschinger, in *Proceedings of the Summer School on Cosmology and Large Scale Structure (Session 60) held 1-28 August 1993 in Les Houches, France*, edited by R. Schaeffer, J. Silk, M. Spiro, and J. Zinn-Justin, (Elsevier, New York, 1996), p. 273.
[34] M. Bruni, S. Matarrese, S. Mollerach, and S. Sonego, Classical Quantum Gravity **14**, 2585 (1997).
[35] J.-P. Uzan and F. Bernardeau, Phys. Rev. D **63**, 023004 (2000).
[36] W. Hu, Phys. Rev. D **62**, 043007 (2000).
[37] T. Okamoto and W. Hu, Phys. Rev. D **67**, 083002 (2003).
[38] R. de Putter and M. Takada, Phys. Rev. D **82**, 103522 (2010).
[39] C. Bonvin, Phys. Rev. D **78**, 123530 (2008).
[40] C. M. Hirata and U. Seljak, Phys. Rev. D **68**, 083002 (2003).
[41] J. M. Maldacena, J. High Energy Phys. 05 (2003) 013.
[42] F. Bernardeau, L. van Waerbeke, and Y. Mellier, Astron. Astrophys. **397**, 405 (2003).
[43] P. J. E. Peebles, *The Large-Scale Structure of the Universe* (Princeton University Press, Princeton, NJ, 1980).
[44] F. Bernardeau, S. Colombi, E. Gaztañaga, and R. Scoccimarro, Phys. Rep. **367**, 1 (2002).
[45] F. Bernardeau and P. Brax, J. Cosmol. Astropart. Phys. 06 (2011) 019.
[46] A. L. Fitzpatrick, L. Senatore, and M. Zaldarriaga, J. Cosmol. Astropart. Phys. 05 (2010) 004.
[47] N. Bartolo, S. Matarrese, and A. Riotto, J. Cosmol. Astropart. Phys. 05 (2006) 010.
[48] L. Boubekeur, P. Creminelli, G. D'Amico, J. Noreña, and F. Vernizzi, J. Cosmol. Astropart. Phys. 08 (2009) 029.
[49] A. Lewis and A. Challinor, Phys. Rep. **429**, 1 (2006).
[50] J. M. Bardeen, J. R. Bond, N. Kaiser, and A. S. Szalay, Astrophys. J. **304**, 15 (1986).
[51] N. Kaiser, Astrophys. J. **388**, 272 (1992).
[52] M. LoVerde and N. Afshordi, Phys. Rev. D **78**, 123506 (2008).
[53] E. Komatsu and D. N. Spergel, Phys. Rev. D **63**, 063002 (2001).
[54] D. H. Lyth and D. Wands, Phys. Lett. B **524**, 5 (2002).
[55] F. Bernardeau and J.-P. Uzan, Phys. Rev. D **66**, 103506 (2002).
[56] G. Dvali, A. Gruzinov, and M. Zaldarriaga, Phys. Rev. D **69**, 083505 (2004).
[57] F. Vernizzi and D. Wands, J. Cosmol. Astropart. Phys. 05 (2006) 019.
[58] D. S. Salopek and J. R. Bond, Phys. Rev. D **42**, 3936 (1990).
[59] E. Sefusatti and E. Komatsu, Phys. Rev. D **76**, 083004 (2007).
[60] E. Komatsu, D, N. Spergel, and B. D. Wandelt, Astrophys. J. **634**, 14 (2005).
[61] D. Babich, P. Creminelli, and M. Zaldarriaga, J. Cosmol. Astropart. Phys. 08 (2004) 009.
[62] D. N. Limber, Astrophys. J. **117**, 134 (1953).

Chapter 10

Appendix: Spherical harmonics and notebooks

Contents

In this appendix, we summarise several equations and results concerning (spin weighted) spherical harmonics. We also describe the structure of my MATHEMATICA notebooks used throughout this project.

10.1 Spin weighted spherical harmonics

The spin weighted spherical harmonics ${}_sY_{lm}(\hat{n})$ are related to the (regular) spherical harmonics $Y_{lm}(\hat{n})$ by acting with spin raising and lowering operators upon them.

$$\text{ł}(l,s)\ {}_sY_{lm}(\hat{n}) = \eth^s Y_{lm}(\hat{n}), \tag{10.1}$$

$$\text{ł}(l,s)\ {}_{-s}Y_{lm}(\hat{n}) = (-1)^s \overline{\eth}^s Y_{lm}(\hat{n}), \tag{10.2}$$

where $0 \leq s \leq l$. The coefficient $\text{ł}(l,s)$ is defined by $\text{ł}(l,s) \equiv \sqrt{\frac{(l+s)!}{(l-s)!}}$, and the spin raising and lowering operators are given, in spherical coordinates, by

$$\eth({}_sX) = -(\sin\theta)^s \left(\frac{\partial}{\partial\theta} + \frac{i}{\sin\theta}\frac{\partial}{\partial\varphi}\right)(\sin\theta)^{-s}({}_sX), \tag{10.3}$$

$$\overline{\eth}({}_sX) = -(\sin\theta)^{-s} \left(\frac{\partial}{\partial\theta} - \frac{i}{\sin\theta}\frac{\partial}{\partial\varphi}\right)(\sin\theta)^{s}({}_sX), \tag{10.4}$$

where ${}_sX$ is a spin-s field. The spin weighted spherical harmonics obey the following relations,

$$
\begin{aligned}
{}_sY^*_{lm}(\hat{n}) &= (-1)^{m+s}\,{}_{-s}Y_{l,-m}(\hat{n}), && (10.5)\\
\overline{\eth}\eth Y_{lm}(\hat{n}) &= -\text{ł}^2(l,1)Y_{lm} = -l(l+1)Y_{lm}(\hat{n}), && (10.6)\\
\int \mathrm{d}^2\hat{n}\ {}_sY_{lm}(\hat{n})\ {}_sY^*_{l'm'}(\hat{n}) &= \delta_{ll'}\delta_{mm'}, && (10.7)\\
\sum_{lm} {}_sY_{lm}(\hat{n})\,{}_sY^*_{lm}(\hat{n}') &= \delta_{\mathrm{D}}(\hat{n}-\hat{n}'). && (10.8)
\end{aligned}
$$

These are all generalisations or implications of the properties of regular spherical harmonics. The operators $\eth$ and $\overline{\eth}$ satisfy the Leibniz rule and the commutation relation

$$(\overline{\eth}\eth - \eth\overline{\eth})\ {}_sY_{lm} = 2s\ {}_sY_{lm}, \tag{10.9}$$

such that

$$\overline{\eth}\eth^2\ Y_{lm} = -\frac{\text{ł}^2(l,2)}{\text{ł}^2(l,1)}\eth\ Y_{lm}. \tag{10.10}$$

The same relation holds when $\eth$ and $\overline{\eth}$ are interchanged. From this we deduce that

$$\overline{\eth}^2\eth^2\ Y_{lm} = \text{ł}^2(l,2)\ Y_{lm}. \tag{10.11}$$

Dropping the boundary term when using integration by parts is valid as long as the integrand has spin zero, i.e.

$$\int \mathrm{d}^2\hat{n}\ \eth([\text{spin} = -1]) = \int \mathrm{d}^2\hat{n}\overline{\eth}([\text{spin} = 1]) = 0. \tag{10.12}$$

The angular integral of three ${}_sY_{lm}$'s, which is called a Gaunt integral, is denoted by

$$\begin{Bmatrix} l_1 & l_2 & l_3 \\ m_1 & m_2 & m_3 \\ s_1 & s_2 & s_3 \end{Bmatrix} \equiv \int \mathrm{d}^2\hat{n}\ {}_{s1}Y_{l_1m_1}(\hat{n})\ {}_{s2}Y_{l_2m_2}(\hat{n})\ {}_{s3}Y_{l_3m_3}(\hat{n}). \tag{10.13}$$

This can be written in terms of Wigner-3j symbols as

$$\begin{Bmatrix} l_1 & l_2 & l_3 \\ m_1 & m_2 & m_3 \\ s_1 & s_2 & s_3 \end{Bmatrix} = \sqrt{\frac{(2l_1+1)(2l_2+1)(2l_3+1)}{4\pi}} \begin{pmatrix} l_1 & l_2 & l_3 \\ m_1 & m_2 & m_3 \end{pmatrix} \begin{pmatrix} l_1 & l_2 & l_3 \\ s_1 & s_2 & s_3 \end{pmatrix}. \tag{10.14}$$

Wigner-3j symbols have many symmetries and satisfy various relations, of which the following is the most important to us:

$$\begin{pmatrix} l_1 & l_2 & l_3 \\ m_1 & m_2 & m_3 \end{pmatrix} = (-1)^{l_1+l_2+l_3} \begin{pmatrix} l_1 & l_2 & l_3 \\ -m_1 & -m_2 & -m_3 \end{pmatrix}. \tag{10.15}$$

10.2 Products of fields

In this section, we expand a spin-2 product of two fields into spin-2 spherical harmonics, see Sec. 8.2.2 for more explanation. We will analyse 5 different cases, covering all the terms of the second-order shear γ given in eq. (6.20). The first case will be analysed in detail, but we will merely state the result for the other cases as the computation is similar.

Case $\left(\eth^2\Xi_1\right)\Xi_2$

Let $\Xi_1(\hat{n})$ and $\Xi_2(\hat{n})$ be spin-0 fields. Therefore, they can naturally be expanded in spin-0 spherical harmonics with expansion coefficients $a_{lm}^{\Xi_1}$ and $a_{lm}^{\Xi_2}$ respectively,

$$\Xi_1(\hat{n}) = \sum_{l,m} a_{lm}^{\Xi_1} Y_l^m(\hat{n}) \qquad \text{and} \qquad \Xi_2(\hat{n}) = \sum_{l,m} a_{lm}^{\Xi_2} Y_l^m(\hat{n}). \tag{10.16}$$

The field $\Upsilon(\hat{n}) \equiv \left(\eth^2\Xi_1(\hat{n})\right)\Xi_2(\hat{n})$ is a spin-2 field and can therefore naturally be expanded into spin-2 spherical harmonics, with expansion coefficients ${}_2a_{lm}$,

$$\Upsilon(\hat{n}) \equiv \left(\eth^2\Xi_1(\hat{n})\right)\Xi_2(\hat{n}) = \sum_{lm} {}_2a_{lm}\ {}_2Y_{lm}(\hat{n}). \tag{10.17}$$

The aim is now to find how the coefficients ${}_2a_{lm}$ are related to the coefficients $a_{lm}^{\Xi_1}$ and $a_{lm}^{\Xi_2}$. First, we plug the expansions from eq. (10.16) into the definition of $\Upsilon(\hat{n})$ and act with $\eth^2$ on the spherical harmonic to find

$$\Upsilon(\hat{n}) = \sum_{l_1m_1}\sum_{l_2m_2} \text{ł}(l_1,2) a_{l_1m_1}^{\Xi_1} a_{l_2m_2}^{\Xi_2}\ {}_2Y_{l_1m_1}(\hat{n})\ Y_{l_2m_2}(\hat{n}), \tag{10.18}$$

which we rewrite, for reasons that will become clear shortly, as

$$\Upsilon(\hat{n}) = \sum_{l_1m_1}\sum_{l_2m_2} \text{ł}(l_1,2) \int \mathrm{d}^2\hat{n}' \delta_{\mathrm{D}}(\hat{n}-\hat{n}') a_{l_1m_1}^{\Xi_1} a_{l_2m_2}^{\Xi_2}\ {}_2Y_{l_1m_1}(\hat{n}')\ Y_{l_2m_2}(\hat{n}'), \tag{10.19}$$

By using eq. (10.8) with $s=2$, i.e. $\sum_{lm} {}_2Y_{lm}(\hat{n}){}_2Y^*_{lm}(\hat{n}') = \delta_{\mathrm{D}}(\hat{n}-\hat{n}')$ we can rewrite the equation above as

$$\Upsilon(\hat{n}) = \sum_{lm}\left(\sum_{l_1m_1}\sum_{l_2m_2} \text{ł}(l_1,2) a_{l_1m_1}^{\Xi_1} a_{l_2m_2}^{\Xi_2} \int \mathrm{d}^2\hat{n}'\ {}_2Y^*_{lm}(\hat{n}')\ {}_2Y_{l_1m_1}(\hat{n}')\ Y_{l_2m_2}(\hat{n}')\right)\ {}_2Y_{lm}(\hat{n}), \tag{10.20}$$

from which we can immediately deduce that

$${}_2a_{lm} = (-1)^m \sum_{l_1,m_1}\sum_{l_2,m_2} \begin{Bmatrix} l & l_1 & l_2 \\ -m & m_1 & m_2 \\ -2 & 2 & 0 \end{Bmatrix} \xi(l_1,2) a_{l_1m_1}^{\Xi_1} a_{l_2m_2}^{\Xi_2}. \tag{10.21}$$

Case $\left(\overline{\eth}^2\Xi_1\right)\Xi_2$

We will now analyse the conjugate case, $\Upsilon^*(\hat{n}) = \left(\overline{\eth}^2\Xi_1(\hat{n})\right)\Xi_2(\hat{n})$ such that $\Upsilon^*(\hat{n})$ is a spin-(-2) field. It is therefore expanded in spin-(-2) spherical harmonics with expansion coefficients ${}_{-2}a_{lm}$, $\Upsilon^*(\hat{n}) = \sum_{lm} {}_{-2}a_{lm}\ {}_{-2}Y_{lm}$. It can be shown, using the same tricks as before, that the expansion coefficients are given by

$${}_{-2}a_{lm} = (-1)^m \sum_{l_1,m_1}\sum_{l_2,m_2} \begin{Bmatrix} l & l_1 & l_2 \\ -m & m_1 & m_2 \\ 2 & -2 & 0 \end{Bmatrix} \text{ł}(l_1,2) a_{l_1m_1}^{\Xi_1} a_{l_2m_2}^{\Xi_2}. \tag{10.22}$$

More generally, the expansion coefficients ${}_{-2}a_{lm}$ of Υ^* are related to the expansion coefficients ${}_2a_{lm}$ of Υ by a change of signs in the last line of the Gaunt integral $\{\vdots\vdots\vdots\}$.

Case $\left(\not{\partial}\Xi_1\right)\left(\not{\partial}\Xi_2\right)$

Using the same techniques for the product

$$\Upsilon(\hat{n}) = \left(\not{\partial}\Xi_1(\hat{n})\right)\left(\not{\partial}\Xi_2(\hat{n})\right) \tag{10.23}$$

yields

$${}_2a_{lm} = (-1)^m \sum_{l_1,m_1}\sum_{l_2,m_2} \begin{Bmatrix} l & l_1 & l_2 \\ -m & m_1 & m_2 \\ -2 & 1 & 1 \end{Bmatrix} \text{ł}(l_1,1)\text{ł}(l_2,1) a^{\Xi_1}_{l_1m_1} a^{\Xi_2}_{l_2m_2}. \tag{10.24}$$

Case $\left(\not{\partial}^3\Xi_1\right)\left(\overline{\not{\partial}}\Xi_2\right)$

Using the same tools for the product

$$\Upsilon(\hat{n}) = \left(\not{\partial}^3\Xi_1(\hat{n})\right)\left(\overline{\not{\partial}}\Xi_2(\hat{n})\right) \tag{10.25}$$

yields

$${}_2a_{lm} = -(-1)^m \sum_{l_1,m_1}\sum_{l_2,m_2} \begin{Bmatrix} l & l_1 & l_2 \\ -m & m_1 & m_2 \\ -2 & 3 & -1 \end{Bmatrix} \text{ł}(l_1,3)\text{ł}(l_2,1) a^{\Xi_1}_{l_1m_1} a^{\Xi_2}_{l_2m_2}. \tag{10.26}$$

Case $\left(\overline{\not{\partial}}\not{\partial}^2\Xi_1\right)\left(\not{\partial}\Xi_2\right)$

Using the same tricks for the decomposition

$$\Upsilon(\hat{n}) = \left(\overline{\not{\partial}}\not{\partial}^2\Xi_1(\hat{n})\right)\left(\not{\partial}\Xi_2(\hat{n})\right) \tag{10.27}$$

yields

$${}_2a_{lm} = -(-1)^m \sum_{l_1,m_1}\sum_{l_2,m_2} \begin{Bmatrix} l & l_1 & l_2 \\ -m & m_1 & m_2 \\ -2 & 1 & 1 \end{Bmatrix} \text{ł}(l_1,1)\text{ł}(l_2,1)(l_1-1)(l_1+2) a^{\Xi_1}_{l_1m_1} a^{\Xi_2}_{l_2m_2}. \tag{10.28}$$

10.3 Mathematica notebooks

This project makes use of three different notebooks. The largest and most important one computes the power spectrum and bispectrum, exports the data and makes the plots. A second notebook computes the Δl_s-dependence of the plots. The last notebook computes $f_{\rm NL}^{\rm loc}$, the cosines and the signal-to-noise. To export data to and import data from the correct location, be sure to update the `directory`.

10.3.1 Bispectrum_AllTerms.nb

This notebook contains the code that computes all the power spectra and bispectra. In the code, the source redshift `zS` $= z_S$ is fixed from the beginning. I decided to make the source redshift a constant (i.e. not a variable), as otherwise the computation would be much slower; the reason being that all the integration boundaries would have to be re-evaluated every time.

The `Code`-section contains all the code needed for the computation of the power spectra and bispectra. If you want to change the cosmological parameters, check the first subsection. Notice that `P[k]` contains both the A_Φ^2/k^3 as the (square of) the transfer function and that A_Φ has been set to unity. Moreover, the command ξ`[l,m]` corresponds to $\ell(l,m)$.

The `Power Spectrum` subsection creates amongst others the commands `ClLimber2[l]`, `ScalingL2[l1,l2,l3]` and `TScalingL2[l1,l2,l3]`. The first one is self explaining, the second one is the factor to reduce the bispectrum, $C_{l_1}C_{l_2} + C_{l_2}C_{l_3} + C_{l_3}C_{l_1}$, whereas the third one is the normalisation of the dot product of two bispectra, i.e. $\Delta_{l_1 l_2 l_3} C_{l_1} C_{l_2} C_{l_3}$. The three commands also exist with `L1` instead of `L2`, corresponding to the first-order Limber approximation. The remaining of this section is devoted to the bispectra. The created commands are `b`i`ElectricLimber2[l1,l2,l3]` where i runs from `1` to `11`, and denotes the part $[i]$; `bNewtonElectricLimber2[l1,l2,l3]`, and `bLocalLimber2` which corresponds to the signal created by a primordial non-Gaussianity of the local type. Like before, every command also exists with `Limber1`. The section also contains the `scalar` and `vector` dynamical corrections (not the `tensor` ones), but they are never used as we used Camille's C++ code for that. I also included the signal created by a primordial non-Gaussianity of the equilateral type.

To summarise, just execute this whole section without thinking; this is very fast because it creates the commands, but does not evaluate anything (except some derived cosmological parameters like χ_s).

The `Results`-section creates the data files and constructs the plots. In the first two subsections (geometric parts and Newtonian terms), a file is created for each `part`, `l` $= l_l$ and `ΔL` $= \Delta l_s$. Each file contains a list of bispectra, with varying `L` $= l_s$. The values of `L` are set in `setL`. They are (crudely) logarithmically distributed between 4 and 1 000.

The structure of the subsection `Specific configuration, designed for varying zS` is different. It creates (or opens) a file, and writes the value of the reduced bispectrum together with the redshift for which it is computed. As the notebook can only handle one redshift at a time, the whole notebook needs to be re-executed when `zS` is changed. This is why the code is able to reopen an existing file, and squeeze the newly computed bispectrum at the right place in the file. This means that if you want to extend the redshift range, or want to add redshifts somewhere, it should all work automatically.

The remaining two subsections, constructing the plots, are self explaining. The reason the "ticks" are removed at the bottom and at the left of the plots is to facilitate the work in `Ipe`. For your information, to import a MATHEMATICA figure in `Ipe`, export it as a `pdf`-file, run `pdftoipe` on your file, and open the newly created `xml`-file in `Ipe`.

10.3.2 Bispectrum_AnalysisOfData.nb

This is the easiest and shortest notebook. It merely expands the prefactors in $1/l_s$, in order to find its Δl_s dependence. Before using it, you need to execute the `Code`-part of the previous notebook to import the prefactors. Notice that you need to overrule the ξ-command (l^m is an approximation when $l \gg m$).

By expanding all the prefactors in $1/l_s$, we find that – to leading order – parts [2] and [6] depend on Δl_s, whereas the other parts do not. This is the reason why the plots bispectra of [2] and [6] are so different than those of the other parts, see Fig. 9.1.

This notebook also contains the computation of the power α defined in eq. (9.6).

10.3.3 Bispectrum_fNL.nb

This notebook contains three sections. Be careful, I'm not sure they are compatible with each other, though I think they are. Nevertheless, be sure to `Quit` before running a section. Unlike the previous notebook, this one does not need the "main" notebook to be executed as I have copied all the necessary commands.

The `zS=1` and `zS=0.5`-sections are similar, so I'll only discuss the first one. The first subsection used to compute the primordial non-Gaussianity bispectrum, but it is set as a "comment" now so that you do not execute it by accident. What the subsection now does, is importing the data computed once. The second and third subsections are the same as in the main notebook. Therefore, you can execute these first three subsections without thinking.

The `results`-subsections contain what you are looking for. The only thing each subsection does, is to implement eq. (9.23). First, it imports the reduced weighted bispectrum data, of which it computes interpolating functions, because we will need to sum over l_s's we haven't computed. These functions are then "unweighted" and "unreduced" to find $B_{l_1 l_2 l_3}$. Afterwards it computes three quantities: $a \equiv B \cdot B^{\rm loc}$, $b \equiv B \cdot B$ and $c = B^{\rm loc} \cdot B^{\rm loc}$, such that $S/N = b$, $\cos = a/\sqrt{b\,c}$ and $f_{\rm NL}^{\rm loc} = a/c$, where the dot-product is defined by eq. (9.21).

The `varying zS`-section is similar, but has some subtle differences. Firstly, as geometrical corrections and redhift corrections behave almost exactly as $b^{\rm loc}$, we just need one configuration to fix $f_{\rm NL}^{\rm loc}$. To be slightly more precise, we perform the sum on l_l and Δl_s, but fix $l_s = 1000$. The maximum value of l_l is left as a variable, but the result does only barely depend on it, as expected. For those terms, we calculate a, b and c in three steps: we first sum over Δl_s for the known values of l_l, we then interpolate these results to find the values for the unknown values of l_l, and then sum over l_l.

For the other terms, those not resembling $b^{\rm loc}$, we need also to sum over all l_l, but the idea is basically the same.

The `Results`-section contains no subtleties, except for the signal-to-noise plot. For the signal-to-noise, we need to sum over all configurations, but – as said before – we did not compute the bispectrum for all configurations and all redhifts for the geometrical and redshift corrections. The trick is to use the bispectra for local primordial non-Gaussianity, multiplied by the corresponding value of $f_{\rm NL}^{\rm loc}$.

Conclusion

Gif-sur-Yvette, May 2012

Dear successor,

This is it, you have reached the end of my thesis. I hope your interest in cosmology has only grown while reading it. But most of all, I hope that this thesis has answered more questions than it has raised!

In Part A we have shown how combining Einstein's general relativity with the collisionless Boltzmann equation can lead to many different kinds of equations. And even if all descriptions are equivalent (remember those dictionaries?) they all have their own advantages. The standard formalism is very well suited for recovering the linear fluid equations. The formalism using the $A^{ij\cdots k}$'s enables us to generalise the results to non-CDM fluids. And the formalism using spherical harmonics is very well suited for scalar-vector-tensor decomposition, and truncation of the hierarchy is more transparent. We believe we will need one of these new hierarchies to properly describe the evolution of neutrinos.

In chapter 3 we described cosmological perturbation theory, our best way to solve the Boltzmann hierarchies. Unfortunately, the standard formalism is unable to handle non-CDM fluids, like neutrinos, in a proper way. Nevertheless, a thorough understanding of cosmological perturbation theory is absolutely necessary to proceed.

In Part B we introduced the eikonal approximation. And even if the formalism is quite simple, its power and range of applicability are beyond compare. The results obtained in EdS spacetime using the very complicated resummed perturbation theory can be recovered with a back-of-the-envelope calculation using the eikonal approximation. Moreover, this formalism can also straightforwardly be applied to multi-component fluids. The results aren't as transparent though, but it works. While these lines are being written, we are finishing a second paper on the eikonal approximation, focussing on the power spectrum. But if you fully understood the first eikonal paper, I have no doubt you'll understand this second one.

In Part C we introduced the concept of cosmic shear. We derived the first-order shear on the sphere, but merely stated the second-order shear, the derivation being rather

lengthy and technical. With these expressions, we computed the power spectrum and bispectrum, using the extended Limber approximation. We showed how the various terms behave and compared them to each other. We saw that the bispectrum they generate is not negligible compared to the bispectrum generated by primordial non-Gaussianity, making this analysis even more interesting.

My dear successor, now it is your turn. I hope I transmitted through this thesis all the information and knowledge you'll need to proceed. I wish you the best of luck in trying to incorporate the hierarchies of Part A into the eikonal framework of Part B. It is not going to be an easy task but succeeding would result in an enormous breakthrough for cosmological perturbation theory. I also wish you the best of luck in computing the magnetic component of the power spectrum and bispectrum of the cosmic shear. This computation is important because the magnetic signal is not dominated by the Newtonian evolution (which only induces an electric component).

As you understood by now, there is still a lot to be done before we will fully understand our Universe. It is now your time to contribute to cosmology. And in a few years from now, you'll also be writing a thesis containing your contributions. I hope you'll be as proud of you work as I'm today of mine.

Nicolas

Bibliography

[1] F. Bernardeau. *Cosmologie: des fondements théoriques aux observations*. Savoirs actuels. Astrophysique. EDP Sciences, 2007.

[2] S.M. Carroll. *Spacetime and geometry: an introduction to general relativity*. Addison Wesley, 2004.

[3] S. Dodelson. *Modern cosmology*. Academic Press. Academic Press, 2003.

[4] G. Lemaître. Un Univers homogène de masse constante et de rayon croissant rendant compte de la vitesse radiale des nébuleuses extra-galactiques. *Annales de la Société Scientifique de Bruxelles*, 47:49–59, 1927.

[5] Chung-Pei Ma and Edmund Bertschinger. Cosmological perturbation theory in the synchronous and conformal Newtonian gauges. *Astrophys.J.*, 455:7–25, 1995.

[6] E. Komatsu et al. Seven-Year Wilkinson Microwave Anisotropy Probe (WMAP) Observations: Cosmological Interpretation. *Astrophys.J.Suppl.*, 192:18, 2011. 57 pages, 20 figures. Accepted for publication in ApJS. (v2) References added. The SZ section expanded with more analysis. The discrepancy between the KS and X-ray derived profiles has been resolved. (v3) New analysis of the SZ effect on individual clusters added (Section 7.3). The LCDM parameters have been updated using the latest recombination history code (RECFAST version 1.5).

[7] Julien Lesgourgues and Sergio Pastor. Massive neutrinos and cosmology. *Phys.Rept.*, 429:307–379, 2006.

[8] Masatoshi Shoji and Eiichiro Komatsu. Massive Neutrinos in Cosmology: Analytic Solutions and Fluid Approximation. *Phys.Rev.*, D81:123516, 2010.

[9] J. Ehlers. General relativity and kinetic theory. In R. K. Sachs, editor, *General Relativity and Cosmology*, pages 1–70, 1971.

[10] S. Weinberg. *Gravitation and Cosmology: Principles and Applications of the General Theory of Relativity*. July 1972.

[11] Emiliano Sefusatti and Filippo Vernizzi. Cosmological structure formation with clustering quintessence. *JCAP*, 1103:047, 2011.

[12] F. Bernardeau, S. Colombi, E. Gaztanaga, and R. Scoccimarro. Large scale structure of the universe and cosmological perturbation theory. *Phys.Rept.*, 367:1–248, 2002.

[13] Martin Crocce and Roman Scoccimarro. Renormalized cosmological perturbation theory. *Phys.Rev.*, D73:063519, 2006.

[14] Roman Scoccimarro. A new angle on gravitational clustering. 2000.

[15] Martin Crocce and Roman Scoccimarro. Memory of initial conditions in gravitational clustering. *Phys.Rev.*, D73:063520, 2006.

[16] Francis Bernardeau, Martin Crocce, and Emiliano Sefusatti. Multi-Point Propagators for Non-Gaussian Initial Conditions. *Phys.Rev.*, D82:083507, 2010.

[17] Francis Bernardeau, Martin Crocce, and Roman Scoccimarro. Multi-Point Propagators in Cosmological Gravitational Instability. *Phys.Rev.*, D78:103521, 2008.

[18] Massimo Pietroni. Flowing with Time: a New Approach to Nonlinear Cosmological Perturbations. *JCAP*, 0810:036, 2008.

[19] Julien Lesgourgues, Sabino Matarrese, Massimo Pietroni, and Antonio Riotto. Non-linear Power Spectrum including Massive Neutrinos: the Time-RG Flow Approach. *JCAP*, 0906:017, 2009.

[20] Benjamin Audren and Julien Lesgourgues. Non-linear matter power spectrum from Time Renormalisation Group: efficient computation and comparison with one-loop. *JCAP*, 1110:037, 2011.

[21] Takashi Hiramatsu and Atsushi Taruya. Chasing the non-linear evolution of matter power spectrum with numerical resummation method: solution of closure equations. *Phys.Rev.*, D79:103526, 2009.

[22] Atsushi Taruya and Takashi Hiramatsu. A Closure Theory for Non-linear Evolution of Cosmological Power Spectra. 2007.

[23] Tomohiro Okamura, Atsushi Taruya, and Takahiko Matsubara. Next-to-leading resummation of cosmological perturbations via the Lagrangian picture: 2-loop correction in real and redshift spaces. *JCAP*, 1108:012, 2011.

[24] Francis Bernardeau and Patrick Valageas. Propagators in Lagrangian space. *Phys.Rev.*, D78:083503, 2008.

[25] Takahiko Matsubara. Resumming Cosmological Perturbations via the Lagrangian Picture: One-loop Results in Real Space and in Redshift Space. *Phys.Rev.*, D77:063530, 2008.

[26] F.R. Bouchet. in Proc. International School Enrico Fermi, Course CXXXII (Dark Matter of the Universe), S. Bonometto, J.R. Primack, A. Provenzale (eds.). IOS Press Amsterdam, 1996.

[27] T. Buchert. in Proc. International School Enrico Fermi, Course CXXXII (Dark Matter of the Universe), S. Bonometto, J.R. Primack, A. Provenzale (eds.). IOS Press Amsterdam, 1996.

[28] Will J. Percival, Robert C. Nichol, Daniel J. Eisenstein, David H. Weinberg, Masataka Fukugita, et al. Measuring the matter density using baryon oscillations in the SDSS. *Astrophys.J.*, 657:51–55, 2007.

[29] Gabor Somogyi and Robert E. Smith. Cosmological perturbation theory for baryons and dark matter I: one-loop corrections in the RPT framework. *Phys.Rev.*, D81:023524, 2010.

[30] Antony Lewis, Anthony Challinor, and Anthony Lasenby. Efficient computation of CMB anisotropies in closed FRW models. *Astrophys.J.*, 538:473–476, 2000. 4 pages, 1 figure. Corrected/updated references. Accepted by ApJ. For the F90 source code see http://www.mrao.cam.ac.uk/ aml1005/cmb/ Journal-ref: Astrophys.J. 538 (2000) 473.

[31] Antony Lewis. CAMB Notes. http://cosmologist.info/notes/CAMB.pdf, 2011.

[32] Henk Hoekstra and Bhuvnesh Jain. Weak Gravitational Lensing and its Cosmological Applications. *Ann.Rev.Nucl.Part.Sci.*, 58:99–123, 2008.

[33] Francis Bernardeau, Camille Bonvin, and Filippo Vernizzi. Full-sky lensing shear at second order. *Phys.Rev.*, D81:083002, 2010.

[34] Francis Bernardeau, Camille Bonvin, Nicolas Van de Rijt, and Filippo Vernizzi. Cosmic shear bispectrum from second-order perturbations in general relativity. *Phys. Rev. D*, 86:023001, Jul 2012.

[35] A. Liam Fitzpatrick, Leonardo Senatore, and Matias Zaldarriaga. Contributions to the Dark Matter 3-Pt Function from the Radiation Era. *JCAP*, 1005:004, 2010.

[36] Marilena LoVerde and Niayesh Afshordi. Extended Limber Approximation. *Phys.Rev.*, D78:123506, 2008.

[37] Wayne Hu. Weak lensing of the CMB: A harmonic approach. *Phys.Rev.*, D62:043007, 2000.

Abstract

The study of the large-scale structure of the Universe is one of the most important tools used to understand the origin and evolution of the Universe. In this thesis, we focus on two different facets of this study: cosmological perturbation theory and cosmic shear.

Cosmological perturbation theory describes how the large-scale structure of the Universe has been created out of the tiny initial perturbations. This evolution is described using fluid equations, and in this thesis, we introduce new versions of this Boltzmann hierarchy. The advantages and disadvantages of each hierarchy are thoroughly analysed. We also introduce a novel technique, dubbed the eikonal approximation, which enables us to better understand the results of existing perturbation theory approaches. Moreover, its broad range of applicability allows us to generalise many results.

Cosmic shear describes how gravitational lensing deforms the image of the sky. In this thesis, we compute in great detail the bispectrum of cosmic shear to second order in the gravitational potentials. The complete calculation is done on the full sky, making the results much more general than the existing ones. To ease the otherwise impossible numerical calculations, we introduce the (extended) Limber approximation.

Résumé

L'étude des grandes structures de l'Univers est un des meilleurs moyens pour comprendre l'origine et l'évolution de l'Univers. Dans cette thèse, nous nous spécialisons aussi bien dans la théorie des perturbations aux échelles cosmologiques, que dans le cisaillement cosmique.

La théorie des perturbations aux échelles cosmologiques décrit comment les grandes structures de l'Univers se sont formées à partir des minuscules fluctuations primordiales. Cette évolution est généralement décrite en se servant des équations du mouvement d'un fluide, et dans cette thèse nous introduisons quelques nouvelles versions de cette hiérarchie de Boltzmann. Les avantages et inconvénients de ces nouvelles hiérarchies sont analysés en détail. Nous introduisons aussi une nouvelle technique, appelée l'approximation eikonal, qui nous permet de mieux comprendre les résultats des autres approches utilisées en théorie des perturbations. En outre, grâce à sa généralité, elle nous permet de généraliser une grande quantité de résultats.

Le cisaillement cosmique décrit comment l'effet des lentilles gravitationnelles déforme notre image du ciel. Dans cette thèse, nous étudions de manière détaillée le bispectre du cisaillement cosmique, au deuxième ordre en les potentiels gravitationnels. Le calcul est intégralement fait en "full sky", généralisant ainsi les résultats existants. Pour simplifier les calculs numériques, nous introduisons et généralisons l'approximation dite de Limber.